Geoenvironmental Reliability of Soil-Bentonite Mixture Cutoff Walls(Dissertation_全文)

AUTHOR(S):

Takai, Atsushi

Geoenvironmental Reliability of Soil-Bentonite Mixture Cutoff Walls

Atsushi TAKAI

ABSTRACT

One of the most effective methods used to prevent the migration of contaminants in aquifers at contaminated sites is their containment with vertical cutoff walls, which are often constructed using Soil-Bentonite Mixtures (SBMs) as barrier materials due to their extremely low hydraulic conductivity (k), high flexibility even after construction, and little surplus-soil discharge. Due to the lack of proper scientific knowledge on the performance of barrier materials, however, these containment techniques are not widely used in Japan, even though excavation and disposal of contaminated soils, the preferred method, should be avoided as much as possible for the preservation of the environment.

To improve on the reliability of this containment technique, hydraulic barrier performance and seismic behavior of SBM cutoff walls were experimentally studied. First, factors affecting the hydraulic barrier performance of SBM cutoff walls were evaluated with a flexible-wall permeameter. From the obtained experimental results, it was found that the k values of SBMs can be reduced to values lower than 1.0×10^{-10} m/s after the addition of 100 kg/m^3 of bentonite-powder, regardless of the type of base soil. Once the bentonite in SBM has been sufficiently hydrated with soil pore water, its k value does not significantly increase by permeating fluids containing inorganic/organic chemicals. On the other hand, when the original ground contains a relatively high concentration of cations in its pore water, subsequent k values become higher than 1.0×10^{-9} m/s, which is the performance-based criterion in this research. Thus, the prehydration of the bentonite in SBM is absolutely vital for chemical compatibility of SBM. Nevertheless, even in the latter cases, the hydraulic barrier performance of SBM cutoff walls can be enhanced by increasing additive amounts of bentonite powder. Regarding their self-sealing capability, which is one of the most important characteristics of SBMs, high k values due to the presence of hydraulic defects can be reduced thanks to both the flexibility of SBM and the reswelling of the bentonite during permeation of distilled water. However, when the permeation is done with a $CaCl_2$ solution, the self-sealing of penetrating circular holes cannot be expected.

The k value of SBM has a strong correlation with some compatible factors such as maximum swelling pressure, plastic index of SBM, and others. Thus, changes in these factors can be useful indices of chemical effects on the k value of SBM. Because they can be easily measured within a couple of weeks or so, these compatible factors are expected to be employed as indicators to roughly estimate the k value at pre- and post-construction stages.

Secondly, the feasibility of using a piezocone test (CPTU) for on-site Quality Control/Quality Assurance (QC/QA) was verified with a large-scale soil tank. From the results of CPTU, corrected cone resistances (q_t) in a SBM layer with low content of bentonite

powder (lean-mixed SBM) were larger than those in a SBM layer with sufficient content of bentonite powder (well-mixed SBM). Although excess pore water pressure was generated in well-mixed SBM layers, pore water pressure (u) in lean-mixed SBM layer was smaller than hydrostatic pressure. However, these differences in q_t and u values can be obtained only when strength characteristics of SBMs depend on the content of bentonite powder.

Horizontal k values obtained from pore pressure dissipation tests during CPTU were almost equivalent regardless of the dissipation degree, being 1.4 - 1.6 times the k values obtained from hydraulic conductivity tests. Since the k values measured by the pore pressure dissipation test show a good correlation with those measured by hydraulic conductivity tests, it is concluded that the hydraulic barrier performance of SBM cutoff walls can be assessed by CPTU on-site with a certain level of accuracy. Besides, considering that boreholes produced by CPTU will self-seal after some time by the self-healing capability of SBM, it can be inferred that SBM cutoff walls can maintain their designed hydraulic barrier performance even after CPTU operation. Thus, CPTU is considered a valid QC/QA method at post-construction stage of SBM cutoff walls. A process of QC/QA using CPTU is also suggested based on the experimental results in a series of discussions.

The seismic behavior of SBM cutoff walls was verified by centrifuge modeling test and cyclic undrained triaxial test. Results of both experiments confirm that the increase in pore water pressure by dynamic loading is relatively small, while large strain is accumulated due to degradation of stiffness. Considering that the acceptable acceleration, back calculated from the factor of liquefaction, F_L, is smaller than 100 gal, SBM cutoff walls can be highly deformed due to seismic excitation, while excess pore water pressure will not increase as much.

From a series of centrifugal modeling tests, although excess pore water pressure ratio in sand layers gradually increased with shaking, regardless of depth, and eventually attained 1.0, that in SBM cutoff wall only reached a maximum of 0.8. Since the predominant frequency of response acceleration corresponds to that of the input wave, SBM cutoff wall shakes together with the adjacent sand layers during seismic excitation. The ground surfaces of the sand layers settled down due to liquefaction; however, the ground surface settlement of the SBM cutoff wall was limited because it did not liquefy. A large deformation of SBM cutoff walls is likely to be produced in shallow zones although various deformation modes can be generated on the SBM cutoff walls even with identical input waves. Since significant damage, such as cracks or fractures, are not observed, we found that SBM cutoff walls could maintain their soundness against the seismic excitation used in this research.

From the viewpoint of practical implications, the experimental results of hydraulic conductivity tests will make a great contribution to the design process for optimizing the mixing conditions in the field. For the QC/QA of constructed SBM cutoff walls, CPTU should be conducted to continuously evaluate vertical homogeneity and on-site k values. Horizontal deformation of SBM cutoff walls should be evaluated by a centrifuge modeling test simulating actual conditions, if necessary, in order to maintain the performance.

ACKNOWLEDGMENTS

The research reported herein mainly originated when the author studied and did research at Kyoto University. The author wishes to acknowledge all supervision, guidance, support, assistance and encouragement of many people.

The author would like to express his deep and sincere gratitude to Professor Takeshi Katsumi, Graduate School of Global Environmental Studies (GSGES), Kyoto University, for his invaluable guidance, encouragement and advice throughout this research work. Professor Katsumi provided a comfortable environment in which the author was able to accomplish his research; and giving him a lot of opportunities to participate domestic and international conferences and social activities. Also, the author is grateful to Professor Katsumi for providing a chance to work together in his laboratory.

The author wishes to express his heartfelt gratitude to Professor Masashi Kamon, Professor Emeritus of Kyoto University, currently President of Kagawa National College of Technology. The author started this research since Professor Kamon gave this research topic to him. Professor Kamon gave numerous suggestions and constructive comments especially during the author's student days. The author was further motivated by encouragement of Professor Kamon even after his graduation and could maintain correct orientation.

Special thanks are due to Professor Mamoru Mimura, Graduate School of Engineering, Kyoto University, for his helpful advice and suggestions. Many results in this dissertation could be obtained with much help of Professor Mimura and members of his former laboratory, Division of Geotechnics, Geohazards, Disaster Prevention Research Institute (DPRI), Kyoto University. Sincere thanks are also extended to Professor Junji Kiyono and Professor Masaki Takaoka, GSGES, Kyoto University, for their reviewing of the author's scholarship.

The author would like to extend his thanks to Dr. Toru Inui, Associate Professor, GSGES, Kyoto University. This research work would not be complete without his technical support, valuable suggestions and kind cooperation. The author could learn a great deal about experiment, data analysis, and how to write academic thesis and papers.

The author also acknowledge to Mr. Susumu Araki, Managing Director, Raito Kogyo, Co., Ltd. for his great contribution and guidance for this research from a viewpoint of practical application. This research would not be possible without the collaboration with Mr. Araki. His arrangement for some opportunities of site visit also helped the successful completion a lot.

The author also wishes to express appreciation to Mr. Mitsugu Yoshimura, Chief Engineer, Soil and Rock Engineering, Co., Ltd. for his technical guidance on CPTU. The author also thanks to Mr. Tsunetaka Terao previously in Soil and Rock Engineering, Co., Ltd.,

for his kind support and advice for interpretation of CPTU.

The author wishes to extend sincere appreciation to all members of the Environmental Infrastructure Engineering Laboratory at Kyoto University. Dr. Giancarlo Flores, Associate Professor, Graduate School of Engineering, Kyoto University, spent many hours encouraging him and proofreading his English in some papers. The author shared a lot of time with Dr. Flores since they were students; and received many stimuli about international sense. Ms. Miho Yasumoto, Administrative Assistant in the laboratory, helped the author with a lot of administrative works. Her kind support is greatly appreciated.

Special thanks are also extended to Mr. Hiroki Shimizu, Technical Officer, DPRI, Kyoto University, for his kind support for many experimental works especially during the author's student days. The author also acknowledge to Dr. Tetsuo Tobita, Associate Professor, DPRI, Kyoto University, for his kind support especially for conducting the centrifuge modeling test.

The author would like to appreciate to Mr. Yasuhiro Ogawa, Mr. Daisaku Matsuhashi, Mr. Futoshi Kurihara, Mr. Hiroyuki Koga, Mr. Hiroki Mogami, and Mr. Kazufumi Sano, former and current graduate students for their substantial contributions to the experiments.

Thanks are also due to the members of the committees that the author is joining, namely, the Technical Committee on Geoenvironmental Engineering (Japanese Geotechnical Society), and the Committee on Ground Improvement (Society of Materials Science, Japan). Special thanks are also extended to Dr. Yoshikazu Otsuka, Okumura Corporation Co., Ltd., for his constructive discussions and continuing encouragement.

Lastly, the author would like to gratefully acknowledge to his wife, Reiko, and two sons, Ryunosuke and Shimpei, for their faithful help. Great appreciations are also due to his father, Masahiko, and his mother, Keiko, for their devotions.

TABLE OF CONTENTS

CHAPTER 1

Introduction

1.1 General remarks

Industrialization and urbanization have caused many serious environmental problems not only in Japan but in the world. In particular, environmental pollution due to the generation and the management of waste materials, toxic chemicals, and other hazardous materials has become one of the most emergent problems to which society should find solutions. The disposal and dumping of such materials caused geoenvironmental problems, typified by contamination in subsurface soil and/or groundwater. Although contamination in soil and/or groundwater is one of the major pollution problems in Japan, countermeasures and legislations for it had been delayed compared with other pollutions (e.g. air pollution, water pollution, noise problem, etc.), because the occurrence of the former is not visible from the ground, and considered a localized problem. After the Japanese government enacted the first Soil Contamination Countermeasure Act (henceforth known as "the Japanese law" or "the law") in 2003, the contamination and its significance started to be commonly recognized, and many researchers started focusing on the possible solutions. The Japanese law was revised in 2010 to enhance the obligation of investigation and to accelerate proper and reasonable countermeasures. Besides, the number of voluntary investigations associated with transactions in land and with the corporate social responsibility (CSR) dramatically increased in the last years. Thus, interest in the geoenvironment is increasing.

Excavation of the contaminated soil and subsequent disposal to landfill sites is one of the conclusive methods in terms of complete removal of the contamination. However, with this method, the contaminants are just transferred to a different place and this is not a fundamental solution to the problem. Furthermore, this method has some environmental risks related to possible secondary contamination with delivery and nature destruction attributed to the extraction of clean soil for backfilling. Besides, in many cases, this method is basically more expensive than other methods. Given such a background, thus far, many kinds and types of techniques have been developed (e.g. Abumaizar and Smith 1999; Reddy 2010; Suhara et al.

2011). One of the techniques is an in-situ containment using vertical cutoff walls, which are used to prevent their migration in the aquifer. Especially, this technique is effective when the contaminants are located under existing structures because, in such cases, the active removal and degradation of contaminants are technically and economically difficult. Soil-Bentonite Mixture (SBM), which is a mixture of in-situ soil and bentonite, is one of the barrier materials used for the cutoff walls. The SBM cutoff walls have to exert high hydraulic barrier performance and high stability as geo-structures in order to completely contain the contaminants.

In this research, hydraulic barrier performance of SBM cutoff wall is evaluated with several laboratory tests in association with physical properties of SBMs. Piezocone test (CPTU) is employed to establish an on-site Quality Control/Quality Assurance (QC/QA) on the SBM cutoff walls at post-construction. Moreover, seismic behavior and liquefaction potential of SBM cutoff walls is assessed using triaxial tests and centrifuge modeling tests.

1.2 Regulations and countermeasures for contaminations

1.2.1 Regulation related to geoenvironment in various countries including Japan

In Japan, the Soil Contamination Countermeasure Act was enacted in 2003 as described above. However, since the conditions to require an investigation for the site characterization were poorly regulated, numerous contaminated sites were outside of its jurisdiction. Besides, in terms of the countermeasures, excavation of contaminated soil had been commonly applied regardless of the types and distribution of the contaminants as shown in Figure 1.1. With such background, the Japanese law was amended in 2010 to enhance the obligation of investigation, and to accelerate proper and reasonable countermeasures. After the amendment of the law, the number of the contaminations under the supervision of public administrations is increasing gradually, and the public administrations specify the type of essential countermeasures to be applied. Figure 1.2 shows the changes in the number of investigations for soil contamination cases in Japan (MOE 2013). As can be seen from this figure, the number of investigations increased around 2002, when the law was promulgated, and then, the number decreased around 2009 under the influence of Lehman's fall and global depression. Currently it has increased again in 2010 as a result of the amendment of the law. According to the results of a survey on soil contamination assessment and countermeasures in the fiscal year 2012 targeting the 120 members (Geo-Environmental Protection Center 2013), the business scale related to the soil contamination was about 88 billion yen in 2012 with total of approximately 7,500 orders.

Not only Japan but a number of advanced countries in Europe and North America have specific legislations to soil and land protection as shown in Table 1.1. In the United States, the Comprehensive Environmental Response, Compensation, and Liability Act (commonly called

"Superfund Act") was enacted in 1980 to clean up sites contaminated with hazardous substances. It was in response to the numerous contaminated sites outside of the jurisdiction of the former Resource Conservation and Recovery Act (Adams and Reddy 2012). In the Netherlands, lots of regulations related to the soil contamination were established. The regulations are collectively called Dutch soil policy, and they address the long-term protection, management, and sustainable use of soil. The 1987 Soil Protection Act (revised in 2008) is

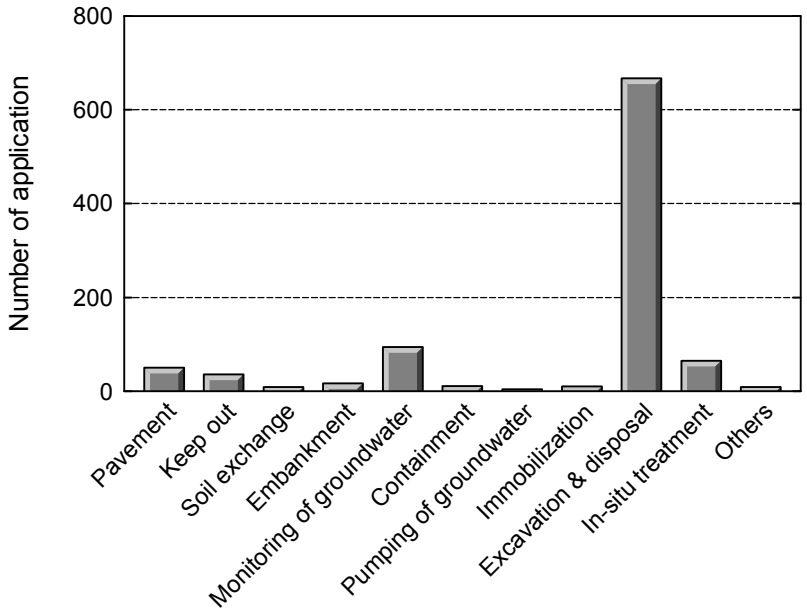

Figure 1.1 Number of countermeasures against soil contamination in Japan (MOE 2013).

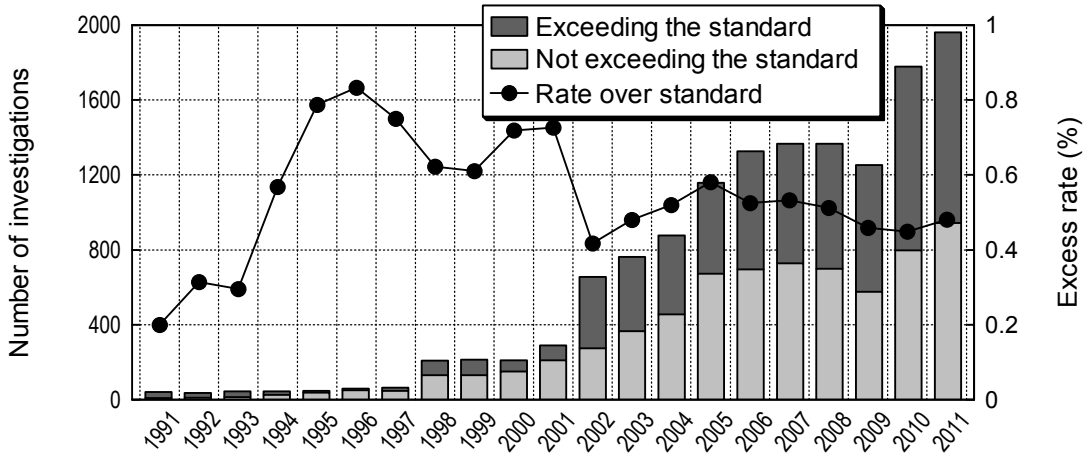

Figure 1.2 Number of investigations on soil contamination in Japan (MOE 2013).

Table 1.1 Regulations in foreign countries

Nations	Regulations (Year of establishment)
United States	Comprehensive Environmental Response, Compensation, and Liability Act: Superfund Act (1980)
Netherlands	Soil Protection Act (1987) Environmental Protection Act (1993) Soil Remediation Circular (2006)
United Kingdom	Waste and Contaminated Land Order (1997) Contaminated Land Regulations (2000)
Germany	Federal Soil Protection Act (1998) Federal Soil Protection and Contaminated Sites Ordinance (1999)
Denmark	Contaminated Land Act (1999)
Taiwan	Soil and Water Conservation Law (1994)
South Korea	Soil Environment Conservation Act (1995)

one of the most important laws that serve as the foundation of the Dutch soil policy, and it contains general rules to prevent soil contamination. The 1993 Environmental Protection Act establishes that permits must be obtained before certain activities may be performed, and the 2006 Soil Remediation Circular establishes objectives of remediation and describes soil remediation requirements. There are 400,000 registered sites that are contaminated or potentially contaminated. In Germany, the 1998 Federal Soil Protection Act and the 1999 Federal Soil Protection and Contaminated Sites Ordinance were enacted so as to unify the regulations in each state. The government conducts a preliminary investigation by itself on the land suspected of contamination, and compels the polluters, the owners, or the users to investigate particularly if the contamination levels exceed the criteria. About 275,000 sites are suspected of being contaminated in Germany. Other countries, such as United Kingdom, Denmark, etc., have legislations to regulate and prevent contamination. In Asian countries, Taiwan and Korea place regulations specializing in soil contamination. However, in most of developing countries, regulations in regard to contamination are not formulated yet. Even China lags behind in legislation because this country is industrializing rapidly and interested in economic growth in this decade without concern to environmental issues. These countries are struggling to formulate legal frameworks as to protect their land, and to remediate contaminated soils. It is said that the Chinese government will prepare relevant laws before 2015 and, similarly, Thailand and Malaysia may legislate about contamination.

As can be seen from the above, legislation about contamination was tightened in these several decades not only in Japan but in the world. Additionally, waste management including radioactive materials due to the 2011 East Japan Earthquake is one of other serious problems related to geoenvironmental issues in Japan. The solutions for such geoenvironmental

problems are significant for the preservation and conservation of the limited natural resources.

1.2.2 Hazardous substances and countermeasures in Japan

In the Japanese law, 24 substances (and their compounds) are designated as hazardous substances. Table 1.2 shows all designated hazardous substances in the law. Criteria for each substance are determined based on the human health with referring the environmental standards in the Basic Environment Law. These substances are categorized into three groups which are volatile organic compounds (VOCs), heavy metals, and agrichemicals (+PCB). VOCs have high mobility and low solubility in water. Heavy metals and agrichemicals have low mobility. Thus, the spreading behaviors of contamination are different by the types of contaminants as shown in Figure 1.3. Some VOCs are heavier than water and others are lighter than water. Hence, the former spread deeply in the aquifer and the latter float at the groundwater level. In any case, once VOCs reach the aquifer, they can spread widely with the flow of groundwater (Flores et al. 2011). Heavy metals and agrichemicals have low-mobility and can be trapped in the subsurface area, therefore, their spread are mostly smaller compared with VOCs.

Figure 1.4 shows various countermeasures against contamination. In considering the spread of contamination, the main concern should be the dissolved contaminants in the groundwater because the mobility of the contaminants in the liquid phase is higher than that of the contaminants adsorbed on the solid surface. Basic concepts of the countermeasures are categorized into the removal of the contaminants or into the prevention of their migration in the aquifer. Biological decomposition, chemical decomposition, pumping techniques, etc. are applied as in-situ techniques with no excavation of the contaminated soils. Thermal treatments, washing techniques, decomposition, etc. can be applied to the excavated soils, and the cleaned soils through the treatments can be reused as geo-materials after proper quality verifications.

Table 1.2 Designated hazardous substances in Japanese law.

VOCs	Heavy metals	Agrichemicals
Carbon tetrachloride	Cadmium and compounds	Simazine
1,2-Dichloroethane	Hexavalent chromium and compounds	Thiuram
1,1-Dichloroethylene	Cyanogen and compounds	Thiobencarb
Cis-1,2-Dichloroethylene	Total mercury and compounds	Polychlorinated biphenyl
Dichloromethane	Selenium and compounds	Organic phosphorus
Tetrachloroethylene	Lead and compounds	compounds
1,1,1-Trichloroethane	Arsenic and compounds	
1,1,2-Trichloroethane	Fluorine and compounds	
Trichloroethylene	Boron and compounds	
Benzene		

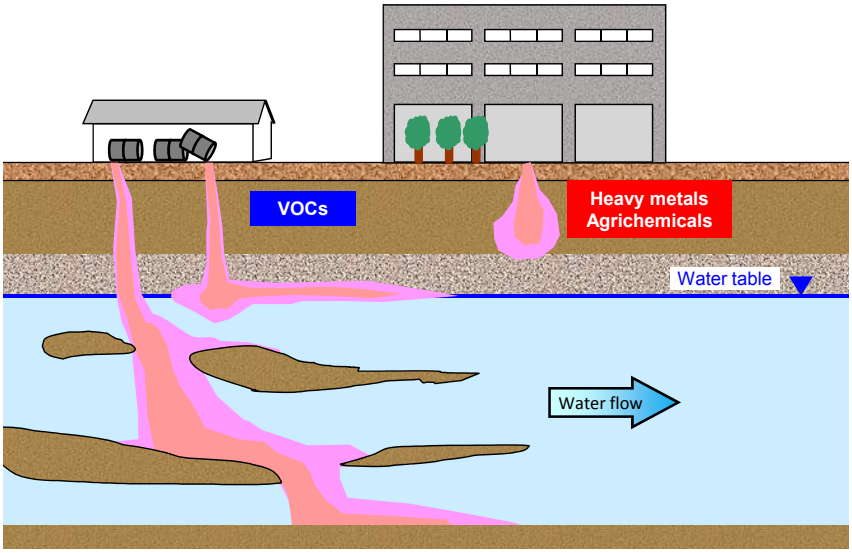

Figure 1.3 Spread of contamination in the ground

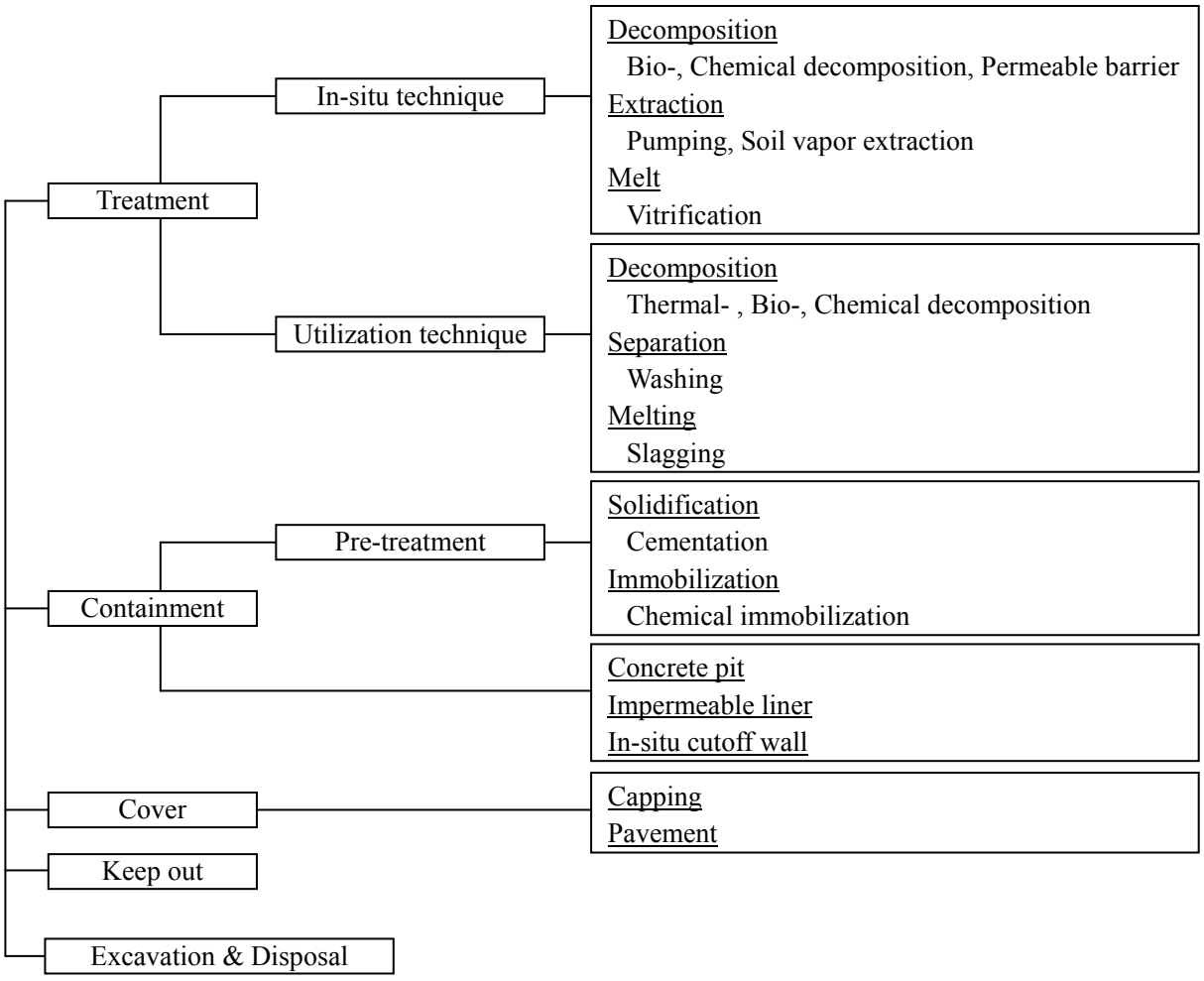

Figure 1.4 Classification of various countermeasures

These techniques are particular solutions of the positive removal of contaminants from the soil.

The containment technique is a typical technique to prevent the contamination from migrating in the aquifer. Mainly vertical cutoff walls and liner systems using clay materials, concrete pits and impermeable sheets are employed as containment techniques. The in-situ containment using cutoff walls can isolate the contaminants from the surrounding environment without any excavations. The containment facilities using liner systems are often placed inside of the contaminated site; and the contaminants can be managed without any transportation.

1.2.3 In-situ containment technique using SBM cutoff walls

As described in 1.1, in-situ containment technique using barrier materials with low hydraulic conductivity is a valid method to prevent the contaminants in subsurface from migrating in the aquifer as shown in Figure 1.5 (e.g. Evans 1993, Katsumi et al. 2009). This technique controls the horizontal groundwater flow and the lateral migration of the contaminants using vertical cutoff walls. In many cases, since the vertical cutoff walls are embedded into a low-permeability stratum, such as clay stratum, with lower hydraulic conductivity than 1.0×10^{-7} m/s and with larger thickness than 5.0 m, the vertical seepage is controlled by the stratum. The vertical cutoff walls are also used in conjunction with some form of pump and/or treat remediation because control of seepage is required on the application of such kinds of remediation techniques (Evans 1995).

In the amended Soil Contamination Countermeasure Act, the in-situ containment technique was positioned as an "Instructed Action", which is a principle of countermeasure required by the local government. However, the number of in-situ containment is not increasing due to lack of scientific knowledge on performance of barrier materials. Thus, improvement of reliability about the barrier materials is vital for acceleration of reasonable and cost-effective countermeasures in Japan.

Until today, various materials are developed and applied for containment systems. They can be categorized into two by their base materials: the steel-base and soil-base materials. The typical materials made of steel include steel sheet piles and steel pipe sheet piles (e.g. Kimura et al. 2007; Watabe et al. 2007), which are also used for the containment at coastal landfill sites and for bracing for underground excavations. The typical materials made of soil include soil-cement mixture and SBM. Soil-cement mixture is a mixture of cement and in-situ soil, and has low hydraulic conductivity and high compression strength due to the hydration reaction of the cement. Therefore, this material is also widely used for the bracing of underground excavations to control the seepage of groundwater and to prevent the ground from being deformed. Furthermore, the constructed vertical cutoff walls can be used as foundations of buildings due to their high strength.

SBM cutoff walls are constructed by blending powder bentonite with in-situ soil without uptake of excavated soil. Hydraulic barrier performance of SBM can be performed by the

swelling of bentonite in SBM as shown in Figure 1.6. SBM cutoff walls also have another distinctive characteristic that the softness can be maintained even after the completion. Even though the application of SBM for bracing is technically difficult because of low compression strength, SBM has some advantages when applied as barrier materials for soil and/or groundwater contaminations compared with other materials (Grube 1992);

- ✓ SBM is not solidified and its high softness can lead the high resistance to cracking even during earthquakes.
- ✓ Self-sealing capability can be performed by the swelling of bentonite in SBM, and the pores will be refilled even in the occurrence of cracks.
- ✓ Bentonite is an inorganic and natural mineral. Hence, SBM has a long-term durability in terms of the corrosion, erosion and deterioration as compared with steel materials.
- ✓ Since SBM cutoff walls are constructed with the addition and mixing of bentonite as powder directly to the in-situ soil, few surplus soils are discharged during its installation.
- ✓ Since bentonite can swell immediately after its contact with a liquid, curing period for the designated performance is shorter than cement-base materials.

In order to achieve high homogeneity of the constructed SBM walls, the Trench cutting and Re-mixing Deep wall (TRD) method is widely considered at construction (Katsumi et al. 2008). The construction processes of SBM cutoff wall by TRD method is as follows (see Figure 1.7):

1) Cutter chains placed at a base machine rotate and cut the trench with supplying bentonite slurry. Trench cutting and mixing of bentonite slurry are conducted at the same time.
2) The cutter chains are drawn back to the initial position.
3) Bentonite powder is added and re-mixed with the soil-slurry mixture while the cutter chains move horizontally again.
4) The cutter chains used for TRD method are shown in Photo 1.1. During the trench cutting, bentonite slurry is initially placed to support the trench and improve the

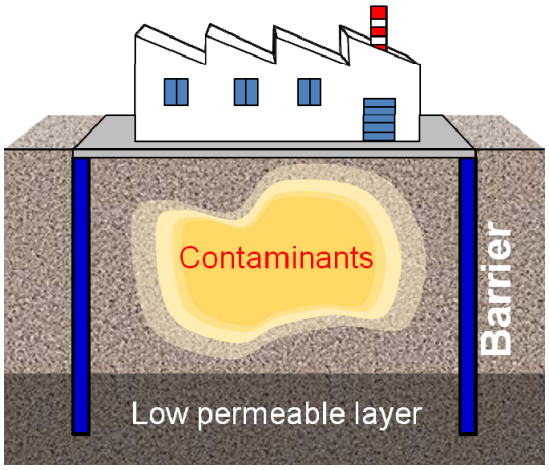

Figure 1.5 Schematic view of in-situ containment technique

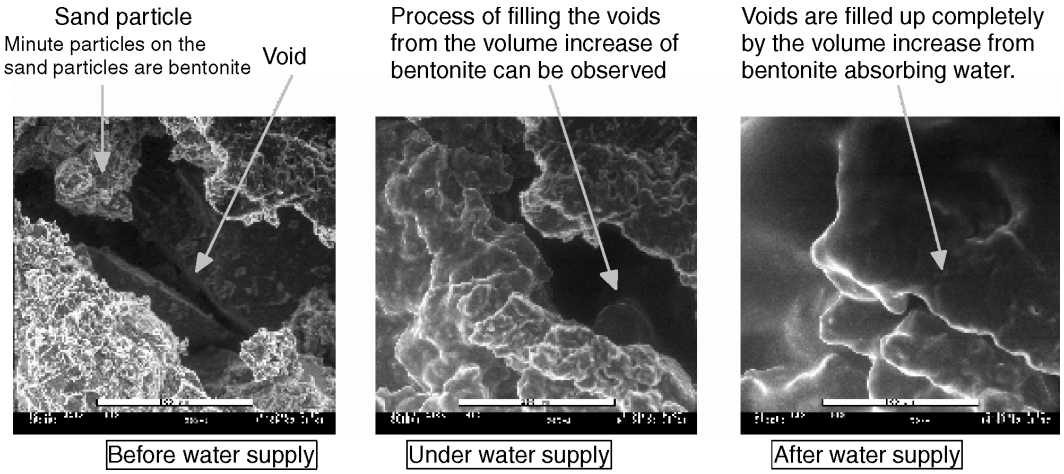

Figure 1.6 Swelling behavior of bentonite in the bentonite-buffer material (Komine and Ogata 2003).

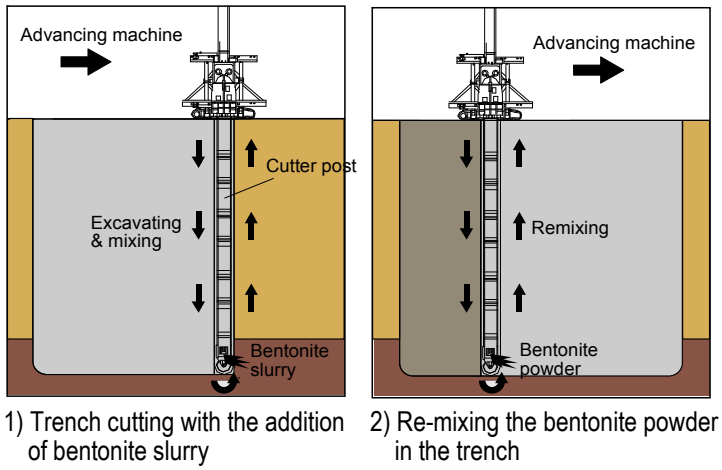

Figure 1.7 Construction processes of SBM cutoff wall by TRD method

Photo 1.1 Cutter chains of TRD machine (Raito Kogyo Co., Ltd. HP).

Photo 1.2 Appearance of SBM cutoff wall after construction.

workability of the excavated soil. Hence, bentonite powder can be mixed sufficiently with the help of the improved workability, even though mixing of bentonite powder is difficult in the case of direct addition to the in-situ soil without bentonite slurry addition. Photo 1.2 shows the appearance of SBM cutoff wall after construction.

1.3 Objectives and contents of the thesis

A main objective of this study is to quantify the effects of various factors on the hydraulic barrier performance of SBM cutoff walls. Quality Control/Quality Assurance (QC/QA) of the constructed SBM wall at the post-construction stage is also experimentally discussed. Seismic behavior of SBM walls installed at sand layer is evaluated in terms of liquefaction and deformation.

The main concerns of in-situ containment barriers are the assurance of hydraulic barrier performance and its vertical homogeneity. Hydraulic barrier performance of SBM is attributed to various factors, such as the swelling of bentonite, bentonite powder content, confining pressure and the types of base sand. The mixing condition of SBM is designed based on laboratory tests using in-situ soil prior to the application and the construction. Therefore, the actual hydraulic barrier performance in the site and its vertical homogeneity should be assured properly because they play fundamental roles on the quality of containment barriers in terms of complete containment. Also, the seismic behavior is crucial to know if the cutoff walls can resist against earthquakes. In this study, the above points are discussed with some laboratory tests. The scientific knowledge obtained through this research can contribute not only to enhance the reliability of in-situ containment itself but to provide reasonable solutions for ground contamination cases instead of the usual excavation and disposal. Besides, such reasonable techniques can contribute to solve problems with brownfield sites which are left for long time due to great expenses for countermeasures. Thus, this research holds much potential to give a significant social impact.

This thesis consists of 5 chapters. The constitution of the thesis is shown in Figure 1.8, and the experimental methodologies applied for this study are shown in Table 1.3.

In this chapter (Chapter 1), the objectives and the contents of the thesis are clarified together with general information related to soil and/or groundwater contamination as a background of this research. Also, fundamental information about advantages and construction processes of SBM are described.

Chapter 2 discusses hydraulic barrier performance of SBM cutoff walls. The hydraulic barrier performance is evaluated by hydraulic conductivity tests with specimens made with water and in permeant, content of bentonite powder, confining pressure and type of base soil are variously changed as parameters, which will influence on the hydraulic conductivity of

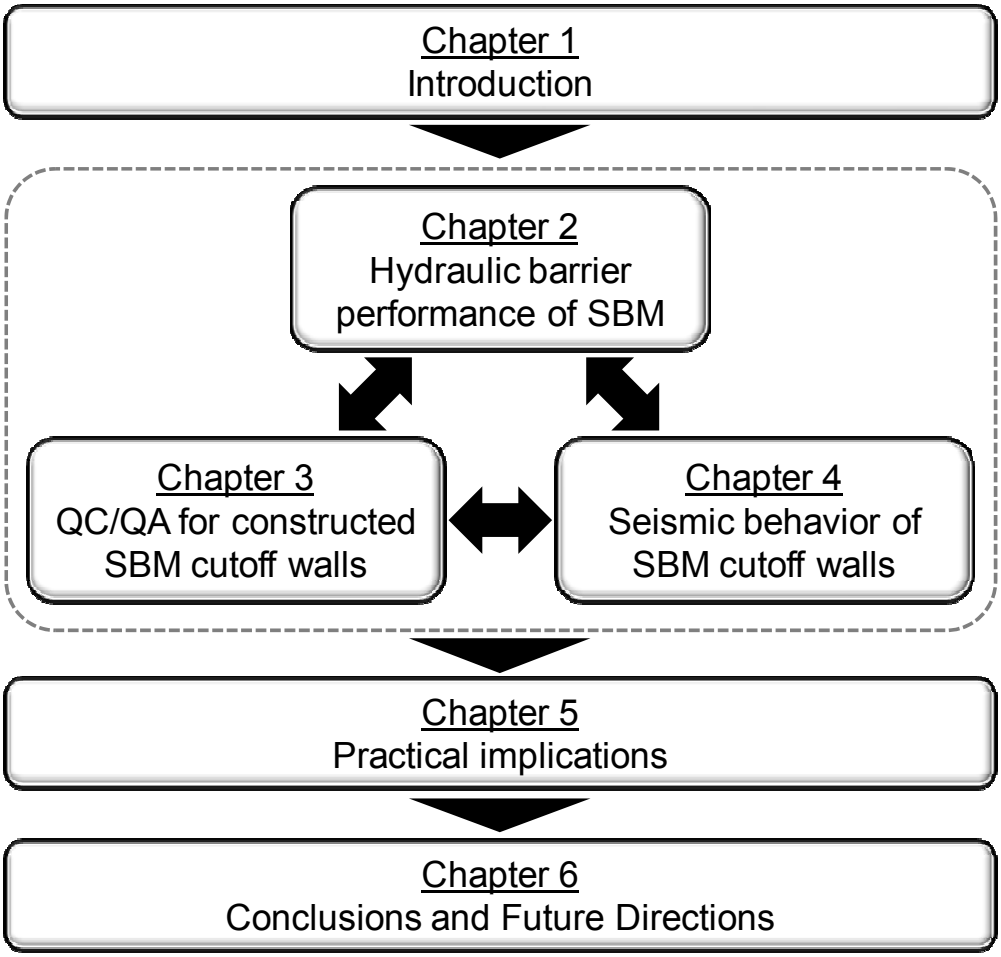

Figure 1.8 Contents of this thesis.

SBMs. Consistency characteristics of SBMs and swelling characteristics of SBMs are also evaluated to verify correlations with the hydraulic conductivity values.

In Chapter 3, establishment of a QC/QA method on the constructed SBM cutoff wall is tested with CPTU by using a large-scale soil tank. CPTU is one of the common techniques applied for ground surveys, and can obtain vertically continuous profiles attributed to a soil classification. Hence, since the values would be unstable if the constructed SBM cutoff walls contain heterogeneous parts, CPTU can be expected to be employed for QC/QA. In this chapter, a process of QC/QA using CPTU is also suggested based on the experimental results in a series of discussion.

In Chapter 4, seismic behavior of SBM cutoff wall is evaluated by a centrifuge modeling test and a cyclic undrained triaxial test. As mentioned above, static/dynamic stability is also an important issue because the SBM is a rather soft material compared with other typical materials. By the centrifuge modeling test, seismic behavior of SBM cutoff wall installed in an underlying clay layer was evaluated by simulating a larger-scale field by loading a centrifugal force on a model cutoff wall.

Chapter 5 describes practical implications based on experimental results obtained in each chapter in terms of design considerations, post-construction verifications and seismic stability assessment. Furthermore, mutual relations among each consideration are discussed.
Chapter 6 summarizes all results and discussions obtained in each chapter as conclusion of this dissertation; and future directions are mentioned.

Table 1.3 Experimental methodologies applied in this study

Chapter	Experimental methodologies
2	Hydraulic conductivity test - Hydraulic conductivity Free swelling test - Free swell index Swelling pressure test - Swelling pressure Swelling deformation test - Deformation characteristics by swelling Consistency test - Consistency characteristics
3	Piezocone test - Vertical profile and homogeneity UU test - UU strength
4	Centrifuge modeling test - Seismic behavior / Lateral deformation CU test - CU strength Cyclic undrained triaxial test - Cyclic strength

References for Chapter 1

Adams, J.A. and Reddy K.R. (2012): State-of-the-Practice of Characterization and Remediation of Contaminated Sites, *Geotechnical Engineering State of the Art and Practice*, *Geotechnical Special Publication*, No.226, K. Rollins and D. Zekkos (eds.), pp.2659-2668.

Abumaizar, R.J. and Smith, E.H. (1999): Heavy Metal Contaminants Removal by Soil Washing, *Journal of Hazardous Materials*, Vol.70, pp.71-86.

Evans, J.C. (1993): Vertical cutoff walls, *Geotechnical Practice for Waste Disposal*, D.E.

Daniel (ed), Chapman and Hall, London, U.K. pp.430-454.

Evans, J.C. (1995): Soil- and Cement-based Vertical Barriers with Focus on Materials, *Assessment of Barrier Containment Technologies: A Comprehensive Treatment for Environmental Remediation Applications*, R. Rumer and J.K. Mitchell. (eds.), U.S. Department of Energy, U.S. Environmental Protection Agency, pp.5-43.

Flores, G., Katsumi, T., Inui, T., and Kamon, M. (2011): A simplified image analysis method to study LNPL migration in porous media, *Soils and Foundations*, Vol.51, No.5, pp.835-847.

Geo-Environmental Protection Center of Japan (2013): Survey Results on "Soil Contamination Assessment and Countermeasures" in the fiscal year 2012, http://www.gepc.or.jp/04result/press24.pdf (accessed on Dec. 25th, 2013). (in Japanese)

Grube, W.E. (1992): Slurry Trench Cut-off Walls for Environmental Pollution Control, *Slurry Walls: Design, Construction, and Quality Control*, ASTM STP 1129, D.B. Paul et al. (eds.), pp.69-77.

Huang, J.W., Chen, J., Berti, W.R., and Cunningham, S.D. (1997): Phytoremediation of Lead-Contaminated Soils: Role of Synthetic Chelates in Lead Phytoextraction, *Environmental Science & Technology*, Vol. 31, No. 3, pp. 800–805.

Katsumi, T., Kamon, M., Inui, T., and Araki, S. (2008): Hydraulic Barrier Performance of SBM Cut-off Wall Constructed by the Trench Cutting and Re-mixing Deep Wall Method, *GeoCongress 2008: Geotechnics of Waste Management and Remediation, Geotechnical Special Publication No.177*, M.V. Khire, A.N. Alshawabkeh and K.R. Reddy (eds.), pp.628-635.

Katsumi, T., Inui, T., and Kamon, M. (2009): In-situ Containment for Waste Landfill and Contaminated Sites, *Advances in Environmental Geotechnics - Proceedings of the International Symposium on Geoenvironmental Engineering* -, Springer, pp.248-258.

Kimura, M., Inazumi, S., Too, A.J.K., Isobe, K., Mitsuda, Y., and Nishiyama, Y. (2007): Development and Application of H-Joint Steel Pipe Sheet Piles in Construction of Foundations for Structures, *Soils and Foundations*, Vol.47, No.2, pp.237-251.

Komine, H., and Ogata, N. (2003): New equations for swelling characteristics of bentonite-based buffer materials, *Canadian Geotechnical Journal*, Vol.40, No.2, pp.460-475.

Ministry of the Environment (2013): The results of the survey on Enforcement Status of the Soil Contamination Countermeasures Act & Numbers and trends of soil contamination investigations and countermeasures in the fiscal year 2011. (in Japanese)

Suhara, H., Arai, Y., Nakakoshi, K., Akagami, M., and Kuroyama H. (2011): A Case Study of a Large Scale Soil/Groundwater Contamination Countermeasure by the Volatile Organic Compound, *Japanese Geotechnical Journal*, Vol.6, No.2, pp.317-329. (in Japanese)

Raito Kogyo Co. Ltd. Home Page, http://www.raito.co.jp/project/doboku/kui/trd/index.html (accessed on Dec. 25th, 2013). (in Japanese)

Reddy, K.R. (2010): Technical Challenges to In-situ Remediation of Polluted Sites,

Geotechnical and Geological Engineering, Vol.28, No.3, pp.211-221.
Watabe, Y., Kinoshita, M., Yamada, K., and Oki, T. (2007): Field Performance and Advanced Application of Impermeable Steel Seawalls for Confined Disposal Facilities in Coastal Areas, *Journal of Japan Society of Civil Engineers, Ser. C*, Vol.63, No.3, pp.662-676.

CHAPTER 2

Hydraulic Barrier Performance of SBM

2.1 General remarks

A key characteristic governing the effectiveness of cutoff walls is the hydraulic barrier performance of the barrier materials (Britton et al. 2004). The hydraulic barrier performance of barrier materials mostly depends on hydraulic conductivity (k) value. The k values are affected by many factors such as chemical property of groundwater, bentonite powder content, stress state, saturation degree, and physical and chemical properties of original soil, etc. Therefore, effect of each factor on the k has to be systematically verified in order to optimize mixing conditions for practical implementation.

2.1.1 Chemical factors

It is well known that the hydraulic barrier performance of bentonite-based barrier materials strongly depends on the swelling characteristics of bentonite (e.g. Komine 2004, Katsumi et al. 2008, Mishra et al. 2011). The swelling characteristics are affected by chemical species and their concentrations in solution, which will be in contact with bentonite. It is because of this that bentonite cannot swell sufficiently against solutions that have high concentration of inorganic chemicals or nonpolar liquids (Norrish and Quirk 1954). The basic mechanism of swelling of bentonite is attributed to "Osmotic swelling" and "Diffuse electrical double layer".

2.1.1.1 Osmotic swelling

A surface of clay mineral is mostly negatively charged due to isomorphous substitution inside of plane crystals of montmorillonite. For electrical neutrality, cations, such as potassium, sodium, or calcium, exist between the plates as exchangeable cations. When the bentonite contacts with water or other polar liquids, negatively-charged side of molecules is attracted to the exchangeable cations to balance the charge. In the case of water, water molecules are attracted to the cations to hydrate one after another. Accordingly, layers of water molecules are electrically intercalated between the montmorillonite interlayer, and the distance between

each crystal sheet is expanded. Thus, bentonite macroscopically expands. This is the basic concept of osmotic swelling of bentonite. When the bentonite is in contact with a fluid, the exchangeable cations are attracted not only to the negative charge of the fluid molecules but with the clay minerals, which also have negative charge. Therefore, when the exchangeable cations are multivalent, the bond between the exchangeable cations and the minerals becomes comparatively strong, and the swell volume of bentonite becomes small as shown in Figure 2.1 (Katsumi et al. 2009).

2.1.1.2 Diffuse electrical double layer

Cations in solution can be tightly adsorbed and held on surfaces of negatively charged clay particles. The adsorbed cations, because of their high concentration near the surfaces of particles, try to diffuse away in order to equalize concentrations throughout the pore fluid. The escaping tendency due to the diffusion and opposing electrostatic attraction lead to ion distributions adjacent to a clay particle in suspension that are often idealized as shown in Figure 2.2. The charged surface and the distributed charge in the adjacent phase are together termed the diffuse electrical double layer. When no or few cation exists in the solution, positively-charged sides of water molecules are adsorbed on the surface of clay particles. These adsorbed water molecules cannot contribute to water permeation through soil because the water molecules are tightly held. Therefore, the thicker diffuse electrical double layer reduces effective porosity. On the other hand, in the case of high cation concentration, those cations are preferentially adsorbed on the clay particles and the diffuse double layer becomes thin. Thus, the thickness of diffuse electrical double layer plays an important role on the hydraulic barrier performance of clay materials.

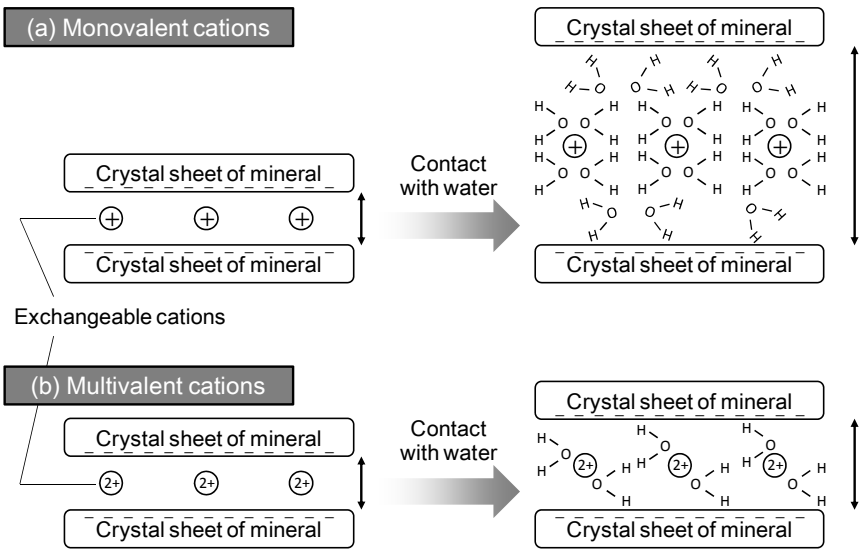

Figure 2.1 Schematic diagram of osmotic swelling.

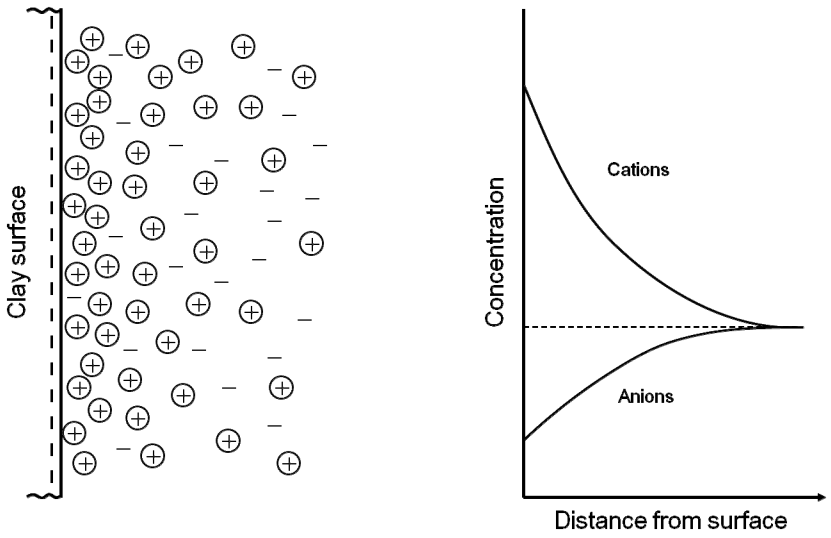

Figure 2.2 Distributions of ions adjacent to a clay surface (modified from Mitchell & Soga 2005).

2.1.2 Physical factors

It is commonly known that hydraulic barrier performance of soils including SBM is affected also by physical factors, such as particle size, void ratio, saturation degree, and viscosity of permeant (Sivapullaiah et al. 2000).

Generally, fine-grained soil has lower k than coarse-grained soil. Uniformity of soil particles also influences k. A soil with uniform particles has higher k because the void in the specimen becomes large in such soil. In a soil with larger void ratio, liquid can move more freely in the soil and the k increases. Also, saturation degree of soil is a key factor affecting on k (e.g. van Genuchten 1980, Durner 1994). The relative k of unsaturated soil is comparatively lower than that of saturated soil due to increase of tortuosity, surface tension, and decrease of cross-sectional area of water flow. From these viewpoints, the k of SBM should be discussed also in consideration of type of base material, i.e. ground conditions of concern.

2.2 Current studies on hydraulic barrier performance of SBM

2.2.1 First exposure effect

Several studies have reported that the sequence in which permeant liquids are introduced to soils containing high swelling clay, such as betonite, can have a significant effect on the k of the soils (e.g. Gleason et al. 1997, Quaranta et at. 1997, Stern and Shackelford 1998, Shackelford et al. 2000, Naka et al. 2012). This effect has been referred to as the "first exposure effect" (Shackelford 1994). Application of multiswellable bentonite or prehydrated bentonite is considered an effective method of improving the chemical compatibility (Onikata

et al. 1996, Shackelford et al. 2000, Katsumi et al. 2004, Kolstad et al. 2004, Katsumi and Fukagawa 2005, Lee and Shackelford 2005, Malusis et al. 2013). Figure 2.3 is a schematic diagram of the effect of prehydration and non-prehydration on the *k*.

Malusis et al. (2013) have studied about the first exposure effect on the *k* values of SBM with flexible-wall permeameters using tap water and calcium chloride ($CaCl_2$) solutions as the permeant liquid. In this research, three different types of powder bentonite, which have 70-85 montmorillonite content, were used and blended with sandy soil as 5% slurry and bentonite powder at 4.5 to 5.7% of total bentonite content (dry weight basis). The experimental results indicated that permeation with tap water before introducing the $CaCl_2$ solutions had no significant effect on the *k* regardless of $CaCl_2$ concentration, although a significant impact on other clay-based materials (GCL2, Compacted S-A-B) with permeation of 500 or 6700 mM $CaCl_2$ solutions were observed as shown in Figure 2.4 (Stern and Shackelford 1998, Shackelford et al. 2000, Lee and Shackelford 2005). Here, the first exposure effect was assessed based on the first exposure ratio (FER), which represents the ratio of the *k* of a specimen permeated initially with a chemical solution relative to that of a separate specimen permeated with the same chemical solution after permeation with water. Based on these results, it was concluded that the SBM backfills were not susceptible to a first exposure effect in which *k* values to chemical solutions were influenced by prior permeation with water. However, the absence of a first exposure effect for SBM backfills were led on the basis that all specimens were fully prehydrated with tap water before permeation as mentioned in the conclusions. In this research, all specimens were prepared by mixing the dry sand-bentonite with bentonite slurry, therefore, the first liquid for powder bentonite was tap water in all cases. In the case that some chemicals exist in the pore water of original ground, swelling of bentonite should be restricted and subsequent hydraulic barrier performance of SBM can be

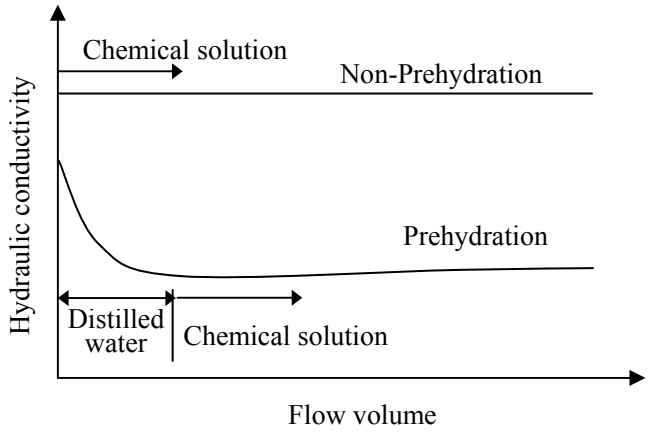

Figure 2.3 Effect of prehydration and non-prehydration on *k* (Katsumi et al. 2004).

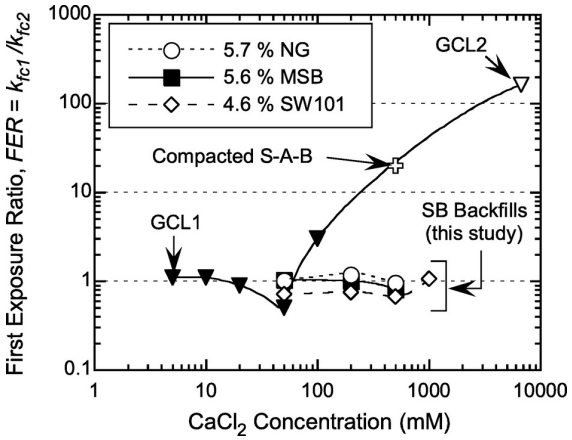

Figure 2.4 Comparison of first exposure effect for SB backfills with other bentonite-based materials (data for GCL1 from Lee and Shackelford 2005; data for GCL2 from Shackelford et al. 2000) and a compacted S-A-B mixture containing 10% attapulgite and 10% bentonite (data from Stern and Shackelford 1998) (Malusis et al. 2013).

affected. It is quite possible that the cutoff walls are installed in a ground that contains chemicals in the pore water, because the land is limited in Japan and the country is surrounded by sea. Therefore, the effect of the actual first exposure effect should be studied.

2.2.2 Effect of wet-dry cycles

Variability in k at post-construction may occur due to changes in the wall induced by some environmental factors (Britton et al. 2005). Evans (1993) discussed potential changes in the k of a cutoff wall due to chemical interactions and cycles of wetting/drying and freezing/thawing. Other sources of variability are variations in the k with depth due to variations in effective stress with depth (Evans 1995, Filz et al. 2001) and high k defects due to cracking that may be caused by large deformations of a cutoff wall.

In particular, the changes in k due to wet-dry cycling are triggered by the water level fluctuation over time due to natural and/or anthropogenic causes. As a result, some portion of an SBM barrier may be located within the zone of a fluctuating water table and may dry when the water table is depressed. If this portion of the barrier does not maintain a low k upon rewetting when the water table rises, the overall effectiveness of the barrier may be compromised. Malusis et al. (2011) evaluated the effect of wet-dry cycles on the hydraulic barrier performance of SBM backfills using leak-free pressure plate extractors (LFPPEs) shown in Figure 2.5 (Wang and Benson 2004). Two different mixture proportions of SBM at 2.7 to 5.6% of total bentonite content by dry weight basis are used for the experiment. For drying cycles, the specimens were dried using compressed air by controlling matric suction under constant pore water pressure in the LEPPE system. The specimens were then resubmerged using tap water for wetting cycles after measurement of air-dried specimen size

and weight. The results in Figure 2.6 showed that significant increases in k occurred after cyclic drying under high matric suctions (≥ 150 kPa) that resulted in saturations lower than 30% although the SBM initially had k of lower than 10^{-9} m/s. Both SBMs exhibited a 500 to 10000-fold increase (≥ 10^{-8} m/s) in the geometric mean k after three or more drying cycles, and the specimens did not heal even after long periods of permeation. These findings illustrate the potential for increases in k for SBM backfills subjected to wet-dry cycling due to water level fluctuation.

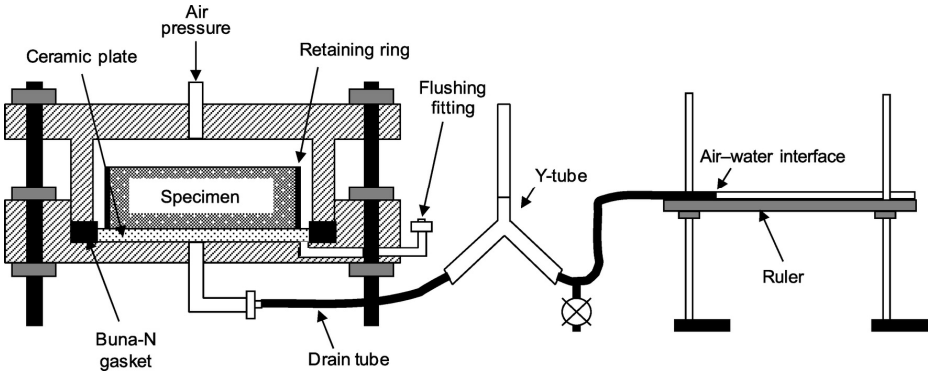

Figure 2.5 Schematic of LFPPE apparatus (redrawn after Wang and Benson 2004).

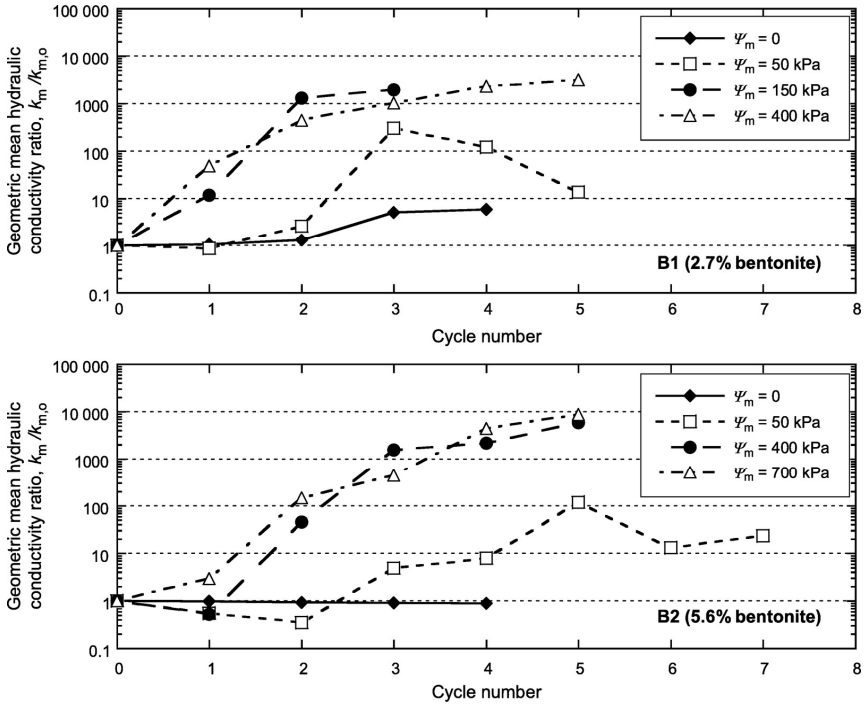

Figure 2.6 Ratios of geometric mean k to initial geometric mean k for replicate specimens of two different bentonite content of SBM as a function of wet-dry cycles and matric suction applied during the drying phase (Malusis et al. 2011).

2.2.3 Effect of additive substances

The effect of zeolite amendment to enhance sorption capacity on the k of a representative SBM backfill for vertical cutoff walls was evaluated by Hong et al. (2012). The k of specimens containing fine sand, 5.8% (dry weight) sodium bentonite, and 0, 2, 5, or 10% (dry weight) of one of three types of zeolite (clinoptilolite, chabazite-lower bed, or chabazite-upper bed) were measured using a fixed-ring oedometers and a flexible-wall permeameter as shown in Figure 2.7. The testing results indicated that amendment of zeolite had little impact on the k of the backfill, regardless of the amount or type of zeolite. The k for the unamended specimen based on flexible-wall tests was 2.4×10^{-10} m/s, whereas those for zeolite-amended specimens were in a range of $1.2 \times 10^{-10} \leq k \leq 3.9 \times 10^{-10}$ m/s.

The k of SBM backfills amended with granular activated carbon (GAC) or powdered activated carbon (PAC) was evaluated to assess an enhancement of SBM backfill with improved attenuation capacity for greater longevity of barrier containment performance by Malusis et al. (2009). Specimens containing fine sand, 5.8% sodium bentonite, and GAC or PAC (0, 2, 5, and 10% by dry weight) were used for the hydraulic conductivity test using flexible-wall permeameter. The results in Figure 2.8 show that amendment with either the GAC or PAC causes no detrimental effects on k of SBM considered in this study. The k values for GAC-amended SBMs are similar to that of the unamended SBM, whereas the values for the PAC-amended SBMs are marginally lower than that of the control backfill due to smaller grain size of PAC.

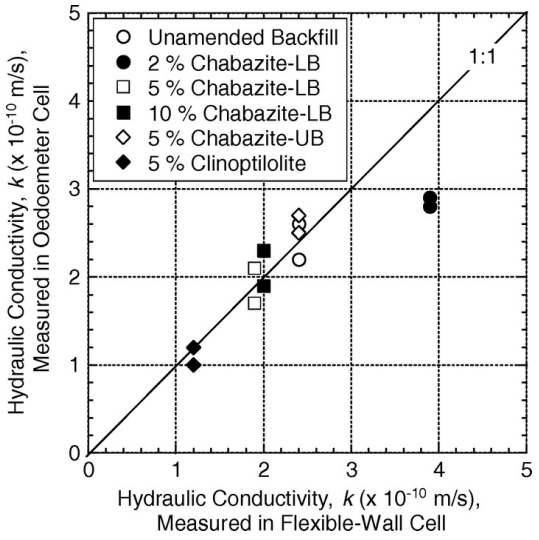

Figure 2.7 Correlation between geometric mean k measured by flexible-wall permeameters at an average effective stress of 34.5 kPa vs. that in fixed-ring oedometer at the average effective stress of 24 and 48 kPa.

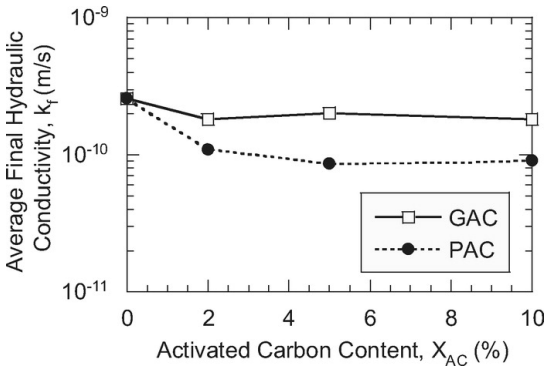

Figure 2.8 Average final *k* of SBM backfills as function of activated carbon content measured by flexible-wall permeameters (average effective stress = 34.5 kPa).

2.3 Experimental methodologies for hydraulic barrier performance of SBM

2.3.1 Materials

2.3.1.1 Bentonite

Bentonite is classified by the types of exchangeable cations existing in the minerals. In this study, sodium-bentonite (Kunigel V1; Kunimine Industry Co., Ltd.) was used for all experiments. Sodium-bentonite is well known for its swelling characteristics higher than calcium-bentonite or other types of bentonite as described in 2.1. The used bentonite is widely used in many researches of geoenvironmental engineering as typified by a buffer material for the repository of high-level radioactive waste (e.g. Komine and Ogata 1996, Komine et al. 2009, Nakamura et al. 2009, Komine 2010, Cui et al. 2011, Suzuki et al. 2013) and by bottom liners in waste disposal facilities (Kochmanova and Tanaka 2011). Typical profile of used bentonite is summarized in Table 2.1.

2.3.1.2 Soils as base material of SBM

In this study, four different soils were used as base soil of SBM: 1) composite soil which is a mixture of volcanic cohesive soil and sandy gravel, 2) silty soil, 3) sandy soil, 4) silica sand #7 and 5) fine sand. All soils were sieved through a 4.75 mm-opening screen before a preparation of SBMs. Physical properties of base soils are shown in Table 2.2.

- ✓ Volcanic cohesive soil and sandy gravel were collected at a pilot scale test site (Shimoishibashi, Shimotsuke-city, Tochigi, Japan). The composite soil was prepared by mixing the sandy gravel with water content of 27% and volcanic cohesive soil with that of 70%. These values correspond to the natural water content of each soil. A mixing ratio of 25:4 by dry mass was determined based on a boring log obtained at the sites as shown in Figure 2.9. In this study, Kanuma soil was not mixed because its thickness was negligible compared with other two layers.

- ✓ Silty soil collected at a construction site (Takakura, Neyagawa-city, Osaka, Japan) was used. Water content was adjusted to 23.6% to be equal to the natural water content.
- ✓ Sandy soil collected at another pilot scale test site (Hanamigawa-ku, Chiba-city, Chiba, Japan) was used. Water content was adjusted to 24.0%.
- ✓ Silica sand #7 used in this study was a commercially manufactured product by sieving into specific grain size (Takeori Kogyo Co., Ltd., collected in Tono district in Gifu Prefecture). Water content was adjusted to 26.0% to simulate general sandy layer.
- ✓ Fine sand was also a commercial product collected at a site (Kita Kenzai, in Soraku district in Kyoto Prefecture). Water content was adjusted to 21.0%.

Figure 2.10 shows grain size distribution curves of each base soil by JIS A 1204 (2009a). Composite soil, silty soil and fine sand are well graded soils, having fine particles of 23.6%, 33.9% and 8.1%, respectively. Sandy soil and silica sand are uniform and poorly graded. Especially fine particle content of silica sand is only 3.5% and few of fine particles are contained. These soils used for SBM preparation for each laboratory test are summarized in Table 2.3.

Table 2.1 Typical profile of sodium-bentonite used in this study (from Komine 2004).

Particle density	2.79 Mg/m^3
Liquid limit	473.9 %
Plastic limit	26.61 %
Plastic index	447.3
Activity	6.93
Clay content [< 0.002 mm]	64.5 %
Montmorillonite content	48.0 %
Cation exchange capacity	0.732 meq/g
Na^+ Exchange capacity	0.405 meq/g
Ca^{2+} Exchange capacity	0.287 meq/g
K^+ Exchange capacity	0.009 meq/g
Mg^{2+} Exchange capacity	0.030 meq/g

Table 2.2 Physical properties of base soils and used soils for each laboratory test.

		Composite soil	Silty soil	Sandy soil	Silica sand	Fine sand
Particle density	(Mg/m^3)	2.72	2.64	2.62	2.61	2.64
Water content	(%)	-	23.6	24.0	26.0	21.0
Liquid limit	(%)	NP	NP	NP	NP	NP
Plastic index	(%)	NP	NP	NP	NP	NP
Particle size distribution						
Gravel [2.00 mm ~]	(%)	5.6	0.9	0	0	6.8
Sand [0.075 ~ 2.00 mm]	(%)	70.8	65.2	87.9	96.5	85.1
Fine [~ 0.075 mm]	(%)	23.6	33.9	12.1	3.5	8.1
Max. grain size (< 4.75 mm)	(mm)	4.75	4.75	2.00	0.425	4.75
Uniformity coefficient		42	250	2.64	2.3	9.3
Curvature coefficient		3.5	10	0.94	0.93	9.3
Specific surface	(cm^2/g)	1896	4200	1746	-	-
Electric conductivity	(mS/m)	39.8	2.4	4.0	-	-

Table 2.3 Base soils used for each laboratory tests

	Composite soil	Silty soil	Sandy soil	Silica sand	Fine sand
Chapter 2					
- Hydraulic conductivity test	✓	✓	✓	✓	✓
- Swelling pressure test	✓	✓	✓		
- Swelling deformation test	✓				
- Consistency test	✓	✓	✓		
- Consolidation test				✓	
Chapter 3					
- Piezocone test				✓	✓
- UU test				✓	✓
Chapter 4					
- Centrifuge modeling test	✓			✓	
- Cyclic undrained triaxial test	✓			✓	

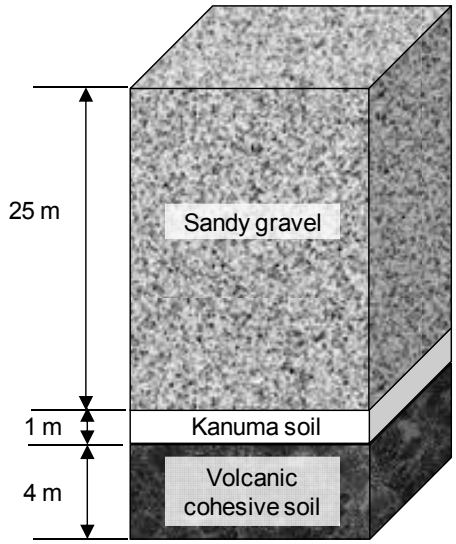

Figure 2.9 Cross-section of ground at a pilot test site.

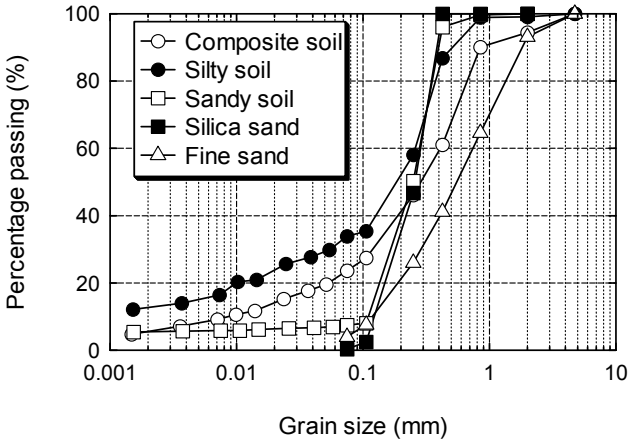

Figure 2.10 Grain size distribution curves of five different base soils.

2.3.1.3 Organic/inorganic chemicals

In order to simulate SBM cutoff wall installation at sites where chemicals originally exist in soil pore water, four different chemicals were used in this study: 1) calcium chloride, 2), ethanol, 3) artificial seawater and 4) heavy-fuel oil A.

- ✓ Calcium chloride ($CaCl_2$) was used to simulate a condition of inorganic chemical contained in groundwater. As described in 2.1.1, the hydraulic barrier performance of SBM strongly depends on the chemical compatibility of bentonite itself. Valency of cations also influences on the swelling characteristics. The effect of divalent cations like Ca^{2+} is larger than monovalent cations like Na^{+}, and it has been verified that the impact by the difference of multivalent cations larger than divalent is not great (Jo et al. 2001). Beside, Ca^{2+} is commonly found in natural aqueous system as well as in water discharged from industrial processes or leached from waste. Therefore, Ca^{2+} is a commonly used in many past researches.
- ✓ Ethanol and heavy-fuel oil A were used to simulate a subsurface area contaminated with organic chemical and oil, respectively. These materials were selected because they are typical chemicals as organic chemical or oil. Table 2.4 shows basic properties of ethanol.
- ✓ Artificial seawater was used to assess an applicability of SBM cutoff walls in a coastal area. The artificial seawater was prepared by solving powder of Aquamarine (Yashima Pure Chemicals Co., Ltd.). Chemical component of the artificial seawater is shown in Table 2.5.

Table 2.4 Basic properties of ethanol used.

Molecular weight	(g/mol)	46.07
Density	(g/cm^3)	0.789
Boiling point	(°C)	78.37
Melting point	(°C)	-114.3
Viscosity	(mPa·s)	1.200

Table 2.5 Chemical composition of the artificial seawater (unit: g/L).

$MgCl_2$	$CaCl_2$	$SrCl_2$	KCl_2	$NaHCO_3$
11.12	1.535	0.0425	0.695	0.201
KBr	H_3BO_3	NaF	Na_2SO_4	NaCl
0.101	0.027	0.003	4.094	24.50

2.3.1.4 SBM preparation

Flow of SBM preparation is schematically shown in Figure 2.11. First, water content of base soil was adjusted using the chemicals mentioned above. Basically distilled water (DW) deaerated for 24 hours was used for all SBM preparation (water content regulation and preparation of chemical solutions). Water content of base soils without chemicals in the pore water were regulated using DW. For SBM samples containing $CaCl_2$ in the pore water, $CaCl_2$ solutions were added to achieve 0.01 - 0.1 M concentration. For the samples that simulate oil contamination, heavy fuel oil A was added to the base soils with a content of 5,000 or 10,000 mg/kg by dry mass after the water content was adjusted to same level. In the case of seawater, the pore water was replaced by the artificial seawater mentioned above in the process of water content regulation.

As explained in 1.2.3, in practical construction procedures of SBM cutoff walls using TRD method, first, the trench cutting is conducted supplying bentonite slurry to maintain the workability of the soil inside the trench. Then, bentonite powder is re-mixed in the trench after the base machine goes back to the initial position. To simulate these construction processes in the laboratory, SBM were prepared according to following steps:

1) Bentonite-water slurry of 10% concentration was prepared by mixing powder bentonite with tap water for 10 minutes using soil mixer. The slurry was allowed to hydrate in constant temperature of 20°C for 24 hours.
2) The slurry was added and blended with the base soil by a soil mixer for 2 minutes to homogenize the mixture. The additive content of the slurry was determined based on a flowability of soil-slurry mixture (150 mm flow value according to JIS R 5201 (1997)).
3) Once a mixture of suitable flowability was achieved, given amount of bentonite powder was added to the soil-slurry mixture and sufficiently remixed using the soil mixer for 2 minutes.

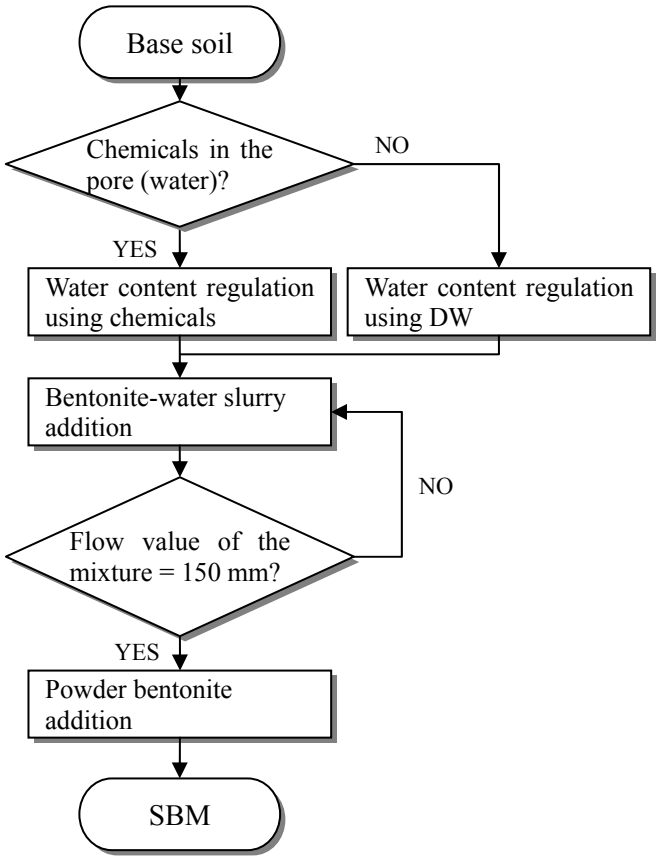

Figure 2.11 Flow chart of SBM preparation.

2.3.2 Experimental procedures

2.3.2.1 Free swelling test of bentonite

Free swelling test is used to measure the swelling volume of bentonite in any solutions. The main purpose of this test is to estimate swelling characteristics of bentonite in SBMs for k reduction. The free swelling test was conducted for nine different liquids and according to ASTM D 5890 "Standard Test Method for Swell Index of Clay Mineral Component of Geosynthetic Clay Liners" (ASTM 2011). The liquids used for this test were DW, tap water, and 7 $CaCl_2$ solutions (0.001, 0.005, 0.01, 0.02, 0.05, 0.1, 1.0 M) and experimental procedure is shown below:

1) Two grams of powder bentonite, which was preliminarily dried in an oven at 110 ± 5 °C and sieved by through a 75 μm-opening screen, was prepared.
2) The bentonite was dusted into a 100 mL graduated cylinder filled with 90 mL of permeant solution in increments of 0.1 g after a prior bentonite aggregate was settled by the hydration.
3) The cylinder was filled up to 100 mL with the same solution and left for 24 hours with a cover.
4) The volume level (in milliliters) was recorded (see Photo 2.1).

Photo 2.1 Appearance after free swelling test.

2.3.2.2 Hydraulic conductivity test

Hydraulic conductivity test was conducted to evaluate the k of SBM made with various conditions against some types of influent liquids. The assessment of k at pre-construction plays an extremely important role on the hydraulic barrier performance of cutoff walls after its construction.

All testing conditions for the hydraulic conductivity test is summarized in Table 2.6 and Table 2.7. The experimental conditions in this study can be categorized into 4 groups (Series-C, P, N and S):

- ✓ Series-C: In this series, various confining pressures were applied during permeation with two different permeant liquids to assess the pressure dependency of k. Figure 2.12 shows the vertical distribution of earth pressure inside the SBM wall (Kamon et al. 2006). This was monitored in an actually constructed vertical wall as a pilot test. Vertical stresses in the SBM wall was proved to be lower than the overburden pressures due to the arching effect (Evans et al. 1995, Filz 1996). When the k of SBM is tested in the laboratory, the stress conditions must be considered so as not to underestimate the k.
- ✓ Series-P: This series was designed to assess the chemical compatibility of SBM attacked by solutions containing $CaCl_2$, $MgCl_2$, seawater, or 50%-ethanol. In this series, bentonite in SBM has been initially hydrated with pore water of original soil (adjusted using DW).
- ✓ Series-N: In this series, the expected detrimental effect of the various chemicals in original soil on the k was verified. In this case, swelling of bentonite in SBM was impeded due to existence of chemicals in the soil and/or the groundwater at a site. The $CaCl_2$ concentration range of 0 - 0.1 M was determined based on the data of actual leachate collected at some waste landfill sites shown in Table 2.8. Although the number of samples is limited, the maximum concentration converted to $CaCl_2$ in terms

of ionic strength was 0.07 M. In this series, the effect of the content of bentonite powder (C_{BP}) was also studied.

- ✓ Series-S: In this series, the effect of soil type used as the base soil on the *k* was studied with five different soil materials. Calcium chloride solution was applied for the pore water regulation and for the permeant with some concentrations. The content of bentonite powder was also differed by the testing cases.

In this study, flexible-wall permeameters were used for all cases according to the ASTM D 5084 "Standard Test Methods for Measurement of Hydraulic Conductivity of Saturated Porous Materials Using a Flexible Wall Permeameter" (ASTM 2010). This equipment allows to apply any pressure via a latex membrane to confine the samples, and is widely used to estimate *k* of samples having low permeability (e.g. Katsumi et al. 2008, Naka et al. 2012). In order to minimize sidewall leakage, a falling head system was employed in this study. A schematic diagram of this system is presented in Figure 2.13. Specimens for the hydraulic conductivity test were prepared by the following procedure:

1) Prepared SBM was carefully poured into an consolidation cell (60 mm in diameter and 20 or 70 mm in height) to avoid the presence of air bubbles in the specimen and not to be overconsolidated with the wet density of 1.75 Mg/m^3.
2) After the specimen in the consolidation cell was saturated using a vacuum deaerator, the specimen was pre-consolidated in a consolidation test apparatus (JIS 2009c) with consolidation pressures listed in Table 2.9. For example, in the cases that confining pressure of 30 kPa would be applied during the hydraulic conductivity test, a pre-consolidation pressure of 20 kPa was applied on the specimen for 24 hours as a first loading. Then, 40 kPa was applied for one more 24 hours as a second loading.
3) After the pre-consolidated SBM specimen was removed from the cell without disturbance, the specimen was shaped to 20-30 mm in height and 60 mm in diameter. The cylindrical specimen was placed between deaerated filter papers, geotextiles, and plastic caps (cap and pedestal) with holes to connect the tubes.
4) A latex membrane was placed to cover the sides after silicone grease was spread around the lateral face of the specimen to minimize the sidewall leakage. After the same solutions as the pore water was supplied from a bottom hole to flush out trapped air between the membrane and specimen, O-rings were attached around the caps to infix the latex membrane. Then, all channels were saturated with the same solutions and connected.
5) After an acrylic cylinder and a top was built up, tap water was supplied in the acrylic cylinder to completely soak the specimen. Air pressure was applied on the specimen via the membrane from an air compressor.
6) A tube from a burette filled with a permeant was connected to the bottom hole, and permeation was started. The hydraulic gradient during permeation was approximately 30-50.

Table 2.6 Testing conditions for hydraulic conductivity test (Series-C, P and N).

Test No.	Type of base soil	Chemical concentration in original soil	Type of permeant	Bentonite powder content (kg/m^3)	Confining pressure (kPa)	Wet density* (Mg/m^3)
C-1	Composite soil	0	DW	100	15	1.74
C-2					60	1.88
C-3					90	1.81
C-4					120	1.80
C-5					150	1.79
C-6			0.1 M-$CaCl_2$		90	1.77
C-7					150	1.87
C-8			1.0 M-$CaCl_2$		15	1.76
C-9					60	1.82
C-10					90	1.86
C-11					120	1.89
C-12					150	1.91
C-13			0.1 M-$MgCl_2$		90	1.82
C-14			1.0 M-$MgCl_2$		90	1.88
C-15					150	1.87
C-16			Seawater		90	1.83
C-17					150	1.90
P-1	Composite soil	0	DW	100	30	1.74
P-2			0.1 M-$CaCl_2$			1.78
P-3			0.25 M-$CaCl_2$			1.76
P-4			1.0 M-$CaCl_2$			1.76
P-5			0.1 M-$MgCl_2$			1.71
P-6			1.0 M-$MgCl_2$			1.80
P-7			Seawater			1.84
P-8			50%-ethanol			1.73
N-1	Composite soil	0	0.1 M-$CaCl_2$	50	30	1.88
N-2		0.01 M-$CaCl_2$	0.1 M-$CaCl_2$	100		1.86
N-3		0.025 M-$CaCl_2$	0.1 M-$CaCl_2$	50		1.74
N-4				75		1.77
N-5				100		1.86
N-6		0.05 M-$CaCl_2$	0.1 M-$CaCl_2$	75		1.76
N-7				100		1.80
N-8				125		1.83
N-9		0.1 M-$CaCl_2$	0.1 M-$CaCl_2$	100		1.82
N-10				125		1.81
N-11				150		1.86
N-12		Sea water	Sea water	100		1.78
N-13		5 g/kg-heavy fuel oil A	0.1 M-$CaCl_2$	100		1.75
N-14		10 g/kg-heavy fuel oil A	0.1 M-$CaCl_2$	100		1.83

* After pre-consolidation before permeation

Table 2.7 Testing conditions for hydraulic conductivity test (Series-S).

Test No.	Type of base soil *	Chemical concentration in original soil *	Type of permeant	Bentonite powder content (kg/m^3)	Confining pressure (kPa)	Wet density* (Mg/m^3)
S-1	Composite soil	0.01 M-$CaCl_2$	0.01 M-$CaCl_2$	100	30	1.76
S-2	Silty clay	0	DW			1.81
S-3		0.01 M-$CaCl_2$	0.01 M-$CaCl_2$			1.82
S-4		0.1 M-$CaCl_2$	0.1 M-$CaCl_2$			1.90
S-5	Sandy soil	0	DW			1.85
S-6		0.01 M-$CaCl_2$	0.01 M-$CaCl_2$			1.84
S-7		0.1 M-$CaCl_2$	0.1 M-$CaCl_2$			1.87
S-8	Silica sand	0	DW	25		1.88
S-9				50		1.86
S-10				100		1.83
S-11	Fine sand	0	DW	25		1.98
S-12				50		1.94
S-13				100		1.93

* After pre-consolidation before permeation

Table 2.8 Chemical composition of leachate collected at waste landfill sites before treatment (unit: M).

Ion	Site A	Site B	Site C	Site D
Ca^{2+}	0.001067	0.004761	0.005856	0.024234
Cl^-	0.000100	0.007402	0.018625	0.309599
Na^+	0.000681	0.003243	0.019096	0.116592
SO_4^{2-}	0.000201	0.000248	0.000142	0.000081
K^+	0.000386	0.001716	0.005740	0.071960
NO_3^-	0.000103	0.000046	0.000046	0.000422

Table 2.9 Pre-consolidation pressure and corresponding confining pressure.

Pre-consolidation pressure (kPa)	Confining pressure during hydraulic conductivity test (kPa)
20	15
40	30
80	60
120	90
160	120
200	150

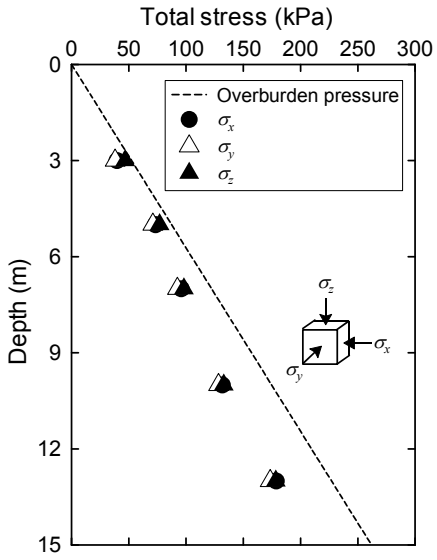

Figure 2.12 Total stress distribution in SBM vertical wall versus overburden pressure (Katsumi et al. 2006).

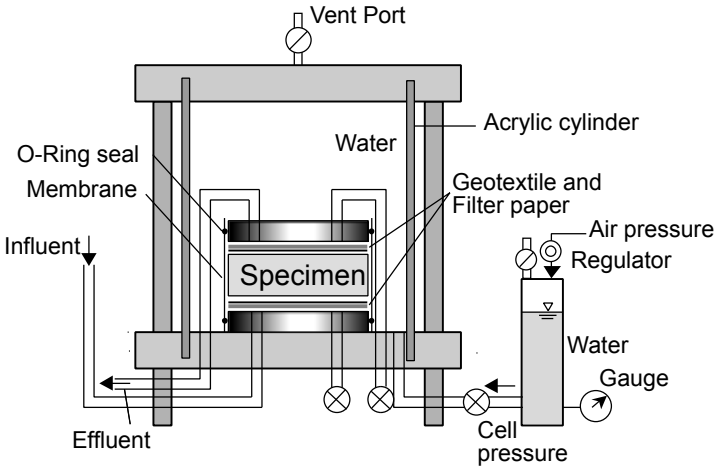

Figure 2.13 Schematic diagram of a flexible-wall permeameter.

Self-sealing capability of SBMs with regard to its hydraulic barrier performance was also evaluated using the same apparatus. To assess the self-sealing capability, two different types of specimens (25 mm height × 60 mm diameter), having a hydraulic defect, were subjected to the hydraulic conductivity test. One specimen has a vertical interface along the diameter of the specimen by cutting into two pieces as shown in Figure 2.14, and another has a circular hole with 2 mm in diameter penetrating the center of the specimen. Testing procedure was according to the flexible-wall hydraulic conductivity test. The hydraulic gradient was 50-60 for the specimen (a) and approximately 5 for the specimen (b).

The permeation was continued until the following requirements were confirmed: 1) the

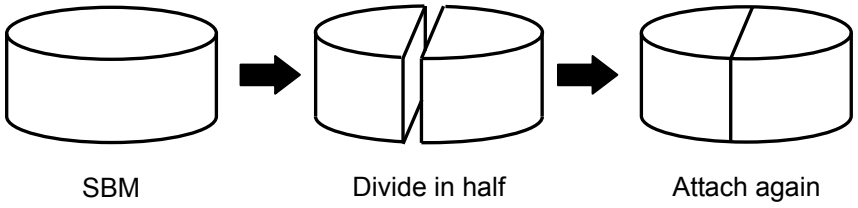

Figure 2.14 Preparation of SBM specimen, having a vertical interface along a diameter.

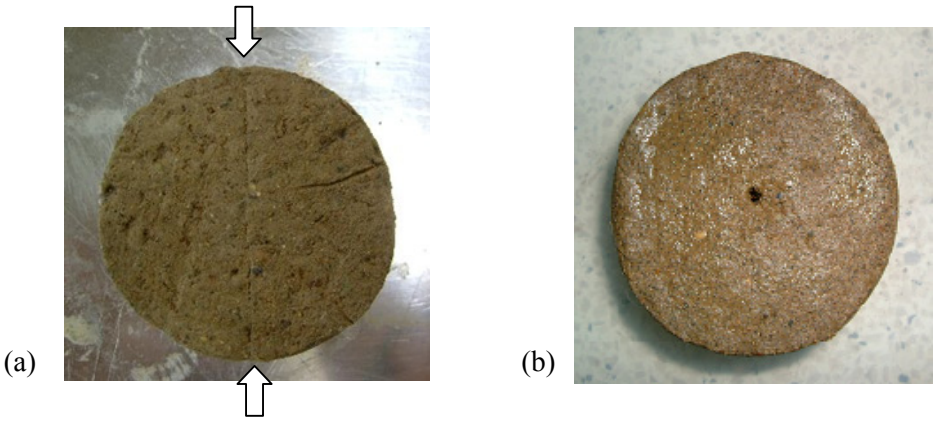

Photo 2.2 Specimen for the self-recovery test with (a) a vertical interface along its diameter and (b) a circular hole (ϕ = 2 mm) penetrating its center.

volume of the effluent and the influent were almost equal, 2) the change in k values with time was negligible, 3) pore volumes of flow (PVF) were greater than 2, and 4) the electrical conductivity (EC) of the effluent was almost equal to that of the influent in the P and N-series (e.g. Shackelford et al. 1999). In some cases, the pore volumes of flow did not reach 2 due to their extremely low k values. The EC values of the effluent were measured after some quantity of the effluent was accumulated in a bottle.

The k values were measured by the following equation (2.1), which is generally used in the falling head hydraulic conductivity test. The k values of SBMs having hydraulic defects were also calculated by the same equation as an apparent hydraulic conductivity.

$$k = (\eta_T / \eta_{15}) \frac{a \cdot L}{A \cdot (t_2 - t_1)} \ln(h_1 / h_2) \times \frac{1}{100} \tag{2.1}$$

where, k = hydraulic conductivity (m/s); a = section area of burette (cm^2); L = height of specimen (cm); A = section area of specimen (cm^2); t_1 = start time of measurement (s); t_2 = finish time of measurement (s); h_1 = initial water head level (cm); h_2 = final water head level (cm); η_T, η_{15} = viscosity coefficient of permeant at T °C or 15 °C.

In this study, the performance-based criterion of k value was set to 1.0×10^{-9} m/s. In

Japan, hydraulic barrier performance of bottom layer for the containment is established to satisfy both the hydraulic conductivity criterion, $k \leq 1.0 \times 10^{-7}$ m/s and the thickness criterion, $L \geq 5.0$ m, according to the Enforcement Regulations of Soil Contamination Countermeasure Law. The value of 1.0×10^{-9} m/s was determined by considering travel time of contaminants through the cutoff wall. The travel time with same groundwater level difference inside/outside the cutoff wall are equivalent with the conditions of "$k = 1.0 \times 10^{-7}$ m/s with $L = 5.0$ m" and "$k = 1.0 \times 10^{-9}$ m/s with $L = 0.5$ m". Therefore, the value of 1.0×10^{-9} m/s can satisfy the regulation in terms of transportation of contaminant with considering that the typical thickness of SBM cutoff walls constructed by TRD method is 55 cm.

2.3.2.3 Consolidation test

Separated SBM specimen in the consolidation cell was saturated by using a vacuum deaerator for 24 hours, and subjected to the standard consolidation test. In this research, consolidation test was conducted using incremental loading according to JIS A 1217 (JIS 2009c), and loading steps were set as five. In the process of data analysis, k value was also calculated by the following equation (2.2).

$$k = \frac{c_V \cdot m_V \cdot \gamma_W}{8.64 \times 10^8} \tag{2.2}$$

where, k = hydraulic conductivity (m/s); c_V = coefficient of consolidation (cm^2/d); m_V = coefficient of volume compressibility (m^2/kN); γ_W = unit weight of water (= 9.81 kN/m^3).

2.3.2.4 Swelling-pressure test

Swelling pressure test was implemented to verify the swelling pressure characteristics of SBMs made with various conditions. In this test, increment of vertical pressure associated with the swelling of bentonite was measured. Swelling pressure of SBM can be expected to behave as that of bentonite itself due to montmorillonite mineral expansion by absorbing water into interlayers as shown in Figure 2.15. (Komine and Ogata 2004, Komine et al. 2009, Wang et al. 2012). Swelling pressure of SBM in a fixed-volume condition should be differed by the mixing conditions as k value because the swelling behavior is sensitive to the chemical agent. This test was conducted on the testing cases of S-1, P-1 and N-1, 9, 11~14 in Table 2.6 and Table 2.7. In this study, only SBMs made from composite soil were subjected to this test to assess the swelling pressure characteristics in association with chemical compatibility. The measurement of swelling pressure should be measured from the moment dry bentonite contact with solutions because the solution quickly begins to infiltrate into interlayers. However, since sufficient mixing is absolutely essential to ensure the homogeneity, an elapsed time from bentonite addition in SBM preparation processes to starting measurement was controlled to be same in all cases in this study. The experimental procedure of the swelling-pressure test is explained below:

1) SBM was filled in an consolidation cell (60 mm in diameter and 20 mm in height), on which a saturated filter paper was placed, with filling carefully not to contain air bubbles in the specimen and not to be overconsolidated with a wet density of approximately 1.80

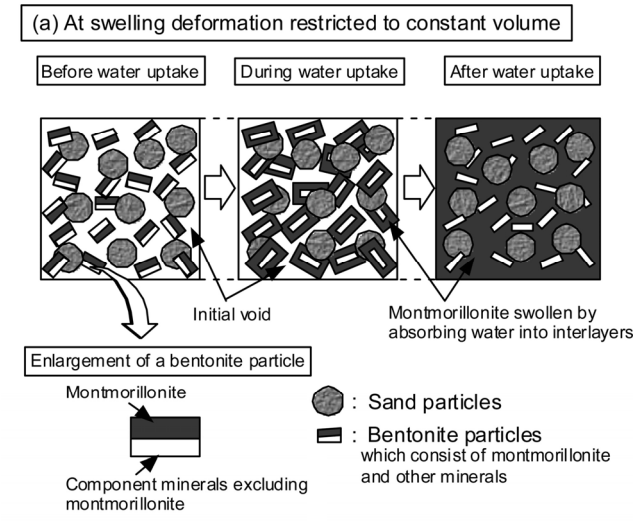

Figure 2.15 Process of swelling behavior in sand-bentonite mixture under constant-volume condition (Komine and Ogata 2004).

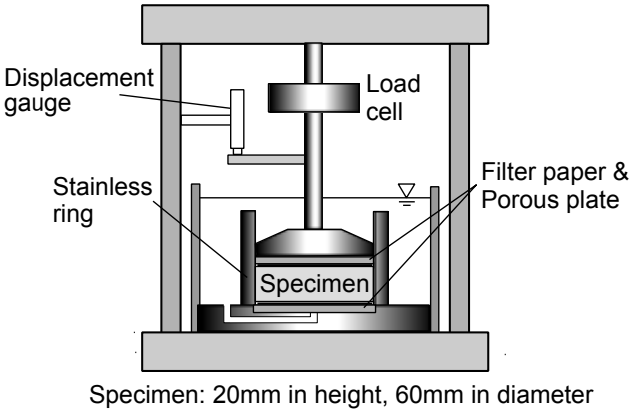

Figure 2.16 Schematic view of apparatus for swelling pressure test.

Mg/m^3.

2) After the surface of specimen was uniformly fixed, an acrylic loading cap with holes was placed onto the specimen with a guide ring. Then, the solution was poured in an immersion solution reservoir to completely submerge the specimen. The chemical concentration of the solution was corresponded to those of the permeant in the hydraulic conductivity test.
3) In a consolidation test apparatus, a vertical consolidation pressure of 40 kPa was applied on the specimen for 24 hours. At this moment, 60 minutes was elapsed in all cases after the bentonite slurry addition. Silicon oil was put on the immersion solution to avoid evaporation during the test. This pre-consolidation step was implemented to improve the

uniformity of the soil surface to minimize the error and to unify the stress state in the specimen.

4) After the pre-consolidation, the specimen was removed from the consolidation test apparatus and placed on an apparatus for swelling pressure test shown in Figure 2.16. This is a modified apparatus for one-dimensional compression test (JIS 2009d). The load cell was replaced to a non-deformable one (Compact Tension/Compression Load Cells; LUR-A-100NSA1, Kyowa Electronic Instruments Co., Ltd.), which was firmly connected to the outer frame with screws. The test was started after 25 hours elapsed from the bentonite slurry addition in SBM preparation.
5) The vertical force was logged at 10 seconds intervals in the first 24 hours and at 1 hour intervals after that. The swelling pressure was evaluated with a maximum value in 168 hours (7 days).

2.3.2.5 Swelling-deformation test

Swelling-deformation characteristics of SBMs also should be differed according to the mixing conditions as the swelling-pressure characteristics mentioned in 2.3.2.4. Swelling-deformation test was conducted to evaluate the swelling deformation characteristics under constant-pressure condition as shown in Figure 2.17 using a consolidation test apparatus (Komine and Ogata 2004, JIS 2009c). In this test, vertical strain change was measured by time. This test was conducted on the testing cases of S-1~7, P-1, and N-9 in Table 2.6 and Table 2.7. In this study, the effects of chemicals in pore water and of base soil on the swelling-deformation characteristics were evaluated. The experimental procedure of the swelling-deformation test is described below:

1) SBM was filled in an consolidation cell (60 mm in diameter and 70 mm in height), on which a saturated filter paper was placed, with filling carefully not to contain air bubbles in the specimen and not to be overconsolidated with the wet density of approximately 1.80 Mg/m^3.
2) After the surface of specimen was uniformly fixed, a stainless loading cap was placed onto the specimen with a guide ring. Then, solution was poured in an immersion reservoir to completely submerge the specimen. The $CaCl_2$ concentration of solution was corresponded to those of the permeant in the hydraulic conductivity test.
3) In a consolidation test apparatus, a vertical consolidation pressure of 100 kPa was applied on the specimen, and the measurement was started.
4) The vertical strain was recorded by time. The test was continued for 168 hours.

For the evaluation of swelling-deformation characteristics, normalized water content, w_{nor}, and effective dry density of bentonite, ρ_{db}, were calculated by the following equation (2.3) and (2.4):

$$w_{nor} = \frac{w_{SBM}}{w_{BS}} \times 100 \tag{2.3}$$

where; w_{SBM} = water content of SBM after swelling-deformation test (%); w_{BS} = water content of base soil after swelling-deformation test (%).

$$\rho_{db} = \frac{m_B}{V_B + V_A + V_W} \tag{2.4}$$

where; ρ_{db} = effective dry density of bentonite (g/cm^3); m_B = mass of bentonite fraction in SBM; V_B = volume of bentonite fraction in SBM; V_A = volume of air in SBM; V_W = volume of water fraction in SBM after the test (see Figure 2.18). As are expressed by these equations, both w_{nor} and ρ_{db} represent the degree of enhancement of soils by converting into SBMs in terms of water retention capability.

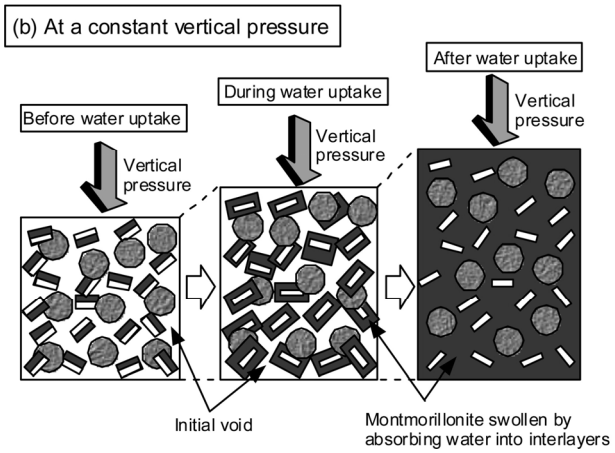

Figure 2.17 Process of swelling behavior in sand-bentonite mixture under constant-pressure condition (Komine and Ogata 2004).

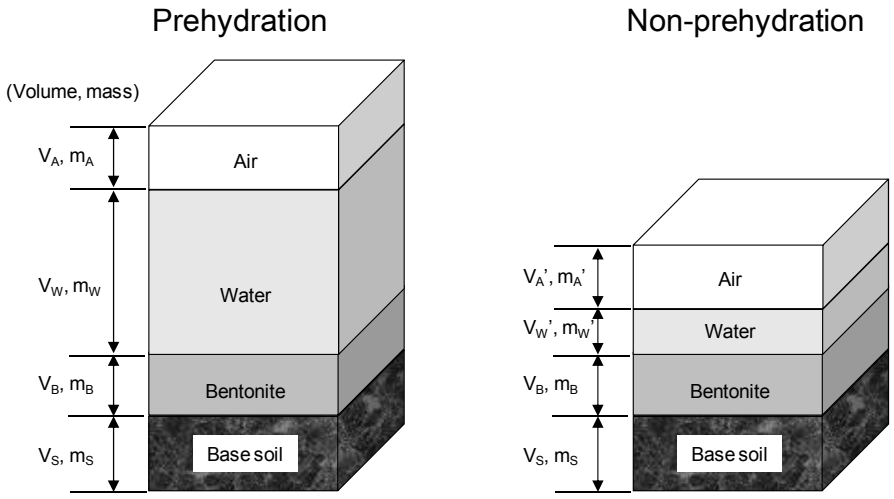

Figure 2.18 Schematic view of composition in SBM for pre or non-prehydration conditions.

2.3.2.6 Consistency characteristics

Liquid limit and plastic limit of SBMs were measured according to JIS A 1205 (2009b). The consistency characteristics were evaluated to verify water retention capability of SBMs made with various conditions shown in Table 2.6 and Table 2.7.

2.4 Factors affecting hydraulic conductivity of SBM

2.4.1 Swell volume of bentonite

Results of free swelling test are shown in Table 2.10 and Figure 2.19. Although the maximum swell volume is 28.6 mL/2g-solid against distilled water, a significant decrease in bentonite swell volume occurs when the $CaCl_2$ concentration is higher than 0.01 M, and the swell volumes against the solutions of $CaCl_2$ concentration higher than 0.1 M are almost similar. As shown in Figure 2.20, the swell volume of bentonite significantly decreased by increase of electrical conductivity (EC) of the solutions because EC is an indicator to represent the electrolyte concentration of the solutions. These results support that it is mostly reasonable to evaluate the chemical compatibility of SBM with the $CaCl_2$ concentration range in 0 to 0.1 M in following sections.

2.4.2 Hydraulic conductivity change with time

Figure 2.21 illustrates an example of k changes with PVF in P-1, P-2, P-4, N-1 and N-9. As

Table 2.10 Swell volume of bentonite with corresponding electrical conductivity of solutions.

		Swell volume (mL/2g-solid)	EC mS/m
DW		28.6	3.5
Tap water		25.9	29.8
Seawater		7.8	4610
$CaCl_2$ solution	0.001 M	25.2	25.2
	0.005 M	22.6	113
	0.01 M	17.4	217
	0.02 M	12.8	414
	0.05 M	9.2	956
	0.1 M	6.0	1800
	1.0 M	5.7	12670

the permeation proceeded, *k* values permeated with the DW (P-1) continuously decreased, particularly at the early stage of the test. This is possibly because the bentonite in the specimen could absorb the influent water with the formation of diffuse double layer and osmotic swelling because it did not fully swell during the pre-consolidation. The *k* values in other cases were almost stable during the permeation. Hereafter, average *k* values after PVF = 1 were adopted as representative values of each testing case when final PVF is larger than 1.In the case that PVF did not reach 1, average value from the beginning was used for further discussions. The *k* values in all cases are summarized in Table 2.11.

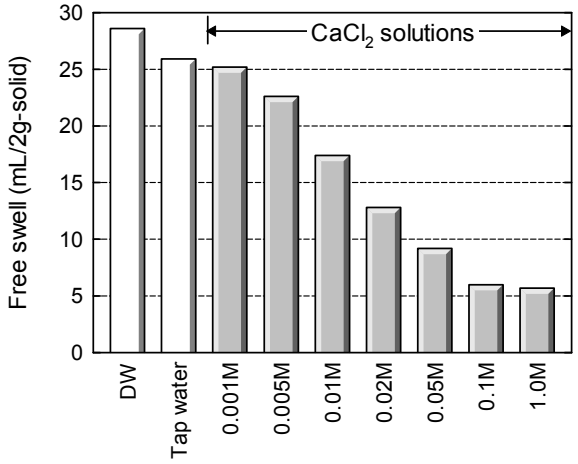

Figure 2.19 Results of free swelling test on various solutions.

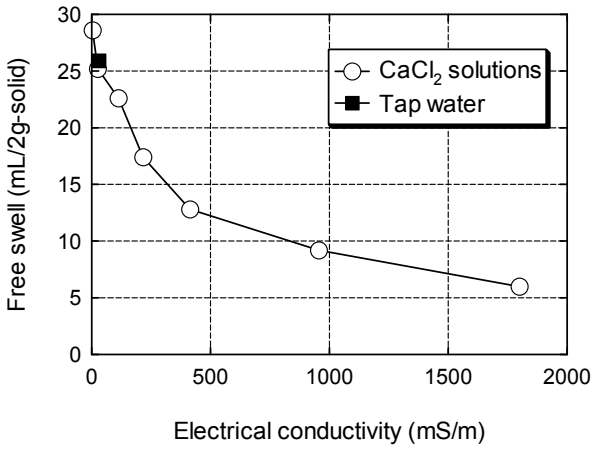

Figure 2.20 Swell volume of bentonite versus electrical conductivity.

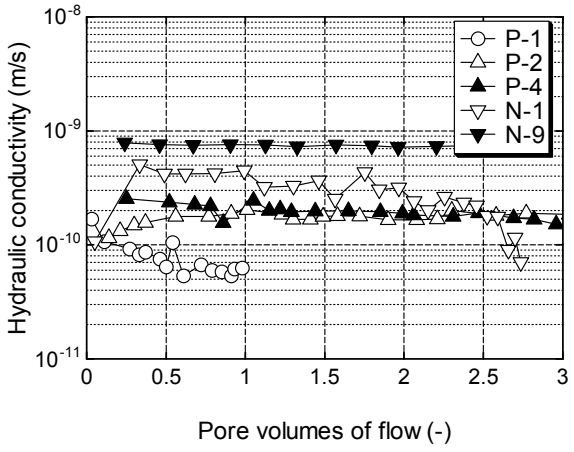

Figure 2.21 Changes in *k* values with the pore volumes of flow (P-1, P-2, P-4, N-1, N-9).

Table 2.11 The k values obtained from hydraulic conductivity test

Test No.	Hydraulic conductivity (m/s)	Void ratio* (-)	Test No.	Hydraulic conductivity (m/s)	Void ratio* (-)
C-1	7.1×10^{-11}	1.06	N-1	2.3×10^{-10}	0.91
C-2	5.5×10^{-11}	0.89	N-2	2.2×10^{-10}	0.95
C-3	4.1×10^{-11}	0.91	N-3	1.5×10^{-9}	0.79
C-4	2.3×10^{-11}	0.90	N-4	6.8×10^{-10}	0.89
C-5	1.8×10^{-11}	0.77	N-5	5.6×10^{-10}	0.82
C-6	6.9×10^{-11}	0.90	N-6	1.1×10^{-9}	0.82
C-7	3.0×10^{-11}	0.81	N-7	1.0×10^{-9}	0.95
C-8	1.9×10^{-10}	0.87	N-8	7.4×10^{-10}	0.89
C-9	6.9×10^{-11}	0.86	N-9	1.3×10^{-9}	0.90
C-10	8.4×10^{-11}	0.79	N-10	1.1×10^{-9}	0.87
C-11	5.6×10^{-11}	0.76	N-11	7.0×10^{-10}	0.88
C-12	4.2×10^{-11}	0.76	N-12	9.8×10^{-10}	0.88
C-13	6.7×10^{-11}	0.87	N-13	1.0×10^{-10}	1.07
C-14	5.0×10^{-11}	0.79	N-14	8.3×10^{-11}	1.01
C-15	4.8×10^{-11}	0.77	S-1	1.0×10^{-10}	1.02
C-16	4.7×10^{-11}	0.85	S-2	2.1×10^{-11}	0.80
C-17	3.8×10^{-11}	0.83	S-3	2.9×10^{-11}	0.80
P-1	5.0×10^{-11}	1.06	S-4	6.3×10^{-10}	0.63
P-2	1.9×10^{-10}	0.95	S-5	3.1×10^{-11}	0.81
P-3	2.2×10^{-10}	1.00	S-6	4.0×10^{-11}	0.75
P-4	1.4×10^{-10}	0.86	S-7	2.5×10^{-10}	0.61
P-5	1.6×10^{-10}	0.97	S-8	2.7×10^{-9}	0.91
P-6	1.1×10^{-10}	0.85	S-9	8.7×10^{-10}	0.93
P-7	1.2×10^{-10}	0.93	S-10	1.1×10^{-10}	0.96
P-8	4.9×10^{-11}	1.09	S-11	1.1×10^{-9}	0.72
			S-12	1.5×10^{-10}	0.78
			S-13	4.3×10^{-11}	0.81

* After permeation

2.4.3 Enhancement of hydraulic barrier performance by bentonite addition

Figure 2.22 shows k values of SBMs made with five different base soils (C_{BP} = 100 kg/m^3) without chemical or permeants in the pore water (P-1, S-2, S-5, S-10, and S-13 in Table 2.6 and Table 2.7). Although the original k values of composite soil, silty clay, sandy soil, silica sand, and fine sand were 1.51×10^{-7}, 6.39×10^{-10}, 1.84×10^{-7}, 3.90×10^{-5}, 2.89×10^{-5} m/s, respectively, the values of SBMs made with each soil could be lower than 1.0×10^{-10} m/s by bentonite addition with C_{BP} = 100 kg/m^3. This result confirms that high hydraulic barrier

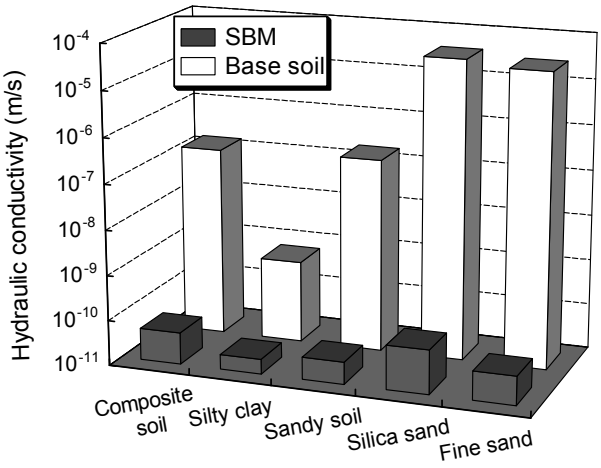

Figure 2.22 Enhancement of hydraulic barrier performance by bentonite addition.

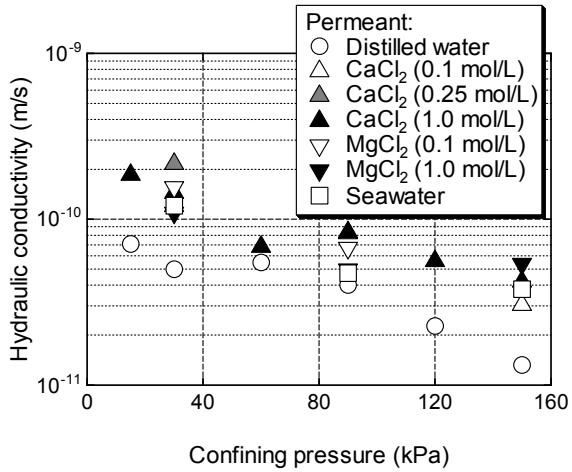

Figure 2.23 Changes in *k* value with confining pressure during permeation (Series-C and P-1~8).

performance of SBMs can be expected by adding bentonite regardless of type of base soil when the bentonite can sufficiently swell and fill voids in the cutoff walls.

2.4.4 Effect of confining pressure

Figure 2.23 illustrates the *k* values of SBMs under different confining pressures and using 7 different permeant liquids. The larger confining pressure led to the lower *k* values of SBMs regardless of types and concentrations of permeant liquid. This is because the lower void ratio induced by the higher pre-consolidation pressure and confining pressure results in the decreasing effective void space that allows the water flow as explained in a previous research (Yeo et al. 2005). Even at the lowest confining pressure of 15 kPa, the *k* value of SBM was approximately 1×10^{-10} m/s. At the confining pressure of 150 kPa, the *k* value was only

one-fourth as high as those at the confining pressure of 15 kPa. Thus, SBM is considered to have a good enough hydraulic barrier performance even when the confining pressure is small. Besides, there is no significant effect of the confining pressure on the k of SBM even if the vertical stresses in the SBM cutoff wall is lower than the overburden pressure due to the arching effect (Evans et al. 1995, Filz 1996).

2.4.5 Chemical compatibility of SBM

Effect of chemicals in permeant on the hydraulic conductivity can be known also from Figure 2.23. The k values permeated with the inorganic solutions were approximately only 1 - 3 times as high as those permeated with the DW regardless of the confining pressure. As previously noted, this is because the osmotic swelling and diffuse double layer collapsed with the effect of divalent cations. However, since the bentonite in SBM was prehydrated during SBM preparation and pre-consolidation, the influence on its hydraulic barrier performance was not significant. Comparing the k values influenced by chemical concentrations of $CaCl_2$ and $MgCl_2$ solutions (see Figure 2.24), the k values were almost similar; however, the values for 1.0 M solution were slightly lower than the values for 0.1 and 0.25 M solutions probably due to the viscosity effect. From this observation, it was confirmed that the concentration of the inorganic solution has no significant effect on the hydraulic barrier performance of the SBM when it is higher than 0.1 M. Katsumi et al. (2001) and Jo et al. (2001) pointed out that increase in the divalent concentration does not affect the swelling property of bentonite nor increase the hydraulic conductivity when the concentration is higher than 0.1 M for non-prehydrated geosynthetic clay liners. From this viewpoint, the effect of chemicals in permeant on the hydraulic barrier performance of SBM are similar with that on other bentonite-based materials.

Figure 2.25 illustrates change in k values of the SBM permeated with 0.1 and 1.0 M $CaCl_2$ solutions at the σ_c = 30 kPa (P-2 and P4). The cumulative flow volume was larger than 6 pore volumes. Although the k values increased or decreased slightly at the beginning of the permeation, they were stable in the range of 1×10^{-10} to 3×10^{-10} m/s after the cumulative flow volume exceeded 3 pore volumes. This observation confirms that SBM can maintain its high hydraulic barrier performance until the cumulative flow volume reaches about 6.5 pore volumes even when the inorganic chemicals flow into the cutoff walls.

Figure 2.26 summarizes the k values in Series-P, in which SBMs were made with C_{BP} = 100 kg/m^3 and σ_c = 30 kPa. This figure also demonstrates that the effect of chemical type and concentration of permeant is negligible and the k values of SBM can be maintained lower than 1×10^{-9} m/s. Permeated with the seawater which contains several species of multivalent cations (e.g. calcium, magnesium), the k became 1 to 2×10^{-10} m/s, which was similar to that for $CaCl_2$ solutions. For 50%-ethanol permeation, k was especially low compare with other cases. To take the effect of the high viscosity of ethanol solution into consideration, the intrinsic permeability, K, of the SBM was calculated by a following equation (2.5).

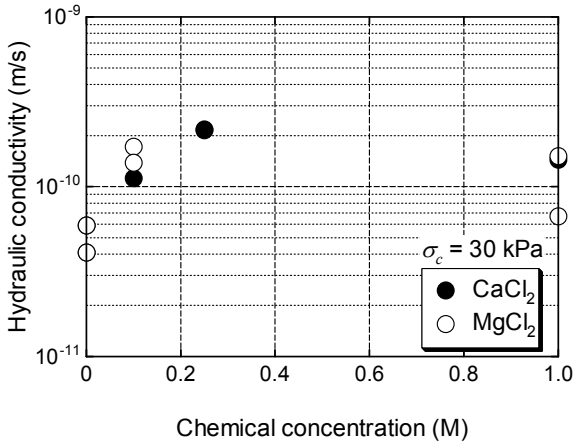

Figure 2.24 The k values versus chemical concentration of permeant.

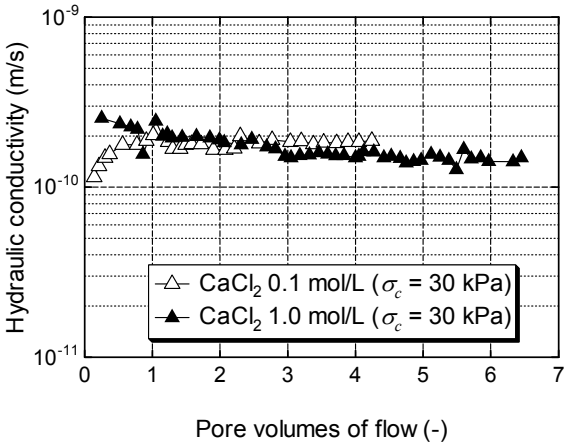

Figure 2.25 Change in the k values with time.

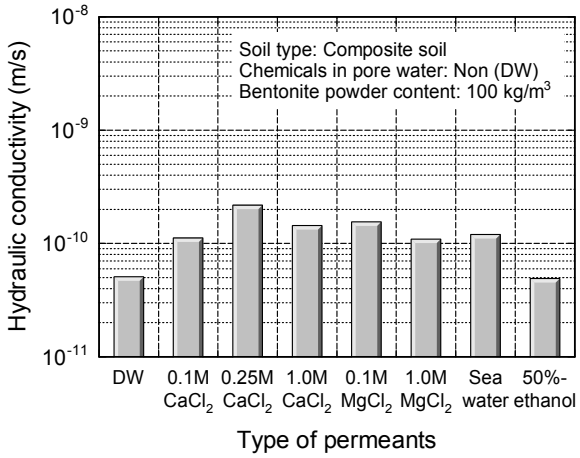

Figure 2.26 Effect of chemicals in permeant liquid on the k (Series-P).

$$K = \frac{\mu}{\rho g} \cdot k \tag{2.5}$$

where, K = intrinsic permeability (m^2); k = hydraulic conductivity (m/s); ρ = density of permeant (g/m^3); g = gravitational acceleration (m/s^2); μ = viscosity of permeant (Pa·s). The obtained value was 1.5×10^{-17} m^2 for 50%-ethanol permeation, which was only 3 times larger than that for the DW permeation, 5.1×10^{-18} m^2. This result indicates that the SBM can maintain its hydraulic barrier performance even when permeated with the high concentration of organic solvents.

As a summary about the hydraulic barrier performance against chemical attack after the construction, the k value of SBM is not significantly increased even against the permeant

containing inorganic/organic chemicals with high concentrations when the bentonite in the SBM can be sufficiently hydrated with the soil pore water.

Figure 2.27 shows the change in hydraulic conductivity of SBM with different $CaCl_2$ concentrations of the soil pore water. Figure 2.28 shows the k values in association with $CaCl_2$ concentration in the soil pore water. For the SBM in which no chemical exist in the soil pore water, k value is 1.1×10^{-10} m/s against permeation of 0.1 M $CaCl_2$ solution. However, the higher $CaCl_2$ concentrations led to the higher k values. As shown in these figures, in the case that $CaCl_2$ concentration in the soil pore water is 0.1 M, the k becomes higher than 1×10^{-10} m/s, which is the performance-based criterion in this study. Although the pore water containing calcium ions is diluted by the water fraction of the bentonite slurry, there is a significant increase to reach the average k value of 1.3×10^{-9} m/s in the case of 0.1 M $CaCl_2$ solution as shown in Figure 2.28. Comparing the chemical effect in permeant and in the soil pore water, it is obvious that the impact of chemicals in the pore water on the k value is much greater than that in permeant as shown in Figure 2.29. Even though the $CaCl_2$ concentration range of the soil pore water is ten times different with that of the permeant, the k value is greatly increased. The k for 0.1 M $CaCl_2$ in the permeant is 3.5 times as high as that for 0 M $CaCl_2$. Contrarily, the increase of the $CaCl_2$ concentration in the pore water resulted in the increase in the k by more than one order of magnitude. Figure 2.30 illustrates k values with EC values of the soil pore water and of permeant. By comparing the effects of divalent cations on the k value when they exist in the permeant or in the pore water, it can be concluded that the cation in the pore water causes more significant increase in the k value. The k for the permeant of 0.1 M $CaCl_2$ is 3.5 times as high as that for the permeant containing no $CaCl_2$ (0 M). In contrast, the increase in the $CaCl_2$ concentration in pore water from 0 to 0.1 M results in the increase in k by more than one order of magnitude. These observations indicate that the prehydration of bentonite is absolutely essential for the chemical compatibility of the SBM. Its effect is not minor even in the case that the divalent cation concentration of the pore water is lower than 0.05 M. Thus, the concentration of the divalent cation and its variation in groundwater at the site of concern should be considered in evaluating the hydraulic barrier performance of SBM.

Figure 2.31 summarizes the k values for the SBMs made with C_{BP} = 100 kg/m^3 in Series-N, where the SBM contains various chemicals in its soil pore water. For the seawater, approximately one order of magnitude higher value was obtained by comparing with the SBM to which no chemical added. This increase is almost equivalent to that caused by 0.05 and 0.1 M $CaCl_2$ solutions due to the multivalent cations. Therefore, there is fear that swell property of bentonite will decay in the construction at coastal areas. For the SBMs containing heavy fuel oil in the pore water, there is no influence on the k value probably due to hydrophobicity of oil.

As described above, the hydraulic barrier performance of SBMs are influenced by the chemicals especially when the chemicals originally exist in soil pore water. The possibility of enhancement on the k value was evaluated from a viewpoint of bentonite content. Data for

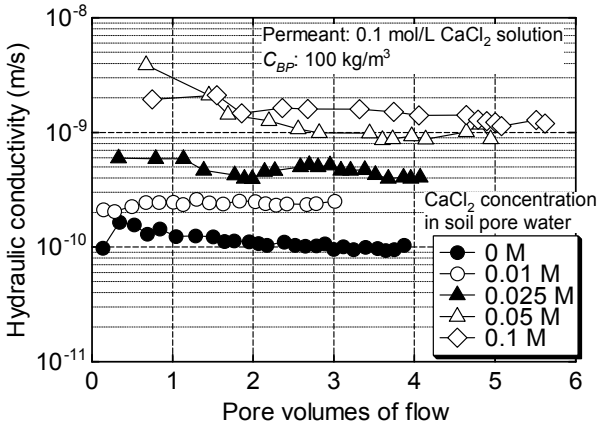

Figure 2.27 Changes in k value of SBM containing $CaCl_2$ in the soil pore water.

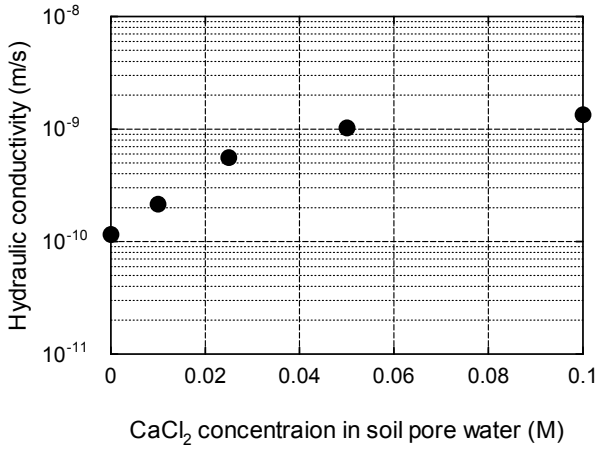

Figure 2.28 The k values versus chemical concentration of soil pore water.

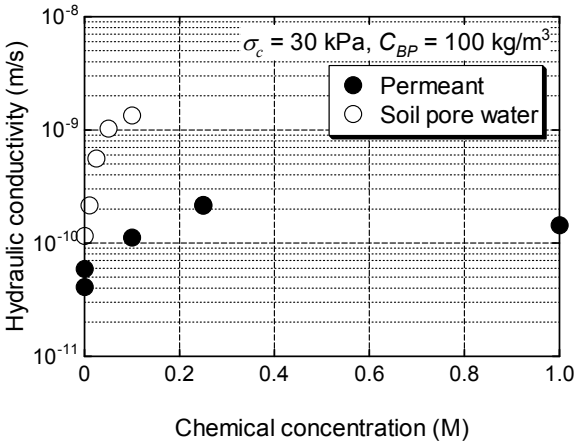

Figure 2.29 Comparison of the chemical effects by permeant and by soil pore water.

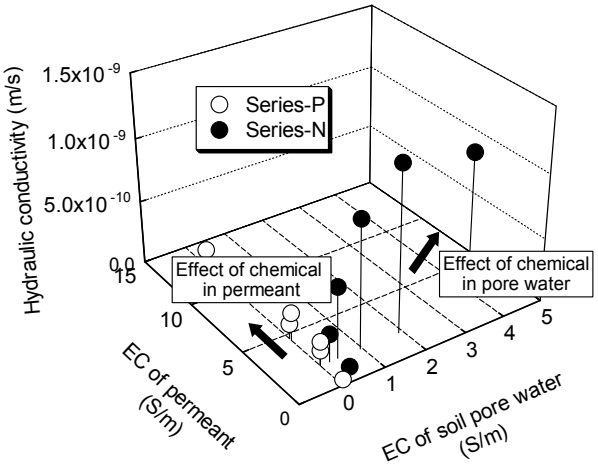

Figure 2.30 Effects of EC value of soil pore water and of permeant on the k value.

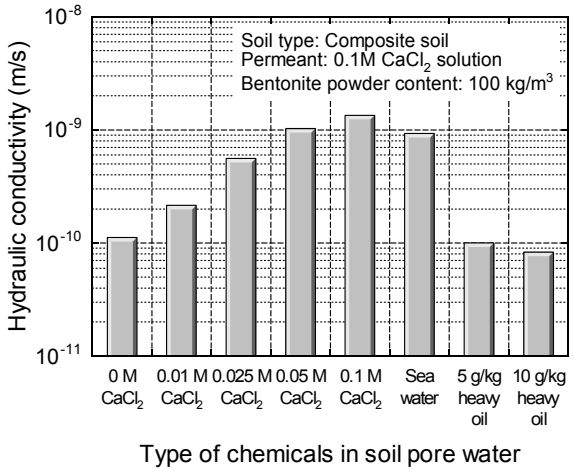

Figure 2.31 Effect of chemicals in the soil pore water on the *k* (P-2, N-2, N-5, N-7, N-9, N-12~14).

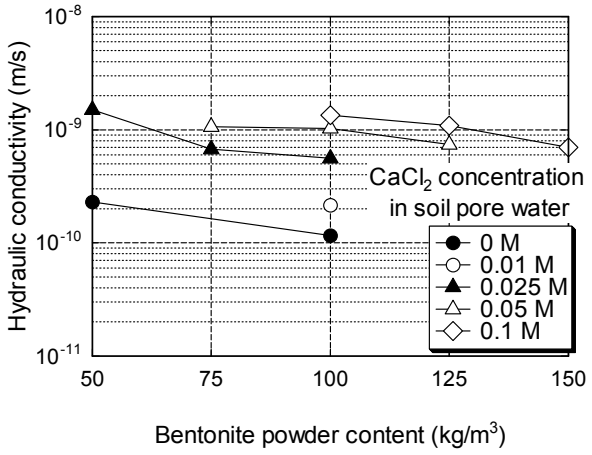

Figure 2.32 Relationship between *k* values and C_{BP} for each $CaCl_2$ concentration in soil pore water (P-2, N-1~N-11).

different bentonite powder contents are plotted in Figure 2.32. For the C_{BP} = 100 kg/m^3, *k* values are increased linearly for $CaCl_2$ concentrations of pore water lower than 0.05 M. However, for $CaCl_2$ concentrations higher than 0.05 M, they are still increased but by the smaller rate. For the C_{BP} = 50 kg/m^3, there is a greater effect of the $CaCl_2$ concentration observed: *k* for 0.025 M is 1.5×10^{-9} m/s, which is more than 6.5 times as high as for 0 M. In the case of 0.1 M $CaCl_2$, the *k* can be lowered by 50% by increasing the bentonite powder content from 100 to 150 kg/m^3. In the case that the SBM was prehydrated ($CaCl_2$ concentration in pore water = 0 M), *k* value of lower 1.0×10^{-9} m/s was achieved by adding 50 kg/m^3 of powder bentonite for the composite soil used in this study. These results indicate that the cation concentration of the pore water is an important factor for determining the additive amount of bentonite powder particularly when it is relatively small, but hydraulic barrier

performance of SBM can be enhanced by increasing the C_{BP}.

2.4.6 Effect of soil type

Figure 2.33 shows the relationship between k values and $CaCl_2$ concentrations in soil pore water and permeant for three types of soil in Series-S, where the initial $CaCl_2$ concentration in pore water and permeant were set equal. For each soil, k increased in association with the $CaCl_2$ concentration. As $CaCl_2$ concentration in soil pore water and permeant increased from 0 to 0.1 M, the k value of SBMs processed from composite soil, silty clay, and sandy soil became 48 times higher, 30 times higher, and 8 times higher, respectively. Figure 2.34 shows the relationship between the void ratio after permeation and the $CaCl_2$ concentration. Void ratio of SBM was lowered more by the higher $CaCl_2$ concentration. For the constant $CaCl_2$ concentration, the void ratio of SBMs made with composite soil was the largest, and those of silty clay-based and sandy soil-based SBMs were almost equal. Comparing the values for $CaCl_2$ concentration of 0.1 M with 0 M, the void ratio of composite soil-based and silty clay-based SBMs became about 20% of magnitude lower. In contrast, decrease in the void ratio of sandy soil-based SBM was only 10% of magnitude. This finding is consistent with the influence of the $CaCl_2$ concentration on the k value shown in Figure 2.33.

Figure 2.35 plots the relationship between the void ratio of SBMs after the experiments and the k of SBMs made with various chemical concentrations and base soils and those of SBMs with various confining pressures during the permeation. In addition, the smaller void ratio led to the lower k value for the SBMs made with same mixing condition due to higher

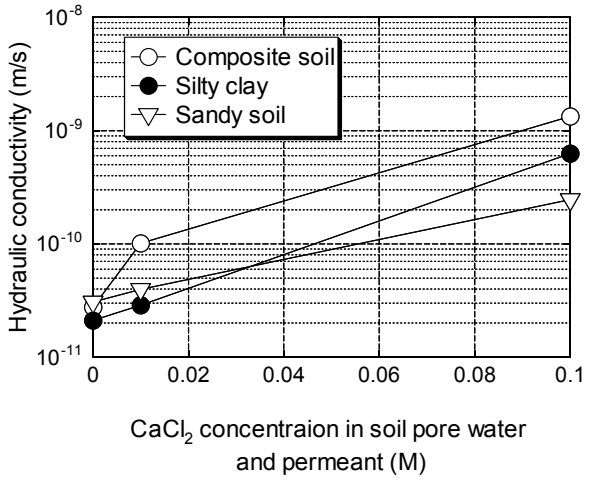

Figure 2.33 Relationship between k values and $CaCl_2$ concentrations in soil pore water and permeant for SBMs made with three different base soils.

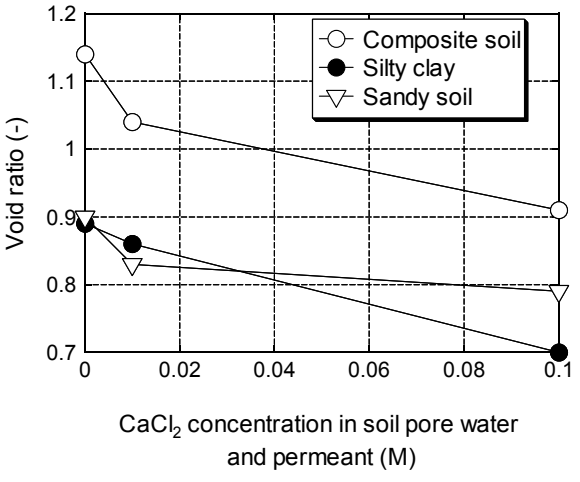

Figure 2.34 Relationship between void ratio of SBMs after permeation and $CaCl_2$ concentrations in soil pore water and permeant for SBMs made with three different base soils.

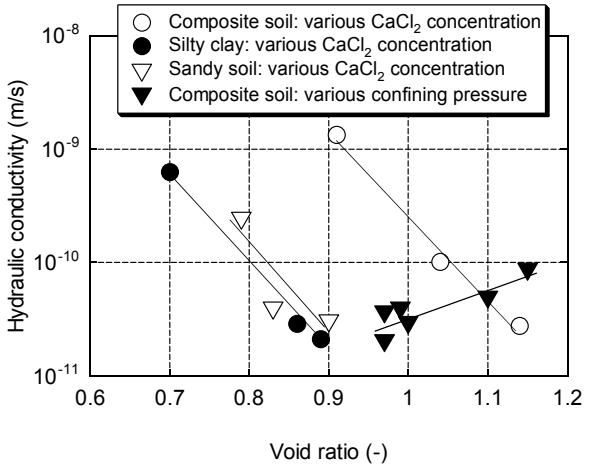

Figure 2.35 Void ratio versus k value.

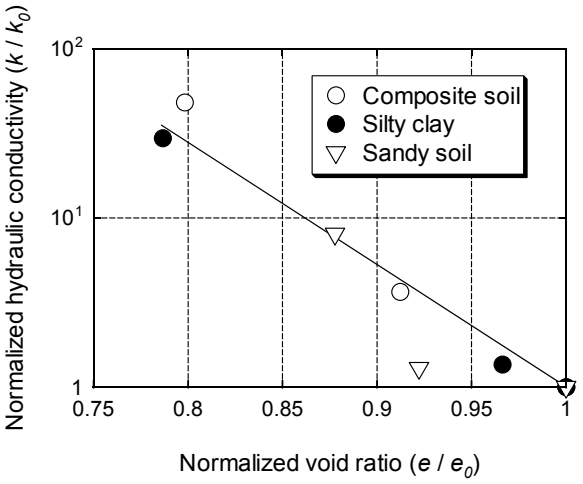

Figure 2.36 Normalized relationship between void ratio and k value.

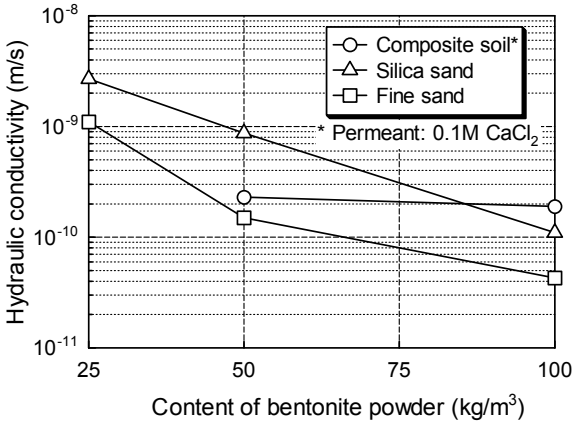

Figure 2.37 The k values versus C_{BP} of SBM made with various base soils (P-2, N-1~N-11).

confining pressure during permeation. Figure 2.36 shows the relationship between void ratio and k value, both of which were normalized with the value for the $CaCl_2$ concentration of 0 M. Correlation between them was observed regardless of the soil type. The lower concentration resulted in the larger void ratio of SBM. As a result, larger volume of water is retained as immovable water, which does not contribute to the permeation. This is why the lower hydraulic conductivity is achieved with the larger void ratio of SBM attacked by $CaCl_2$. This finding supports that the void ratio change can become a good indicator for the hydraulic barrier performance of SBM attacked by the divalent cation for various types of soil.

Figure 2.37 plots the k values of silica sand-based SBM and fine sand-based SBM permeated with DW as well as the value of composite soil-based SBM permeated with 0.1 M $CaCl_2$ solution in association with C_{BP} of SBM. Although a similar increasing tendency with

decreasing in C_{BP} can be observed, the significant k values have a certain amount of difference according to the type of base soil and of permeant. Comparing the result of silica sand-based SBM and fine sand-based SBM in light of each fine particle content of base soil, fine sand-based SBM, which contains more fine particle in the base soil, represents lower k values regardless of C_{BP}. Even though composite soil contains more fine particles than fine sand, composite soil-based SBM shows higher k values probably due to the permeation of 0.1 M $CaCl_2$ solution. Due to the large fine particle content of composite soil, the increment of k value associated with decrease in C_{BP} can be assumed to be small.

2.4.7 Self-sealing capability of SBM

Figure 2.38 shows the apparent hydraulic conductivity values for the cylindrical SBM specimen having a vertical interface along its diameter in the case of σ_c = 30 kPa. The apparent hydraulic conductivity was calculated by dividing the effluent rate by the section area of the specimen and the hydraulic gradient. Apparent hydraulic conductivity values were very similar to those of the SBM specimens with no defect both for distilled water and 1.0 M $CaCl_2$ solutions. Thus, a leakage through the interface in the SBM, such as a slip surface, can be negligible because both the flexibility of SBM and the re-swelling of the bentonite were effective under a confining pressure. Figure 2.39 shows the apparent hydraulic conductivity values for the cylindrical SBM specimen initially penetrated by a circular hole (ϕ = 2 mm). After the permeation started, a significant leakage was observed in every specimen, and apparent hydraulic conductivity values were in the range of 10^{-5} to 10^{-6} m/s. Then, those of the specimens permeated with the distilled water were lowered gradually to approximately 1×10^{-9} m/s, while those of the specimens permeated with the $CaCl_2$ solution were stabilized in the range of 10^{-5} to 10^{-6} m/s even when the confining pressure was high (σ_c = 150 kPa).

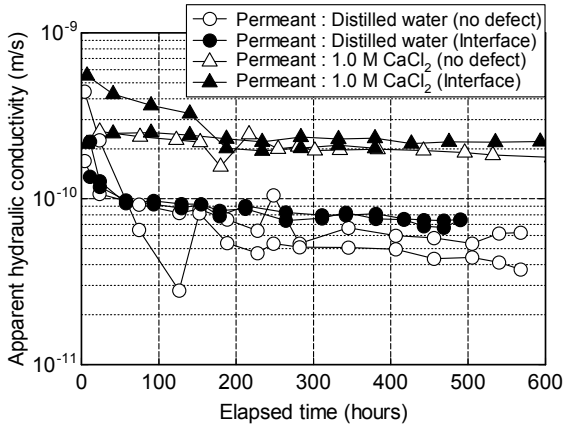

Figure 2.38 Apparent hydraulic conductivity of the SBM specimen containing a vertical interface along its diameter (σ_c = 30 kPa).

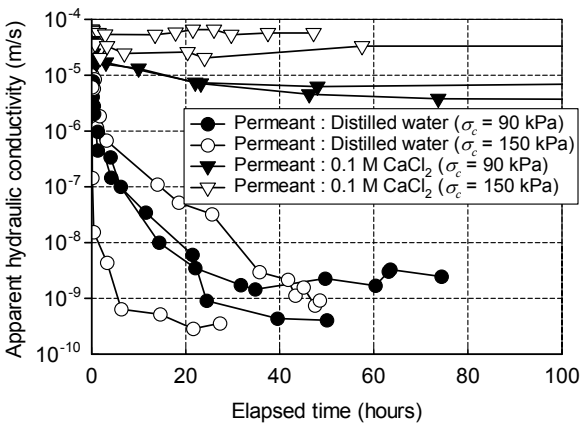

Figure 2.39 Apparent hydraulic conductivity of the SBM specimen with a circular hole (ϕ = 2 mm).

Photo 2.3 Specimens with hole after permeation (L) DW permeation; (R) 0.1 M $CaCl_2$ permeation.

These changes in hydraulic conductivity values confirm that the reswelling of bentonite plays an important role to reduce the leakage flow rate. Photo 2.3 shows appearance of specimens after the permeation. These photos also demonstrate that the hole was filled with a gel of reswelled bentonite in conjunction with the erosion around the hole by permeation of DW; however, the hole was maintained even after the permeation of 0.1 M $CaCl_2$ solution. Thus, when permeated with $CaCl_2$ solution, the SBM specimen did not recover its hydraulic barrier performance since the swelling of the bentonite was prevented.

2.4.8 Hydraulic conductivity assessment by consolidation test

Figure 2.40 shows the k values of SBMs made with silica sand obtained from hydraulic conductivity test and consolidation test. Comparing the values obtained by the two experimental methodologies, those corresponding to the hydraulic conductivity test have a clear linear relationship with the C_{BP}, whereas those from the consolidation test have variability. This is probably because the clay fraction in SBM of C_{BP} = 50kg/m^3 is

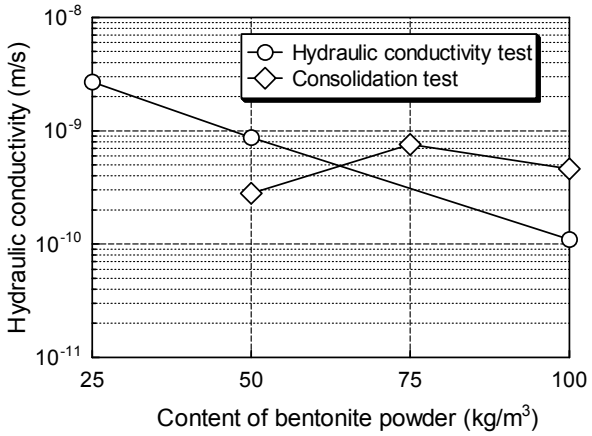

Figure 2.40 Comparison of k values obtained from hydraulic conductivity test and consolidation test (Base soil: silica sand).

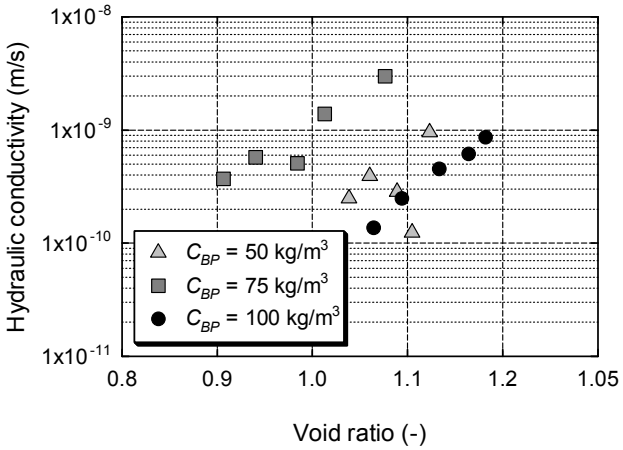

Figure 2.41 Relationship between void ratio after settlement and *k* value

approximately only 4%, and the sand fraction, which acts as the skeleton of SBM, supported the consolidation pressure. As shown in Figure 2.41, in the case of SBM of C_{BP} = 50kg/m^3, there is no clear relationship even between void ratios and *k* values due to few clay fraction as same as shown in Figure 2.40. As described in previous researches (e.g., Tavenas et al. 1983), *k* values cannot be accurately estimated by the consolidation tests because; 1) consolidation tests are conducted only with vertical one-dimensional consolidation and do not simulate in-situ stress state, and 2) leakage between specimen and rigid cell might occur. Also in this research, the results indicate that it is difficult to evaluate accurate permeability; however, the order of magnitude of hydraulic conductivity can be estimated by this method. Hydraulic conductivity test continues running for approximately 1 or 2 months to obtain a constant value because this method is conducted against low- permeable materials. Thus, by carrying out consolidation test, there are some possibilities that the general value of hydraulic conductivity can be estimated more quickly compared to permeability test.

2.5 Indicators for hydraulic barrier performance

2.5.1 Swell volume of bentonite

Figure 2.42 illustrates the relationship between swell volume of bentonite measured by the free swelling test and *k* value of SBMs in which chemicals exist in the soil pore water. When the swell volume of bentonite is larger than 17.4 mL/2g-solid, *k* values lower than 2.2×10^{-10} m/s can be achieved by adding 100 kg/m^3 of powder bentonite even when $CaCl_2$ solution is permeated. The smaller swell volume leads to the higher *k* value and it comes close to the value of 1.0×10^{-9} m/s when the swell volume of bentonite is smaller than 9.2 mL/2g-solid. It can be seen that the swelling property of bentonite strongly contribute to the subsequent *k*

value of SBM. Once the bentonite can be sufficiently swelled by the prehydration with the soil pore water, SBMs can maintain high hydraulic barrier performance even against the chemical attack regardless of soil type.

2.5.2 Physical properties of SBMs

Figure 2.43 illustrates the relationship between total fine content in SBMs and the *k* value (P-1, S-2, S-5 and S-9~13). The total fine content was calculated with taking both fine particles in base soils and added bentonite amount into account. There is an apparent correlation between these two values as previously indicated by Ryan (1987); and the total fine particle content larger than 10% should be achieve on the determination of additive amount of bentonite powder at pre-construction stage. However, since silty clay originally contains many fines of 33.9% as shown in Table 2.2, this correlation can be applied on SBM.

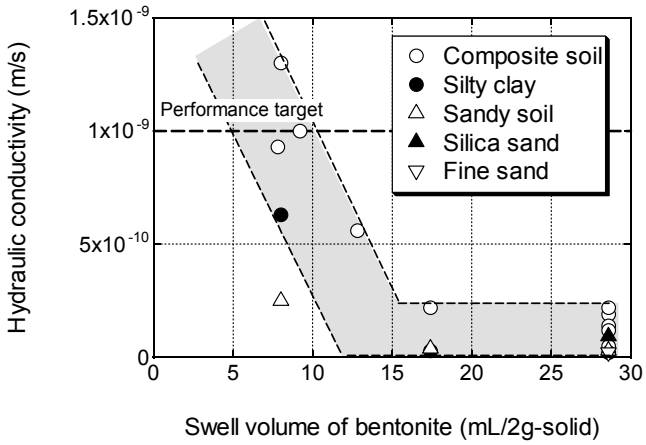

Figure 2.42 Relationship between swell volume of bentonite and *k* value of SBMs.

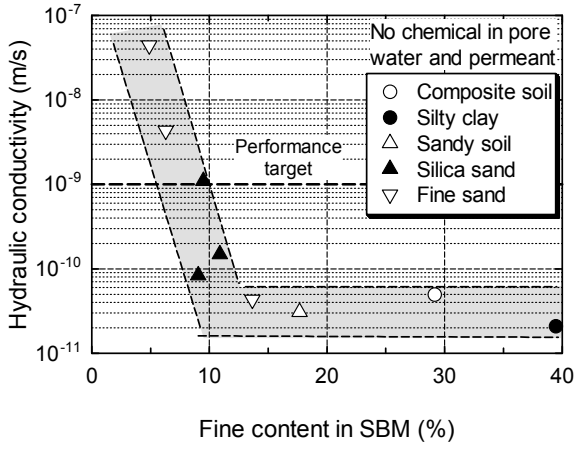

Figure 2.43 Total fine content in SBM versus *k* values.

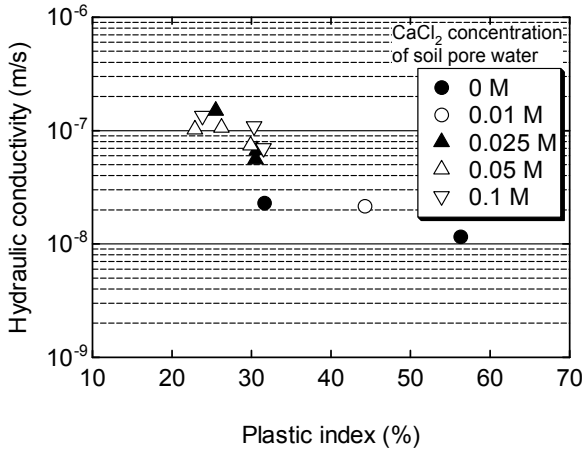

Figure 2.44 Plastic indices of SBMs versus *k* values.

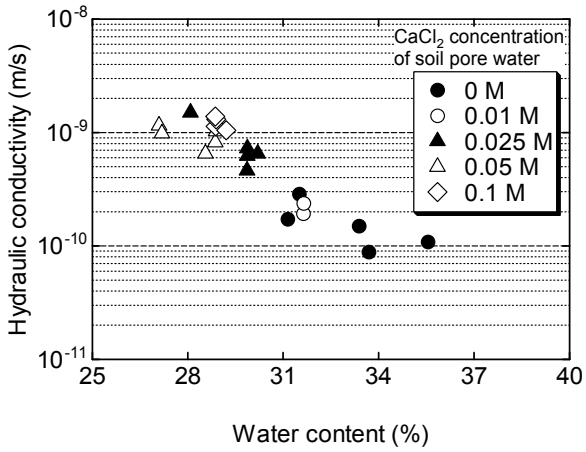

Figure 2.45 Water contents of SBMs after permeation versus *k* values.

Figure 2.44 plots *k* values obtained for every SBM specimen with itsplastic index (P-2 and N-1~11). Figure 2.45 shows the relationship between the *k* values and its water content after the hydraulic conductivity test. Hydraulic conductivity has strong negative correlations with both the plastic index and the water content. Fundamentally, hydraulic conductivity is deeply related to how much adsorbed water molecules, which are immovable and do not contribute to the water flow, are attracted in the SBM. Thus, the SBM with the higher plasticity and water content can retain much water inside and results in the lower hydraulic conductivity. These correlations confirm that the change in the plasticity index of SBM, increased by the lower $CaCl_2$ concentration of pore water and the higher bentonite content, become a useful indicator of these effect on the *k* value.

2.5.3 Swelling-pressure characteristics of SBMs

Figure 2.46 shows profiles of swelling pressure obtained from the swelling-pressure test. This figure plots the data for SBMs which contain $CaCl_2$ in its soil pore water as a representative example. The profiles have two different stages in all cases: 1) drastic increase at the beginning of the test as a primary swelling, and 2) gradual increase after the primary swelling as secondary swelling. In lower $CaCl_2$ concentration case in the soil pore water, the swelling pressures remained at a higher level due to the swelling property of bentonite. Another finding from this result is that the inflection point of the profile also differed by the $CaCl_2$ concentration in the soil pore water. For the SBMs with low $CaCl_2$ concentration, such as 0 M or 0.01 M, the primary swelling is continued for 6 to 8 hours, however, the profile changed from the primary to secondary swelling at around 2 hours of elapsed time in the case of 0.1 M $CaCl_2$. This result confirms that the infiltration into the montmorillonite mineral takes longer time in the case of lower $CaCl_2$ concentration in the soil pore water.

Figure 2.47 shows a relationship between the maximum swelling pressure and *k* value of

SBMs (P-2, N-1, N-2, N-9 and N-11~14). In these cases, 0.1 M $CaCl_2$ solution was used as permeant liquid. As shown in this figure, a good linear correlation between the two values is observed for the SBMs exposed to divalent cation, seawater and heavy fuel oil. The relatively lower swelling pressure values were observed for the SBMs exposed to the high concentrations of divalent cation, which had the higher *k* values. Although it takes a long period to measure the *k* of low-permeable materials such as SBM with enough accuracy, swelling pressure can be tested within a week or so. Considering this fact, the swelling pressure is expected to be employed as a good indicator for the estimation of the hydraulic barrier performance of the SBM. To verify and generalize the applicability of the swelling test to a simple evaluation, test results on the SBMs processed from different types of soil, however, should be collected and analyzed.

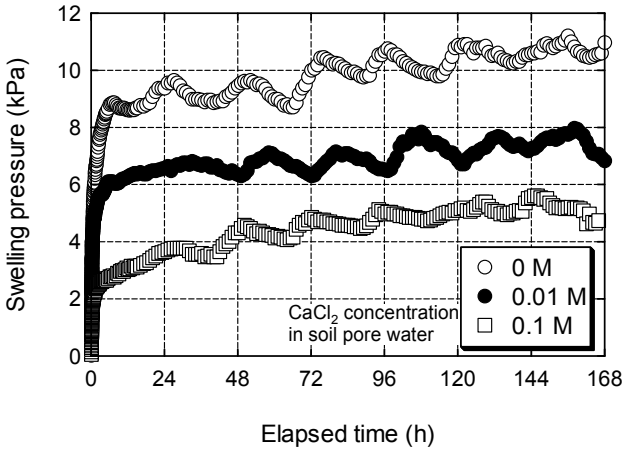

Figure 2.46 Changes in swelling pressure of SBMs with time.

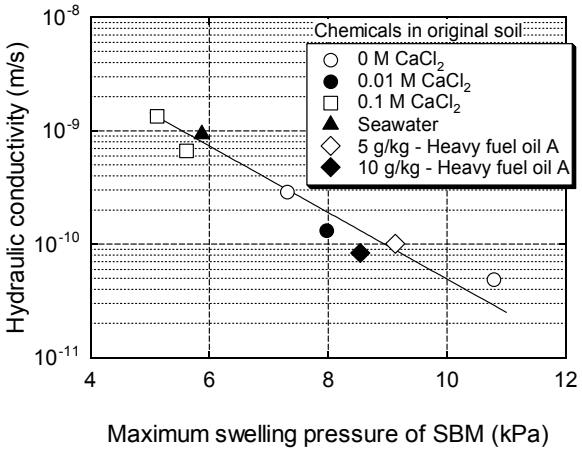

Figure 2.47 Maximum swelling pressure versus *k* value.

2.5.4 Swelling-deformation characteristics of SBMs

Figure 2.48 illustrates the normalized water content of SBM, which represents relative water content to the base soil without bentonite, obtained from the swelling-deformation tests conducted on the SBMs containing $CaCl_2$ in its pore water. As demonstrated in this figure, even though there is no significant effect on the normalized water content when $CaCl_2$ concentration is lower than 0.01 M, the value is decreased from 137.3% to 120.9% for the SBM made with composite soil. The trend is similar in other base soil cases. Figure 2.49 shows effective dry density of bentonite in SBM with $CaCl_2$ concentration in the soil pore water and immersion solution. The higher $CaCl_2$ concentration leads to the larger effective dry density of bentonite regardless of soil type. The large effective dry density of bentonite represents void volume is comparatively small because the mass and volume of solid bentonite fraction is constant for all cases. These observations confirm that the water retention capability of SBM decayed under high $CaCl_2$ concentration, such as 0.1 M $CaCl_2$ solution.

Figure 2.50 and Figure 2.51 show *k* values obtained from the hydraulic conductivity test with the normalized water content and effective dry density of bentonite, respectively. Large normalized water content means that SBM contains immovable water, such as adsorbed water, in large quantity. Also, the large effective dry density of bentonite indicates that the swell of bentonite is restricted. Thus, the larger normalized water content and the smaller effective dry density of bentonite can lead to the lower *k* values as shown in the figures. Each SBM made with three different base soils has almost linear correlation separately. To generalize the swelling deformation and apply the swelling-deformation characteristics as another indicator for estimation of *k* value, unified evaluation method should be developed.

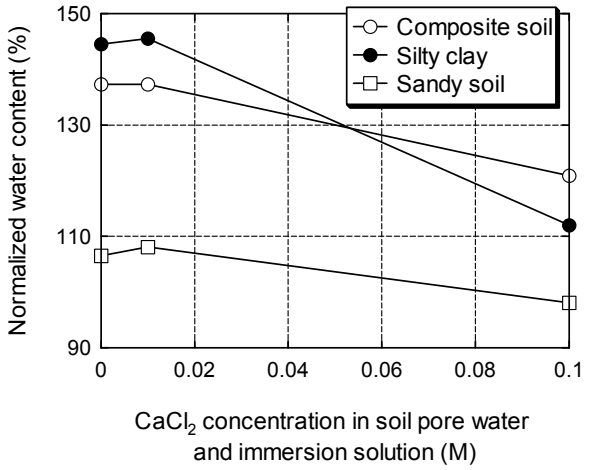

Figure 2.48 Normalized water content versus $CaCl_2$ concentration in soil pore water and immersion solution.

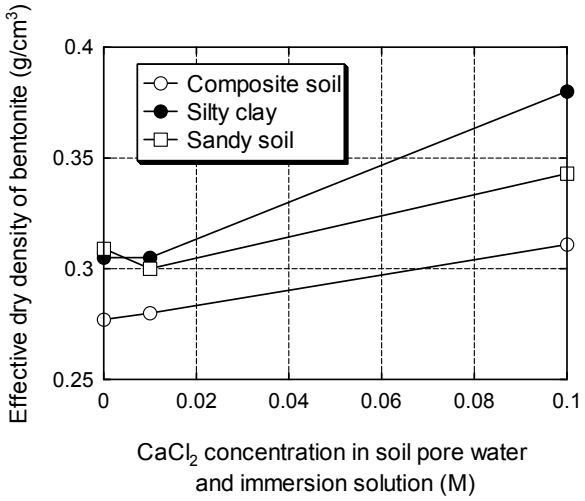

Figure 2.49 Effective dry density of bentonite versus $CaCl_2$ concentration in soil pore water and immersion solution.

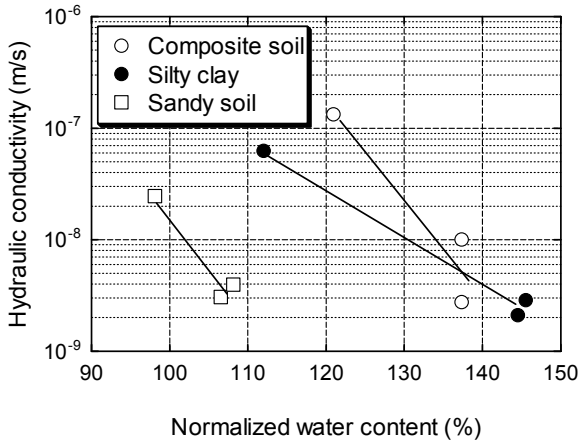

Figure 2.50 Relationship between normalized water content and *k* value.

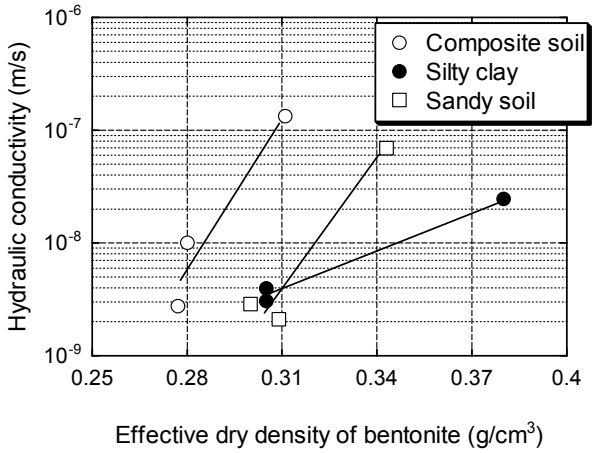

Figure 2.51 Relationship between effective dry density of bentonite and *k* value.

2.6 Summary and conclusions

The hydraulic barrier performance of SBM strongly depends on the swelling property of bentonite. In this chapter, hydraulic barrier performance of SBM was discussed in terms of *k* value based on the results of laboratory hydraulic conductivity test, swelling-pressure test, and swelling-deformation test from the viewpoint of bentonite behavior inside SBMs. Chemical compatibility of SBM was evaluated regarding the effect of chemicals in the soil pore water and in permeant. The effect of bentonite powder content was also discussed using various SBMs which contain chemicals in the soil pore water. Physical properties of SBMs were also verified in association with the hydraulic barrier performance. The main achievement obtained in this chapter can be summarized as follows:

(1) The bentonite used in this study results in a significant decrease in its swell volume when the $CaCl_2$ concentration is higher than 0.01 M, and the swell volumes against the solutions of $CaCl_2$ concentration higher than 0.1 M were almost similar. The swell volume of bentonite significantly decreased according to increase of EC value of the solutions.

(2) In hydraulic conductivity test, *k* values permeated with DW continuously decreased as the permeation proceeded particularly at the early stage of the test. This is possibly because the bentonite in the specimen could absorb the influent water with the formation of diffuse double layer and osmotic swelling because it did not fully swell during the pre-consolidation.

(3) Although the original *k* values of base soils have variation ranging from 10^{-5} to 10^{-10} m/s, the values of SBMs made with each soil could be lower than 1.0×10^{-10} m/s by the

addition of 100 kg/m^3 of bentonite powder. SBMs can achieve high hydraulic barrier performance regardless of soil type at sites when the bentonite can sufficiently swell and fill voids in the cutoff walls.

(4) Even at the lowest confining pressure of 15 kPa, the k value of SBM was approximately 1×10^{-10} m/s. At the confining pressure of 150 kPa, the k value was only one-fourth as high as those at the confining pressure of 15 kPa. Thus, SBM is considered to have an enough hydraulic barrier performance even when the confining pressure is small, besides, there is no significant effect of the confining pressure on the k of SBM even if the in-situ vertical stresses inside the SBM cutoff wall is lower than the overburden pressure due to the arching effect.

(5) The k values permeated with the inorganic solutions were approximately only 1 - 3 times as high as those permeated with the DW regardless of the confining pressure. Since the bentonite in SBM was prehydrated during SBM preparation and the pre-consolidation, the influence on its barrier performance was limited.

(6) Although the k values have slight variation at the beginning of the permeation, they were stable in the range of 1×10^{-10} to 3×10^{-10} m/s after the cumulative flow volume exceeded 3 pore volumes. Thus, SBM can maintain its hydraulic barrier performance until the cumulative flow volume reaches about 6.5 pore volumes even when the inorganic chemicals flow into the cutoff walls.

(7) Prehydrated SBM could maintain its hydraulic barrier performance also against the permeation of seawater and 50%-ethanol. Thus, it can be concluded that the k value of SBM does not significantly increase against the permeant containing inorganic/organic chemicals when the bentonite in the SBM can be preliminarily sufficiently hydrated with the soil pore water.

(8) In the case that $CaCl_2$ concentration in the soil pore water is 0.1 M, the k becomes higher than 1×10^{-10} m/s, which is the performance-based criterion in this study. Although the pore water containing calcium ions is diluted by the water fraction of the bentonite slurry, there is a significant increase to reach the average k value of 1.3×10^{-9} m/s when the pore water has 0.1 M $CaCl_2$.

(9) By comparing the effects of divalent cations on the k when they exist in the permeant or in the pore water, the cation in the pore water causes more significant increase in the k value. Thus, the prehydration of bentonite is an important factor for the chemical compatibility of the SBM. The concentration of the divalent cation and its variation in groundwater at the site of concern should be considered in evaluating the hydraulic barrier performance of SBM.

(10) When the soil pore water was replaced by the artificial seawater, approximately one order of magnitude higher value was obtained by comparing with the SBM to which no chemical added. This result indicates that the swelling of bentonite will be impeded in the construction at coastal areas. For the SBMs containing heavy fuel oil in the pore water, there is no influence on the k value probably due to hydrophobicity of oil.

(11) In the case of 0.1 M $CaCl_2$ in the soil pore water, the *k* can be lowered by 50% by increasing the bentonite powder content from 100 to 150 kg/m^3. In the case that the SBM was prehydrated ($CaCl_2$ concentration in pore water = 0 M), *k* value of lower 1.0×10^{-9} m/s was achieved by adding 50 kg/m^3 of powder bentonite for the composite soil used in this study. These results indicate that the cation concentration of the pore water is an important factor for determining the additive amount of bentonite powder, and the hydraulic barrier performance of SBM can be enhanced by increasing the additive amount of bentonite powder.

(12) There is a strong negative correlation between the normalized void ratio and the *k* of the SBM, for three different soils used. Thus, the change in void ratio can become a good indicator to estimate the hydraulic barrier performance of SBM attacked by the divalent cation.

(13) The SBM can recover its hydraulic barrier performance when the specimen has an intentional defect (a vertical interface or a circular hole penetrating the specimen) due to the combined effects of its deformability and the reswelling of bentonite. However, when permeated with $CaCl_2$ solution, the leakage through a circular hole was continuously observed since the swelling of the bentonite was prevented.

(14) When the swell volume of bentonite is larger than 17.4 mL/2g-solid, *k* value of SBM lower than 2.2×10^{-10} m/s can be achieved by adding 100 kg/m^3 of powder bentonite even against the permeation of $CaCl_2$ solution. The smaller swell volume of bentonite leads to the higher *k* value of SBM and it comes close to the value of 1.0×10^{-9} m/s when the swell volume of bentonite is smaller than 9.2 mL/2g-solid.

(15) The *k* value of SBM showed strong negative correlations with its plastic index and the water content of the specimen after permeation. From this observation, the change in these values, influenced by the cation concentration of the pore water and the bentonite content, can become useful indices of these effects on the *k* value.

(16) A good linear correlation between the maximum swelling pressure and *k* values is observed for the SBMs exposed to divalent cation, seawater and heavy fuel oil. The relatively lower swelling pressure values were observed for the SBMs exposed to the high concentrations of divalent cation, which had the higher *k* values. Although it takes a long period to measure the *k* of low-permeable materials such as SBM with enough accuracy, swelling pressure can be tested within a week or so. Considering this fact, the swelling pressure is expected to be employed as a good indicator for the estimation of the hydraulic barrier performance of the SBM.

(17) The larger normalized water content and the smaller effective dry density of bentonite can lead to the lower *k* values due to the higher water retention capacity of SBM.

References for Chapter 2

ASTM (2010): D5084-10 Standard Test Methods for Measurement of Hydraulic Conductivity of Saturated Porous Materials Using a Flexible Wall Permeameter.

ASTM (2011): D5890-11 Standard Test Method for Swell Index of Clay Mineral Component of Geosynthetic Clay Liners.

Britton, J.P., Filz, G.M., and Herring, W.E. (2004): Measuring the Hydraulic Conductivity of Soil-Bentonite Backfill, *Journal of Geotechnical and Geoenvironmental Engineering*, ASCE, Vol.130, No.12, pp.1250-1258.

Britton, J.P., Filz, G.M., and Little, J.C. (2005): The Effect of Variability in Hydraulic Conductivity on Contaminant Transport through Soil–Bentonite Cutoff Walls, *Journal of Geotechnical and Geoenvironmental Engineering*, Vol.131, No.8, pp.951-957.

Cui, Y.J., Tang, A.M., Qian, L.X., Ye, W.M., and Chen, B. (2011): Thermal-mechanical behavior of compacted GMZ bentonite, *Soils and Foundations*, Vol.51, No.6, pp.1065-1074.

Durner, W. (1994): Hydraulic conductivity estimation for soils with heterogeneous pore structure, *Water Resources Research*, Vol.30, No.2, pp.211-223.

Evans, J.C. (1993): Vertical cutoff walls, *Geotechnical practice for waste disposal*, D.E. Daniel (ed), Chapman and Hall, London, U.K. pp.430-454.

Evans, J.C. (1995): Soil- and Cement-based Vertical Barriers with Focus on Materials, *Assessment of Barrier Containment Technologies: A Comprehensive Treatment for Environmental Remediation Applications*, R. Rumer and J.K. Mitchell. (eds.), U.S. Department of Energy, U.S. Environmental Protection Agency, pp.5-43.

Evans, J.C., Costa, M., and Cooley B. (1995): The state-of-stress in soil-bentonite slurry trench cutoff walls, *Geoenvironment 2000*, Y.B. Acar and D.E. Daniel (eds.), ASCE, pp.1173-1191.

Filz, G.M. (1996): Consolidation stresses in soil-bentonite backfilled trenches, *Environmental Geotechnics*, M. Kamon, (ed.), Balkema, Rotterdam, pp.497-502.

Filz, G.M., Henry, L.B., Heslin, G.M., and Davidson, R.R. (2001): Determining hydraulic conductivity of soil-bentonite using the API filter press, *Geotechnical Testing Journal*, Vol.24, No.1, pp.61-71.

Gleason, M.H., Daniel, D.E., and Eykholt, G.R. (1997): Calcium and sodium bentonite for hydraulic containment applications, *Journal of Geotechnical and Geoenvironmental Engineering*, ASCE, Vol.123, No.5, pp.438-445.

Hong, C.S., Shackelford, C.D., and Malusis, M.A. (2012): Consolidation and hydraulic conductivity of zeolite-amended soil-bentonite backfills, *Journal of Geotechnical and Geoenvironmental Engineering*, ASCE, Vol.138, No.1, pp.15-25.

JIS (1997): JIS R 5201, Physical testing methods for cement.

JIS (2009a): JIS A 1204, Test method for particle size distribution of soils.

JIS (2009b): JIS A 1205, Test method for liquid limit and plastic limit of soils.

JIS (2009c): JIS A 1217, Test method for one-dimensional consolidation properties of soils using incremental loading

JIS (2009d): JIS A 1216, Method for unconfined compression test of soils.

Jo, H., Katsumi, T., Benson, C., and Edil, T. (2001): Hydraulic conductivity and swelling of nonprehydrated GCLs permeated with single-species salt solutions, *Journal of Geotechnical and Geoenvironmental Engineering*, Vol.127, No.7, pp.557-567.

Kamon, M., Katsumi, T., Inui, T., Ogawa, Y. and Araki, S. (2006): Hydraulic performance of soil-bentonite mixture barrier, *5ICEG Environmental Geotechnics*, H.R. Thomas (ed.), Thomas Telford Publishing, London, pp.733-740.

Katsumi, T., Benson, C.H., and Kamon, M. (2001): Chemical compatibility of bentonite liner material, *Soil Mechanics and Foundation Engineering*, Japan Geotechnical Society, Vol.49, No.2, pp.21-24 (in Japanese).

Katsumi, T., Ogawa, A., and Fukagawa, R. (2004): Effect of chemical solutions on hydraulic barrier performance of clay geosynthetic barriers, *Proceedings of the Third European Geosynthetics Conference - Geotechnical Engineering with Geosynthetics*, R. Floss, G. Braeu, M. Nussbaumer, and K. Laackmann (eds.), pp.701-706.

Katsumi, T., and Fukagawa, R. (2005): Factors affecting chemical compatibility and barrier performance of GCLs, *Proceedings of the 16th ICSMGE*, Millpress Science Publishers, pp.2285-2288.

Katsumi, T., Ishimori, H., Onikata, M., and Fukagawa, R. (2008): Long-term barrier performance of modified bentonite materials against sodium and calcium permeant solutions, *Geotextiles and Geomembranes*, Vol.26, Issue 1, pp.14-30.

Katsumi, T., Inui, T., and Kamon, M. (2009): Chemical effects on the performance of soil-bentonite cut-off walls for in-situ containment, *Proceedings of the 17th International Conference on Soil Mechanics and Geotechnical Engineering*, M. Hamza, M. Shahien, and Y. ElMossallamy (eds.), IOS Press, pp.2552-2555.

Kochmanova, N., and Tanaka, H. (2011): Influence of the soil fabric on the mechanical properties of unsaturated clays, *Soils and Foundations*, Vol.51, No.2, pp.275-286.

Kolstad, D.C., Benson, C.H., and Edil, T.B. (2004): Hydraulic conductivity and swell of nonprehydrated geosynthetic clay liners permeated with multispecies inorganic solutions, *Journal of Geotechnical and Geoenvironmental Engineering*, ASCE, Vol.130, No.12, pp.1236-1249.

Komine, H., and Ogata, N. (1996): Prediction for swelling characteristics of compacted bentonite, *Canadian Geotechnical Journal*, Vol.33, No.1, pp.11-22.

Komine, H. (2004): Simplified evaluation for swelling characteristics of bentonites, *Engineering Geology*, Vol.71, pp.265-279.

Komine, H., and Ogata, N. (2004): Predicting swelling characteristics of bentonites, *Journal of Geotechnical and Geoenvironmental Engineering*, ASCE, Vol.138, No.8, pp.818-829.

Komine, H., Yasuhara, Y., and Murakami, S. (2009): Swelling characteristics of bentonites in artificial seawater, *Canadian Geotechnical Journal*, Vol.46, No.2, pp.177-189.

Komine, H. (2010): Predicting hydraulic conductivity of sand-bentonite mixture backfill before and after swelling deformation for underground disposal of radioactive wastes, *Engineering Geology*, Vol.114, Issues 3-4, pp.123-134.

Lee, J.M., and Shackelford, C.D. (2005): Concentration dependency of the prehydration effect for a geosynthetic clay liner, *Soils and Foundations*, Vol.45, No.4, pp.27-41.

Malusis, M.A., Barben, E.J., and Evans, J.C. (2009): Hydraulic conductivity and compressibility of soil-bentonite backfill amended with activated carbon, *Journal of Geotechnical and Geoenvironmental Engineering*, ASCE, Vol.135, No.5, pp.664-672.

Malusis, M.A., Yeom, S., and Evans, J.C. (2011): Hydraulic conductivity of model soil-bentonite backfills subjected to wet-dry cycling, *Canadian Geotechnical Journal*, Vol.48, No.8, pp.1198-1211.

Malusis, M., and McKeehan, M. (2013): Chemical Compatibility of Model Soil-Bentonite Backfill Containing Multiswellable Bentonite, *Journal of Geotechnical and Geoenvironmental Engineering*, ASCE, Vol.139, No.2, pp.189-198.

Mishra, A.K., Ohtsubo, M., Li, L., and Higashi, T. (2011): Controlling factors of the swelling of various bentonites and their correlations with the hydraulic conductivity of soil-bentonite mixtures, *Applied Clay Science*, Vol.52, Issues 1-2, pp.78-84.

Mitchell, J.K., and Soga, K. (2005): *Fundamentals of soil behavior*, John Wiley & Sons, pp.153-156.

Naka, A., Katsumi, T., Ohta, T., Flores, G., Inui, T., and Takai, A. (2012): Geosynthetic clay liner permeated with acid rock drainage: The role of iron in arsenic immobilization, *Geosynthetics Engineering Journal*, Vol.27, pp.39-46.

Nakamura, M., Kawano, K., Thai, B., Uchimura, T., Sugo, K., and Towhata, I. (2009): Preparation of water-saturated bentonite samples and their use in torsion shear tests, *Soils and Foundations*, Vol.49, No.6, pp.981-991.

Norrish, K., and Quirk, J. (1954): Cristalline swelling of montmorillonite, Use of electrolytes to control swelling, *Nature*, Vol.173, pp.255-257.

Onikata, M., Kondo, M., and Kamon, M. (1996): Development and characterization of multiswellable bentonite, *Environmental Geotechnics*, A.A. Balkema Publishers, pp.587-590.

Quaranta, J.D., Gabr, M.A., and Bowders, J.J. (1997): First-exposure performance of the bentonite component of a GCL in a low-pH. Calcium enriched environment, *Testing and acceptance criteria for geosynthetic clay liners*, L.W. Well (ed.), ASTM, West Conshohocken, pp.162-177.

Ryan, C.R. (1987): Vertical barriers in soil for pollution containment, *Geotechnical Practice for Waste Disposal '87, Geotechnical Special Publication No.13*, R. Woods (ed.), ASCE, pp.182-204.

Sivapullaiah, P.V., Sridharan, A., Stalin, V.K. (2000): Hydraulic conductivity of bentonite-sand mixtures, *Canadian Geotechnical Journal*, Vol.37, No.2, pp.406-413.

Shackelford, C.D. (1994): Waste-soil interactions that alter hydraulic conductivity, *Hydraulic*

conductivity and waste contaminant transport in soil, D.E. Daniel and S.J. Trautwein, eds. ASTM, West Conshohocken, pp.111-168.

Shackelford, C.D., Malusis, M.A., Majeski, M.J., and Stern, R.T. (1999): Electrical conductivity breakthrough curves, *Journal of Geotechnical and Geoenvironmental Engineering*, Vol.125, No.4, pp.260-270.

Shackelford, C.D., Benson, C.H., Katsumi, T., Edil, T.B., and Lin, L (2000): Evaluating the hydraulic conductivity of GCLs permeated with non-standard liquids, *Geotextiles and Geomembranes*, Vol.18, Issues 2–4, pp.133-161.

Stern, R.T., and Shackelford, C.D. (1998): Permeability of sand-processed clay mixtures with calcium chloride solutions, *Journal of Geotechical and Geoenvironmental Engineering*, Vol.124, No.3, pp.231-241.

Suzuki, K., Asano, H., Yahagi, R., Kobayashi, I., Sellin, P., Svemar, C., and Holmqvist, M. (2013): Experimental investigations of piping phenomena in bentonite-based buffer materials for an HLW repository, *Clay Minerals*, Vol.48, pp.363-382.

Tavenas, F., Leblond, P., Jean, P., and Leroueil, S. (1983): The permeability of natural soft clays. Part I: Methods of laboratory measurement, *Canadian Geotechnical Journal*, Vol.20, pp.629-644.

van Genuchten, M.T. (1980): A closed form equation for predicting the hydraulic conductivity of unsaturated soils, *Soil Science Society of America Journal*, Vol.44, pp.892-898.

Wang, X., and Benson, C.H. (2004): Leak-free pressure plate extractor for measuring the soil-water characteristic curve, *Geotechnical Testing Journal*, Vol.27, No.2, pp.1-10.

Wang Q., Tang, A.M., Cui, Y.J., Delage P., Gatmiri, B. (2012): Experimental study on the swelling behaviour of bentonite/claystone mixture, *Engineering Geology*, Vol.124, pp.59-66.

Yeo, S.S., Shackelford, C.D., and Evans, J.C. (2005): Consolidation and hydraulic conductivity of nine model soil-bentonite backfills, *Journal of Geotechnical and Geoenvironmental Engineering*, ASCE, Vol.131, No.10, pp.1189-1198.

CHAPTER 3

QC/QA for Constructed SBM Cutoff Walls

3.1 General remarks

Since the contaminants must be completely contained to prevent their migration into the aquifer, cutoff walls must be constructed with both low hydraulic conductivity and high homogeneity. The main concerns of containment barriers are the assurance of their hydraulic barrier performance and homogeneity. Homogeneity plays a fundamental role on the quality of containment barriers since a larger variability in the hydraulic conductivity leads to a higher flux of contaminant out of the barrier system even if the average hydraulic conductivity values are equivalent (Britton and Filz 2007, Yesiller and Shackelford 2010). However, since SBM maintains its softness even after its construction, it is technically and

Photo 3.1 Various piezocone probes (Robertson 2009a)

economically difficult to collect high-quality solid core samples to assess the homogeneity of constructed SBM cutoff walls. Therefore, in-situ quality control/quality assurance (QC/QA) methods for SBM cutoff walls should be developed. In this chapter, applicability of piezocone test (CPTU) (see Photo 3.1) as QC/QA method is experimentally verified.

3.2 Variability in hydraulic conductivity in the field

3.2.1 Sources of variability in hydraulic conductivity

Since laboratory devices can only permeate relatively small specimens of soil; in situ tests offer the opportunity to test larger, more representative volumes of material and to include flow through secondary features, e.g., macropores, fissures, and slickensides, in a manner that often cannot be simulated properly in small, laboratory test specimens (Daniel 1989). Not only such scale effect but also many sources may cause the variability in k value of vertical/sloping cutoff walls in the field. Evans (1993) mentioned the following three factors to raise the variability in SBM: 1) Natural variability in the base soils, 2) accumulation of soil particles at the bottom and 3) time-dependent chemical interactions. First, there is always some degree of natural variability in the base soil's composition, especially if the base soil is the excavation spoils from the trench and not an off-site soil from a more homogeneous source. For example, Bergstom et al. (1987) measured a mean and standard deviation in fines content of field-mixed soil-bentonite, which strongly influences hydraulic conductivity, of 43.5% and 7.4%. Second, there may be a significant accumulation of soil particles at the bottom of the trench or on the sloping backfill due to settlement through the support slurry or spalling from the trench walls. Third, there may be time-dependent changes in the hydraulic conductivity of cutoff walls from point to point due to chemical interactions and wetting/drying and freezing/thawing cycles of the wall material (Kraus et al. 1997, Malusis et al. 2011).

Barvenik and Ayres (1987) discussed variability in the amount of bentonite added to the base soil and the degree of mixing of the backfill. Ryan (1987) found, using field sample test data from approximately thirty soil-bentonite cutoff wall projects, that both the average permeability and the deviation from the average were reduced at increased dry bentonite contents. This observation indicates that higher bentonite contents may reduce the variability from mixing. Manassero (1994) added to the list by mentioning cracks caused by large deformations of the surrounding ground, which may be more likely for the brittle cement-bentonite walls.

The sources of variability can be categorized into two groups.

- ✓ The SBM itself: This category is greatly dependent on the mixing procedure and intensity. Besides, it includes variations in the composition of the base soil used in the

SBM and variations in the bentonite content from place to place in the cutoff walls.

- ✓ Variability induced by the environment: This kind of variability may not develop until well after construction of the cutoff wall, and may be difficult to detect and/or anticipate: 1) Variations in hydraulic conductivity with depth due to variations in effective stress with depth and time (Evans 1995, Filz et al. 2001), 2) various chemical interactions with the SBM, 3) wetting/drying and freezing/thawing cycles and 4) high *k* defects due to cracking or large deformations of the cutoff wall.

In addition to those factors, variability of hydraulic barrier performance in the cutoff walls will be caused by the construction processes itself especially when they are processed by TRD method. Since the ground is invisibly cut by a chain and the bentonite slurry and bentonite powder are added to the in-situ soil under the ground, there is no way to check the quality directly and visibly. Hydraulic defects are sources of variability that have been identified as having a major impact on the performance of cutoff walls. Tachavises and Benson (1997) investigated the influence of defects on the flow rate through cutoff walls. They used a three-dimensional numerical groundwater model to show that even relatively small, fully penetrating, high permeability defects can render a wall ineffective at reducing the flow rate, while partially penetrating defects or defects of moderate permeability are not nearly as significant. Britton et al. (2005b) numerically demonstrated that the influence of variability is greatest when the hydraulic gradient and concentration gradient act in opposite directions, which is the case with an inward directed hydraulic gradient.

3.2.2 Case histories with variability in hydraulic conductivity of SBM samples

Five case histories have been collected where laboratory hydraulic conductivity tests were made on samples of SBM obtained in the fields, usually grab samples obtained during cutoff wall construction (Barvenik and Ayres 1987, GeoSyntec Consultants 1997, Hayward Baker Inc. 1998, Koelling et al. 1997, Zamojski et al. 1995). In all cases, SBM cutoff walls were used to contain contaminants. Britton et al. (2005b) summarized the type and number of samples and the type of hydraulic conductivity test equipment for each case history with *k* value and its standard deviation as shown in Table 3.1.

For each case history, the data set of *k* was converted into a data set of the negative logarithm of hydraulic conductivity, -log *k*. Table 3.1 shows the average and standard deviation of each data set of *k* and -log *k*. A wealth of evidence suggests that the log-normal probability density function provides a good fit for soil hydraulic conductivity (Freeze 1975, Hoeksema and Kitanidis 1985, Sudicky 1986, Russo and Bouton 1992). Both the normal function and the log-normal function were evaluated as fits for the hydraulic conductivity data from the five case histories. This was done by evaluating the fit of the normal function to both the *k* data sets and the -log *k* data sets. A fit between the normal function and −log *k* data is equivalent to a fit between the log-normal function and *k* data. For the –log *k* data, Table 3.1 shows a range of standard deviation values for field-mixed soil–bentonite from 0.13 to 0.32. For comparison, the case histories compiled by Freeze (1975), which cover a variety of

Table 3.1 Case histories of SBM cutoff walls (edited by Britton et al. (2005b)).

Reference	Sample type	Test equipment	Number of samples	Average k (m/s)	Standard deviation (m/s)
Barvenik and Ayres (1987)	Grab	API	68	1.0×10^{-9}	9.5×10^{-10}
Barvenik and Ayres (1987)	Grab	API	68	9.1	0.32
GeoSyntec Consultants (1997)	Grab	Flexible wall	30	1.5×10^{-10}	4.8×10^{-11}
GeoSyntec Consultants (1997)	Grab	Flexible wall	30	9.8	0.13
Hayward Baker (1988)	Grab	Flexible wall	55	1.5×10^{-10}	1.5×10^{-10}
Hayward Baker (1988)	Grab	Flexible wall	55	9.9	0.30
Hayward Baker (1988)	Grab	Rigid wall	33	1.5×10^{-10}	7.8×10^{-11}
Koelling et al. (1997)	Grab	Flexible wall	15	3.0×10^{-10}	1.7×10^{-10}
Koelling et al. (1997)	Grab	Flexible wall	15	9.6	0.23
Zamojski et al. (1995)	Undisturbed	Flexible wall	54	2.2×10^{-10}	9.2×10^{-11}
Zamojski et al. (1995)	Undisturbed	Flexible wall	54	9.7	0.16

natural soils and rocks, have values of the standard deviation of -log k between 0.2 and 2.0.

3.2.3 Case histories with in-situ QC/QA for barrier materials

Manassero (1994) describes the possible usage of the piezocone penetration tests to provide a continuous assessment of k value for a cement-bentonite barrier. The assessment procedure uses an empirical relation between k and three piezocone penetration parameters: the pore pressure increment, the total point resistance, and the sleeve friction. Use of the piezocone in a hardened CB backfill that is relatively stiff, hard, and brittle may not give a reasonable estimation of k value because the cone penetration could cause cracking. Hydraulic conductivity measured from the piezocone pore pressure dissipation test in the standard mix slurry was found to be several orders of magnitude larger than laboratory and other in-situ measurements (Tedd et al. 1995a).

The more commonly used in-situ method for measurement of k is a single-well, falling-head or rising-head test, commonly termed a “slug test.” A slug test is initiated by causing an instantaneous change in the water level in a borehole through the sudden introduction or removal of a known volume of water. A rate of water rise or drop in a bore-hole after withdrawing or adding a known volume of water is measured and used to determine k value in the slug test. The recovery of the water level with time is analyzed as a graph of head versus time history. The slug test has been used routinely by hydrogeologists to evaluate k value of aquifers and aquitards (Hyder et al. 1994, Butler 1998). There are three fundamental problems in the interpretation of data from slug tests: 1) Available slug test analysis methods are applicable to porous media that extend infinitely in the horizontal direction; 2) the distance from the well to the edge of the wall is usually not known or even knowable; and 3) most methods of data analysis assume that the porous medium is incompressible and barrier materials such as SBM are highly permeable. Choi and Daniel

(2006a, b) conducted slug tests in vertical cutoff walls for *k* assessment. By this method, the *k* value can be assessed with relatively high accuracy since a well is directly placed inside cutoff wall. In this case, however, since the thickness of cutoff wall gets thin due to the well installation, backfill of the borehole is necessary to maintain the hydraulic barrier performance after the assessment. Britton et al. (2005a) described the procedures for performing slug tests using a push-in piezometer tip to produce measurements of *k* value of SBM backfill that are in very good agreement with the results of other reliable test methods. By performing falling head tests and evaluating the data over a limited range of head drops, it was not necessary to complicate data reduction by taking backfill compressibility into account for the measurement. However, he suggested that the excess heads/hydraulic gradient applied in falling head tests must be small to avoid hydraulic fracture because the effective stresses in the backfill are small.

Table 3.1 lists representative examples of methodologies for *k* assessment with the type of barrier materials studied in previous researches. Benson et al. (1997) independently assessed the *k* value with four different tests including two laboratory tests. One is sealed double-ring infiltrometer (SDRI), and another is two-stage borehole permeameters. Analysis of the test results shows that the two field-scale test methods generally yield similar hydraulic conductivities. Joshi et al. (2010) verified *k* value with laboratory test, CPTU and packer test on the slag-cement-bentonite cutoff walls with different age. The *k* value was evaluated from excess pore pressure dissipation during the CPTU; however, the value was unrealistically high due to axial leakage. The *k* values obtained from the self-boring permeameter were comparable with those obtained by the falling-head and constant-flow packer system. Nishigaki and Komatsu (2007) developed and applied an air entry permeameter (Bouwer 1966) modified with combining a moisture sensor on SBM liner. The *k* value of 10^{-8} m/s order of magnitude could be measured accurately in 10 minutes. Tomura et al. (2005) conducted in-situ hydraulic conductivity test with a falling-head system and two slug tests: 1) normal slug test system which allows water drainage around the whole borehole, and 2) partially sealed slug test system which allows water drainage only from a bottom part. The test results confirmed that the values obtained from each test are in a same range.

Figure 3.1 schematically shows some configurations in Table 3.2. The field assessment should take advantages of each method, such as testing time, simpleness, cost-efficiency, or accuracy, however, a continuous assessment should be performed to assure the homogeneity of constructed cutoff walls.

3.2.4 Piezocone for hydraulic conductivity assessment

CPTU is commonly used to estimate profiles of soil characteristics; and its interpretations for results are particularly addressed by some researchers (e.g., Jeffries et al. 1993, Lunne et al. 2007, Robertson 2009b). There are several advantages of the CPTU in measuring *k* of vertical barriers. The method is fast and cost effective. A continuous log of *k* value versus depth can be obtained. This point is essential for the confirmation of high hydraulic barrier performance

of cutoff walls because the k values for grabbed samples during construction are not continuous, and some values will represent for the quality of whole cutoff walls. Furthermore, CPTU is an assurable method. A disadvantage is that the CPTU permeates only a tiny volume of material relative to other in-situ test methods. This method may, on insertion into the barrier, create sufficient disturbance (or even cracks) to alter k value. Tedd et al. (1995b) conducted CPTU on cement-bentonite slurry trench cutoff walls to measure the in-situ hydraulic properties. He concluded that excess pore pressure dissipation tests do not give representative k value for the hardened slurry; however cone resistance profiles have provided some interesting data about the wall properties.

Britton et al. (2004) measured k values of pilot-scale SBM backfill using five different tests: 1) Laboratory tests in American Petroleum Institute (API) filter press test, 2) global measurement of average hydraulic conductivity, 3) piezometer test, 4) excess pore pressure dissipation test during piezocone sounding and 5) laboratory tests on undisturbed samples. For the API filter press test, grab samples were taken during the backfilling stage. For laboratory hydraulic conductivity test, undisturbed samples were obtained during destructive evaluation of the cutoff walls. Comparing the test results, the following trend in k values can was observed:

$$k_{API} < k_{labtest} < k_{piezocone} < k_{piezometer} < k_{global}$$

The main factors differentiating these values were remolding and sample volume. The specimen fabrication process for test performed in API filter press equipment involves rodding the SBM into the filter press, however, the other four methods imparted less remolding and disturbance of samples. The sample volume for the tests also affected on the measured k values as shown in Figure 3.2.

Table 3.2 Case histories with in-situ measurement of k for barrier materials

Reference	Type of barrier material	Methodology
Benson et al. (1997)	Compacted clay liner	Sealed double-ring infiltrometer (SDRI)
		Two-stage borehole permeameters
Britton et al. (2004)	Soil-bentonite backfill	Piezometer test
		CPTU
Britton et al. (2005a)	Soil-bentonite backfill	Slug test
Joshi et al. (2010)	Slag-cement-bentonite	CPTU
		Packer test
		Self-boring permeameter
Manassero (1994)	Cement-bentonite slurry	Piezocone
Nishigaki and Komatsu (2007)	Soil-bentonite liner	Modified air entry permeameter
Tomura et al. (2005)	Soil-bentonite liner	Slug test

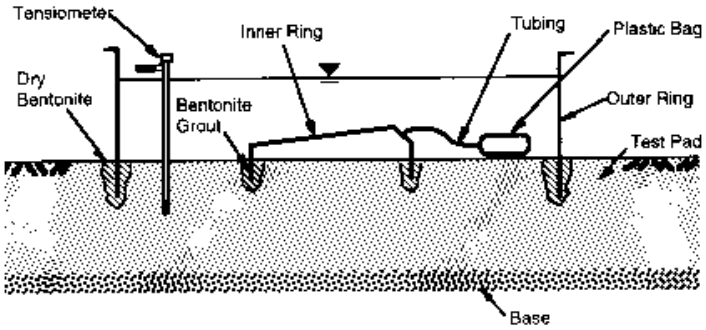

a) Sealed double-ring infiltrometer (SDRI) (Benson et al. 1997)

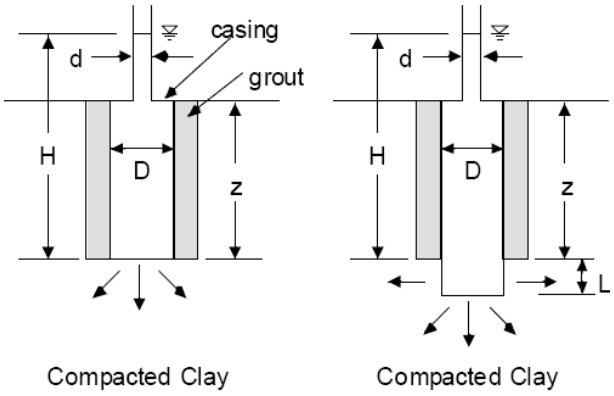

b) Two-stage borehole permeameter (Benson et al. 1997)

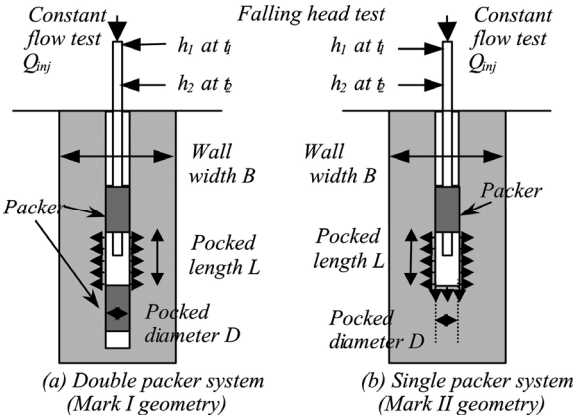

c) Packer test (Joshi et al. 2010)

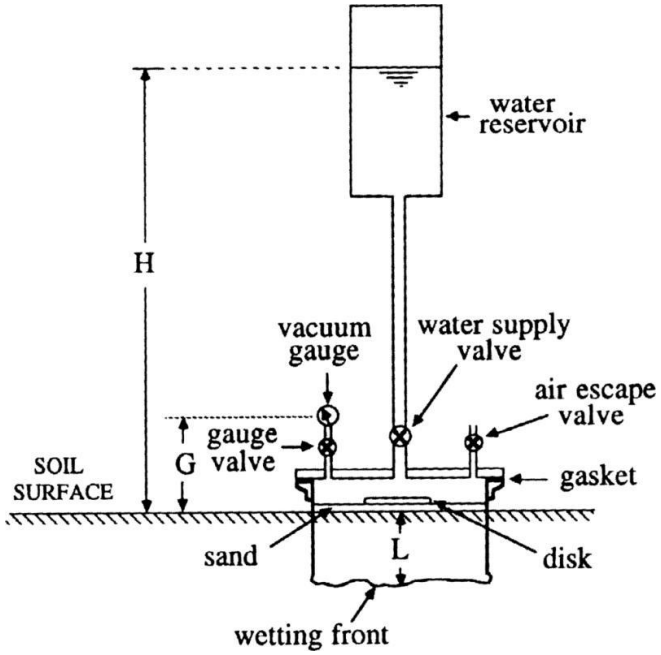

d) Air-entry permeameter (Topp and Binns 1976)

Figure 3.1 Schematic view of various in-situ methods for *k* assessment.

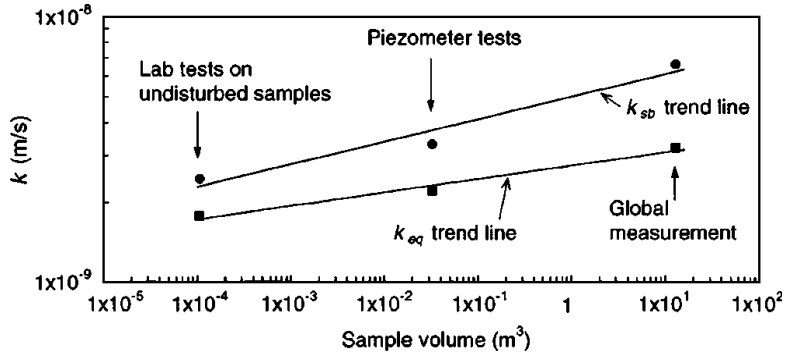

Figure 3.2 Comparison of average k value and equivalent k value versus sample volume.

Joshi et al. (2010) also conducted both laboratory and in-situ hydraulic conductivity tests on the slag-cement-bentonite slurry trench cutoff walls as described in the previous section. The results confirms that the k values determined by in-situ testing were larger than those found from laboratory testing. This observation can be primarily due to inclusions and fissures that form a network of flow paths leading to a higher k value for larger-scale test section. It is concluded that in-situ testing is better suited to estimate actual field behavior since it allows the testing of materials at various scales.

Thus, these observations derive that CPTU cannot evaluate the properties of hard barrier materials, such as cement-bentonite, however it is applicable for soft materials such as SBM cutoff walls.

3.3 Experimental methodologies for QC/QA method for constructed SBM cutoff walls

In this chapter, applicability of CPTU as a QC/QA method of constructed SBM cutoff walls is experimentally studied. Since the values of the physical properties obtained from CPTU, which are total cone resistance (q_c), sleeve friction (f_s), and pore pressure (u), change according to the soil characteristics, it is possible to classify the soil type by penetration. Therefore, CPTU may detect hydraulic fractures inside SBM cutoff walls. In this study, variability in k value caused by construction process was specifically verified. As confirmed in Chapter 2, lean-mix of bentonite may cause increase in k value. Since the termination of bentonite swelling is long when the bentonite can sufficiently swell, aggregation of bentonite powder (or lump) will possibly form during the construction. In such a case, variability in bentonite powder content may be caused from point to point. Thus, partial lean-mix of bentonite may exist inside the cutoff walls, which may results in hydraulic fracture.

3.3.1 Materials

For CPTU, SBM made with silica sand #7 and fine sand were used. To minimize the variability of base soil, these commercial products were employed. SBM samples were prepared according to the same procedure described in 2.3.1.4. Since much volume of soil samples were necessary for CPTU, a mortar mixer (PM-38G, Mazelar Co., Ltd.; 97 L, 40 rpm) was used to blend the soil with bentonite powder or bentonite slurry. To simulate the SBM cutoff wall with variability in k value, SBMs with bentonite powder content of 25, 50 and 100 kg/m^3 were prepared.

3.3.2 Experimental procedures

3.3.2.1 Laboratory CPTU

The feasibility of CPTU as QC/QA of SBM cutoff walls was studied using a large-scale soil tank in the laboratory. The cone probe used in this study is schematically drawn in Figure 3.3. An additional probe can attached to the cone to provide wet density of a small volume around the probe together with other usual three parameters of q_c, f_s and u (e.g. Shibata et al. 1993, Mimura and Yoshimura 2007), but this function to measure wet density was not employed in this study to verify an applicability of standard CPTU for QC/QA. The probe used in this study has 35.6 mm in diameter (= 10 cm^2 in its section area) and a ceramic filter for pore pressure measurement is located on a shoulder of the cone tip. One thermometer and two inclinometers are also embedded in the probe as shown in the figure.

The detailed view of large-scale soil tank used for CPTU is shown in Figure 3.4. The soil tank has 1.0 m in inner diameter and 0.8 m in height. A self-standing steel mesh with 0.5 m diameter was set in the center of soil tank. The mesh played the role of a boundary between

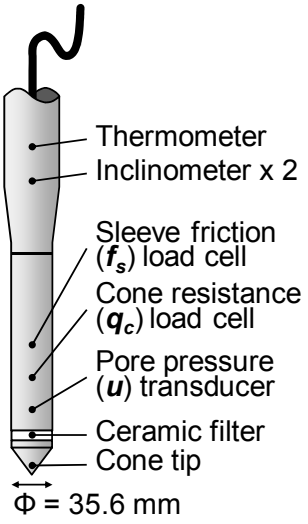

Figure 3.3 Schematic diagram of cone probe

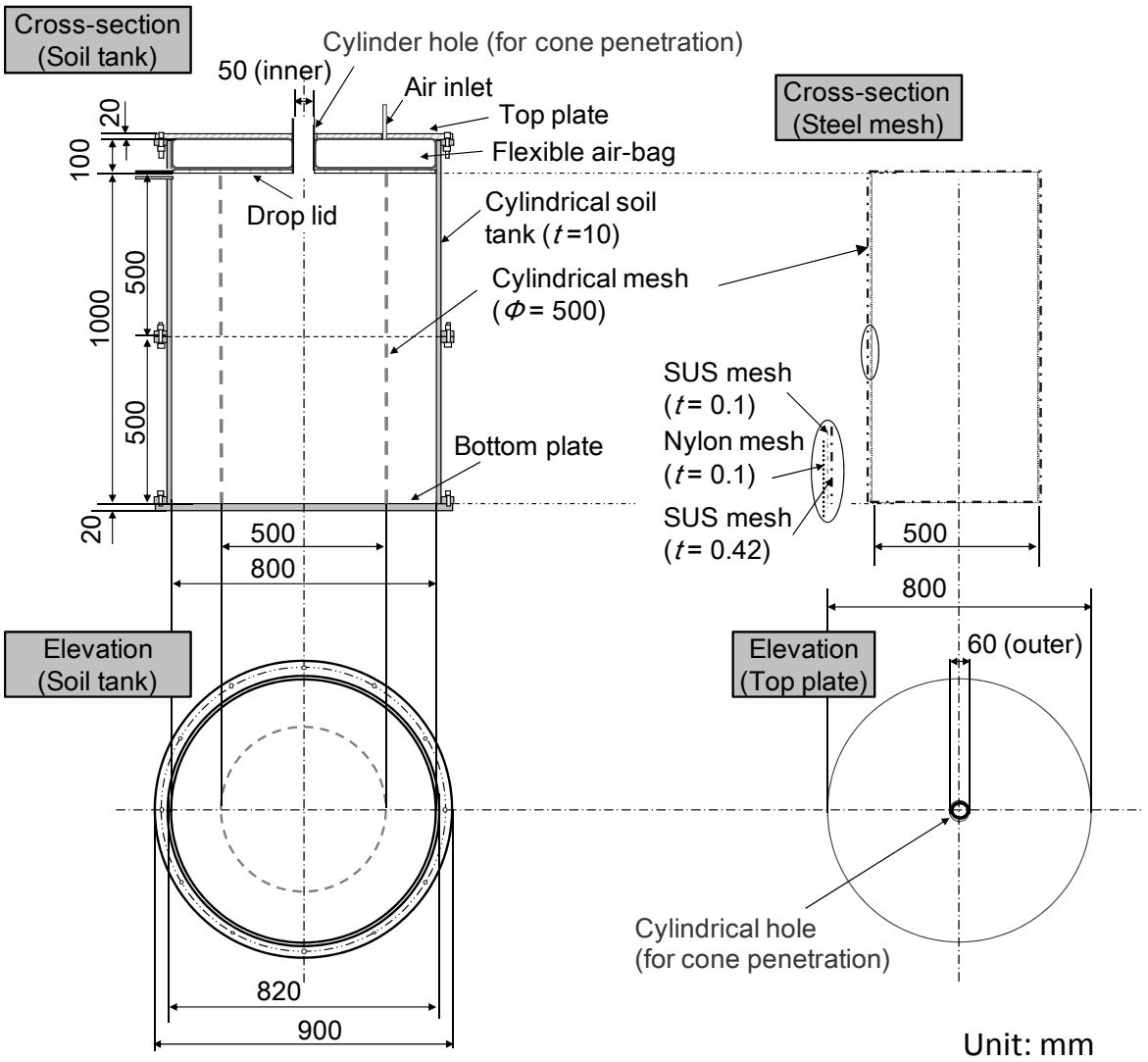

Figure 3.4 Schematic diagram of soil tank and belongings for Piezocone test.

SBM layer and surrounding soil layer and it allowed drainage from SBM layer during cone penetration. Rubber packings were placed at each contacting face (upper and lower tank, or with top/bottom plates) not to allow water leakage from the connection parts. A circular hole of 5.0 cm diameter is equipped on the top steel plate for cone penetration. Air pressure can be supplied on the surface of soil layer via an flexible air-bag to avoid any volume change of the soil layers. To transport the air pressure equally on the surface, A drop lid was placed between soil surface and air-bag. During the cone penetration, the specimen was loaded with air pressure of 30 kPa. Soil layers in the soil tank was prepared by the following procedure:

1) The lower half (0.5 m) of the cylindrical steel mesh was filled up with SBM of known C_{BP} with a target mean wet density, and surrounding part outside the steel mesh was filled up with fresh base soil in approximately 12 hours. Water level in the tank was kept higher than

the soil surface during preparation to assure that no air exists in the soil.

2) After jointing the upper tank to lower tank with the rubber packing and screws, the tank was left undisturbed for 12 hours to enhance the saturation degree inside specimen.
3) Afterward, the upper half (0.5 m) was filled up with SBM of same or different C_{BP} to achieve a target wet density, and surrounding part outside the mesh was filled up with fresh base soil in approximately 12 hours. Then, the tank was left for 12 hours again.
4) A top part was set up in the order corresponding to drop lid, flexible air-bag and top steel plate from bottom up with rubber packings and screws.
5) After the tank was left for several hours with the air pressure of 30 kPa, cone penetration was started with recording the penetration depth with a depth recorder.

The obtained data were automatically transmitted to a data logger (TDS-303, Tokyo Measuring Instruments Laboratory Co., Ltd.) and also to a PC. Thus, the data profiles could be monitored in real-time on the PC. At certain depth, the penetration was suspended to evaluate the k value with the pore pressure dissipation test. Target rate of penetration was set up to 1.0 cm/s to enhance the precision of detection, while the penetration rate of 2.0 cm/s is commonly used for the field investigations.

The experimental conditions for CPTU are summarized in Table 3.3. Figure 3.5 shows diagrammatic sketch of these testing conditions along with the depth for implementation of pore pressure dissipation test. In this figure, the dense color represents well bentonite added SBM layer, and the light color represents poorly bentonite added SBM layer. For both base soils, vertically homogeneous cutoff walls were simulated with different C_{BP} (Si-1, Si-2, Fi-1, Fi-2). In addition to these conditions, double or triple layers with different C_{BP} were subjected to CPTU to simulate vertically heterogeneous conditions. In Si-3, the lower half of the cylindrical steel mesh was filled up with SBM of C_{BP} = 100 kg/m^3, and the upper half was filled up with SBM of C_{BP} = 50 kg/m^3. In Si-4, multiple layers were made in the steel mesh. In this case, a SBM layer of C_{BP} = 50 kg/m^3, simulating a lean-mix part, was sandwiched in

Table 3.3 Experimental conditions for CPTU

Test No.	Base soil of SBM	C_{BP} (kg/m^3) – mean wet density (g/cm^3)			Depth for pore pressure dissipation test (m)
		Upper half		Lower half	
Si-1	Silica sand	100 – 1.87		100 – 1.87	G.L.-0.50, 0.75
Si-2		50 – 1.93		50 – 1.93	
Si-3		50 – 1.91		100 – 1.87	G.L.-0.75
Si-4*		100 – 1.87	50 – 1.91	100 – 1.87	
Fi-1	Fine sand	100 – No data		100 – No data	G.L.-0.25, 0.75
Fi-2		25 – 1.81		25 – 1.81	

* Three layer condition

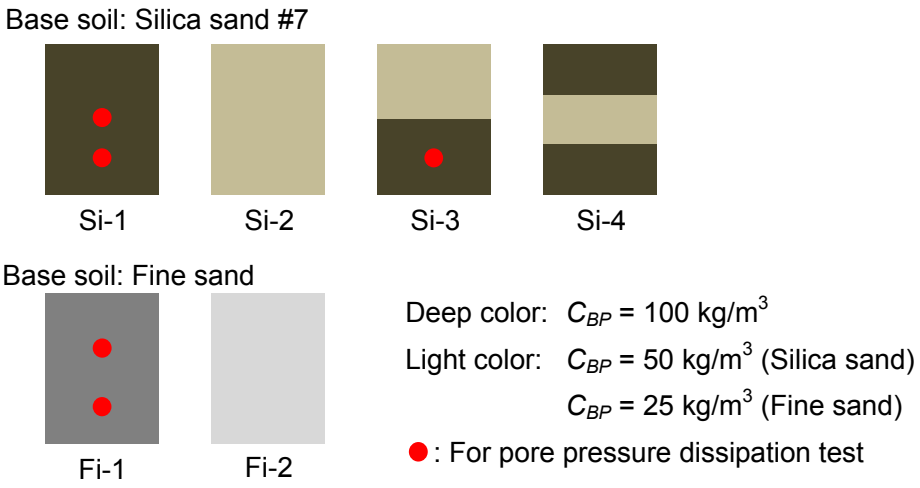

Figure 3.5 Diagrammatic sketch of each condition

between two SBM layers C_{BP} = 50 kg/m^3. In this testing case, top and bottom SBM layers of C_{BP} = 100 kg/m^3 have 0.35 m thickness, and the intermediate SBM layer has 0.30 thickness. Wet density of each SBM layer was determined based on the property after the hydraulic conductivity test.

3.3.2.2 Unconsolidated-Undrained triaxial compression test

To evaluate the strength-deformation characteristics of SBM, triaxial compression test was conducted under unconsolidated-undrained (UU) condition according to JGS 0521-2009 (JGS 2009) with a standard laboratory-scale specimen. The characteristics were evaluated under UU condition to be able to compare the results from triaxial compression test and CPTU in the aspect of strength. Considering a practical implementation, the QC/QA using CPTU will be operated almost immediately after the construction of the cutoff wall to ensure the quality; thus, the consolidation inside the cutoff wall does not begin at the moment, corresponding to UU condition in the triaxial compression test.

The specimens were prepared using a halved cylindrical acryl tube (50 mm in inner diameter and 100 mm in height). After the tube was filled with SBM with known wet density, the specimen was saturated by submersion in a tank by using a vacuum deaerator for 7 days. The wet densities correspond to that of specimen in the soil tank for CPTU. After the saturation step, the cylindrical specimen was placed between filter papers, and caps (cap and pedestal). The chamber of triaxial compression test was build up, and then, the specimen was subjected to UU triaxial compression test. The vertical strain rate was set up to 1.0%/min during the compression process. The compression continued until the vertical strain of 15% was achieved. The test was conducted with the confining pressure of 10, 20, and 40 kPa in consideration the fact that the vertical effective stress is approximately 40 kPa at the bottom in the soil tank during CPTU. To verify the characteristics of pore water pressure increase in CPTU, pore water pressure was also measured during the compression.

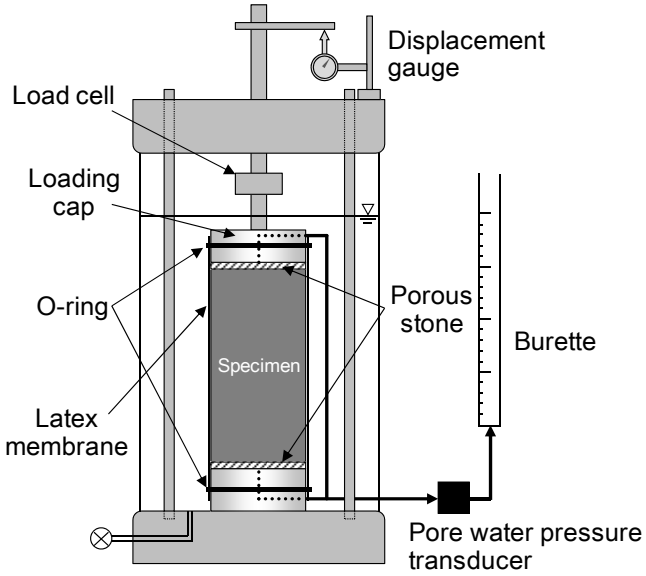

Figure 3.6 Schematic diagram of triaxial compression test apparatus.

3.4 QC/QA for SBM cutoff walls using piezocone

In this study, physical property of SBM was evaluated by three continuous data of q_c, f_s and u. Furthermore, k value was evaluated by implementing pore pressure dissipation test with a temporal suspension of cone penetration.

3.4.1 Post-construction verification

Vertically continuous changes with penetration depth in each experimental condition are shown in Figure 3.7~3.10 for silica sand-based SBM and in Figure 3.11 and 3.12 for fine sand-based SBM. Each graph in the figures illustrates SBM composition in the soil tank, corrected cone resistance (q_t), sleeve friction (f_s), and pore water pressure (u), respectively, from left to right.

As shown in Figure 3.7, when SBM was made by adding bentonite with 100 kg/m^3, which simulates well bentonite added part in the actual condition, obtained q_t and f_s values are extremely low enough to be almost zero. This is because of high flexibility and softness, which are SBM's especially-important characteristics. In contrast, a maximum value of q_t from SBM layer with 50 kg/m^3 bentonite powder is approximately 4.1 MPa as shown in Figure 3.8. Since SBM with 50 kg/m^3 bentonite powder contains less clay fraction (approximately 6%) and is classified into sandy gravel (SG) according to JGS 0051-2009, SBM behaved almost similar with pure sand. Considerably variable u values are measured in both cases and the lower values than the hydrostatic pressure are observed in some depth due

to positive dilatancy during the cone penetration. Generally, cone resistance values and sleeve friction values from sand stratum are higher than those values from silty soil and/or clay stratum due to their particle sizes (e.g. Pradhan 1998, Mayne et al. 2009). Considering cutoff walls are mainly constructed in sand stratum, partial lean-mix of bentonite in constructed SBM cutoff walls may also acts as sand stratum.

Figure 3.9 shows CPTU results conducted on SBMs with double layer structure. These results indicate that three values change notably around 0.5 m depth, which is the boundary of the two different compositions of SBM. The q_t values in upper layer (C_{BP} = 50 kg/m^3) become larger than those in lower layer (C_{BP} = 100 kg/m^3). In the upper layer, the q_t values attain approximately 1.3 MPa, and in the lower layer it is approximately 0.1 MPa regardless of the depth. The maximum value in upper layer of 1.3 MPa is small compare with the result of mono-layer of the same SBM composition (4.1 MPa, see Figure 3.8) because of the higher flexibility and compressibility of lower half, which was filled up with SBM of C_{BP} = 100 kg/m^3. Similarly for f_s values, higher values were attained in the upper layer than in the lower layer. Although larger variations were observed on f_s values, the same trend as q_t can be confirmed. However, considering the facts that 1) the f_s values in Figure 3.7 and Figure 3.8 are extremely low regardless of C_{BP} and 2) the f_s values at the soil surface is not zero, the uncertainty of measurement and calibration of the sensors could have been occurred. Pore water pressure values in the upper layer became so reduced that reached negative values, and those in the lower layer recovered until they reached values near the hydrostatic pressure. Figure 3.10 shows profiles obtained from SBMs with three layers. This result clearly confirms that q_t values in the middle layer (C_{BP} = 50 kg/m^3) are larger than the values in the top and bottom layers (C_{BP} = 100 kg/m^3). In the middle layer, the q_t values attain approximately 1.9 MPa, and in the lower layer it is approximately 0.1 MPa regardless of the depth. Pore water pressure values also has obviously different trend in the middle layer and in the top and bottom layers. Furthermore, the fact that the f_s values are almost zero regardless of the penetration depth is consistent with the results in Figure 3.7 and Figure 3.8. Although excess pore water pressure was generated in the top and bottom layers, u values in the middle layer are negative values throughout the layer. These results indicate that CPTU has some possibility to be able to detect hydraulic defects in SBM cutoff walls when the physical properties in the lean-mix part are obviously different.

However, the physical properties obtained from CPTU are almost equal for both cases of fine sand-based SBMs as shown in Figure 3.11 and Figure 3.12. This is because of the high flowability of SBMs regardless of C_{BP} as shown in Table 3.4. Considering the fact that SBM with 25 kg/m^3 bentonite has flow value of 145 mm, although that of SBM with 100 kg/m^3 bentonite is 140 mm, SBM with 25 kg/m^3 cannot resist to the cone strike and deforms as fluid. In contrast, the u value continues to increase with same rate regardless of SBM composition. These facts confirm that the profiles of physical properties are varied by base soil, and preliminary calibration is necessary when CPTU is applied in the field. If the profiles of physical property have no significant differences with C_{BP}, CPTU should overestimate the

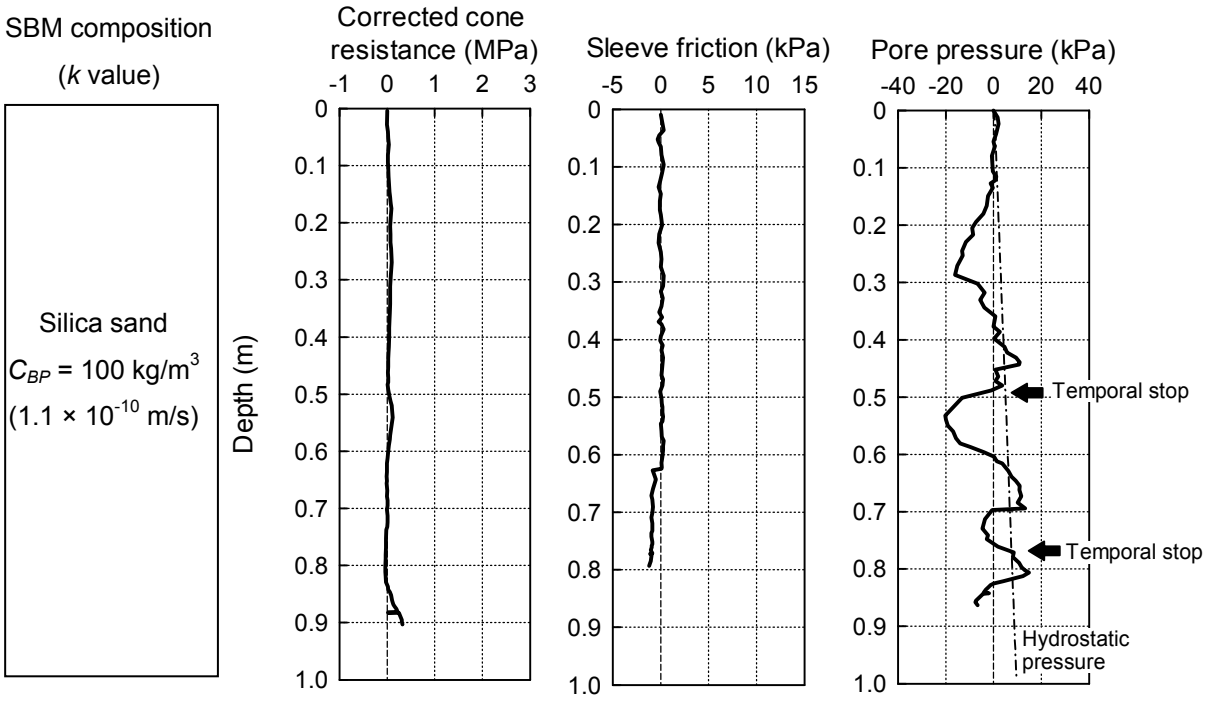

Figure 3.7 CPTU results (Si-1)

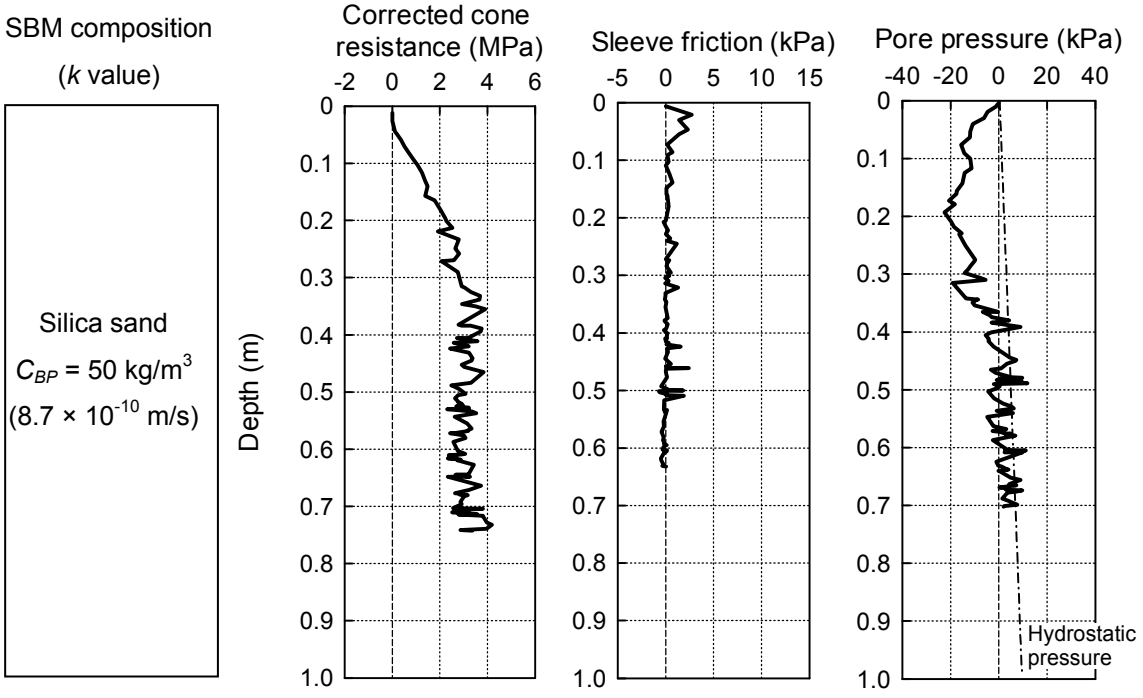

Figure 3.8 CPTU results (Si-2)

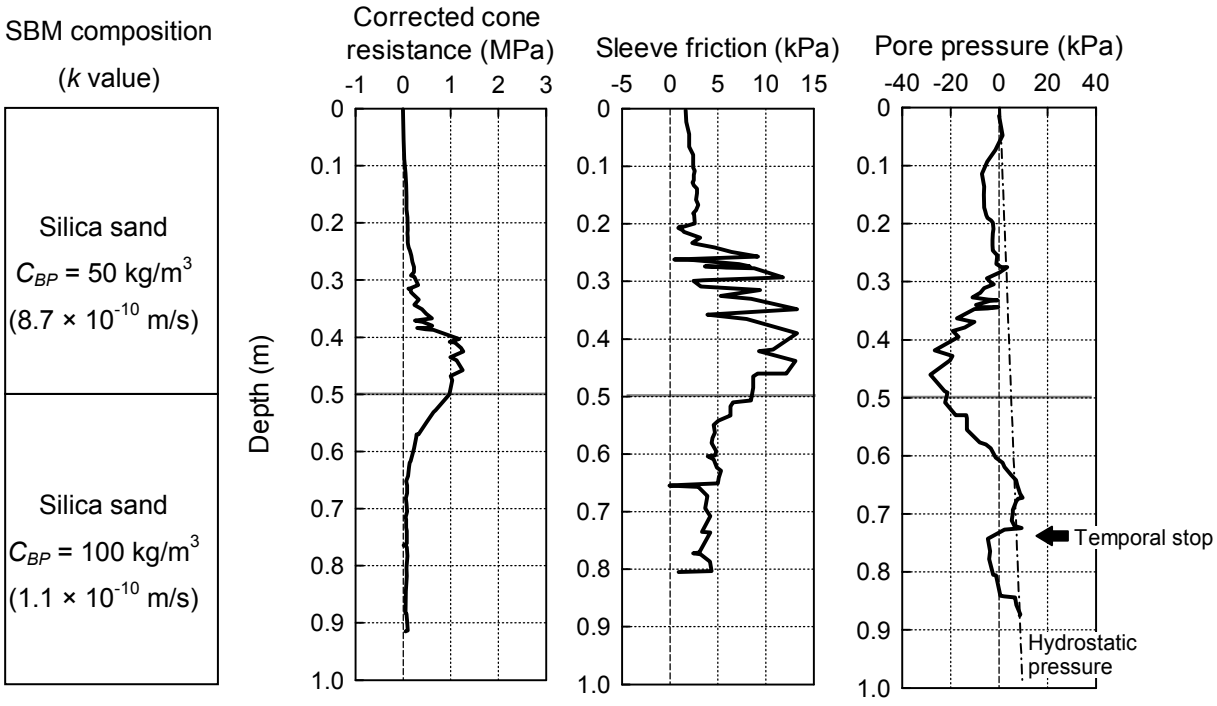

Figure 3.9 CPTU results (Si-3)

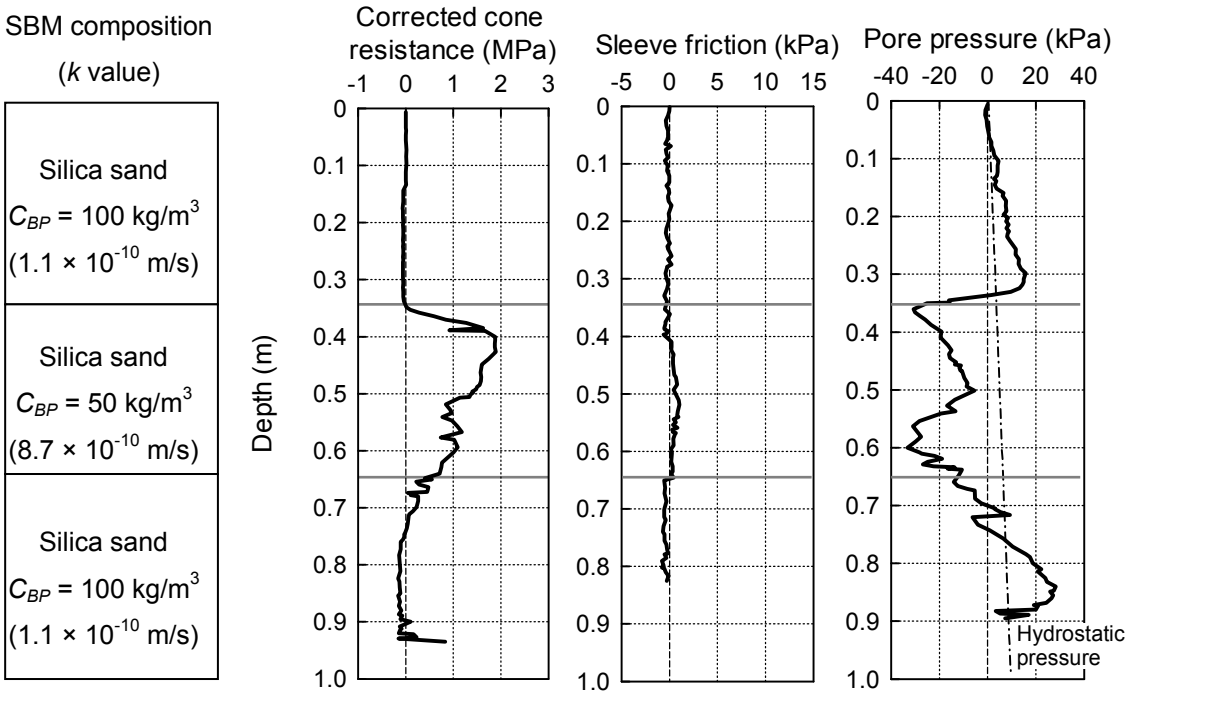

Figure 3.10 CPTU results (Si-4)

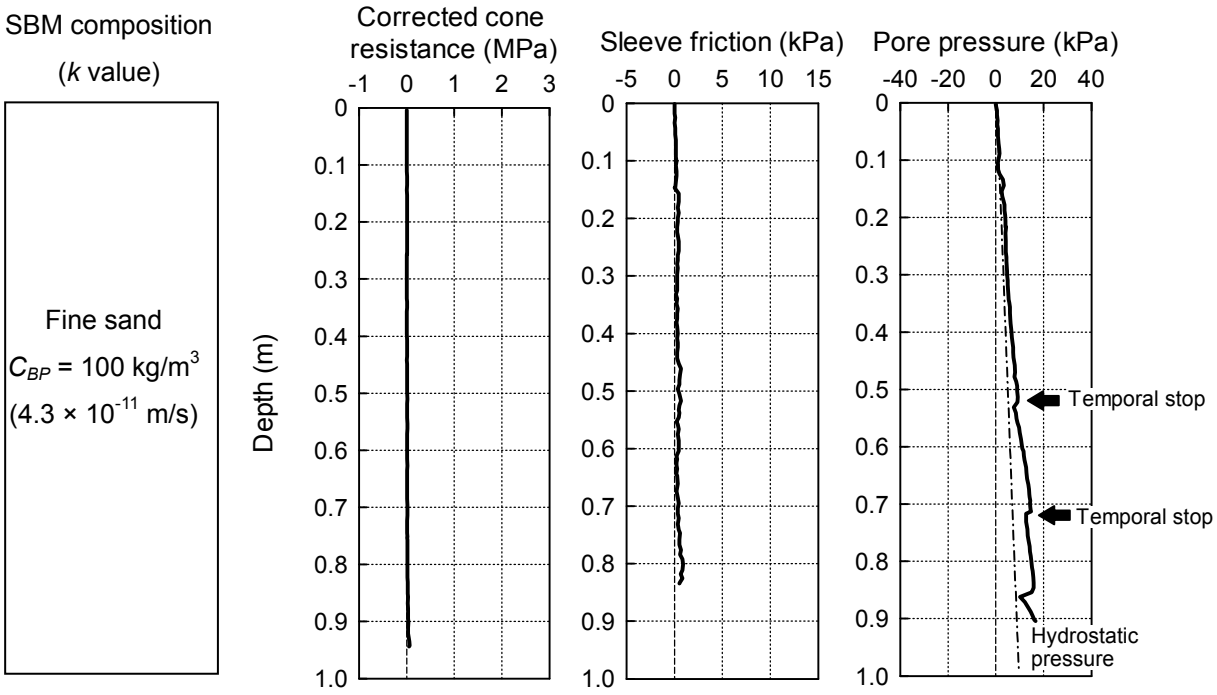

Figure 3.11 CPTU results (Fi-1)

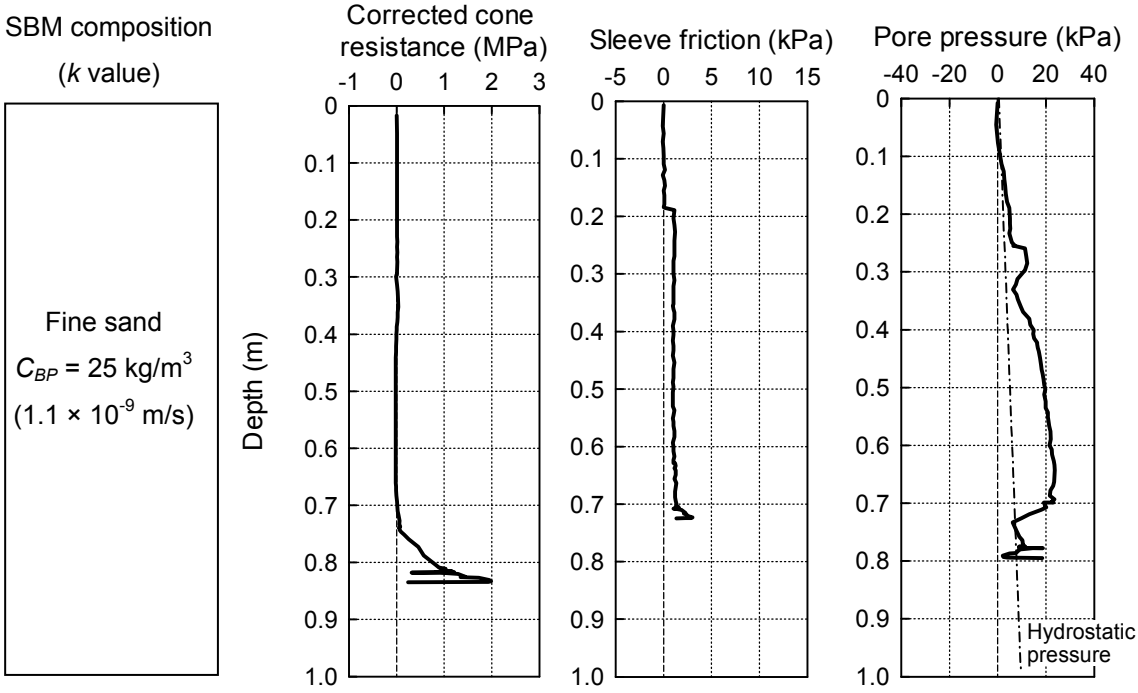

Figure 3.12 CPTU results (Fi-2)

homogeneity of SBM cutoff walls; however, CPTU can be employed when those profiles have significant differences.

Figure 3.13 shows results of unconsolidated-undrained triaxial compression test on silica sand-based SBM. As shown in this figure, clear peaks are not observed in deviator stress changes with time regardless of content of bentonite powder. These results indicate that SBM presents ductile fracture against the compression due to its high softness. Although pore water pressure of SBM with C_{BP} = 100 kg/m^3 is kept with constant positive value during the compression, that of SBM with C_{BP} = 50 kg/m^3 decreased after 5% strain regardless of confining pressure. The values drop into negative values under confining pressure of 10 and 20 kPa. These results are consistent with the fact that pore water pressure lower than hydrostatic pressure was observed during CPTU. This is probably because SBM with C_{BP} = 50 kg/m^3 behaves like sand due to less bentonite, and negative dilatancy occurred during the shearing step. Particles run on other particles with compression and sharing because silica sand is poorly-graded sand material. In contrast, a significant difference is not observed between two fine sand-based SBMs as shown in Figure 3.14. This is because fine particles are originally contained in the fine sand to some degree, therefore, the contact between particles are maintained even during the shearing steps.

Table 3.5 summarizes undrained shear strength of SBMs obtained from triaxial compression test. As explained above, the undrained shear strength is increased with lower bentonite content for silica sand-based SBM; however, significant difference is not observed for fine sand-based SBM. Figure 3.15 illustrates relationship between the undrained shear strength obtained by triaxial compression test and corrected cone resistance values from CPTU. Although further research should be conducted to confirm the correlation between these values, there is a possibility that the CPTU can detect the lean-mix part when the undrained shear strength is larger than 58 kPa. Therefore, the difference of q_t value with penetration depth can be used for the verification when SBM has significant difference in undrained shear strength with C_{BP}. Further research is necessary when SBM has similar shear properties regardless of C_{BP}; however, the trend of pore water pressure may change C_{BP} because the magnitude of pore water pressure increase is different by C_{BP} both in CPTU results and triaxial compression test results.

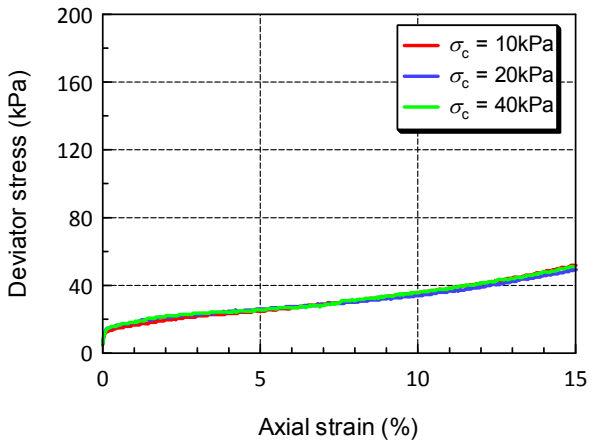

a-1) Changes in deviator stress with time

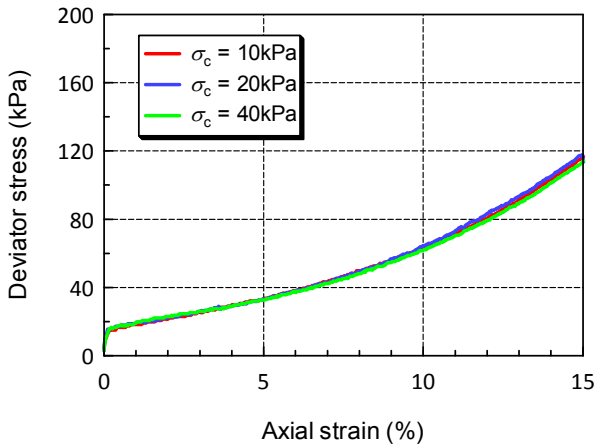

a-2) Changes in deviator stress with time

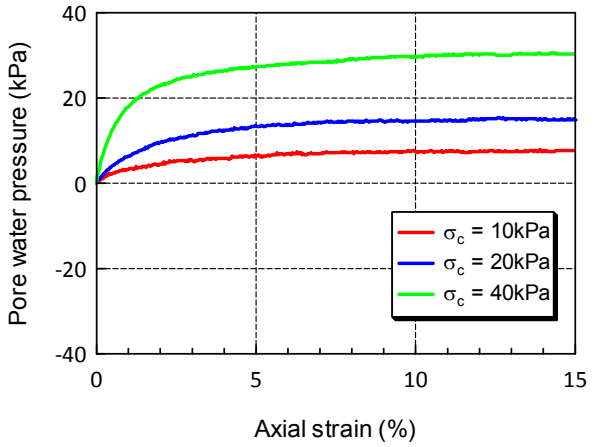

b-1) Changes in pore water pressure with time

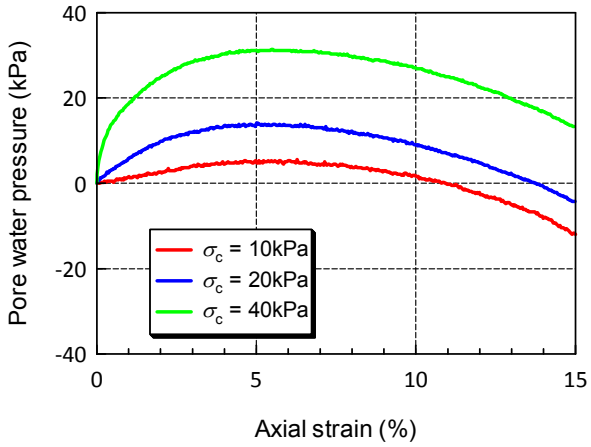

b-2) Changes in pore water pressure with time

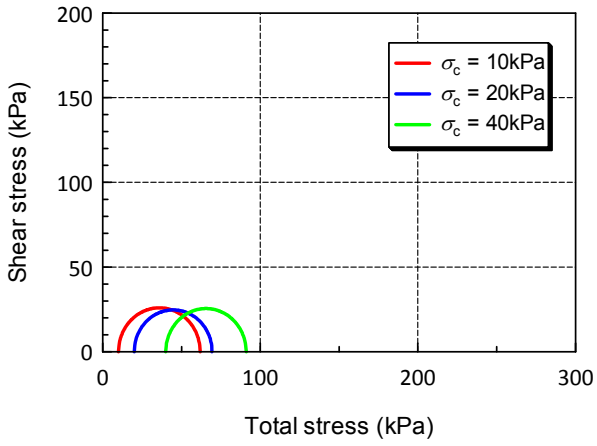

c-1) Mohr's circle about total stress

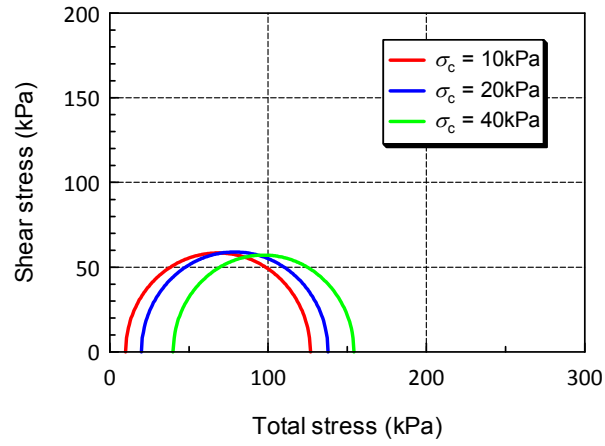

c-2) Mohr's circle about total stress

Figure 3.13 Results of triaxial compression test of silica sand-based SBM
(Left) C_{BP}: 100 kg/m^3, (Right) C_{BP}: 50 kg/m^3

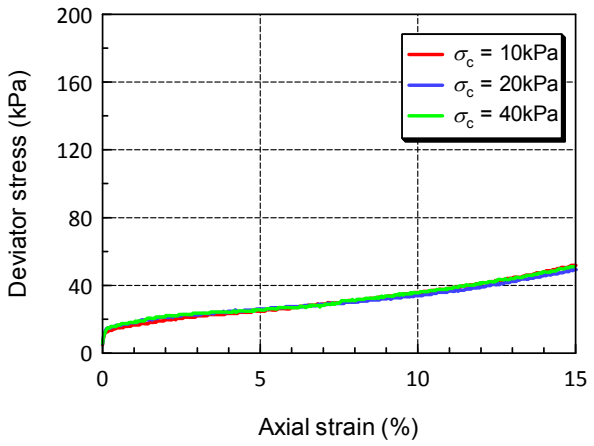

a-1) Changes in deviator stress with time

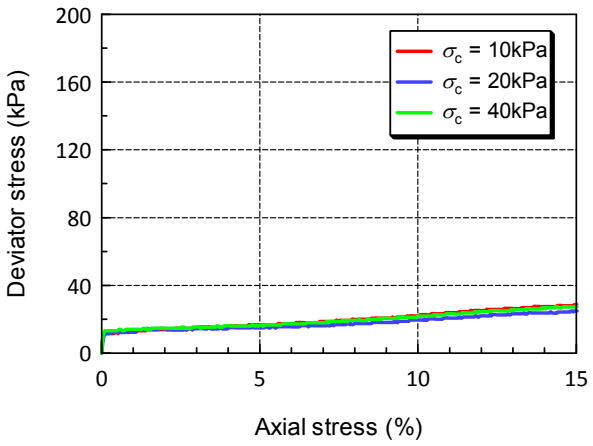

a-2) Changes in deviator stress with time

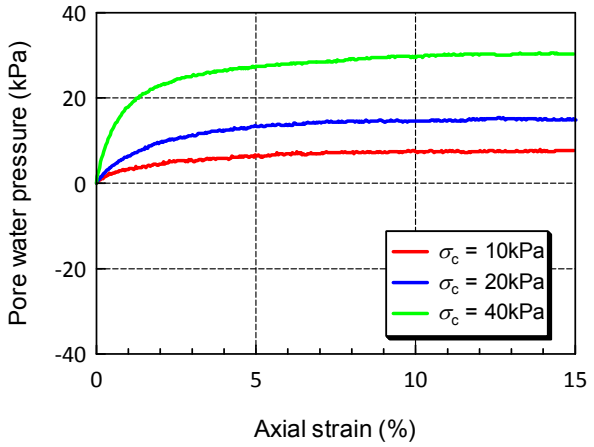

b-1) Changes in pore water pressure with time

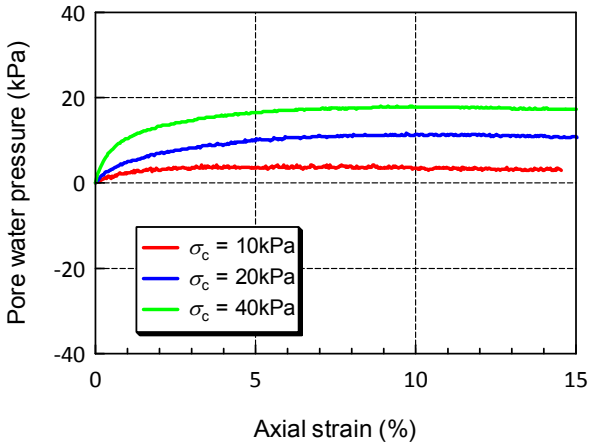

b-2) Changes in pore water pressure with time

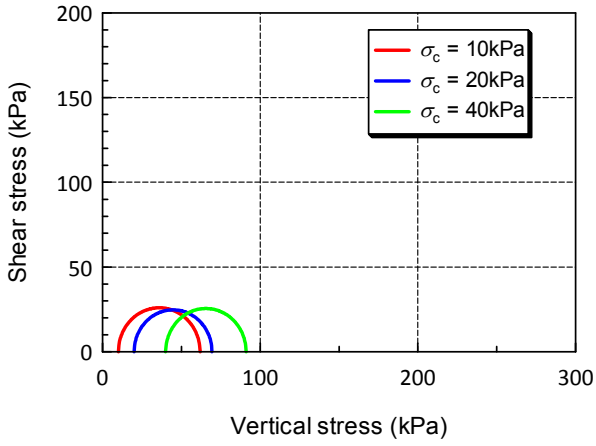

c-1) Mohr's circle for total stress

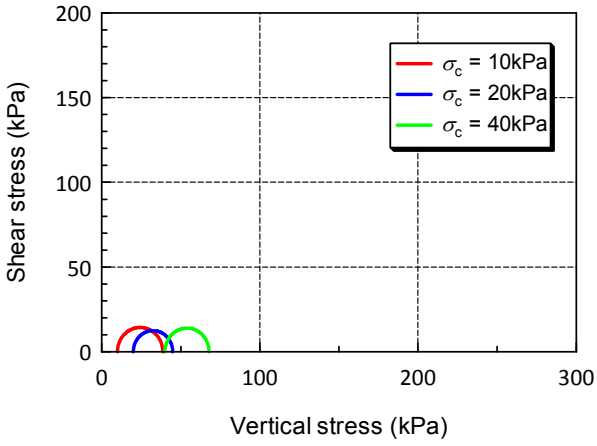

c-2) Mohr's circle for total stress

Figure 3.14 Results of triaxial compression test of fine sand-based SBM (Left) C_{BP}: 100 kg/m^3, (Right) C_{BP}: 25 kg/m^3

Table 3.4 Flow values of SBMs made with various content of bentonite powder

Base soil	Silica sand		Fine sand	
Content of bentonite powder (kg/m^3)	50	100	25	100
Flow value (mm)	10.33	12.83	14.45	14.05

Table 3.5 Effect of C_{BP} on undrained shear strength of SBM

Base soil	Content of bentonite powder (kg/m^3)	Undrained shear strength (kPa)
Silica sand	100	25.4
	50	58.1
Fine sand	100	20.3
	25	13.6

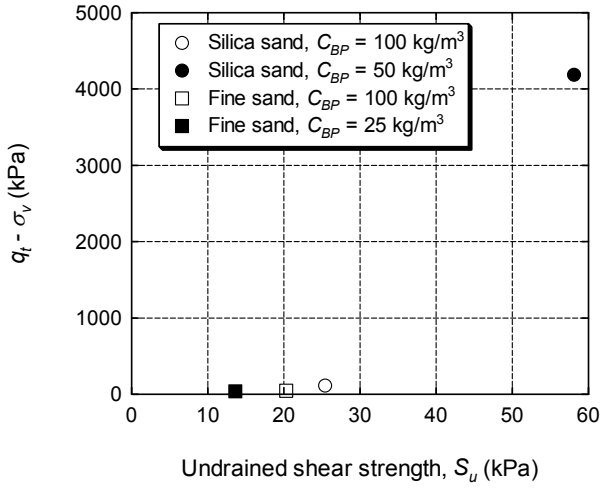

Figure 3.15 Relationship between undrained shear strength from UU test and cone resistance from CPTU.

3.4.2 Hydraulic conductivity assessment by pore pressure dissipation test

In this research, the pore pressures were collected at 1 second intervals at certain depth after cone penetration was suspended. Figure 3.16 shows a result of pore pressure dissipation test at 0.75 m-depth in Si-3. Here, degree of excess pore pressure dissipation (U) defined by the following equation (3.1) are plotted on the vertical axis. The horizontal axis is elapsed time with a logarithmic scale.

$$U = \frac{u_t - u_0}{u_i - u_0} \tag{3.1}$$

where u_t = pore pressure at time t (kPa); u_0 = hydrostatic pore pressure in situ (kPa); and u_i = initial pore pressure at start of dissipation test (kPa). Since dissipation rate varies by compressibility and permeability of the surrounding soil around the cone probe, hydraulic conductivity of SBM can be estimated by the dissipation process. In the calculation of hydraulic conductivity, it is frequently recommended to use the time for 50% dissipation, t_{50}. In this research, both of the time for 30% dissipation, t_{30}, and the time for 20% dissipation, t_{20}, were also used for the prediction to shorten the time for quality evaluation on-site.

After each time (t_{20}, t_{30}, and t_{50}) were determined from the experimental results, horizontal coefficient of consolidation was calculated from the following equation (3.2).

$$c_h = \frac{T^* R^2}{t\sqrt{I_r}} \times 8.64 \times 10^{-2} \tag{3.2}$$

where, c_h = horizontal coefficient of consolidation (m^2/day); T^* = time factor (-); R = penetrometer radius (= 17.8 mm); t = time (s); and I_r = rigidity index. Time factor T^* is a dimensionless factor that depends on the location of the pore pressure element, and analytically calculated as shown in Table 3.6 by Houlsby and Teh (1988) for the cone probe which has the element above cone base as used in this study. Rigidity index I_r of 25 was used for all SBMs with referring the average value of soft clay. Based on the calculated c_h, horizontal hydraulic conductivity can be estimated by the following equation (3.3).

$$k_h = \frac{c_h m_v \gamma_w}{8.64 \times 10^4} \tag{3.3}$$

where, k_h = horizontal hydraulic conductivity (m/s); c_h = horizontal coefficient of consolidation (m^2/day); m_v = coefficient of volume compressibility (m^2/kN); and γ_w = unit weight of water (= 9.81 kN/m^3). In this research, m_v values measured in the process of consolidation test was applied on the assumption that the compression of the surrounding of the probe is one-dimensional; the same as specimen in the consolidation test. Table 3.8 shows m_v values of each SBM obtained from the consolidation test. From the above equations, it can be seen that the k value estimated by the pore pressure dissipation test has an inverse correlation with time for the dissipation as shown in the following equation (3.4).

$$k_h = \frac{m_v \gamma_w T^* R^2}{t\sqrt{I_r}} \times 10^{-6} \tag{3.4}$$

Calculated horizontal c_h values and k_h values at each degree of excess pore water dissipation are summarized in Table 3.7. As shown here, the variation of values is negligible regardless of the degree of excess pore water dissipation. Moreover, the k values calculated by CPTU are in the range of 1.4 - 1.6 times of those values calculated by the hydraulic

conductivity test as shown in Figure 3.17. Figure 3.18 illustrates a relationship between k values obtained from the pore pressure dissipation test during CPTU with 50% dissipation and that values obtained from hydraulic conductivity test with 30 kPa confining pressure. In Si-2 and Fi-2, k values could not be measured because pore water pressure was not converged to hydrostatic pressure due to some error. The reasons why such error occurred have to be revealed in further research; however, the k values measured by the pore pressure dissipation test have good correlation with that values measured by hydraulic conductivity test. Overall trend of this relationship is that the k values from CPTU are larger than that from hydraulic conductivity test. This difference is caused probably because; 1) the piezocone permeates only a tiny volume of liquid, 2) water penetration in the hydraulic conductivity test is one-dimensional, while the pore water pressure during CPTU is dissipated three-dimensionally, 3) the soil tank test in this study allows two-dimensional drainage, even though the one-dimensional drainage will be occurred in a short time in actual conditions as shown in Figure 3.19. However, it is possible to measure k value by implementation of pore pressure dissipation test within one order of magnitude difference.

These observations confirm that k of SBM can be approximately estimated by the pore pressure dissipation test. This fact suggests that the operation of dissipation test is suitable as quality assurance for hydraulic barrier performance at post-construction of SBM cutoff walls.

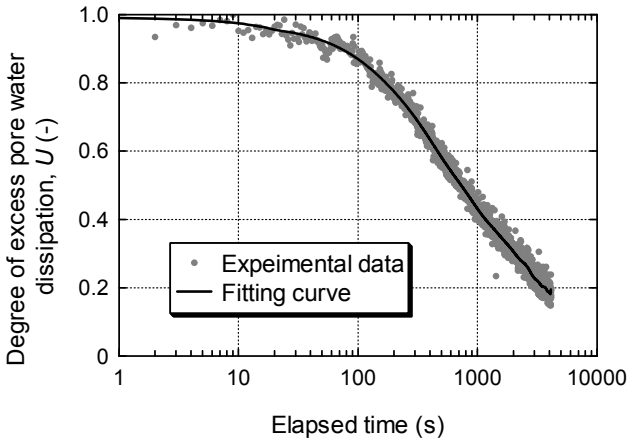

Figure 3.16 Example of pore pressure dissipation test result (Si-3, at 0.75 m-depth).

Table 3.6 Time factors T^* at each degree of dissipation (from Houlsby and Teh 1988)

Degree of dissipation (%)	Time factor (-)
20	0.038
30	0.078
50	0.245

Table 3.7 c_h and k at each degree of dissipation.

Degree of dissipation (%)	Horizontal coefficient of consolidation, c_h (m^2/kN)	Horizontal hydraulic conductivity, k_h (m/s)
20	2.5×10^{-3}	1.5×10^{-10}
30	2.4×10^{-3}	1.4×10^{-10}
50	2.9×10^{-3}	1.8×10^{-10}

Table 3.8 m_v values of each SBM obtained from consolidation test

	Content of bentonite powder (kg/m^3)		
	25	50	100
Silica sand	—	3.36×10^{-4}	4.20×10^{-4}
Fine sand	5.75×10^{-4}	—	8.24×10^{-4}

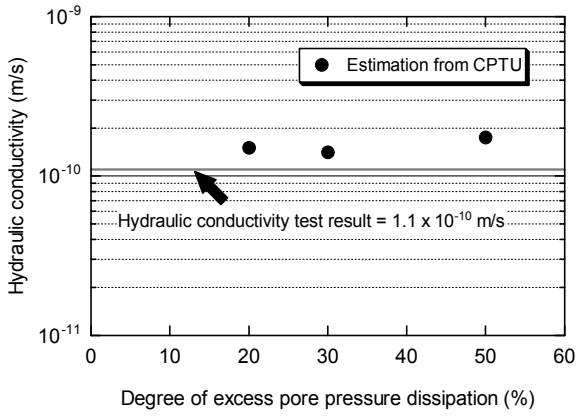

Figure 3.17 k values from CPTU at each degree of dissipation.

Table 3.9 k values obtained from each case at 50% dissipation.

Case No.	Depth from soil surface (m)	Hydraulic conductivity (m/s)
Si-1	0.5	2.3×10^{-10}
	0.75	8.5×10^{-10}
Si-3	0.75	5.7×10^{-10}
Fi-1	0.25	1.6×10^{-10}
	0.75	1.8×10^{-10}

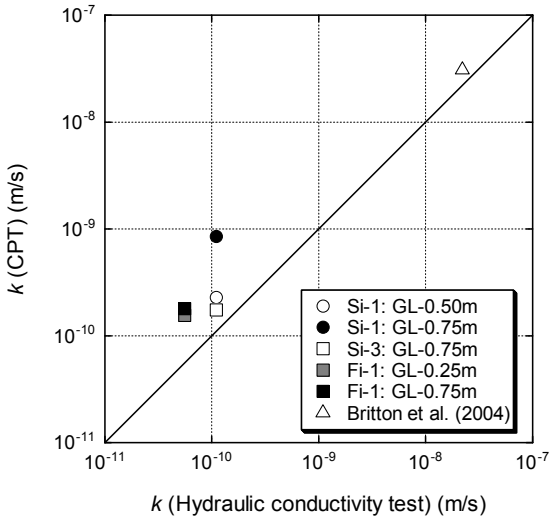

Figure 3.18 Comparison of k values from CPTU at 50% dissipation and from hydraulic conductivity test

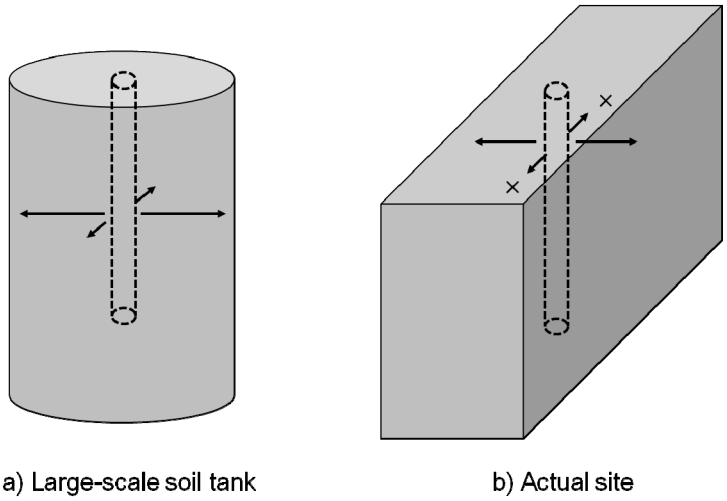

Figure 3.19 Horizontal directions of drainage around the probe

3.4.3 Self-sealing of borehole after CPTU

Borehole after CPTU must be sealed or refilled with another material with k value low enough to ensure adequate wall thickness. Since the high softness even after the construction is one of the most significant characteristics of SBM, unlike other hard materials, it can be expected that the boreholes after CPTU will be sealed by themselves given enough time.

Photo 3.2 shows the appearance of SBM layer in the soil tank before and after CPTU operation in case of Si-3. As seen in these photos, although a residual deformation due to the cone penetration is observed within approximately 2.0 cm depth, the deeper area of the borehole is sealed by SBM itself with time. Even though the self-sealing capability can be

confirmed only in the area where can be seen visibly, the borehole in deeper zone can be expected to be sealed due to higher earth pressure. These observations indicate that SBM cutoff walls can maintain the designed hydraulic barrier performance due to the self-sealing capacity even after CPTU operation.

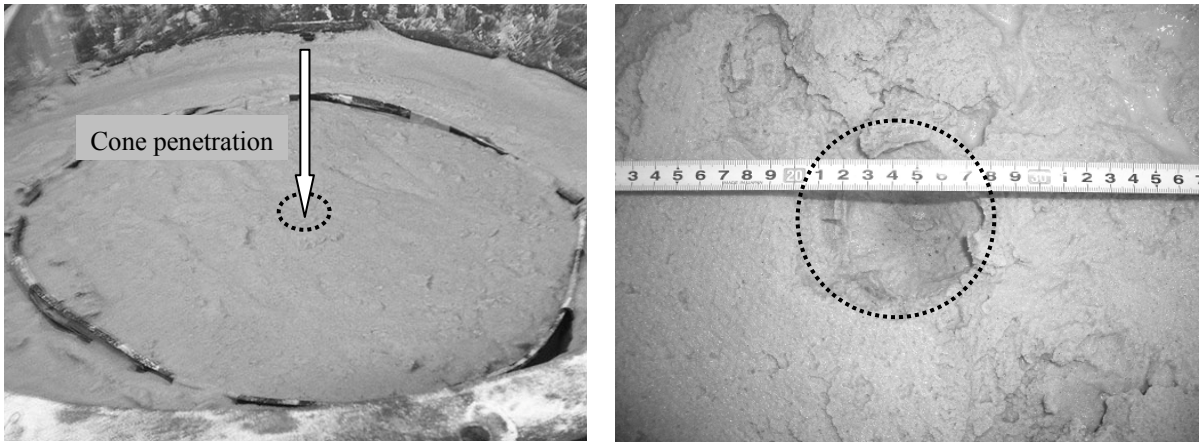

Photo 3.2 Appearance of soil surface in the tank (Left) before CPTU, (Right) after CPTU.

3.4.4 QC/QA flow by CPTU

As described above, although it depends on the soil type of original ground, SBM has different characteristics with different C_{BP}. Using this fact, QC/QA of constructed SBM cutoff walls should be implemented using CPTU as shown in Figure 3.20 after the laboratory-scale calibration to obtain the dependency of strength characteristic of SBM on bentonite powder amount.

First, CPTU should be operated on the constructed SBM cutoff wall to obtain the profiles of three physical properties, q_t and u at a certain intervals along the wall. If q_t values have variation with penetration depth or u values change with different rate, SBM cutoff walls may have heterogeneous part inside. In such cases, re-mixing of the cutoff wall by TRD method is required to enhance its homogeneity. If those values have constant values regardless of the penetration depth, the vertical homogeneity is reliable. After the verification of the homogeneity, pore pressure dissipation test should be implemented at a certain depth intervals to ensure the actual hydraulic barrier performance. Since the k values obtained from the pore pressure dissipation test have correlation with the k values from hydraulic conductivity test, pore pressure dissipation test is effective method to measure k value on-site. Although k values from CPTU are usually higher than those from hydraulic conductivity test, k value can be briefly estimated. If the k values from CPTU are more than one order of magnitude higher than k values obtained by hydraulic conductivity test, there is a possibility that on-site hydraulic barrier performance is not so high as the designed one because of less bentonite swelling due to unconfirmed chemicals in the groundwater, etc. In this case, re-addition of bentonite powder should be considered to enhance the hydraulic barrier performance.

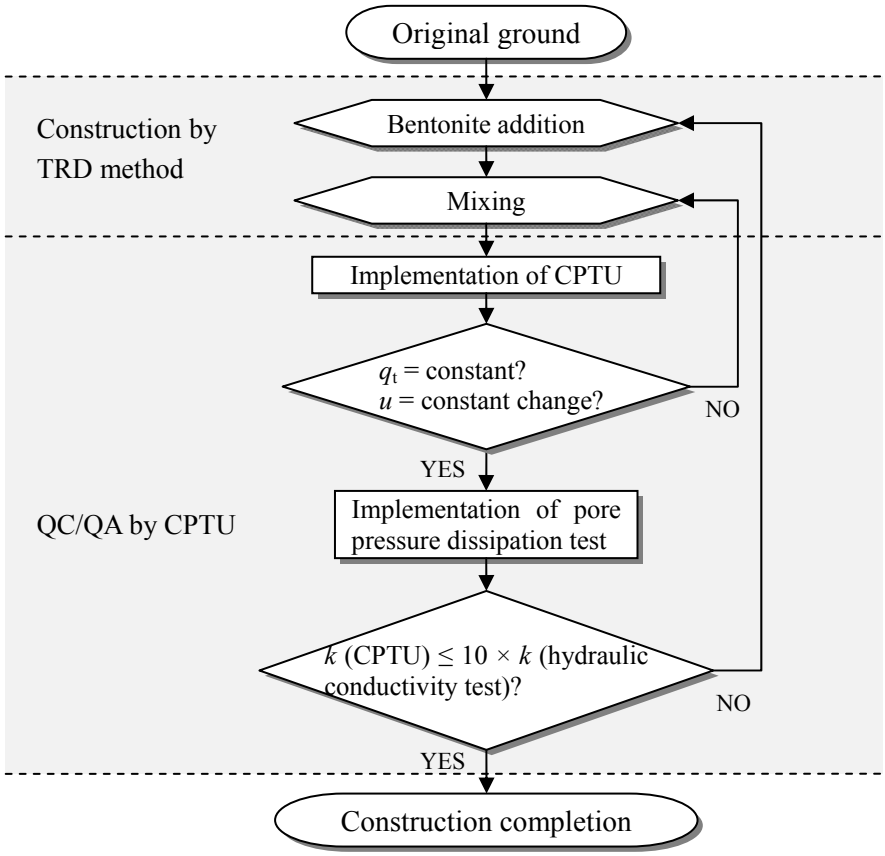

Figure 3.20 Processes of QC/QA by CPTU on SBM cutoff walls

3.5 Summary and conclusions

On-site QC/QA is one of the crucial issues to enhance the reliability of containment barrier system. In this chapter, applicability of CPTU as an on-site QC/QA method of constructed SBM cutoff walls was experimentally studied. The application of CPU is superior in terms of the fact that a continuous log of k value versus depth can be obtained, unlike the laboratory hydraulic conductivity test on the grabbed samples. CPTU was conducted using a large-scale soil tank, which was filled with various SBMs. Vertical homogeneity was assessed by basic three parameters, q_t, f_s and u, obtained during the cone penetration. These values were compared with unconsolidated-undrained triaxial compression test results. Representative k values of SBM layer were measured by conducting pore pressure dissipation test with temporal stop of the penetration. The main achievements obtained in this chapter can be summarized as follows:

(1) When a cone probe was penetrated into a single layer of silica sand-based SBM with 100 kg/m^3 bentonite powder, which simulates a well of bentonite-added fraction in an actual site, the obtained q_t values were extremely low, enough to be almost zero, because such SBM has high flexibility and softness.
(2) The maximum value of q_t in a single layer of silica sand-based SBM with 50 kg/m^3

bentonite powder was approximately 4.1 MPa. Since SBM with 50 kg/m^3 bentonite powder contains less clay fraction (approximately 6% by dry mass basis), SBM performed similarly with pure sand.

(3) From results of CPTU conducted on SBMs with multi-layers, it was confirmed that q_t values in SBM layer with C_{BP} = 50 kg/m^3 are larger than the values in the SBM layers with C_{BP} = 100 kg/m^3. Although the values in the SBM layer with C_{BP} = 50 kg/m^3 attain approximately 1.9 MPa, the values in the SBM layer with C_{BP} = 100 kg/m^3 was converged to almost 0 MPa regardless of the penetration depth.

(4) Pore water pressure values also has obviously different trend in the SBM layer with C_{BP} = 50 kg/m^3 and in the SBM layers with C_{BP} = 100 kg/m^3. Although excess pore water pressure was generated in the top and bottom layers, u values in the middle layer are negative values throughout the layer. Therefore, CPTU has some possibility to be able to detect hydraulic defects in SBM cutoff walls when the physical properties in the lean-mix part are obviously different.

(5) In the results of unconsolidated-undrained triaxial compression test, clear peaks are not observed in deviator stress changes with time regardless of base soil and C_{BP}. Thus, it was confirmed that SBM presents ductile fracture against the compression due to its high softness.

(6) Although pore water pressure of silica sand-based SBM with C_{BP} = 100 kg/m^3 is kept with constant positive value during the compression, that of SBM with C_{BP} = 50 kg/m^3 decreased after 5% strain regardless of confining pressure. The values drop into negative values under some confining pressure. These observations are consistent with the fact that pore water pressure lower than hydrostatic pressure was observed during CPTU. This is due to negative dilatancy during the shearing steps caused by less clay fraction. In contrast, a significant difference is not observed in fine sand-based SBMs with two different C_{BP} because fine particles are originally contained in the fine sand itself.

(7) While further data should be collected to ensure the correlation, relatively higher q_t values could be obtained from CPTU from the SBMs with higher undrained shear strength. Thus, CPTU might detect the lean-mix part with using the q_t values as an indicator of bentonite powder amount.

(8) Horizontal k values were measured by conducting pore pressure dissipation test with a temporal stop of cone penetration at each dissipation degree of 20%, 30% and 50%. The calculated horizontal k values were almost equivalent regardless of the dissipation degree. The k values calculated at any degree of pore water pressure dissipation are in the range of 1.4 - 1.6 times of those values measured by the hydraulic conductivity test in the case of silica sand-based SBM with 100 kg/m^3 powder bentonite. Thus, the hydraulic barrier performance of SBM can be measured with shorter time with accuracy.

(9) The k value measured by the pore pressure dissipation test shows a good correlation with the k value measured by hydraulic conductivity test regardless of base soil and C_{BP}. The k values can be measured by implementation of pore pressure dissipation test within one order of magnitude difference. Therefore, the operation of dissipation test is suitable as quality assurance for hydraulic barrier performance at post-construction of SBM cutoff walls.

(10) Although a residual deformation due to the cone penetration is observed within approximately 2.0 cm depth at the soil surface, the deeper area of the borehole is sealed

by SBM itself with time. This observation indicates that SBM cutoff walls can maintain the designed hydraulic barrier performance due to its self-sealing capacity even after CPTU operation.

(11) The QC/QA using CPTU should be implemented after the laboratory-scale calibration to obtain the dependency of strength characteristic of SBM on the bentonite powder amount. During the CPTU, if q_t values have variation or u values change with different rate with penetration depth, SBM cutoff walls may have heterogeneous portion inside. In such cases, re-mixing of the cutoff wall by TRD method is required to enhance its homogeneity. After the verification of the homogeneity, pore pressure dissipation test should be implemented at a certain depth intervals to ensure the actual hydraulic barrier performance. Since the k values obtained from the pore pressure dissipation test have correlation with the k values from hydraulic conductivity test, pore pressure dissipation test is effective method to measure k value on-site. If the k values from CPTU are more than one order of magnitude higher than those values obtained from hydraulic conductivity test, re-addition of bentonite powder should be considered to enhance the hydraulic barrier performance.

References for Chapter 3

Barvenik, M.J., and Ayres, J.E. (1987): *Construction quality control and post-construction performance verification for the Gilson road hazardous waste site cutoff wall*, U.S. Environmental Protection Agency (EPA).

Benson, C.H., Gunter, J.A., Boutwell, G.P., Trautwein, S.J., and Berzanskis, P.H. (1997): Comparison of four methods to assess hydraulic conductivity, *Journal of Geotechnical and Geoenvironmental Engineering*, ASCE, Vol.123, No.10, pp.929-937.

Bergstrom, W.R., Sweatman, M.B., and Dodt, M.E. (1987): Slurry Trench Construction - Collier Road Landfill, *Geotechnical Practice for Waste Disposal '87*, Geotechnical Special Publication No.13, R. Woods (ed.), ASCE, pp.260-274.

Bouwer, H. (1966): Rapid field measurement of air entry value and hydraulic conductivity of soil as significant parameters in flow system analysis, Water Resources Research, Vol.2, No.4, pp.729-738.

Britton, J.P., Filz, G.M., and Herring, W.E. (2004): Measuring the Hydraulic Conductivity of Soil-Bentonite Backfill, *Journal of Geotechnical and Geoenvironmental Engineering*, ASCE, Vol.130, No.12, pp.1250-1258.

Britton, J.P., Filz, G.M., and Herring, W.E. (2005a) Slug Test in Soil-Bentonite Cutoff Walls Using a Push-In Piezometer Tip. Waste Containment and Remediation: pp. 1-13.

Britton, J.P., Filz, G.M., and Little, J.C. (2005b): The Effect of Variability in Hydraulic Conductivity on Contaminant Transport through Soil-Bentonite Cutoff Walls, *Journal of Geotechnical and Geoenvironmental Engineering*, ASCE, Vol.131, No.8, pp.951-957.

Britton, J.P. and Filz, G.M. (2007): High uniformity versus low hydraulic conductivity for vertical barriers in contaminant containment applications, *Geoenvironmental*

Engineering, S.E. Burns, P.J. Culligan, J.C. Evans, P.J. Fox, K.R. Reddy, and N. Yesiller (eds.), pp.1-10.

Choi, H., and Daniel, D.E. (2006a, b): Slug test analysis in vertical cutoff walls, I: Analysis Methods, and II: Applications, *Journal of Geotechnical and Geoenvironmental Engineering*, Vol.132, No.4, pp.429-447.

Daniel, D.E. (1989): In situ hydraulic conductivity tests for compacted clay, *Journal of Geotechnical Engineering*, Vol.115, No.9, pp.1205-1226.

Evans, J.C. (1993): Vertical cutoff walls, *Geotechnical practice for waste disposal*, D.E. Daniel (ed), Chapman and Hall, London, U.K. pp.430-454.

Evans, J.C. (1995): Soil- and Cement-based Vertical Barriers with Focus on Materials, *Assessment of Barrier Containment Technologies: A Comprehensive Treatment for Environmental Remediation Applications*, R. Rumer and J.K. Mitchell. (eds.), U.S. Department of Energy, U.S. Environmental Protection Agency, pp.5-43.

Filz, G.M., Henry, L.B., Heslin, G.M., and Davidson, R.R. (2001): Determining hydraulic conductivity of soil-bentonite using the API filter press, *Geotechnical Testing Journal*, Vol. 24, No. 1, pp.61-71.

Freeze, R.A. (1975): A stochastic-conceptual analysis of one-dimensional groundwater flow in nonuniform homogeneous media, *Water Resources Research*, Vol.11, No.5, pp.725-741.

GeoSyntec Consultants. (1997): Construction quality assurance report, Vol. II of III, Appendix D, McColl superfund site, Huntington Beach, California.

Hayward Baker Inc. (1988): Slurry trench cut-off wall, Raytheon Company, Mountain View, California, *Case history flyer*, Odenton, Maryland.

Hoeksema, R.J., and Kitanidis, P.K. (1985): Analysis of the spatial structure of properties of selected aquifers, *Water Resources Research*, Vol.21, No.4, pp.563-572.

Houlsby, G.T. and Teh, C.I. (1991): An analytical study of the cone penetration test in clay, *Geotechnique*, Vol.41, No.1, pp.17-34.

JGS (2003): 1435-2003 Method for electric cone penetration test.

JGS (2009): 0521-2009 Method for unconsolidated-undrained triaxial compression test on soils.

Jeffries, M.G., and Davies, M.P. (1993): Use of CPTu to estimate equivalent SPT N_{60}, *Geotechnical Testing Journal*, Vol.16, No.4, pp.458-468.

Joshi, K., Kechavarzi, C., Sutherland, K., Ng, M.Y.A., Soga, K., and Tedd, P. (2010): Laboratory and in situ tests for long-term hydraulic conductivity of a cement-bentonite cutoff wall, *Journal of Geotechnical and Geoenvironmental Engineering*, ASCE, Vol. 136, No. 4, pp.562-572.

Koelling, M.A., Kovac, C.P., and Norris, J.E. (1997): Case history: Vertical barrier wall system for superfund site, *Proceedings of International Containment Technology Conference*, St. Petersburg, Florida State University, Tallahassee, Florida.

Kraus, J.F., Benson, C.H., Erickson, A.E., and Chamberlain, E.J. (1997): Freeze-Thaw Cycling and Hydraulic Conductivity of Bentonitic Barriers, *Journal of Geotechnical and Geoenvironmental Engineering*, Vol.123, No.3, pp.229-238.

Lunne, T., Robertson, P.K., and Powell, J.J.M. (2007): *Cone penetration testing in geotechnical practice*, Spon Press.

Malusis, M.A., Yeom, S., and Evans, J.C. (2011): Hydraulic conductivity of model

soil-bentonite backfills subjected to wet-dry cycling, *Canadian Geotechnical Journal*, Vol.48, No.8, pp.1198-1211.

Malusis, M., and McKeehan, M. (2013): Chemical Compatibility of Model Soil-Bentonite Backfill Containing Multiswellable Bentonite, *Journal of Geotechnical and Geoenvironmental Engineering*, ASCE, Vol.139, No.2, pp.189-198.

Manassero, M. (1994): Hydraulic conductivity assessment of slurry wall using piezocone test, *Journal of Geotechnical Engineering*, Vol.120, No.10, pp.1725-1746.

Mayne, P.W., Matthew, R.C., Sarah, M.S., An-Bin, H., Jorge, G.Z. (2009): Geomaterial behavior and testing, *Proceedings of the 17th International Conference on Soil Mechanics and Geotechnical Engineering, The Academia and Practice of Geotechnical Engineering*, Vol.4, M. Hamza, M. Shahien and Y. El-Mossallamy (eds.), pp.2777-2872.

Mimura, M., and Yoshimura, M. (2007): Development of new radio isotope density cone penetrometer and progress in accuracy of measurement, Journal of JSCE, Vol.63, No.2, pp.649-661. (in Japanese)

Nishigaki, M., and Komatsu, M. (2007): In-situ method for measuring hydraulic conductivity of the bentonite mixture soil liner, Journal of JSCE, Division C, Vol.63, No.1, pp.299-311. (in Japanese)

Pradhan, T.B.S. (1998): Soil identification using piezocone data by fuzzy method, *Soils and Foundations*, Vol.38, No.1, pp.255-262.

Robertson, P.K. (2009a): *Guide to cone penetration testing for geo-environmental engineering*.

Robertson, P.K. (2009b): Interpretation of Cone Penetration Tests – a unified approach, *Canadian Geotechnical Journal*, Vol.46, No.11, pp.1337-1355

Robertson, P.K. (2010): Estimating in-situ soil permeability from CPT & CPTu, Proceedings of 2nd International Symposium on Cone Penetration Testing, Huntington Beach, CA, USA., Volume 2&3: Technical Papers, Session 2: Interpretation, Paper No. 51.

Russo, D., and Bouton, M. (1992): Statistical analysis of spatial variability in unsaturated flow parameters, *Water Resourses Research*, Vol.28, No.7, pp.1911-1925.

Ryan, C.R. (1987): Vertical barriers in soil for pollution containment, Geotechnical Practice for Waste Disposal '87, Geotechnical Special Publication No.13. R. Woods, (ed.), ASCE, pp.182-204.

Shibata, T., Mimura, M., Shrivastava, A.K. and Nobuyama, M. (1993): RI Cone Penetrometer experience in marine clays in Japan, *Proceedings of 4th Canadian Conference on Marine Geotechnical Engineering*, Vol.3, pp.1024-1033.

Sudicky, E.A. (1986): A natural gradient experiment on solute transport in a sand aquifer: spatial variability of hydraulic conductivity and its role in the dispersion process, *Water Resourses Research*, Vol.22, No.13, pp.2069-2082.

Tachavises, C. and Benson, C.H. (1997): Hydraulic importance of defects in vertical groundwater cut-off walls. *In Situ Remediation of the Geoenvironment*, Minneapolis, Minnesota, ASCE.

Tedd, P., Quarterman, R.S.T., and Holton, I.R. (1995a): Development of an instrument to measure in-situ permeability of slurry trench cut-off walls, Proceedings of 4th International Symposium on Field Measurements in Geomechanics, Bergamo, Italy, pp.441-446.

Tedd, P., Butcher, A.P., and Powell, J.J.M. (1995b): Assessment of the piezocone to measure

the in-situ properties of cement-bentonite slurry cut-off walls, *Geoenvironmental Engineering Contaminated Ground: Fate of Pollutants and Remediation*, R. Yong and H.R. Thomas (eds.), pp.48-55.

Tomura, G., Nakata, M., Kita, H., Kuroshima, I. (2005): Quality assurance techniques for bentonite mixture soil liner at final disposal sites, *Reports of Technical Research Institute of Sumitomo Mitsui Construction Co.Ltd.*, pp.71-81. (in Japanese)

Topp, G.C., and Binns, M.R. (1976): Field measurement of hydraulic conductivity with a modified air-entry permeameter, Canadian Journal of Soil Science, Vol.56, pp.139-147.

Voyiadjis, G.Z., and Song, C.R. (2003): Determination of hydraulic conductivity using piezocone penetration test, *International Journal of Geomechanics*, Vol.3, No.2, pp.217-224.

Yesiller, N., and Shackelford, C.D. (2010): Chapter 13: Geoenvironmental Engineering, B.M. Das (ed.), *Geotechnical Engineering Handbook*, pp.13-52.

Zamojski, L., Perkin, S., and Reinknecht, D. (1995): Design and construction evaluation of a slurry wall at FLR landfill superfund site, *Proceedings of Geoenvironment 2000*, New York, ASCE, pp.1192-1206.

CHAPTER 4

Seismic Behavior of SBM Cutoff Walls

4.1 General remarks

Containment barriers, including SBM cutoff walls, should maintain their hydraulic barrier performance even under the occurrence of an earthquake to completely contain the contaminants for a long period. In the case of rigid cutoff walls, such as concrete and soil-cement, a high strength is required to resist the seismic behavior. On the other hand, physical resistance by the strength cannot be expected for SBM cutoff walls because their high flexibility is one of their significant characteristics. Therefore, performance of SBM cutoff walls against seismic events is a crucial issue to be studied. However, few researches have dealt with the seismic behavior of cutoff walls especially as containment barriers. In this chapter, the dynamic behavior of SBM cutoff walls against seismic loading is verified by centrifuge modeling test and cyclic undrained triaxial test.

4.2 Importance of seismic behavior for structures

4.2.1 Damage to the underground structures due to seismic loading

Japan is prone to earthquakes. Several huge earthquakes have occurred even within these decades, such as the Great Hanshin Earthquake in 1995, Mid Niigata Prefecture Earthquake in 2004 and the Great East Japan Earthquake in 2011. Many previous studies related to the seismic behavior can be categorized into three groups.

- ✓ Ground failure: Ground failure as a result of seismic shaking includes liquefaction, slope instability, and fault displacement. Ground failure is particularly prevalent at tunnel portals and in shallow tunnels. Special design considerations are required for cases where ground failure is involved. Shear failure and slope failure will be triggered by the earthquake loading due to the oblique earth pressure on the slope. Gravity

retaining walls will be inclined as well as the slope.

- ✓ Aboveground structures: The existing structures will be affected by the earthquake due to many causes, such as the seismic impact itself on the structures and the ground deformation. Critical damage on the base ground and foundation may also significantly affect on the aboveground structure (Iai and Ichii 2011). Since aboveground pipelines and storage tanks will be damaged by these causes, from a viewpoint of geoenvironmental engineering, subsurface contamination could be caused during a seismic event.
- ✓ Underground structures: The underground structures will be affected in association with the liquefaction of surrounding ground. For example, manholes can be uplifted by a strong earthquake because the trench backfill is low-compacted (Tobita et al. 2011, Kang et al. 2013). A major collapse of the Daikai subway station in Kobe was caused by the 1995 Great Hanshin Earthquake, Japan (Iida et al. 1996, Nakamura et al. 1996). This station designed in 1962 did not include specific seismic provisions. It represents the first modern underground structure to fail during a seismic event.

The major factors influencing shaking damage of underground structures include: 1) the shape, dimensions and depth of the structure, 2) the properties of the surrounding soil or rock, 3) the properties of the structure, and 4) the severity of the ground shaking (Dowding and Rozen, 1978, St. John and Zahrah, 1987). The American Society of Civil Engineers (1974) describes the damage in the Los Angeles area as a result of the 1971 San Fernando Earthquake. The Japan Society of Civil Engineers (1988) describes the performance of several underground structures, including an immersed tube tunnel during shaking in Japan. Owen and Scholl (1981) have updated Dowding and Rozen's work with 127 case histories. Sharma

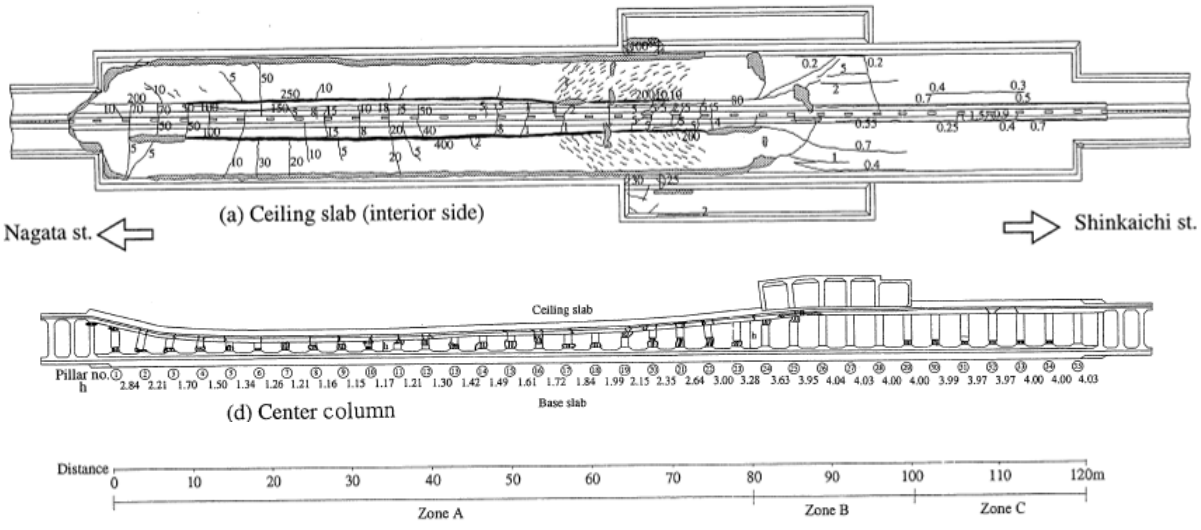

Figure 4.1 Sketch of damage to Daikai subway station (Iida et al. 1996).

and Judd (1991) generated an extensive database of seismic damage to underground structures using 192 case histories. Power et al. (1998) provide a further update with 217 case histories, and Wang et al. (2001) collected the data about the seismic damage by Chi-Chi Earthquake in Taiwan. The following issues are selected confirmations related to the cutoff walls from the summary of the seismic performance of underground structures (Hashash et al. 2001):

1. Underground structures suffer appreciably less damage than surface structures.
2. Reported damage decreases with increasing overburden depth. Deep tunnels seem to be safer and less vulnerable to earthquake shaking than are shallow tunnels.
4. Damage may be related to peak ground acceleration and velocity based on the magnitude and epicentral distance of the affected earthquake.
5. Duration of strong-motion shaking during earthquakes is of utmost importance because it may cause fatigue failure and, therefore, large deformations.
6. High frequency motions may explain the local spalling of rock or concrete along planes of weakness. These frequencies, which rapidly attenuate with distance, may be expected mainly at small distances from the causative fault.

4.2.2 Seismic performance of slurry walls

Although cutoff walls have been widely used in many countries, their behavior under seismic forces is unknown. In areas that are susceptible to seismic activity, the slurry wall in the ground could be damaged: micro and macro cracks can develop, large lateral deformations can occur, and permeability may significantly increase.

Graham et al. (2012) studied the seismic performance of slurry walls, used as seepage barriers in levees, by a one dimensional shaking table test as shown in Photo 4.1. In this study, cement-bentonite (CB) and soil-cement-bentonite (SCB) were used as the slurry cutoff walls. Wyoming bentonite and Portland cement were respectively used as bentonite and cement. A slurry wall with the following dimensions 150 cm × 160 cm × 20 cm was constructed in a formwork (see Photo 4.2) and tested on a one dimensional shaking table that is capable of replicating the 6.7 magnitude Northridge earthquake. A 150 cm × 187 cm × 180 cm rigid steel-frame box that is anchored on the shaking table contained the slurry walls and the sandy soil that was compacted on both sides of the wall to simulate a levee section. In each shake table test, the slurry walls and the confining soil are instrumented with accelerometers, LVDT transducers, linear potentiometers, and dynamic soil stress gauges to respectively record the accelerations, vertical and horizontal deformations of the wall, and transient dynamic soil pressures on the wall during the simulated earthquake excitations. Although the accelerations produced by the shake table contained a few outliers, which are higher than the actual one (1.7g), the wall did not settle more that 0.2 cm (or 0.12% strain to the wall height) throughout the shaking in the case of CB slurry wall as shown in Figure 4.2. The sand had an initial significant upward heaving followed by settlement at the conclusion of the test. This is the first segment of the 36-second test and the complete graph shows a descending trend that corresponds to soil settlement. After the shaking table test, the adjacent soil was removed so

that the slurry wall could be examined for any cracks that were caused by the shaking. In the case of SCB slurry wall, a large crack that was caused by the shaking was clearly observed along the upper 40 cm as shown in Photo 4.3. The crack developed along the entire length of the wall and the top 40 cm section shifted laterally approximately 1.5 cm. No visible cracks were observed in the lower section, possibly due to the higher confining soil pressure and smaller accelerations. The same results were obtained from the repeated test with the same conditions. The CB wall, which is lighter and more plastic than the SCB slurry wall, performed well without any visible cracks, as shown in Photo 4.4. The lines on the CB wall as shown in Photo 4.4 were not cracks, and they were the surface indentations that are caused by the formwork.

Hioki et al. (2007) studied the physical and dynamic properties of soil-cement (SC) and SCB cutoff walls with various laboratory tests. To enhance the plasticity of the cutoff walls, SCBs were prepared with hardening materials made by various cement amounts against bentonite amount with 2, 0.5 and 0.25 (cement/bentonite). In addition, seismic response was

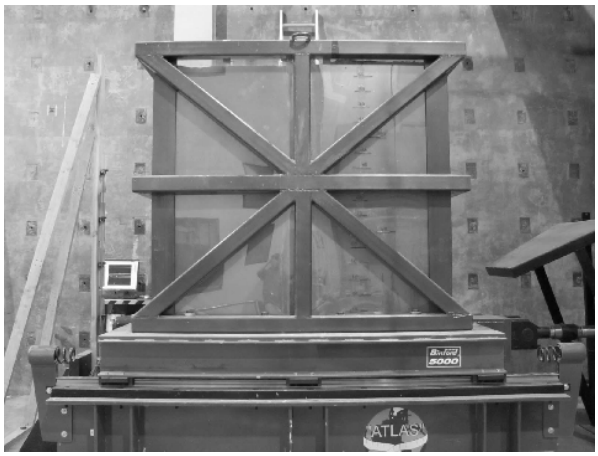

Photo 4.1 Seismic table and box

Photo 4.2 Formwork for slurry wall installation

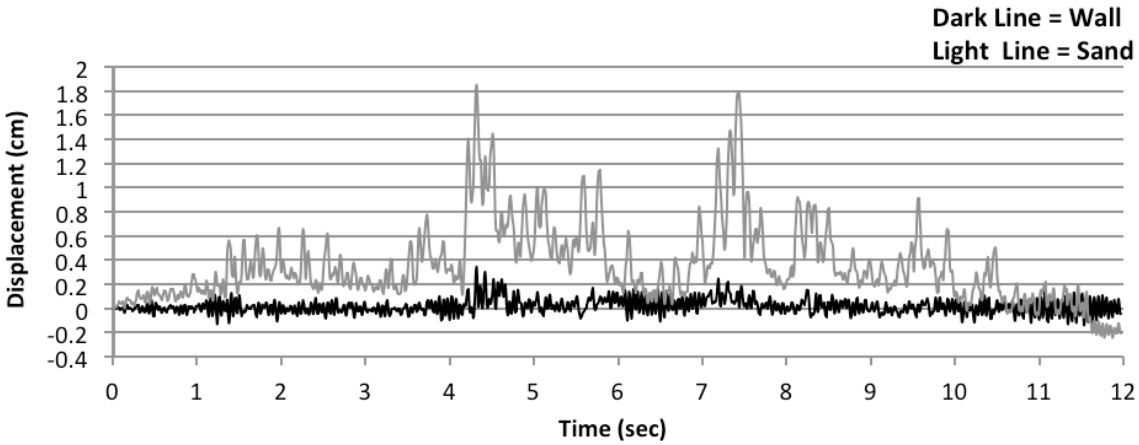

Figure 4.2 Dynamic settlements of the slurry wall and the sand during the excitation

Photo 4.3 SCB wall with crack, after shaking

Photo 4.4 CB wall after shaking

numerically analyzed to evaluate the seismic performance of SC cutoff walls. Results of two-dimensional seismic response analysis using physical properties obtained from the laboratory experiments revealed that SC cutoff walls (without bentonite) might suffer cracks during a large earthquake as the Great Hanshin Earthquake because of their low tensile strength. Especially, the maximum tensile stress was observed just above the embedded part (build-in edge) regardless of the mixing condition. Those cracks might degrade seepage control performance. On the other hand, SCB cutoff walls showed plastic behavior even after cement solidification due to the existence of bentonite. Hydraulic barrier performance of all SCBs was also improved from the SC with the hardening material of any mixing ratios. However, it was mentioned that shear failure should be taken into account in the case of SCB because of its low shear strength.

These observations suggest that shear stress in shallow zone becomes high due to the small lateral earth pressure when the embedment of cutoff wall into the bottom layer. On the other hand, when the embedment into the bottom layer must be taken into account in deep zone, the shear stress just above the embedded part become high because the cutoff wall will behave like a cantilever. Considering the fact that the cutoff walls are installed with embedding into the low-permeable bottom layer in the actual condition, the shear stress just above the embedded zone could become high. However, the shear failure in shallow zone might be caused when the cutoff walls are so deep that the effect of embedment is negligible.

4.3 Experimental methodologies for seismic behavior of SBM cutoff walls

In this chapter, seismic behavior of SBM cutoff walls is experimentally studied. In particular, cyclic strength of SBMs is measured by cyclic undrained triaxial test to fundamentally

evaluate the liquefaction potential of SBMs under dynamic condition. The cyclic undrained triaxial test is widely employed to measure the seismic soil property under the undrained condition (e.g. Procter and Khaffaf 1984, Tatsuoka et al. 1986, Toki et al. 1986, Yasuhara et al. 2005, Gratchev and Sassa 2013). The seismic behavior of SBM cutoff walls is evaluated by a centrifuge modeling test under 50 G centrifugal acceleration field. By applying high centrifugal acceleration to a scaled model ground, a confining pressure of the ground in prototype scale can be simulated in a scaled model, which is one of the advantages of using a geotechnical centrifuge facility. (Iai et al. 2005a). This test is especially commonly employed to assess the seismic behavior of the structures, such as slope, levee and engineered barrier, etc. (e.g. Brandenberg et al. 2005, Viswanadham and Rajesh 2009, Ling and Ling 2012). However, there are no previous researches about the vertical cutoff walls from a viewpoint of dynamic response against seismic excitation.

4.3.1 Materials

For the experiments, SBM constructed with composite soil (a mixture of volcanic cohesive soil and sandy gravel) and silica sand #7 were used as base soil. SBM samples were prepared according to the same procedure described in 2.3.1.4. Distilled water was used for the water content regulation and bentonite powder was added to achieve C_{BP} = 100 kg/m^3. Since composite soil-based SBMs with a maximum grain size of 0.85 mm were employed for the centrifuge modeling test because of the specimen thickness (11 mm in model scale), cyclic undrained property of SBMs were evaluated with both 0.85 mm and 4.75 mm for the maximum grain size. Since the maximum grain size of silica sand is 0.425 mm without sieving, the whole material was directly used for both experiments.

4.3.2 Experimental procedures

4.3.3 Cyclic undrained triaxial test

Cyclic undrained triaxial test was conducted according to JGS 0541-2000 (JGS 2000). Since the reproduction of actual wave profiles is technically difficult due to their variability and irregularity, the cyclic strength of soil is generally evaluated by cyclic loading of compression and extension with a model sine wave.

The specimens were prepared using a halved cylindrical steel tube (50 mm in inner diameter and 100 mm in height). To fill the SBM into the tube, a latex membrane was vacuumed to fit to the inner wall of the tube. After the tube was filled with SBM with wet density of 1.80 g/cm^3, the specimen was saturated by submerging it in a tank using a vacuum deaerator for 7 days. After the saturation was completed, the cylindrical specimen was placed between filter papers and caps (cap and pedestal). The chamber of triaxial compression test was build up, and then, deaired water was infiltrated from a porous stone at the bottom for 24 hours to remove the air between the specimen and the latex membrane. Figure 4.3 shows a schematic diagram of cyclic undrained triaxial test apparatus. In the consolidation process, a isotropic pressure of 196 kPa was applied on the specimen in all cases. The consolidation step

was continued for approximately 7 days until the change of drainage volume and of vertical settlement with time became negligible. The drainage volume and vertical settlement were recorded by a data logger (TDS-303, Tokyo Measuring Instruments Laboratory Co., Ltd.). After the consolidation step, cyclic loading was applied under undrained condition. During the cyclic loading step, axial load (P), pore water pressure (u) and axial displacement was measured. Testing condition is summarized in Table 4.1. Cyclic stress ratio is defined by the following equation (5.1) and (5.2).

$$\sigma_d = \frac{\Delta P_c + \Delta P_e}{2A_c} \tag{5.1}$$

$$CSR = \frac{\sigma_d}{2\sigma_0'} \tag{5.2}$$

where, σ_d = cyclic deviator stress (kPa); ΔP_c = peak cyclic load in compression (kN); ΔP_e = peak cyclic load in extension (kN); A_c = area of specimen after the consolidation (m^2); CSR = cyclic stress ratio (dimensionless); σ_0' = effective confining pressure (kPa).

The definition of ΔP_c in compression and ΔP_e in the cyclic sine wave is shown in Figure 4.4. The terms of test are defined to satisfy either of the following requirement; 1) cyclic numbers exceed 200, and 2) double amplitude strain, DA, become larger than 5%. Double amplitude strain is the difference between the maximum axial strain in compression and extension during the cycles as expressed by the following equation (5.3).

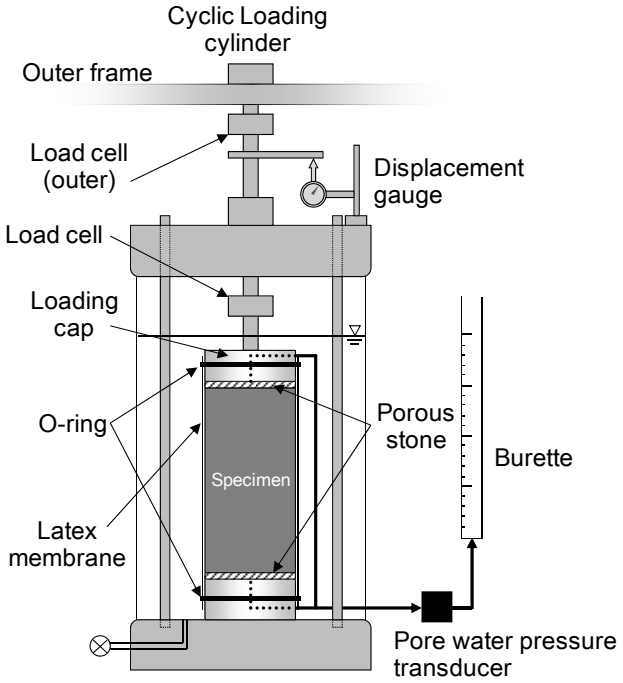

Figure 4.3 Schematic diagram of cyclic undrained triaxial test apparatus.

Table 4.1 Testing conditions for cyclic undrained triaxial test

Case No.	Type of base soil for SBM	Maximum diameter (mm)	Cyclic stress ratio	Wet density of SBM after the consolidation step (g/cm^3)
Case-1	Composite soil	4.75	0.229	1.89
Case-2			0.216	1.89
Case-3			0.205	1.90
Case-4		0.85	0.240	2.04
Case-5			0.235	2.03
Case-6			0.224	2.00
Case-7	Silica sand	0.425	0.195	2.00
Case-8			0.161	1.89
Case-9			0.157	1.90
Case-10			0.155	1.95

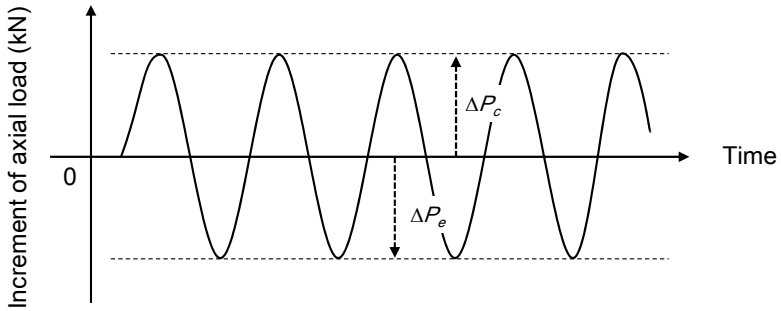

Figure 4.4 Definition of ΔP_c and ΔP_e in the cyclic sine wave.

$$DA = \frac{\Delta L}{H_c} \times 100 \tag{5.3}$$

where, DA = double amplitude strain (%); ΔL = double amplitude of axial displacement during the cyclic loading (cm); H_c = Height of specimen after the consolidation step (cm).

4.3.4 Centrifuge modeling test

4.3.4.1(1) Detail of geotechnical centrifuge used in this study

In this study, the geotechnical centrifuge at the Disaster Prevention Research Institute (DPRI), Kyoto University, was used. The specifications of the geotechnical centrifuge is shown in Table 4.2. Figure 4.5 and Photo 4.5 show schematic view of the facility and panoramic view of centrifuge room, respectively. Effective radius, which is the distance between the rotation axis and the platform, is 2.5 m. Maximum loading capacity, which is one of the indicators for the performance of geotechnical centrifuge, is calculated by multiplying the maximum centrifugal acceleration by the maximum weight of model. The swingable platform can be horizontally lifted by the centrifugal force. Seismic excitation is given in longitudinal

direction. A shake table unidirectionally driven by a servo hydraulic actuator is mounted on a platform and can be controlled through a laptop computer on the centrifuge arm. All the equipment necessary for shake table control is put together on the arm. The laptop PC is accessible from a PC in the control room through wireless LAN and "Remote Desktop Environment." The experimental data can be automatically transmitted to a PC in the control room via wireless LAN (Iai et al. 2005). The front image of model is recorded during the test with a high-speed camera, which can take 21,000 images per second. Besides, a configuration of shaking device is schematically shown in Figure 4.6.

Since the gravity force in the centrifugal field is different from the actual field, a scaling rule has to be considered to expand the experimental results to prototype scale. The scaling rules used in this study are summarized in Table 4.3. As described above, all tests were conducted under 50 G centrifugal acceleration field in this study.

Table 4.2 Specifications of geotechnical centrifuge at DPRI, Kyoto University.

Effective radius	2.50 m
Maximum scale of model container	W 0.80 m × D 0.355 m × H 0.80 m (for static test)
	W 0.61 m × D 0.35 m × H 0.62 m (for dynamic test)
Maximum loading capacity	24G ton
Maximum centrifugal acceleration	200 G
Maximum number of rotations	270 rpm
Maximum weight of model	120 kg

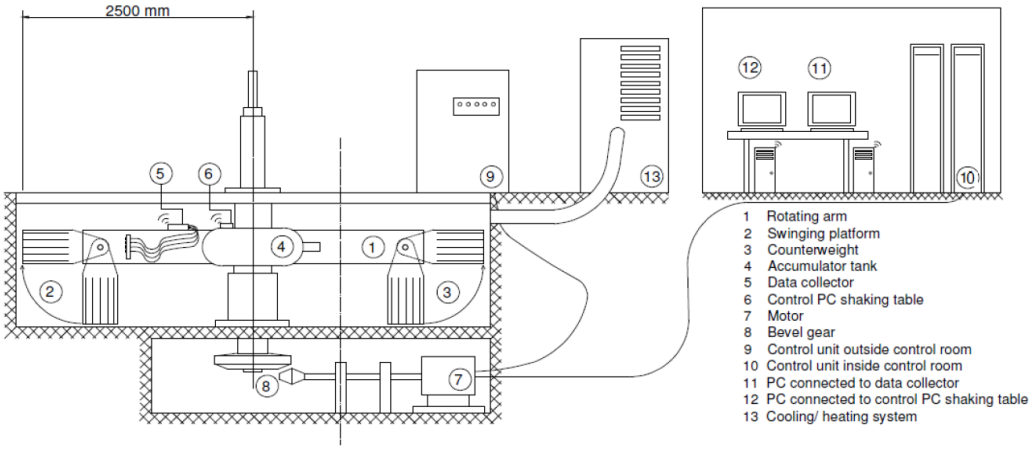

Figure 4.5 Schematic view for centrifuge facility.

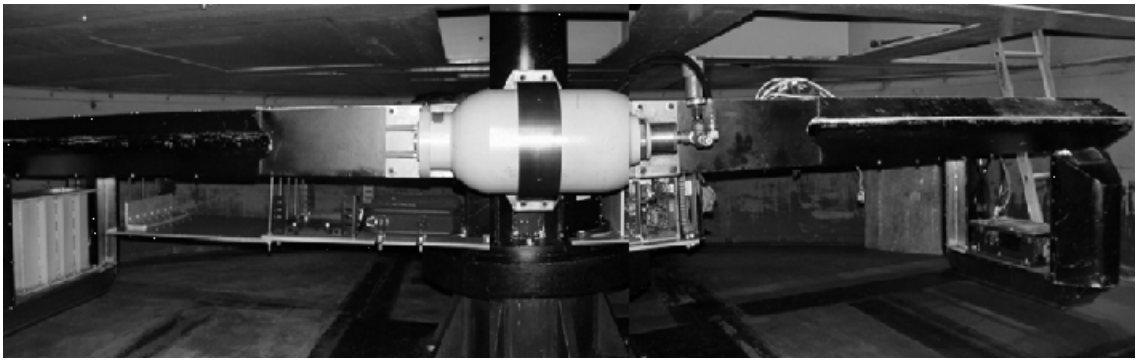

Photo 4.5 Panoramic view of centrifuge room.

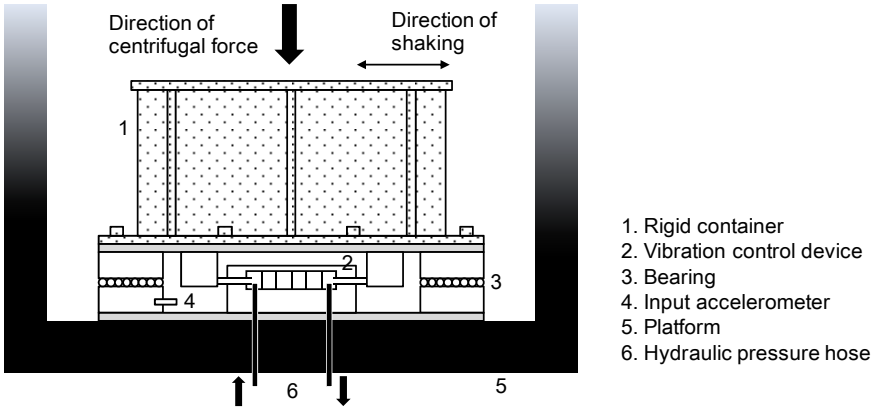

Figure 4.6 Schematic view for shaking device.

Table 4.3 Scaling rule used in this study.

Quantity	Symbol	Similarity		Qantity	Symbol	Similarity	
		N G	1 G			N G	1 G
Acceleration	a	N	1	Viscosity	η	1	$N^{-1/2}$
Length	l	1/N	1/N	Saturation degree	S_r	1	1
Solid density	ρ	1	1	Fluid density	ρ_l	1	1
Grain size	d	1 (1/N)	1 (1/N)	Rigidity	E	1	1/N
Void ratio	e	1	1	Time	t_i	1/N	$N^{-1/2}$

4.3.4.2(2) Model configuration

Figure 4.7 and Figure 4.8 show the model configuration in rigid container in this study with section view and plan view, respectively. The model configuration are the same in all testing cases. Overall inner dimensions of the rigid container are 450 × 150 × 294 mm in length, width, and height, respectively. The bottom part of SBM cutoff wall was installed into a channel of an acrylic resin to simulate the embedment of SBM cutoff walls into the

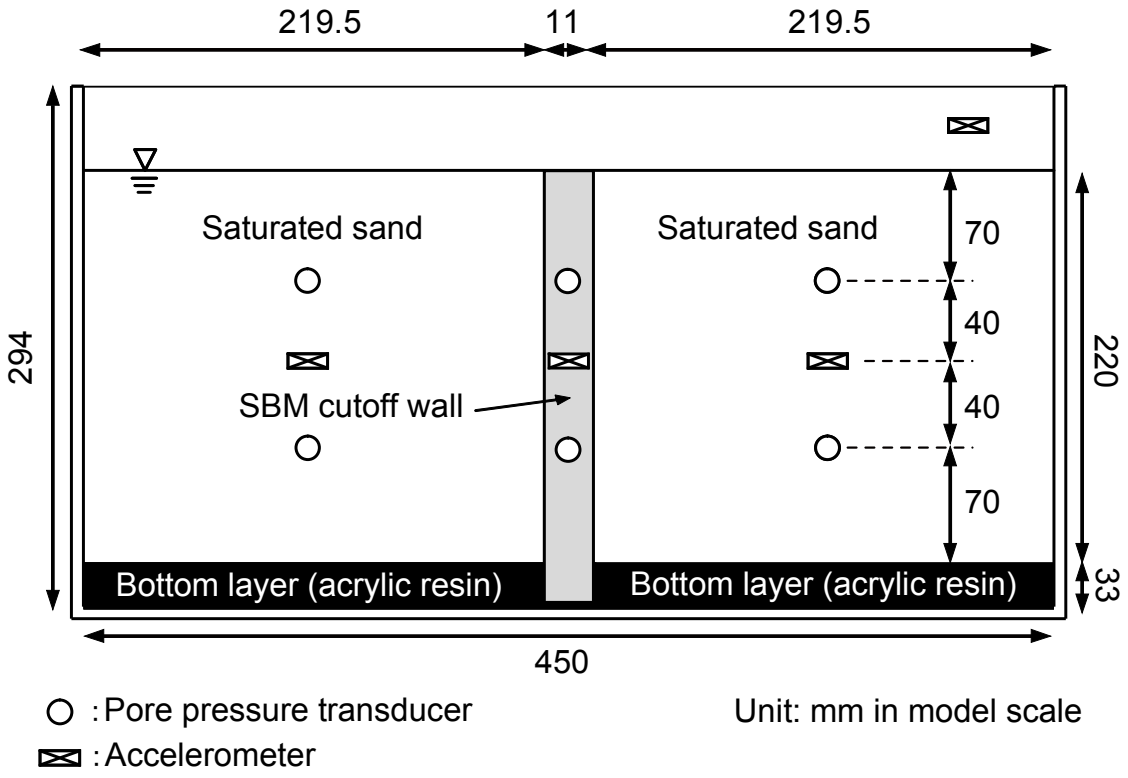

Figure 4.7 Cross-sectional model configuration in rigid container.

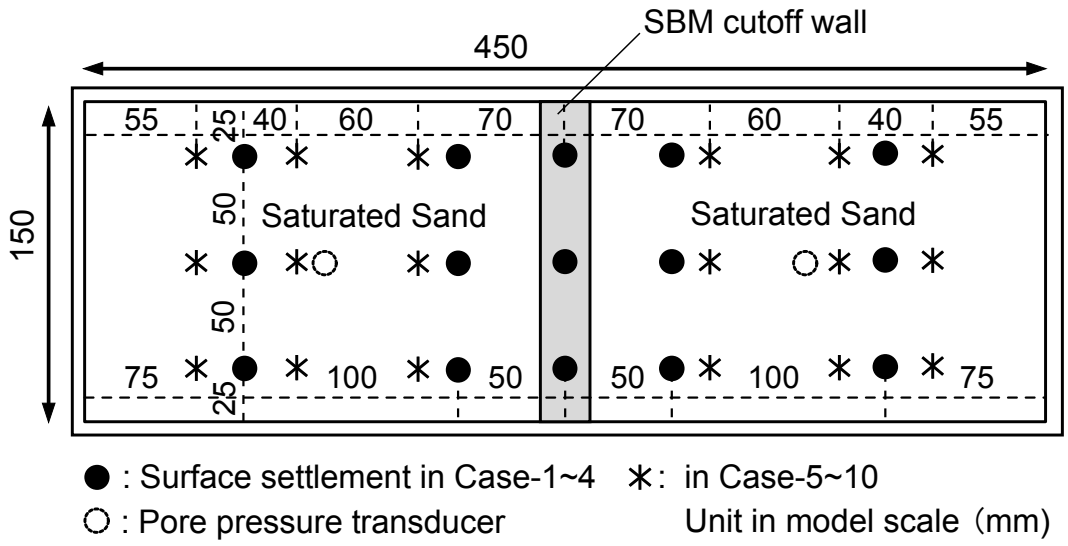

Figure 4.8 Planar model configuration in rigid container.

low-permeable clay layer. The channel was made in the center with the dimension of 11 × 150 × 30 mm in length, width, and height. The acrylic bottom was made with stacking 11 sheets of acrylic plate of 3 mm thickness as shown in Photo 4.6. Adjacent sand layers were prepared by water pluviation to simulate the saturated condition so that the height of sand layers from the

top of acryl become approximately 220 mm after the consolidation. This model ground simulates SBM vertical cutoff wall of total 12.5 m height with 1.5 m embedment in prototype scale. Both sand layers and SBM cutoff wall was instrumented with 2 pore pressure transducers (P306A-2, SSK Co., Ltd.) at 70 and 150 mm-depth from the soil surface to measure the pore water pressure change by the seismic excitation. In after-mentioned Case 6~10, one pore pressure transducer was mounted in each layer at 110 mm-depth. One accelerometer (A6H-50, SSK Co., Ltd.) was also mounted in each layer at 110 mm-depth from the surface to measure the response acceleration spectra. Another accelerometer (A6H-50, SSK Co., Ltd.) was separately attached on the sidewall of rigid container to measure the response acceleration. Surface settlement by seismic excitation was measured at measurement point shown in Figure 4.8.

4.3.4.3(3) Centrifuge model preparation

The aluminum formwork shown in Photo 4.7 was filled with the prepared SBM whose maximum grain size is 0.85 mm, to achieve its wet density of approximately 1.80 g/cm^3. The dimension of formwork is 300 × 200 × 20 mm in length, width, and height. As shown in the photo, the formwork allows vertical drainage from the top and bottom plates with holes. To avoid runoff of soil particles during the consolidation step, filter papers were set between

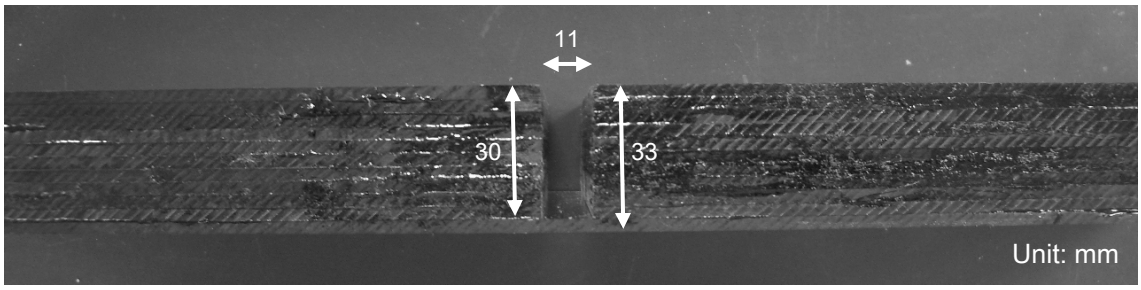

Photo 4.6 Acrylic resin used as a bottom layer.

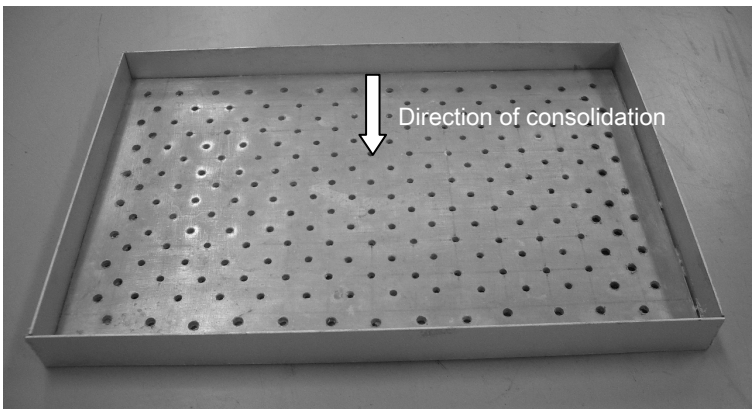

Photo 4.7 Formwork for the preparation of SBM cutoff wall.

water to completely submerge the specimen. Under this condition, the SBM specimen was consolidated for 12 hours with a consolidation pressure of approximately 58.8 kPa in vertical direction, which means horizontal direction in the centrifuge model. After the consolidated SBM specimen was removed from the formwork without disturbance, SBM specimen was cut

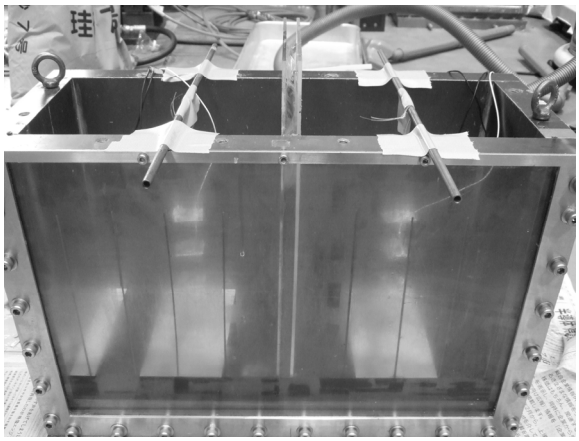

a)

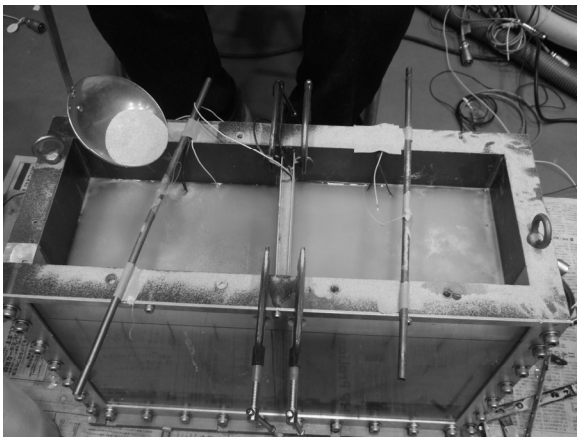

b)

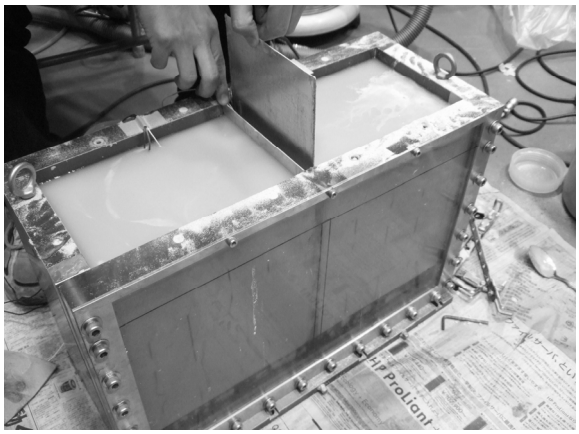

c)

d)

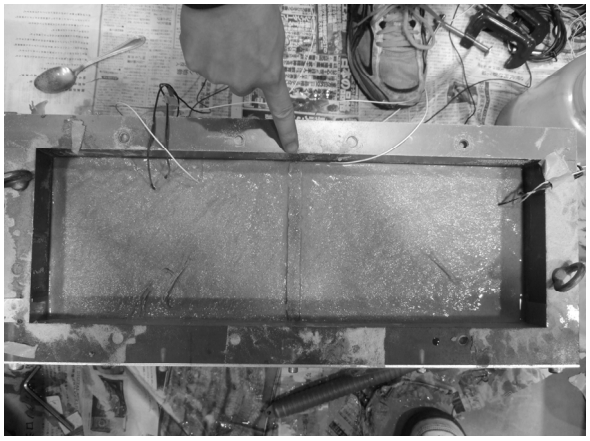

e)

Photo 4.8 Preparation steps for centrifuge model

into 250 × 148 × 11 mm in length, width, and height. The width of specimen was adjusted to 148 mm with consideration for the side friction between SBM cutoff wall and rigid container.

The centrifuge model was set up by following steps as shown in Photo 4.8. First, acrylic bottom layer was set on the bottom of model. All measurement instruments were preliminarily fixed at the known position by hanging them with strained fishlines connected to bars (Photo 4.8 a)). SBM cutoff wall was installed into the channel located in the acrylic bottom layer with lateral support by stainless plates not to deform during the model preparation. After a viscous fluid (Metolose, SM-25 Shin-Etsu Chemical Co.) whose viscosity was adjusted to 50 times of water (50 cSt) was poured into the container, silica sand was deposited by water pluviation (Photo 4.8 b)). When the sand layer was made up to certain height, the stainless plates to support SBM cutoff wall was gradually upward slid. After the completion of sand layer preparation, the stainless plates were withdrawn (Photo 4.8 c)). The centrifuge model was placed on and anchored to the shaking table (Photo 4.8 d)). Under 50 G centrifugal acceleration field, the model was left for 3 hours to consolidate the model ground. The pre-consolidation was finished when the pore water pressure in sand layer and in the SBM cutoff wall became equivalent.

4.3.4.4(4) Experimental procedures

After the pre-consolidation, the model was removed from the shaking table to measure the height of each layer and horizontal position of SBM cutoff wall. These lengths were directly measured, not by a sensor, but by a caliper. After the measurement of the initial conditions, the model was once again placed on and anchored to the shaking table. The consolidation step lasted for approximately 2 hours until the difference of pore water pressure between the sand layers and SBM cutoff wall became negligible. A predetermined wave was applied to the model from a PC in the control room, and the response data of each sensor was measured in the PC. The front view of model during the shake was recorded on DVD. The centrifugal loading was stopped after a negligible change in pore water pressure value was observed. The horizontal displacement of SBM cutoff wall and the vertical settlement of the ground were measured at the prescribed points. After dismantling the centrifuge model, water content of SBM cutoff wall was measured by cutting into 5 pieces, which were an embedded part and vertically quadrisected rest.

All testing conditions for centrifuge modeling test are summarized in Table 4.4. In Case-1~3, the model with loosely prepared sand layers was used to verify the effect of input wave with three different waves: 1) sinusoidal wave with 0.4 Hz in frequency, 150 mm in amplitude, and 25 cycles in prototype scale, 2) sinusoidal wave with 2.0 Hz in frequency, 100 mm in amplitude, and 10 cycles in prototype scale, and 3) a wave with relatively high acceleration whose maximum acceleration is approximately 500 gal. The second wave has higher frequency, smaller amplitude and fewer cycles compared with the first wave. In Case-4, one sand layer was prepared with higher density to assess the effect of unsymmetrical earth pressure on the deformation of SBM cutoff wall against the above-mentioned sinusoidal wave no.1. In Case-1~4, composite soil-based SBM was used for the cutoff wall, and silicone

Table 4.4 Testing condition for centrifuge modeling test

Case No.	Base soil for SBM	Contact between SBM and front face	Density of sand layer [1]		Input wave [2]
			Left	Right	
Case-1	Composite soil	Silicone grease	Loose	Loose	0.4 Hz-150 mm-25 cycles
Case-2			Loose	Loose	2.0 Hz-100 mm-10 cycles
Case-3			Loose	Loose	A wave with high acceleration
Case-4			Dense	Loose	0.4 Hz-150 mm-25 cycles
Case-5	Silica sand	Round head pin	Loose	Loose	0.4 Hz-150 mm-25 cycles
Case-6			Loose	Loose	
Case-7			Loose	Loose	
Case-8			Dense	Dense	
Case-9			Dense	Dense	
Case-10			Dense	Dense	

[1] Loose: relative density = approx. 40%; Dense: relative density = approx. 70%
[2] Frequency-amplitude-cyclic numbers, respectively in prototype scale

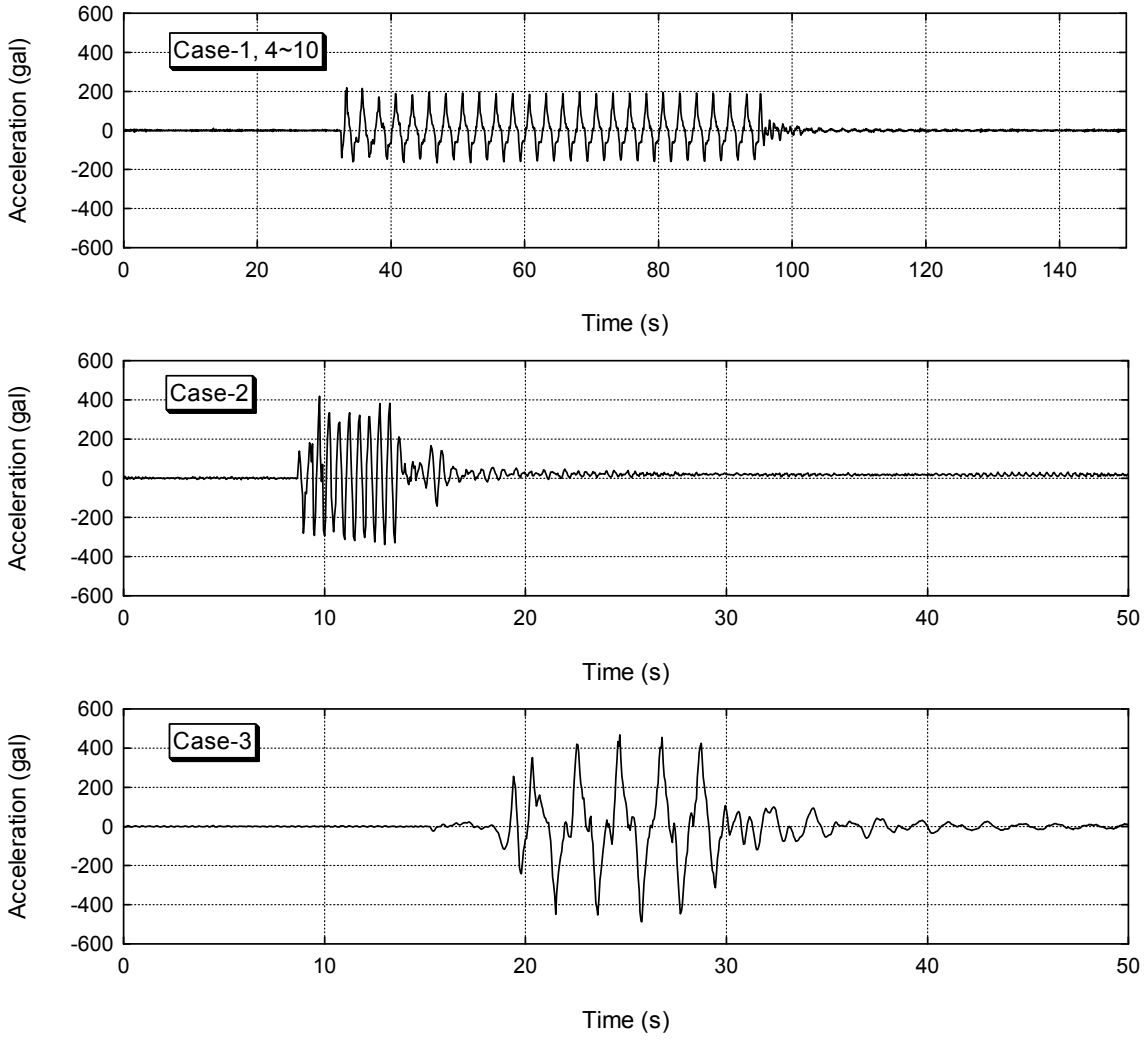

Figure 4.9 Input acceleration of the container in each case in prototype scale.

grease was spread on the both sides to joint the gap between SBM cutoff wall and the front face of rigid container. In Case-5~10, above-mentioned sinusoidal wave no.1 was applied on the model ground with silica sand-based SBM cutoff wall. Both sand layers were prepared loosely in Case-5~7 and densely in Case-8~10, respectively. In these cases, repeatability of experiments were verified on two different density of sand layers. Sides of SBM cutoff wall were instrumented with round head pins at intervals of 20 mm from top to bottom to visualize the deformation and to allow SBM cutoff wall to deform as freely as possible. Waveforms of each response acceleration of the container are shown in Figure 4.9. As shown in this figure, the amplitude was not constant even for the sinusoidal waves. This might be due to the effect of mechanical resonance with the centrifuge arm during shaking.

4.4 Strength characteristics of SBM against cyclic loading

4.4.1 Degradation of stiffness and liquefaction potential of SBM

Figure 4.10 and Figure 4.11 show examples of results of cyclic undrained triaxial test. As shown in Figure 4.10, axial strain of composite soil-based SBM exponentially increased from 1% to 5% after the gradual increase within approximately 1%. The same trend was observed in all cases in Case-1~6. There was little change in excess pore water pressure of composite soil-based SBM. Thus, the increase of axial strain was caused not by the decrease of effective stress but by the degradation of stiffness with the cyclic loading. On the other hand, the axial strain of silica sand-based SBM increased at the same rate from 1% to 5%. By comparing the increasing rate in axial strain of silica sand-based SBM with that of composite soil-based SBM, the former was approximately 0.40% per cycle regardless of the cycle, but the latter was approximately 1.30% per cycle in the last cycle. Furthermore, the excess pore water pressure was large in comparison with the composite soil-based SBM. This is because the silica sand-based SBM showed sand-like behavior due to few fine particles of base soil. However, the maximum excess pore water pressure is smaller than the effective confining pressure. Figure 4.12 and Figure 4.13 show stress-strain curves of composite soil-based SBM and those of silica sand-based SBM, respectively. As mentioned above, it can be seen that the axial strain of composite soil-based SBM dramatically increased after certain point, though the SBM showed elastic deformation for a while after the loading. This trend was observed in all cases regardless of maximum grain size of base soil. The fact that the axial strain of silica sand-based SBM increased more gradually than the composite soil-based SBM is also expressed in Figure 4.13. Figure 4.14 and Figure 4.15 present the effective stress paths of composite soil-based SBM and those of silica sand-based SBM, respectively. The effective stress paths confirm that few excess pore water pressure was generated during the cyclic loading in composite soil-based SBM. For the silica sand-based SBM, while the effective

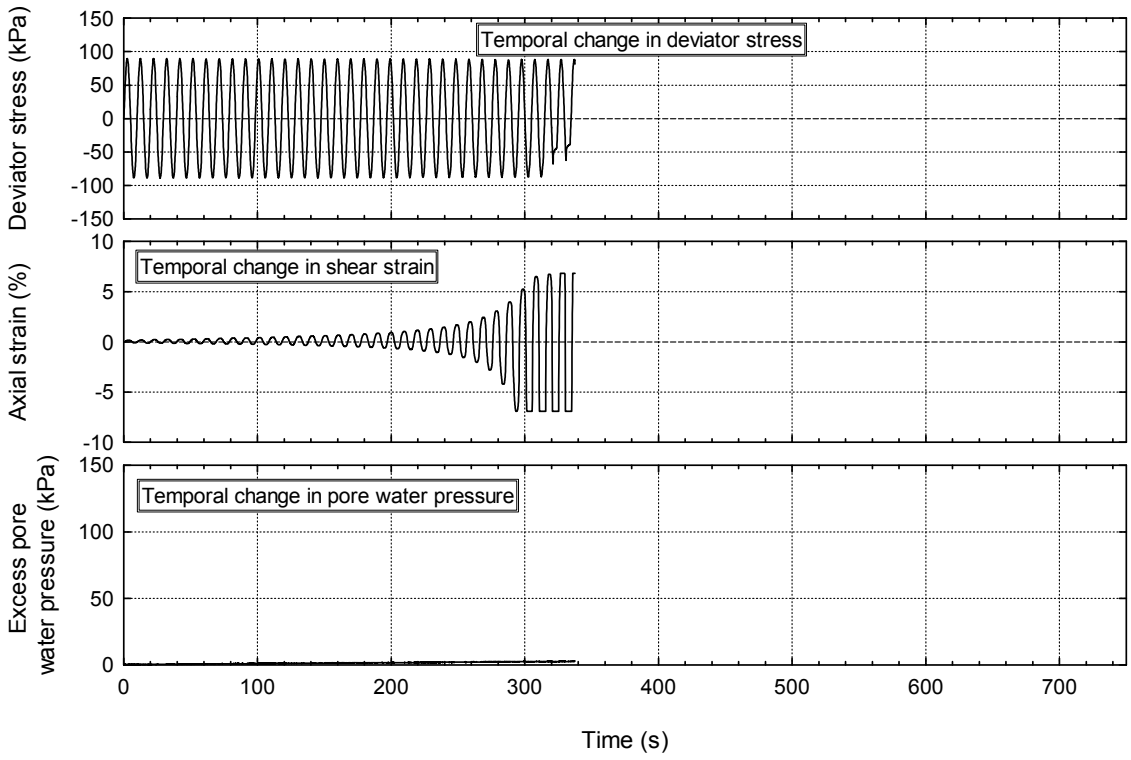

Figure 4.10 Result of cyclic undrained triaxial test (Case-6).

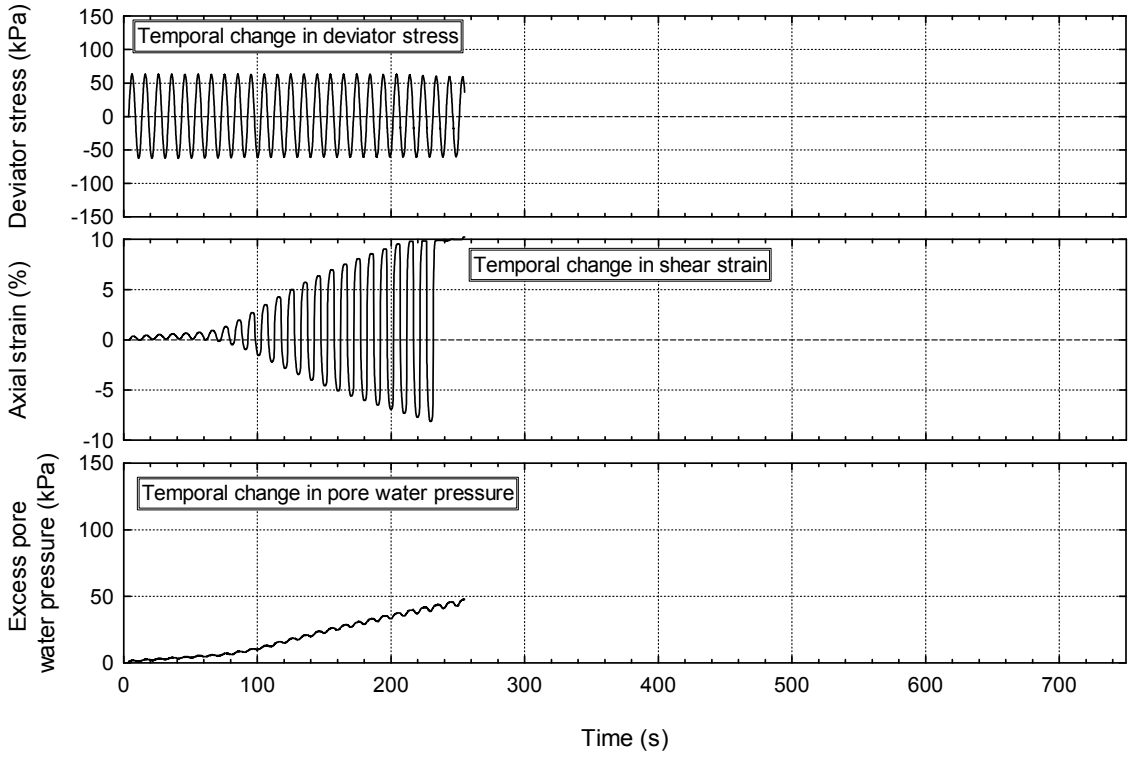

Figure 4.11 Result of cyclic undrained triaxial test (Case-9).

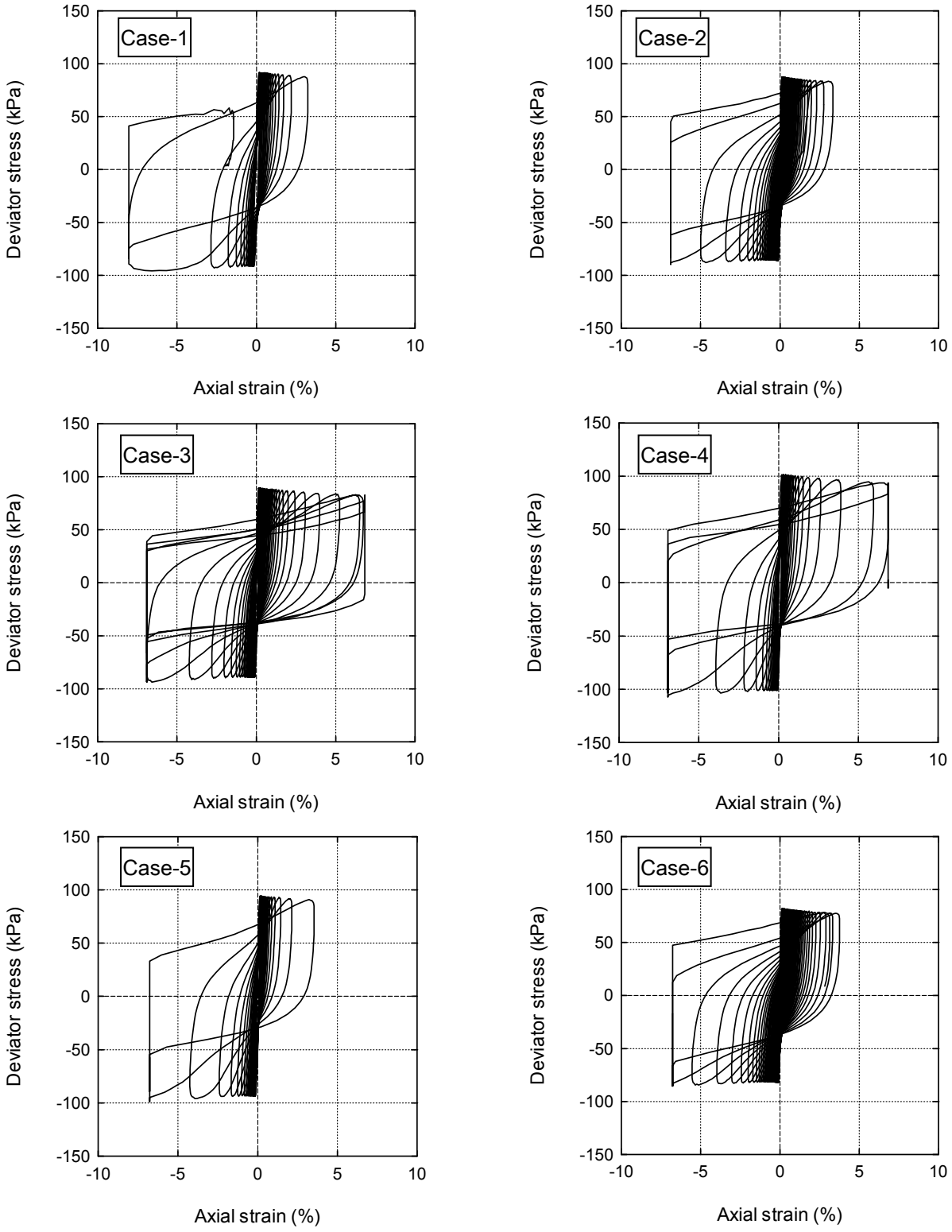

Figure 4.12 Stress-strain curve of composite soil-based SBM (Max. grain size = 4.75 and 0.85 mm).

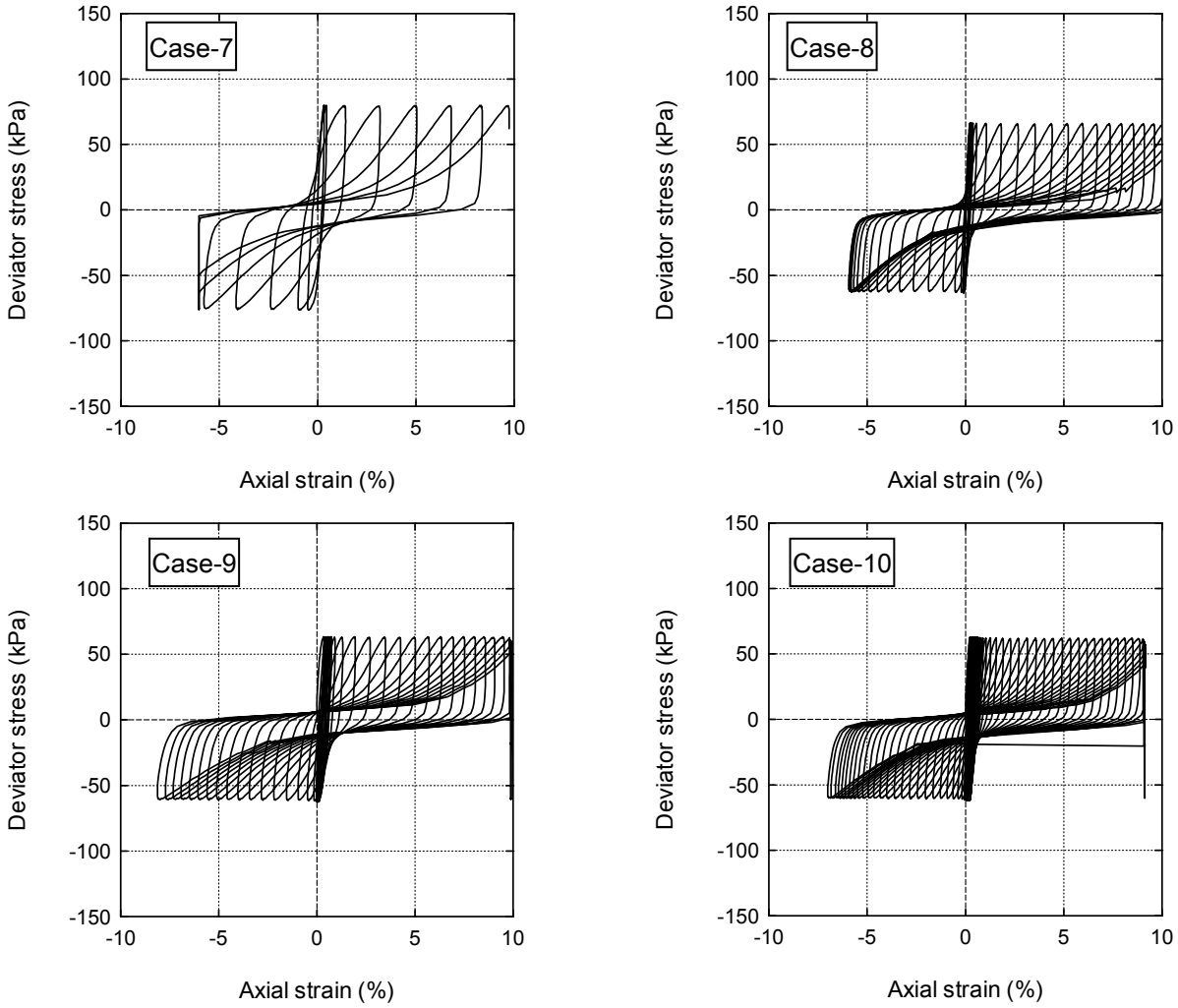

Figure 4.13 Stress-strain curve of silica sand-based SBM (Max. grain size = 0.425 mm).

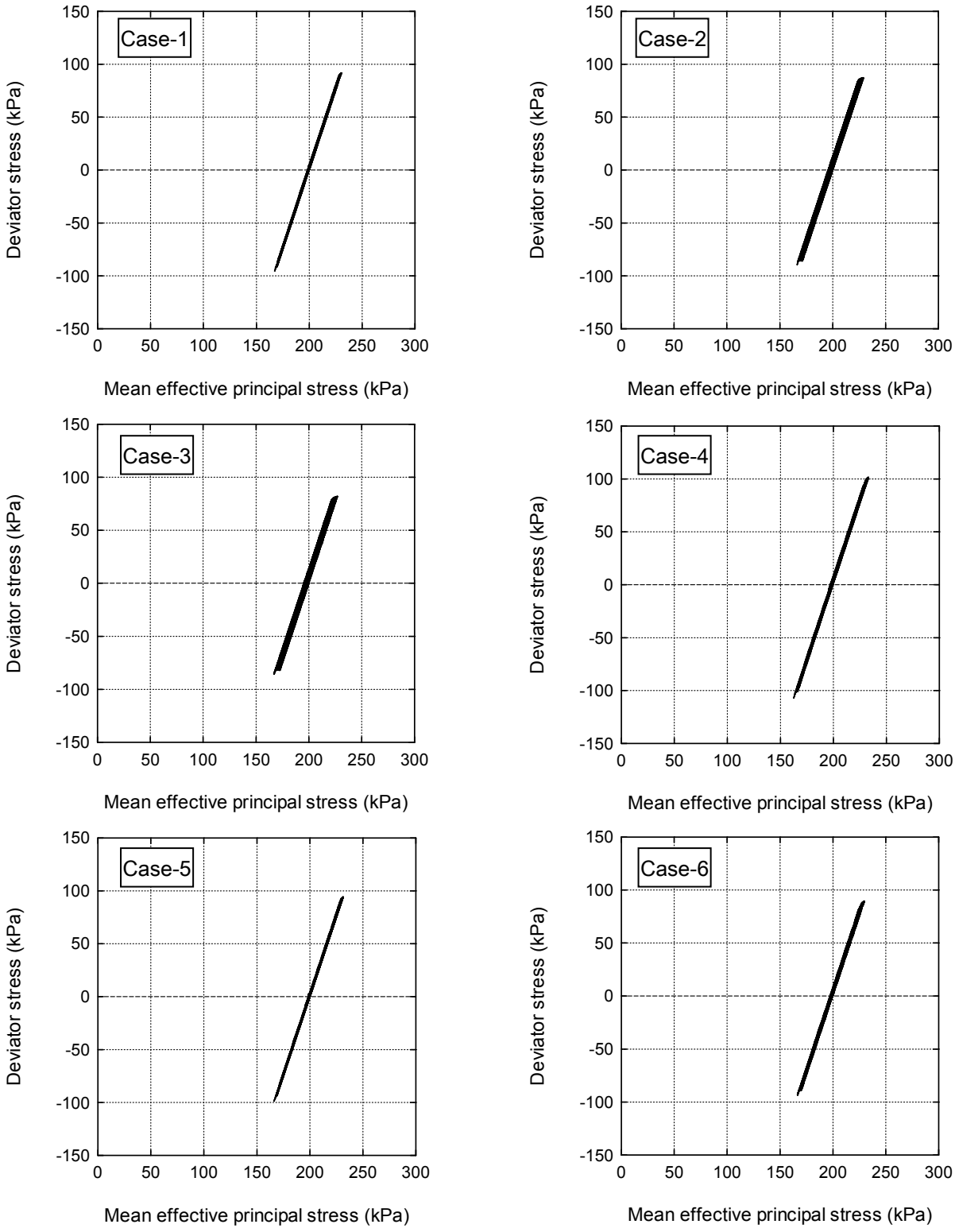

Figure 4.14 Effective stress path of composite soil-based SBM
(Max. grain size = 4.75 and 0.85 mm)

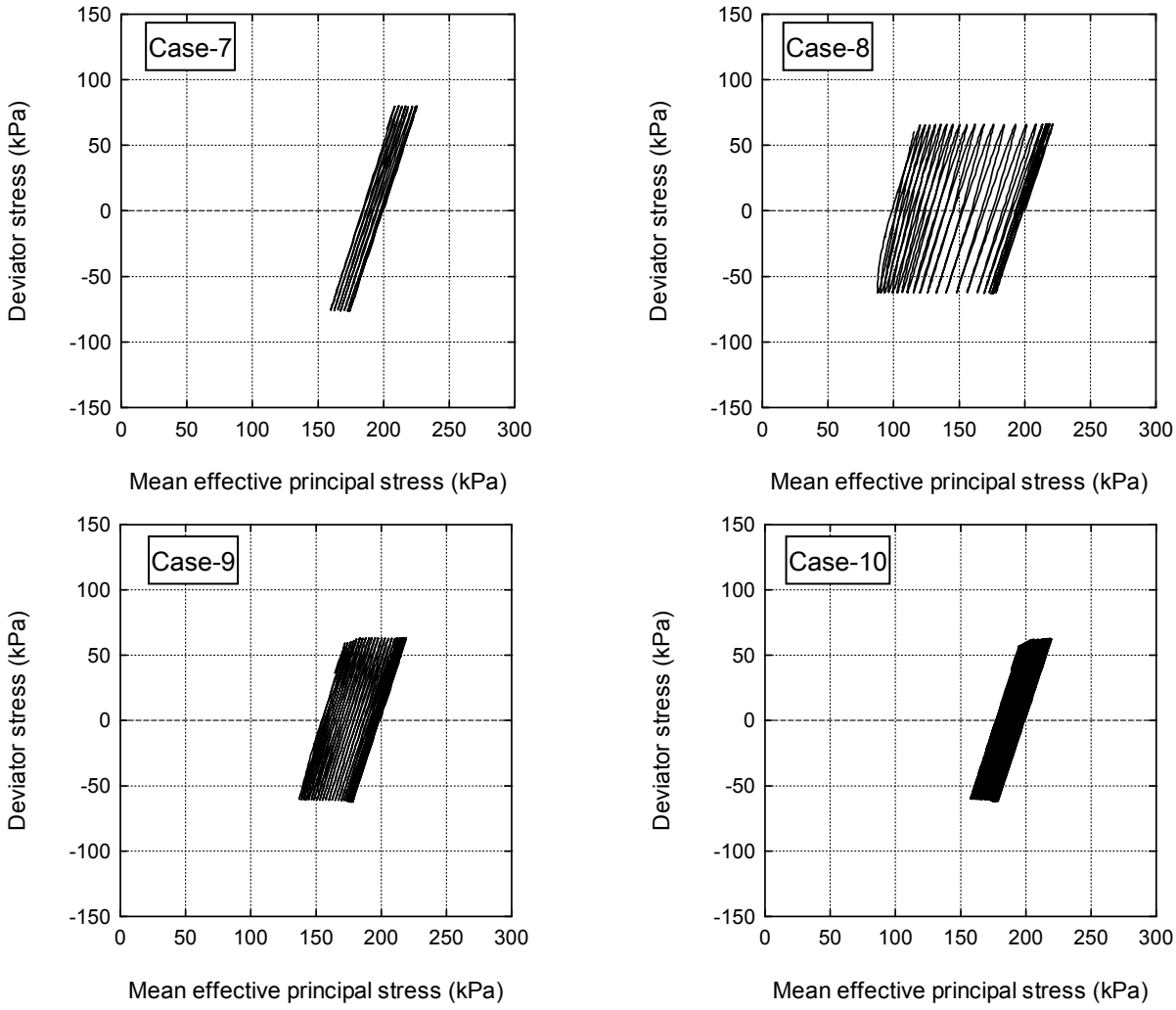

Figure 4.15 Effective stress path of silica sand-based SBM
(Max. grain size = 0.425 mm)

stress path shifted to left with the cyclic loading, approximately 50% of effective stress remained in the specimen at the minimum (Case-8). The maximum excess pore water pressure ratio (the ratio of excess pore water pressure to the effective confining pressure) in each case is summarized in Table 4.5. As seen in this table, the excess pore water pressure ratio is approximately 0.5 at the maximum. Thus, the liquefaction may not be occurred in SBM cutoff wall due to little change in the excess pore water pressure. These observations confirm that stiffness of SBM can be degraded by the seismic excitation, although the liquefaction may not be occurred because of its low hydraulic conductivity.

Table 4.5 Excess pore water pressure in each case

Type of base soil for SBM	Maximum diameter (mm)	Cyclic stress ratio	Excess pore water pressure ratio ($\times 10^{-2}$)
Composite soil	4.75	0.229	1.1
		0.216	2.2
		0.205	2.6
	0.85	0.240	0.9
		0.235	0.9
		0.224	1.5
Silica sand	0.425	0.195	9.4
		0.161	53.3
		0.157	24.4
		0.155	12.4

4.4.2 Cyclic strength of SBM

Figure 4.16 illustrates the cyclic strength curve. In this study, since the excess pore water pressure was comparatively small, the condition with DA = 5% was defined as a failure of specimen. The cyclic strength of two composite soil-based SBM have similar strength characteristics. The slightly higher strength in the SBM with the maximum grain size of 0.85 mm was caused probably due to higher densities of specimens. The silica sand-based SBM has lower cyclic strength. This is because of the less fine particle content. Since the silica-sand base SBM shows sand-like behavior due to less fine particles, relatively high excess pore water pressure can cause the weakening of the specimen due to the decrease in effective stress.

By using the results shown in Figure 4.16, cyclic strength ratio, R_L, was calculated for each SBM. The cyclic strength ratio is defined as the cyclic stress ratio when the number of cycles reaches 20. As a result, the cyclic strength ratio of composite soil-based SBM with the maximum grain size of 4.75 mm, that of 0.85 mm, and silica sand-based SBM were calculated to be approximately 0.225, 0.230, and 0.155, respectively. Ito et al. (2001) conducted cyclic undrained triaxial test on laboratory samples with various fine content, F_c, . The cyclic strength ratios of composite soil-based SBM and of silica sand-based SBM are respectively equivalent with the soil of F_c = 24~32% and that of F_c = 8~16%. Considering that the fine content of composite soil-based SBM and that of silica sand-based SBM are 29.2% and 9.1%, respectively, the cyclic strength ratios obtained in this study can be considered reasonable. For damage prediction of structures on the ground by liquefaction, factor of liquefaction, F_L, calculated by following equation (5.4), (5.5) and (5.6) is commonly used (e.g. Tatsuoka et al. 1980):

$$F_L = \frac{R}{L} \tag{5.4}$$

$$L = \gamma_d \cdot \frac{\alpha_{\max}}{g} \cdot \frac{\sigma_v}{\sigma_v'} \tag{5.5}$$

$$\gamma_d = 1.0 - 0.015x \tag{5.6}$$

where, F_L = factor of safety liquefaction (dimensionless); R = undrained cyclic strength ratio (dimensionless); L = dynamic load induced in the soil element by a seismic excitation (dimensionless); γ_d = reduction factor for dynamic shear stress (dimensionless); $\alpha_{\max}$ = maximum acceleration at the ground surface (gal); g = gravity acceleration (= 980 gal); σ_v = total overburden pressure (kPa); σ_v' = effective overburden pressure (kPa).

This factor can be applied for the sandy ground, but is not suitable to estimate the liquefaction potential in SBM cutoff wall because the excess pore water pressure is not generated during the cyclic loading in SBM. However, acceptable accelerations are respectively calculated as approximately 100 gal and 60 gal for composite soil-based SBM and silica sand-based SBM by these equations, applying the R value obtained not by the liquefaction but by the degradation of stiffness with cyclic loading. Therefore, while the excess pore water pressure will progressively increase, the SBM cutoff wall can be deformed with seismic excitation of acceleration larger than these values.

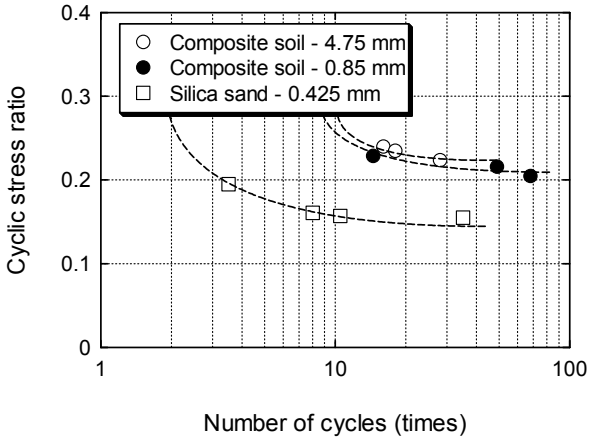

Figure 4.16 Cyclic strength curve at *DA* = 5%.

4.5 Seismic behavior of SBM cutoff wall

4.5.1 Response of model ground against seismic excitation

Response of accelerometers and pore pressure transducers during and after the shaking was monitored and recorded in the control room. In this section, response of SBM cutoff wall and sand layers is discussed with the spectra of each sensor. In this study, excess pore water pressure ratio was applied as an indicator of occurrence of liquefaction. Since the magnitude

of acceleration strongly depends on the direction of accelerometer, the values were not converged into zero in some cases due to the slide of the sensors by the shaking. In the following figures, the experimental results are illustrated in prototype scale unless otherwise noted.

4.5.1.1 In loose sand layer (silicone grease joint)

In this section, seismic behavior of SBM cutoff wall installed in loose sand layer is discussed. In this series, composite soil-based SBM was used for the cutoff wall, and silicone grease was spread on the sides of SBM as joints between SBM cutoff wall and the rigid container.

(1) Input wave: 0.4 Hz-150 mm-25 cycles

Figure 4.17 shows time history of acceleration in each layer and the container at 5.5 m-depth from the soil surface. As shown in this figure, the maximum magnitude of response acceleration is observed at 4 cycles in both sand layers and SBM cutoff wall. Since the response accelerations of sand layer drastically decreased after 10 cycles, it can be considered that the liquefaction occurred at this moment in the sand layers. The magnitude of response acceleration in SBM cutoff wall gradually becomes small with the cycles, but a certain level of the response acceleration remained throughout the entire shaking. Fourier spectra of each response acceleration, shown in Figure 4.18, is drawn to verify the predominant frequency of each response waveform. The fact that the predominant frequency of all waveform is 0.4 Hz is consistent with the frequency of input sinusoidal wave of 0.4 Hz. Thus, SBM cutoff wall can be assumed to be shaken together with the adjacent sand layers during the seismic excitation. The vibration characteristics of SBM cutoff wall depends on that of surrounding ground even when the liquefaction is occurred in the adjacent ground.

Figure 4.19 and Figure 4.20 present temporal changes in excess pore water pressure ratio with the shaking at 3.5 m-depth and 7.5 m-depth, respectively. The excess pore water pressure ratio is the ratio of generated excess pore water pressure to the initial effective stress. Therefore, it can be judged that the liquefaction occurred when the excess pore water pressure ratio reaches 1. The excess pore water pressure ratio in sand layers gradually increased with shaking regardless of the depth, and reached approximately 1.0. Therefore, the sand layers can be liquefied by the shaking. However, the maximum excess pore water pressure ratio is only 0.1 in SBM cutoff wall. These observations confirm that the liquefaction did not occur in SBM cutoff wall because the excess pore water pressure is not generated throughout the entire shaking, although the sand layers are liquefied.

(2) Input wave: 2.0 Hz-100 mm-10 cycles

In Case-2, a sinusoidal wave with higher frequency, smaller amplitude and fewer cycles compared with Case-1 was applied on model ground with same conditions. The acceleration spectra of the ground and container are shown in Figure 4.21. The response acceleration is minimized at 4 cycles, but is recovered to a certain level with cycles. The magnitude of recovered acceleration is two-thirds of the input acceleration at the maximum. Fourier spectra of each response acceleration is shown in Figure 4.22. The frequency of 2.0 Hz is predominant in all sensors because the sinusoidal wave of 2.0 Hz was input. All spectra of

sand layers and SBM cutoff wall show similar form and they are well accorded each other. However, they are poorly fit with the spectrum of the container, and the second and third peak values were varied probably due to the high acceleration and high frequency.

Figure 4.23 and Figure 4.24 present temporal changes in excess pore water pressure ratio with the shaking. Although the larger excess pore water pressure ratio is observed in SBM cutoff wall compared with Case-1, the value is approximately 0.3 in upper SBM at the maximum. The excess pore water pressure ratio in sand layers immediately increased by the shaking, and showed constant value of approximately 1.0 after the shaking. These results also confirm that the liquefaction did not occur in SBM cutoff wall even against the sinusoidal wave with higher frequency, although the adjacent sand layers are liquefied.

(3) Input wave: a realistic wave with high acceleration

Figure 4.25 illustrates the spectra of acceleration obtained from each accelerometer. In Case-3, a realistic wave with high acceleration was applied as an input wave. This wave has the acceleration of approximately 500 gal at the maximum. Although the maximum acceleration of the input wave is 500 gal, the high maximum accelerations of approximately 700 gal and 1000 gal are measured in sand layer and SBM cutoff wall, respectively. Figure 4.26 shows each Fourier spectrum about the acceleration waveform. As seen from this figure, each layer has different vibration characteristics. Considering the fact that the acceleration in the ground was amplified with the shaking at a certain point, cyclic mobility might have occurred in the ground. The cyclic mobility is a phenomenon where the stiffness of the ground is enhanced during the shaking due to a positive dilatancy, and cause a reduction of pore water pressure and amplification of acceleration. Thus, the waveform of the container was not well transmitted to the ground because of the cyclic mobility.

Figure 4.23 and Figure 4.24 show time histories of excess pore water pressure ratio with the shaking. In this case, the excess pore water pressure ratio in the upper SBM cutoff wall increased to 0.8 during the shaking. These observations suggest that the pore water pressure can be increased by the shaking with high acceleration, although a certain amount of effective stress can be maintained in SBM cutoff wall. In these figures, drastic reduction of pore water pressure, which is assumed to be due to the cyclic mobility during the shaking, can be observed in the sand layers after elapsed time of 20 s.

4.5.1.2 With unsymmetrical earth pressure (silicone grease joint)

In Case-4, the same sinusoidal wave as Case-1 was applied on the ground with unsymmetrical densities. The left sand layer was prepared with relative density of approximately 70% and the right one was prepared with that of approximately 40%. Silicone grease was spread on the sides of SBM cutoff wall to fill the gap between the cutoff wall and the container.

Figure 4.29 shows time history of acceleration in each layer and the container at 5.5 m-depth from the soil surface. As shown in this figure, the constant acceleration is obtained in the dense sand layer, and the amplitude is not attenuated during the entire shaking. Compared with the response acceleration in Case-1 shown in Figure 4.17, it is obvious that the high acceleration was maintained in the dense sand layer. On the other hand, the response

acceleration in loose sand layer has variation with the cycles. The value becomes larger than the value of container at 14~16 cycles, and decreases after 17 cycles. The response acceleration in SBM cutoff wall shows similar waveform with that in the dense sand layer; thus, the more constant acceleration was input during the shaking compared with Case-1. Fourier spectrum of each response acceleration is shown in Figure 4.30. Since the frequency of input sinusoidal wave is 0.4 Hz as same as Case-1, the predominant frequencies of all waveform are 0.4 Hz. While one adjacent sand layer is liquefied as mentioned below, the whole model ground shows same vibration characteristics.

The time histories of excess pore water pressure ratio at 3.5 m-depth and 7.5 m-depth are shown in Figure 4.31 and Figure 4.32, respectively. Although the excess pore water pressure ratio in the loose sand layer increased to more than 0.8, that values at 3.5 m-depth and 7.5 m-depth respectively increased no further than approximately 0.6 and 0.4 in the dense sand layer. Furthermore, the value in dense sand layer gradually decreased after the shaking. Considering the facts that the excess pore water pressure ratio in loose sand layer reached to 1.0 with the same input wave in Case-1 and the constant value is observed after the shaking, the liquefaction might be occurred in the upper part of loose sand layer as well as in Case-4; but, the occurrence of liquefaction in lower part is difficult to be judged from Figure 4.32 because the excess pore water pressure ratio increased only to 0.8 at the maximum and gradually decreased after the shaking. Anyway, it can be seen that the increment of excess pore water pressure in the dense sand layer is inhibited compared with in the loose sand layer. The excess pore water pressure ratio in SBM cutoff wall is smaller than 0.1 during the shaking regardless of the depth.

4.5.1.3 In loose sand layer (round head pin joint)

In Case-5~7, the same sinusoidal wave as Case-1 was applied on the ground with loose sand layer. All conditions in these cases are same with Case-1 except a base soil of SBM cutoff wall and a material at a gap between SBM cutoff wall and rigid container. In Case-5~10, silica sand-based SBM was used for cutoff wall by considering that the sand layers were prepared by silica sand. Besides, in these cases, in order to visualize the deformation of SBM cutoff wall with the shaking and to minimize the friction between SBM cutoff wall and the rigid container, round head pins were mounted at intervals of 20 mm from top to bottom on the sides of SBM cutoff wall instead of silicone grease. Thus, SBM cutoff wall can move more freely in these cases. In this section, the experimental result of Case-6 is shown and discussed as a representative example. Basically same results are obtained in Case-5 and 7. The detail of experimental results obtained from each case is summarized as appendix at the end of this dissertation.

Figure 4.33 shows time histories of acceleration in each layer and the container at 5.5 m-depth from the soil surface. As shown in this figure, the amplitude of input acceleration is smaller than Case-1, although the same sinusoidal wave was applied. Besides, the response accelerations after the shaking are not converged into zero due to rotation of the sensors. From this figure, it can be seen that the magnitude of acceleration becomes small after 9

cycles in all layers. As same as the results of Case-1 shown in Figure 4.17, the response acceleration in SBM cutoff wall is remained at a certain amplitude during the shaking. Fourier spectra of each response acceleration shown in Figure 4.34 are similar with the experimental result of Case-1 shown in Figure 4.18. The predominant frequencies of all acceleration is 0.4 Hz, which is the frequency of input sinusoidal wave.

Figure 4.35 shows temporal changes in excess pore water pressure ratio with the shaking at 5.5 m-depth. In Case-6~10, one pore pressure transducer was embedded in each layer at 110 mm-depth in model scale. The excess pore water pressure ratio in sand layers increases with shaking, and maintains the value larger than 1.0 after the shaking. Therefore, the sand layers can be assumed to be liquefied by the shaking. However, the maximum excess pore water pressure ratio is only 0.2 in SBM cutoff wall, even though the silica sand-based SBM were used in this case. These observations confirm that liquefaction did not occur in SBM cutoff wall because the excess pore water pressure is not generated throughout the entire shaking, although the sand layers are liquefied.

4.5.1.4 In dense sand layer (round head pin joint)

In Case-8~10, the same sinusoidal wave as Case-1 and 5~7 was applied on the ground with dense sand layer. Both sand layers were prepared with their relative densities of approximately 70%. In this section, the experimental result of Case-9 is shown and discussed as a representative example because basically same results are also obtained in Case-8 and 10. The detail of experimental results obtained from each case is summarized as appendix at the end of this dissertation.

Time histories of acceleration in each layer and the container at 5.5 m-depth are shown in Figure 4.36. As shown in this figure, the waveform of input acceleration is completely same with that in Case-6 shown in Figure 4.33. From this figure, although the amplitude of response accelerations in left sand layer and SBM cutoff wall are small compared with input acceleration, it can be seen that the constant acceleration is obtained in both sand layers, and the amplitudes are not attenuated during the entire shaking compared with the result in Case-6. Fourier spectra of each response acceleration shown in Figure 4.37 are similar with the experimental result of Case-1 shown in Figure 4.18. Since the frequency of 0.4 Hz is predominant in all accelerations, it can be assumed that the sand layers and SBM cutoff wall in the model displaced monolithically.

Figure 4.38 shows changes in excess pore water pressure ratio with the shaking at 5.5 m-depth. Although the excess pore water pressure ratio in sand layers increases with shaking and attained approximately 1.0 after the shaking, that in SBM cutoff wall increases no further than approximately 0.2. Therefore, it can be concluded that the SBM cutoff wall did not liquefy for the applied sinusoidal wave regardless of type of base soil.

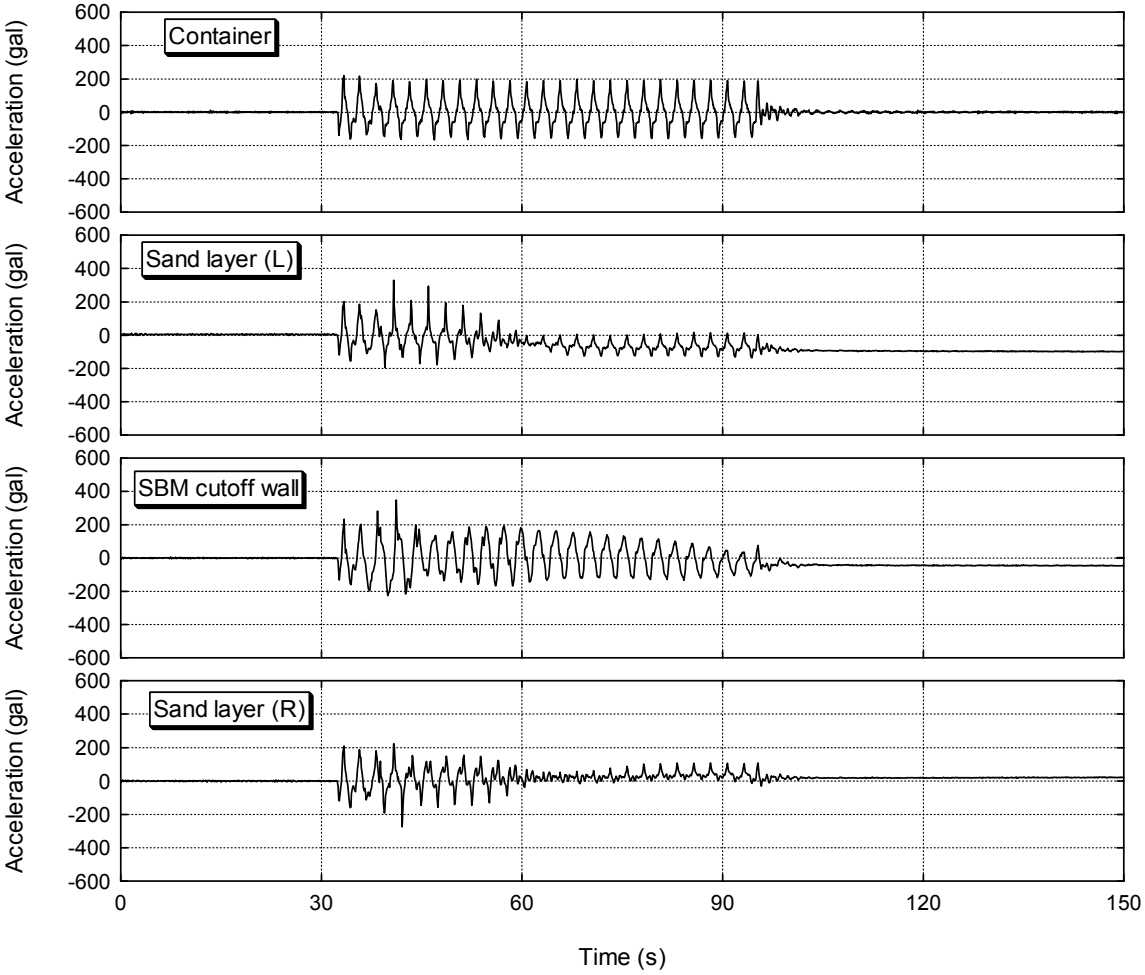

Figure 4.17 Time history of acceleration (Case-1, at 5.5 m-depth).

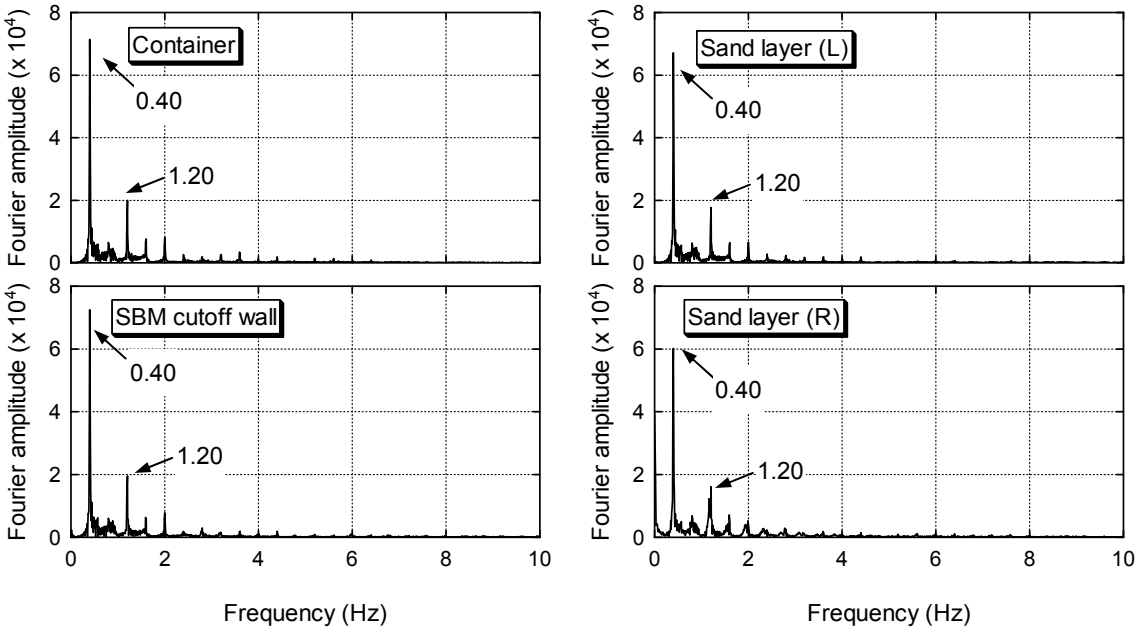

Figure 4.18 Comparison of Fourier spectrum (Case-1, at 5.5 m-depth).

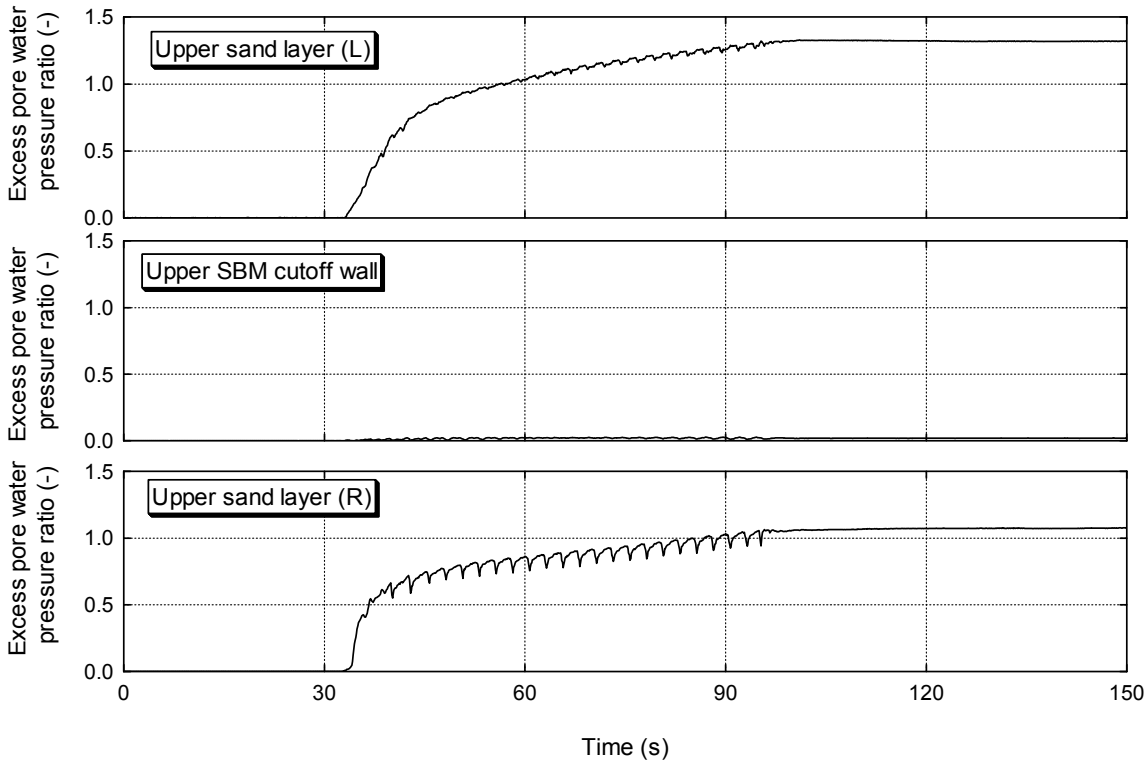

Figure 4.19 Time history of excess pore water pressure ratio (Case-1, at 3.5 m-depth).

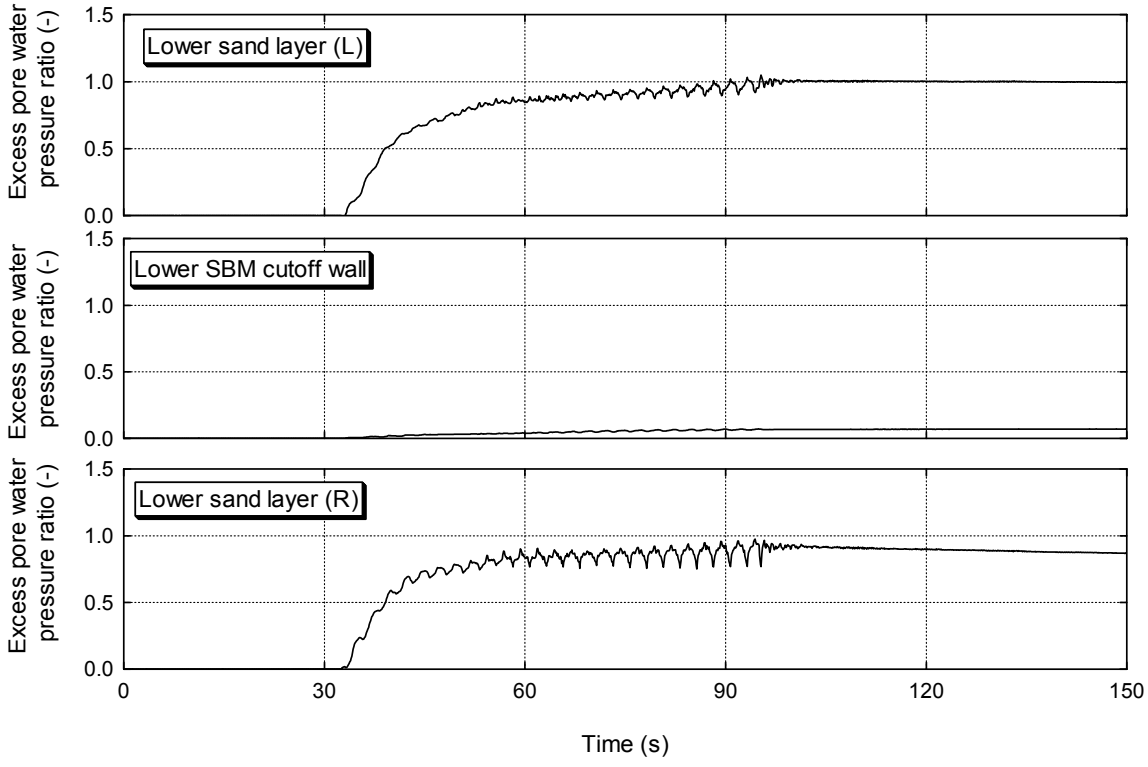

Figure 4.20 Time history of excess pore water pressure ratio (Case-1, at 7.5 m-depth).

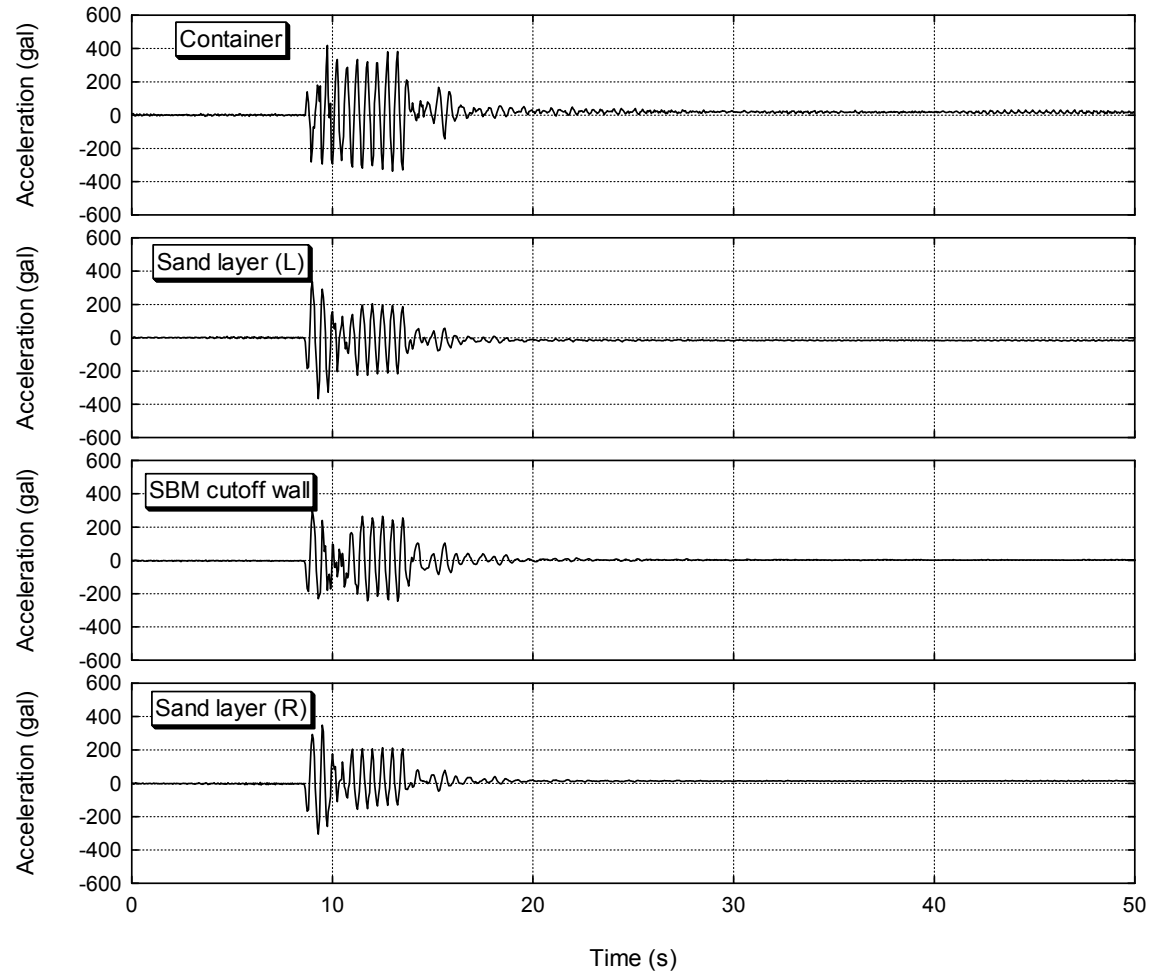

Figure 4.21 Time history of acceleration (Case-2, at 5.5 m-depth).

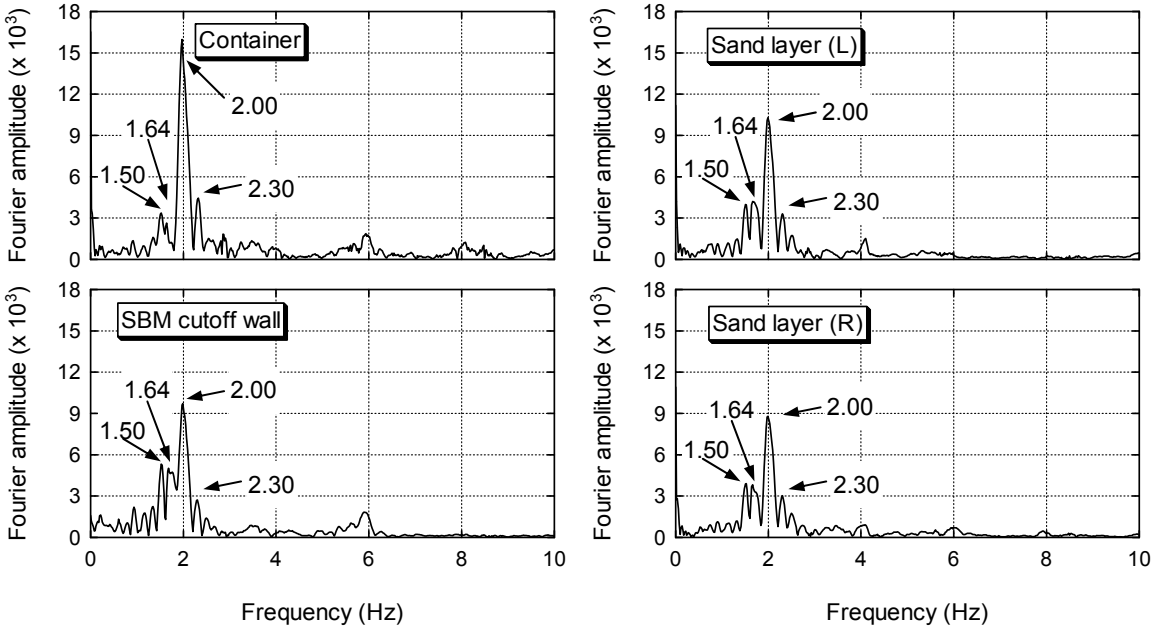

Figure 4.22 Comparison of Fourier spectrum (Case-2, at 5.5 m-depth).

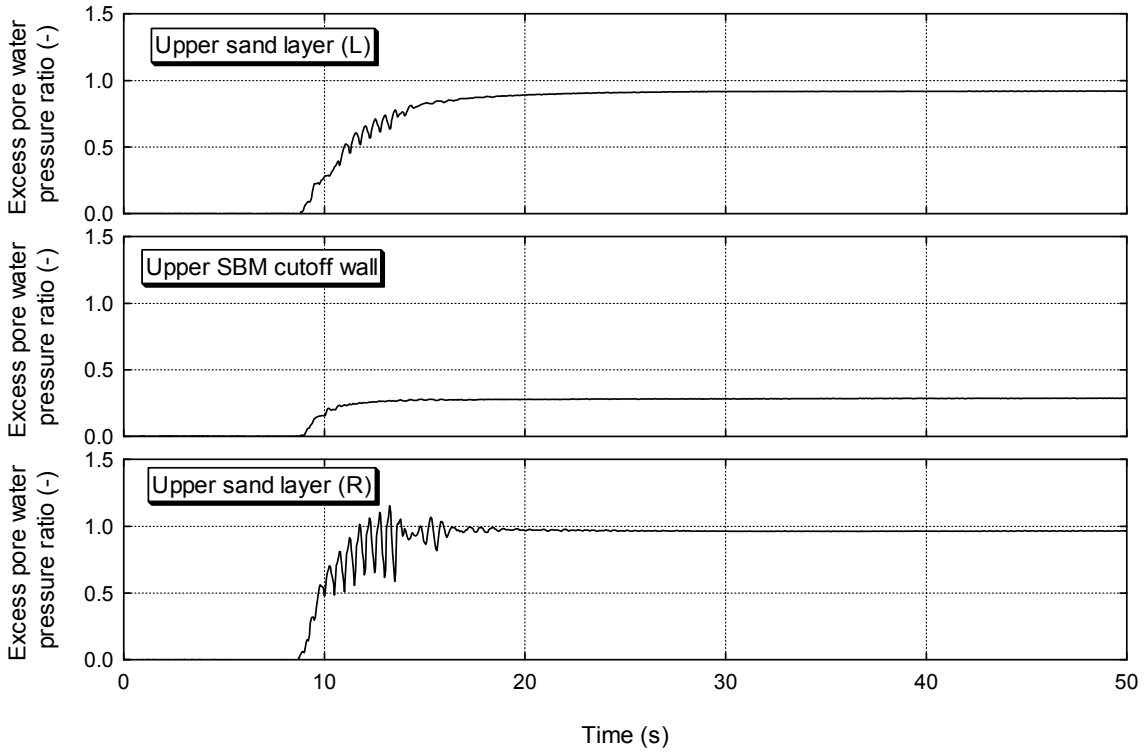

Figure 4.23 Time history of excess pore water pressure ratio (Case-2, at 3.5 m-depth).

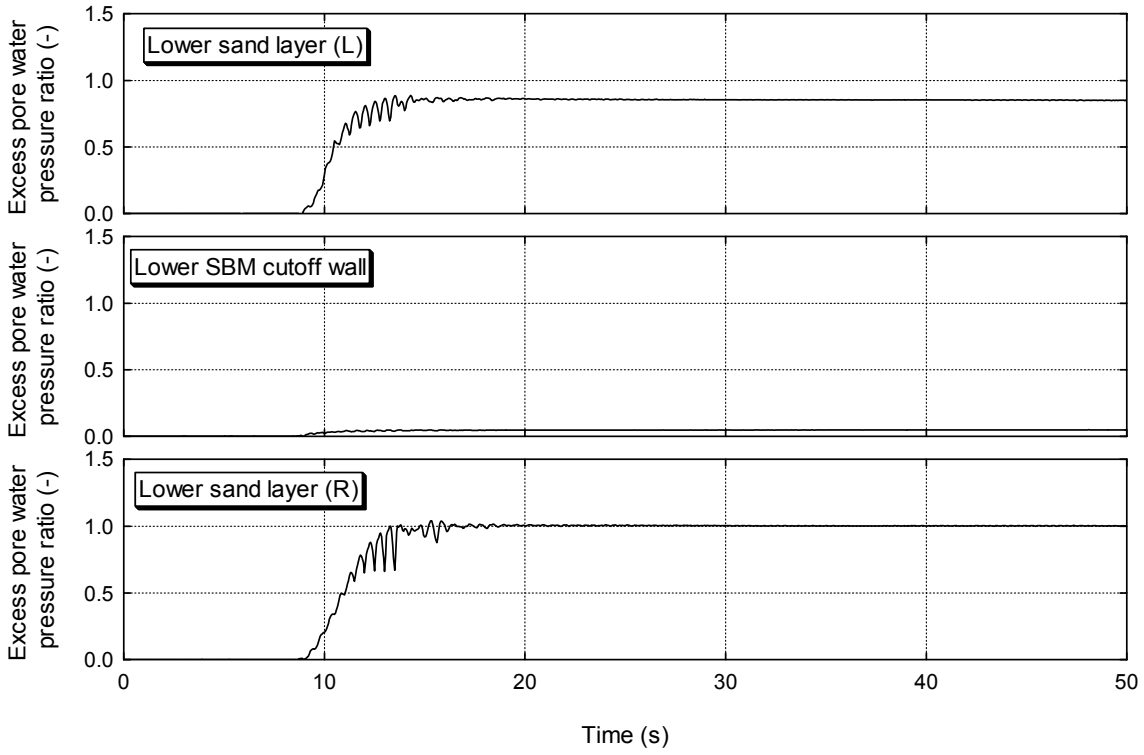

Figure 4.24 Time history of excess pore water pressure ratio (Case-2, at 7.5 m-depth).

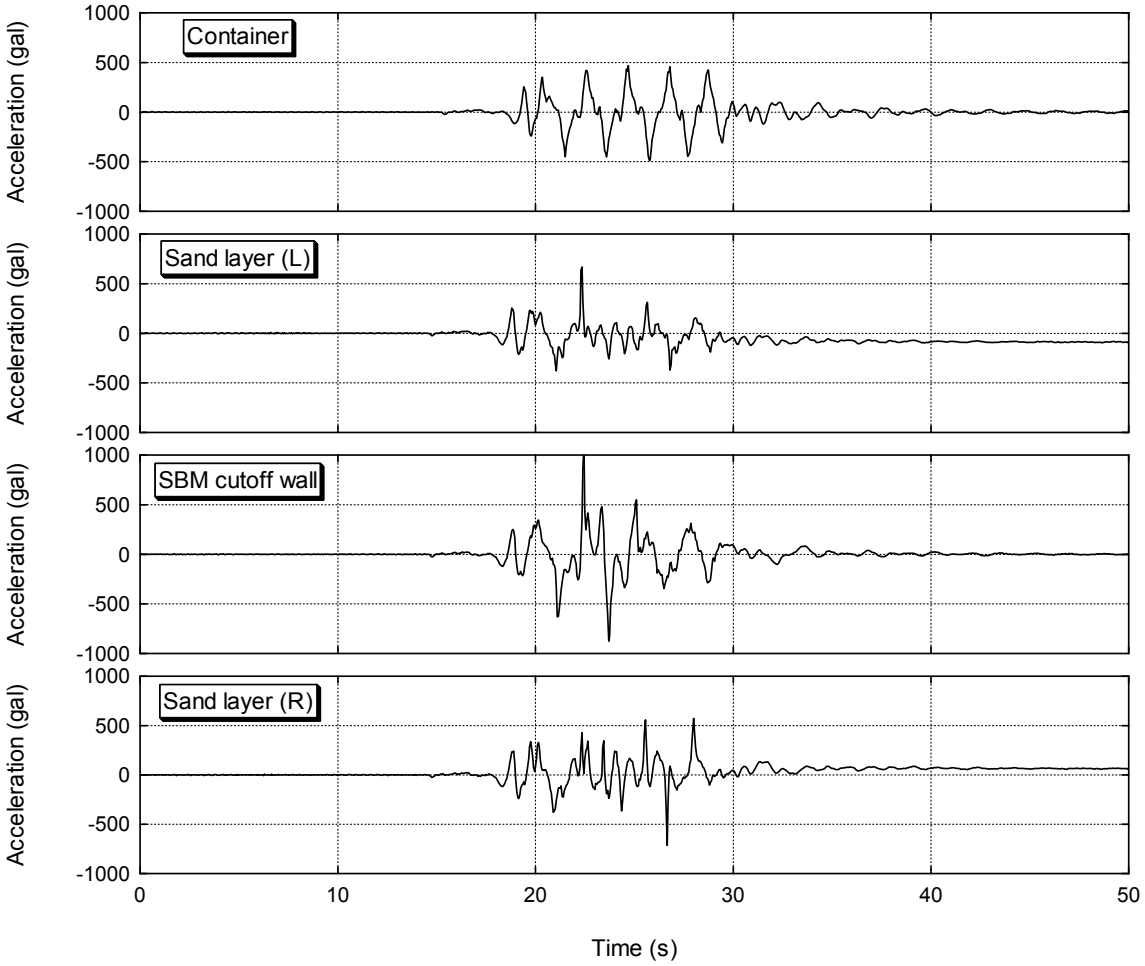

Figure 4.25 Time history of acceleration (Case-3, at 5.5 m-depth).

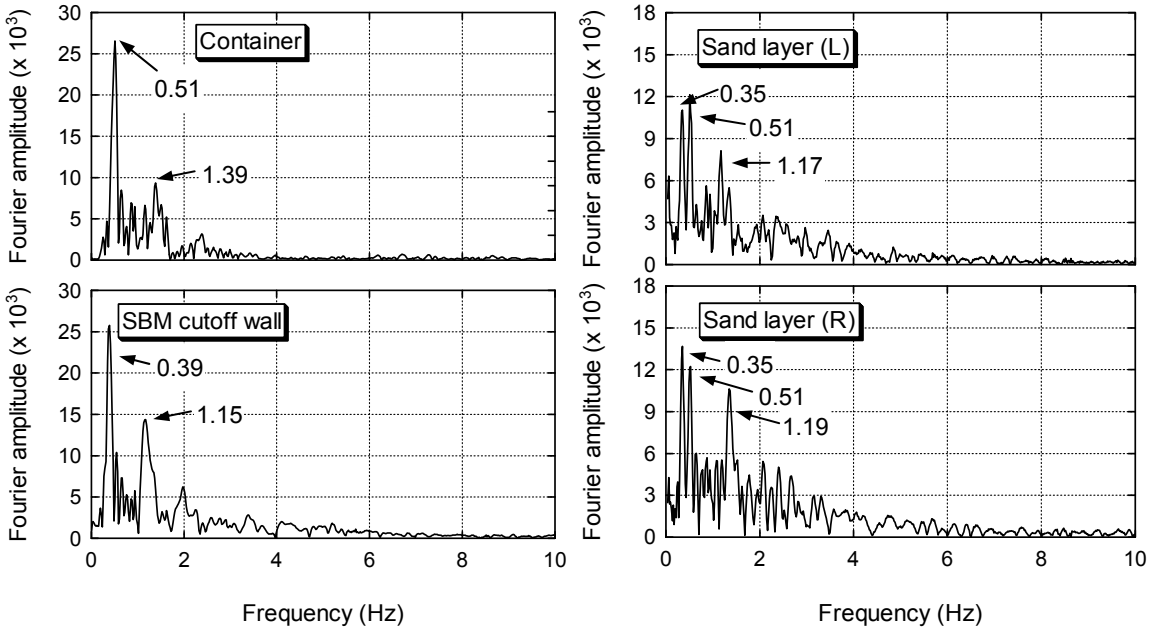

Figure 4.26 Comparison of Fourier spectrum (Case-3, at 5.5 m-depth).

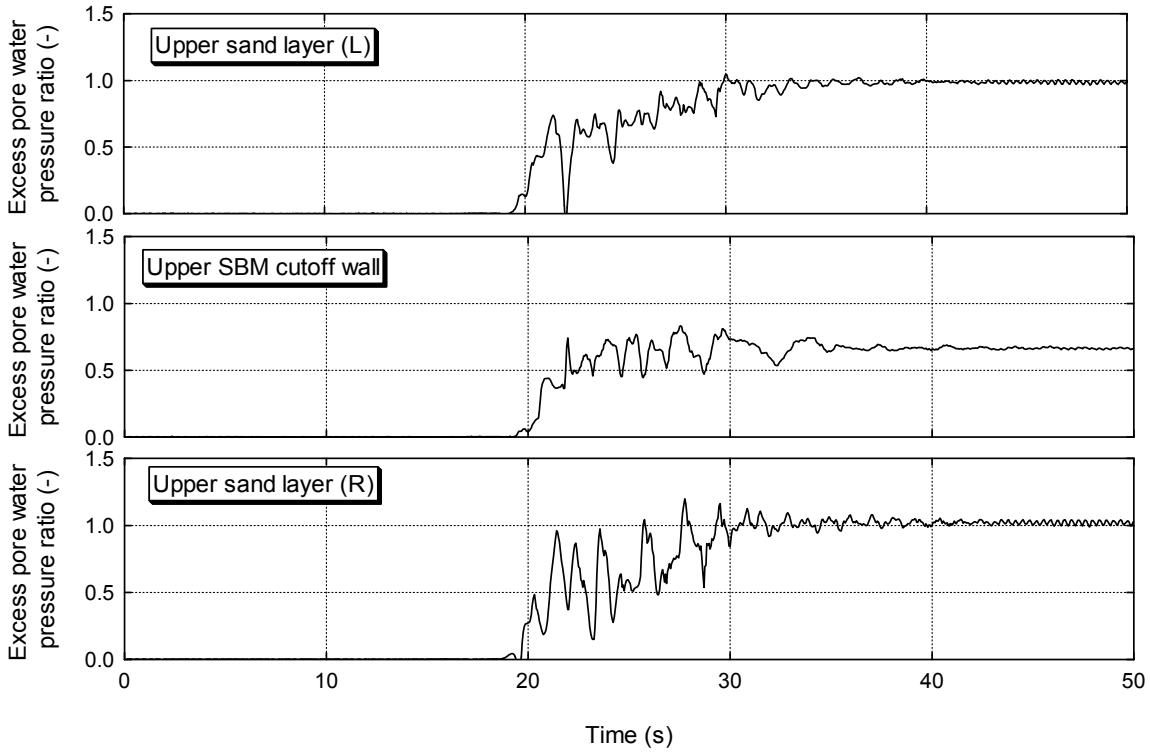

Figure 4.27 Time history of excess pore water pressure ratio (Case-3, at 3.5 m-depth).

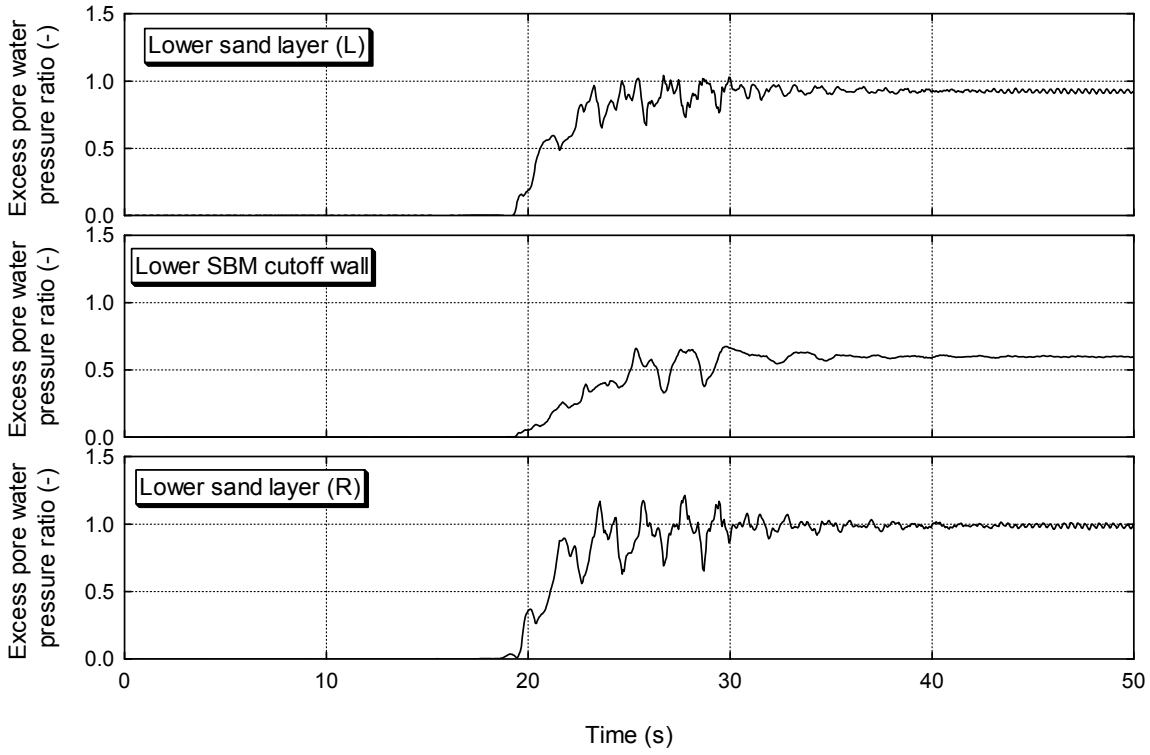

Figure 4.28 Time history of excess pore water pressure ratio (Case-3, at 7.5 m-depth).

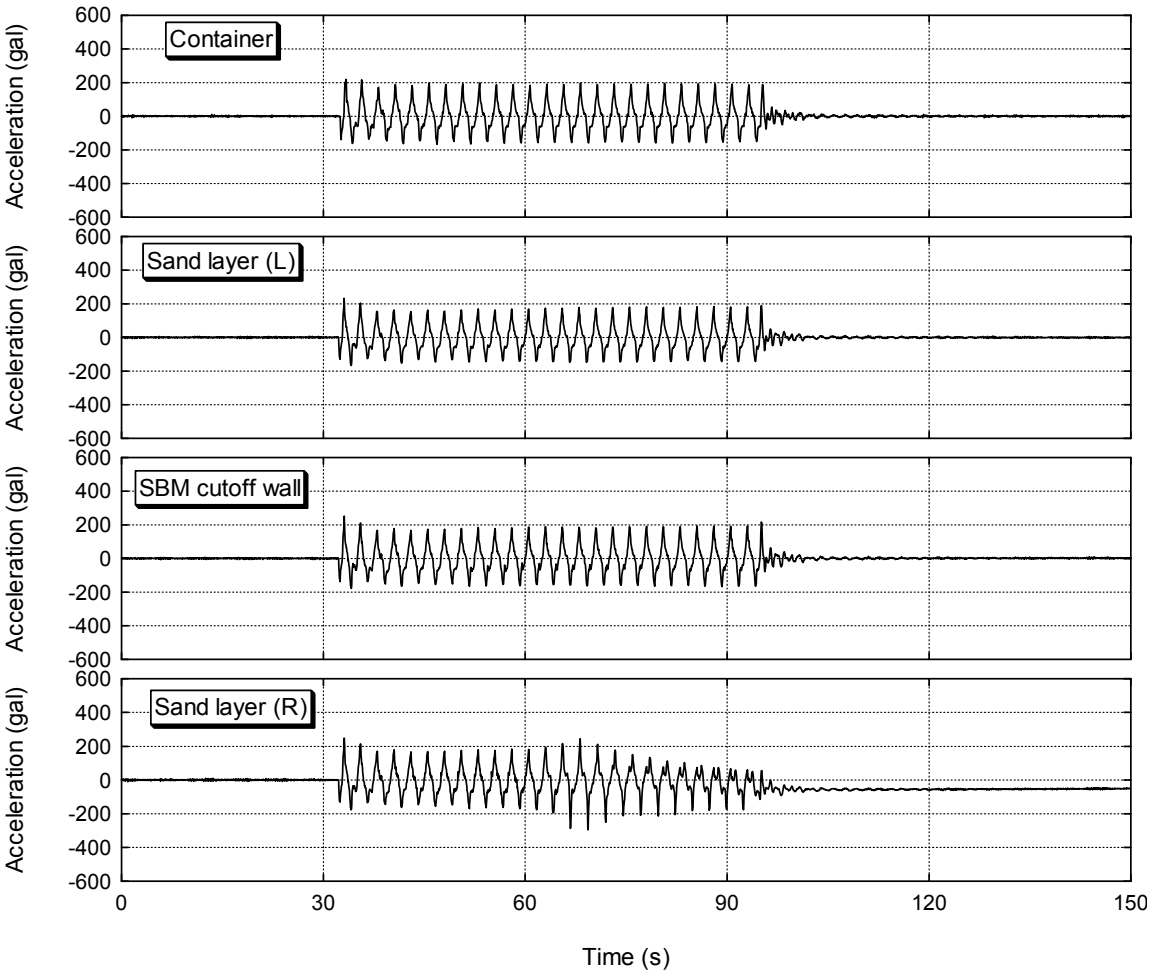

Figure 4.29 Time history of acceleration (Case-4, at 5.5 m-depth).

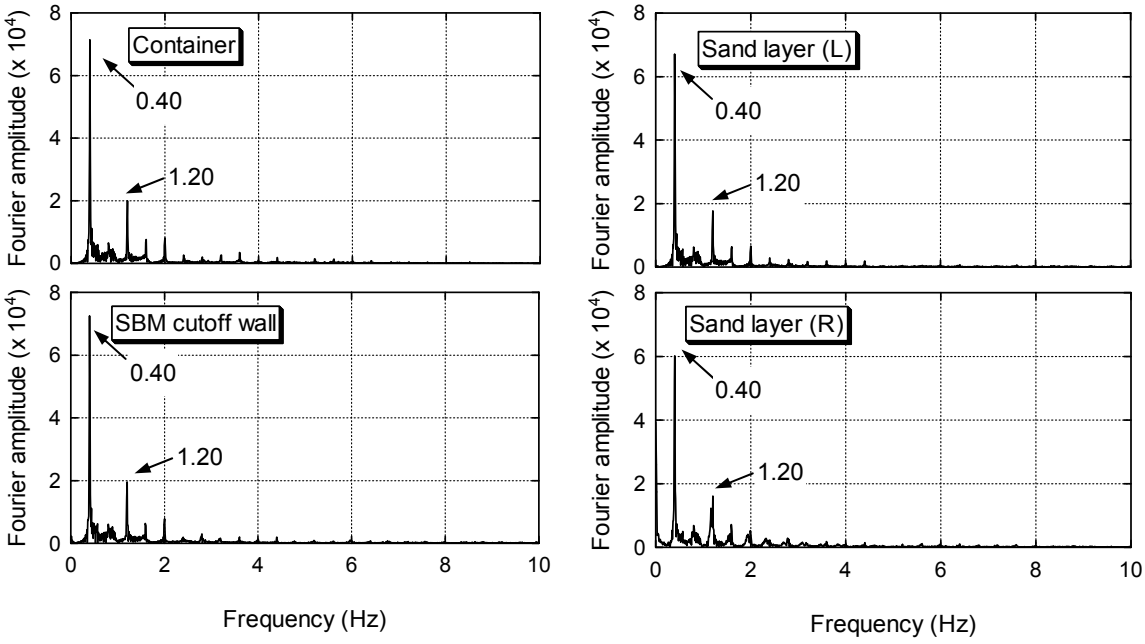

Figure 4.30 Comparison of Fourier spectrum (Case-4, at 5.5 m-depth).

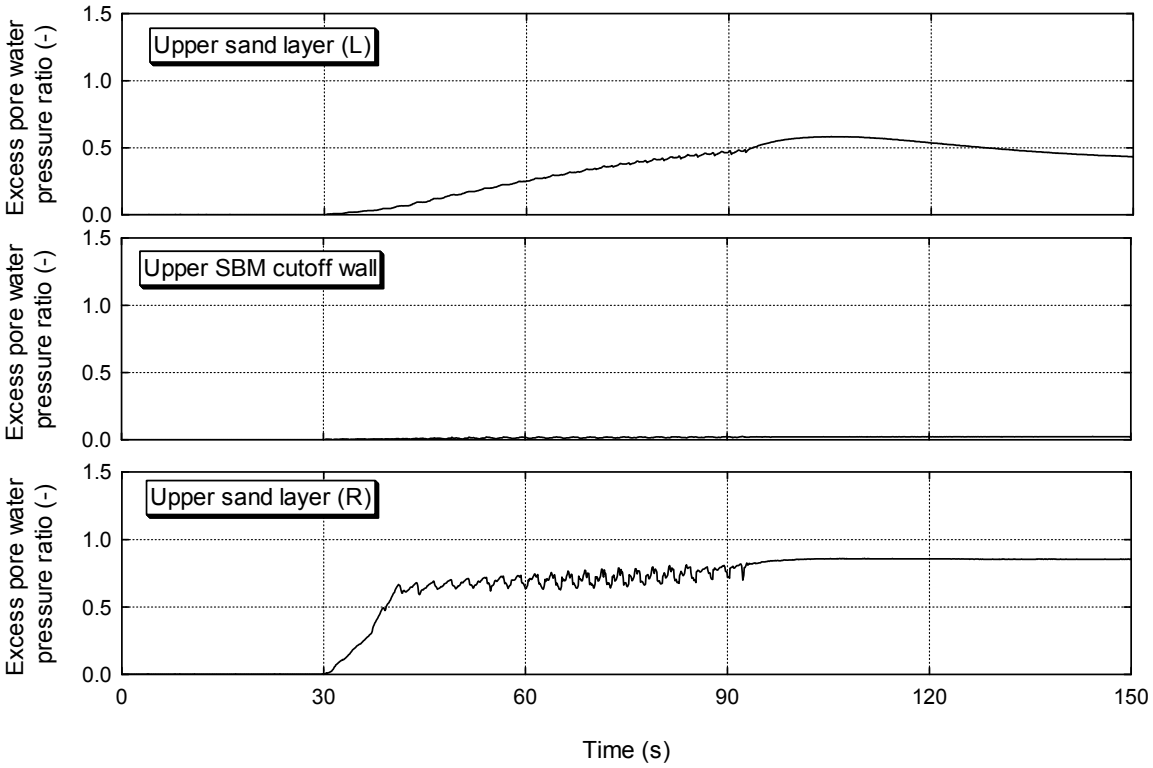

Figure 4.31 Time history of excess pore water pressure ratio (Case-4, at 3.5 m-depth).

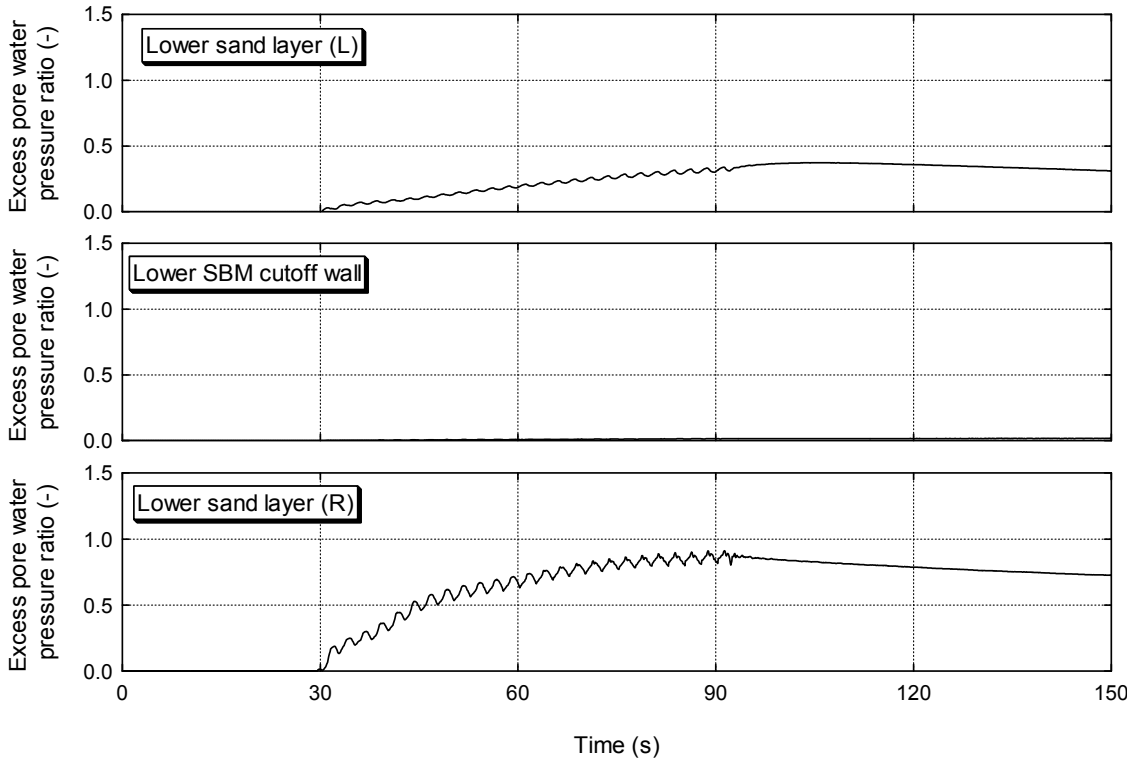

Figure 4.32 Time history of excess pore water pressure ratio (Case-4, at 7.5 m-depth).

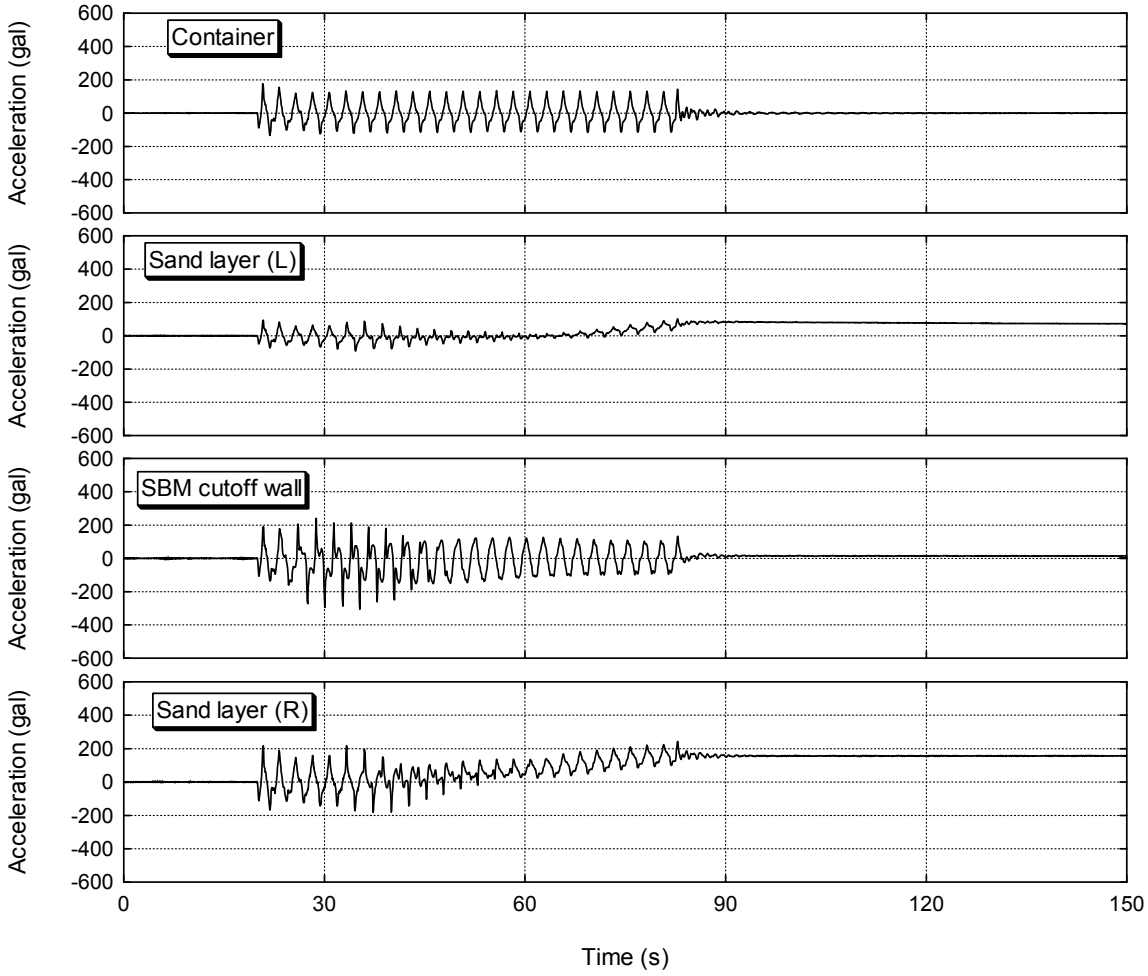

Figure 4.33 Time history of acceleration (Case-6, at 5.5 m-depth).

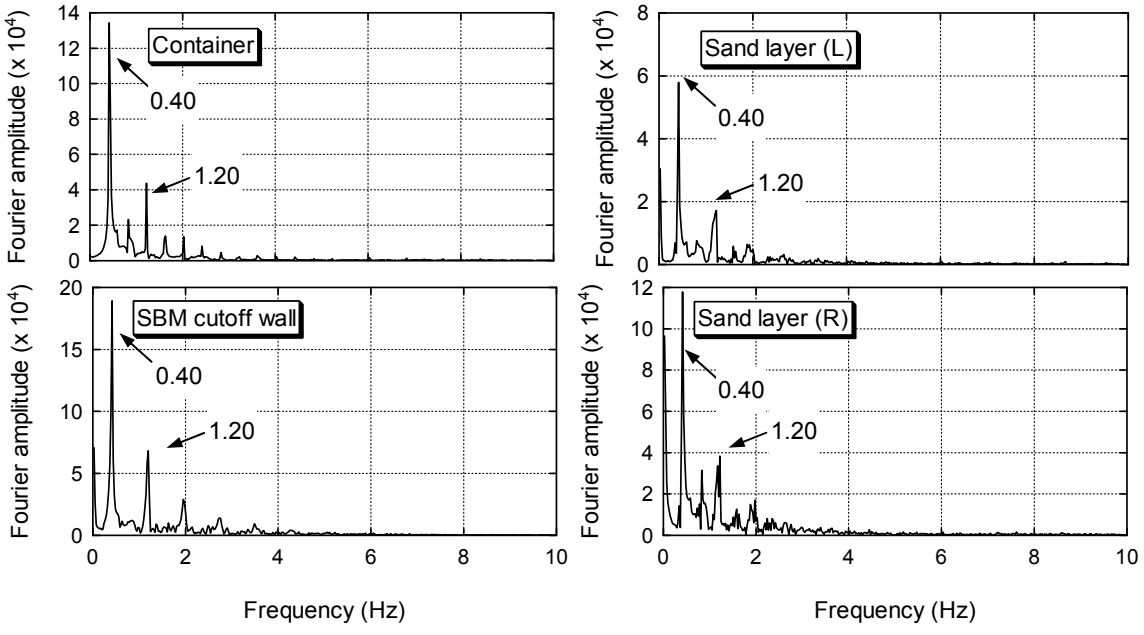

Figure 4.34 Comparison of Fourier spectrum (Case-6, at 5.5 m-depth).

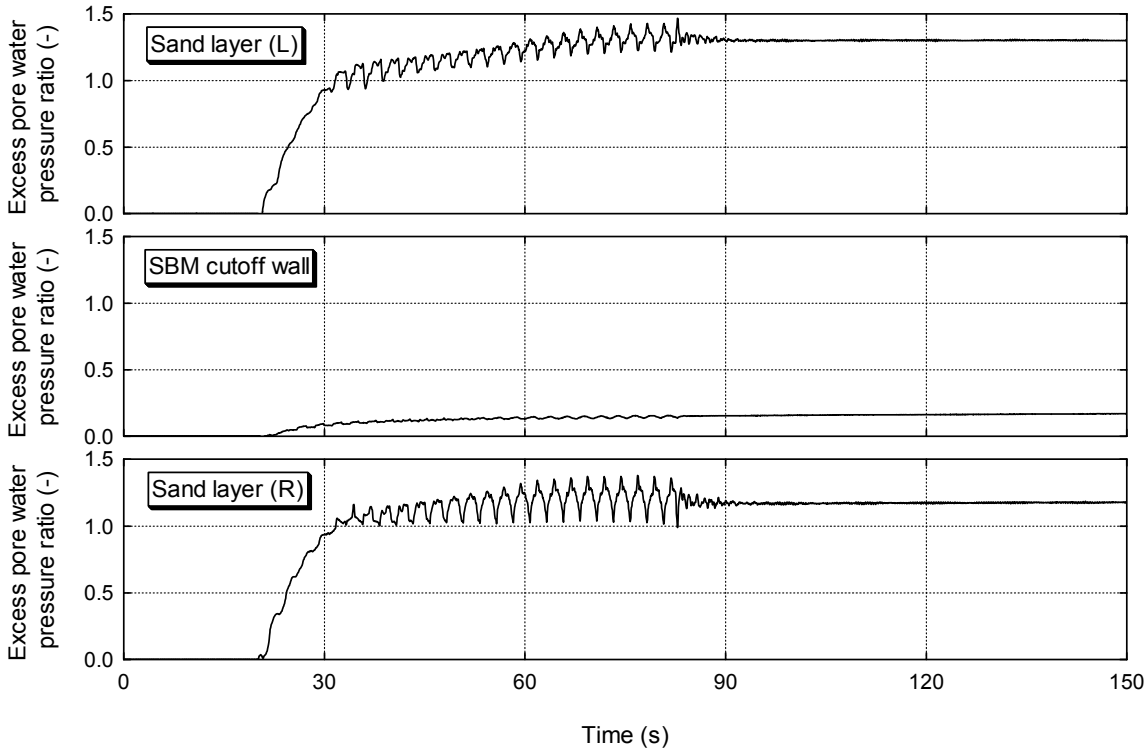

Figure 4.35 Time history of excess pore water pressure ratio (Case-6, at 5.5 m-depth).

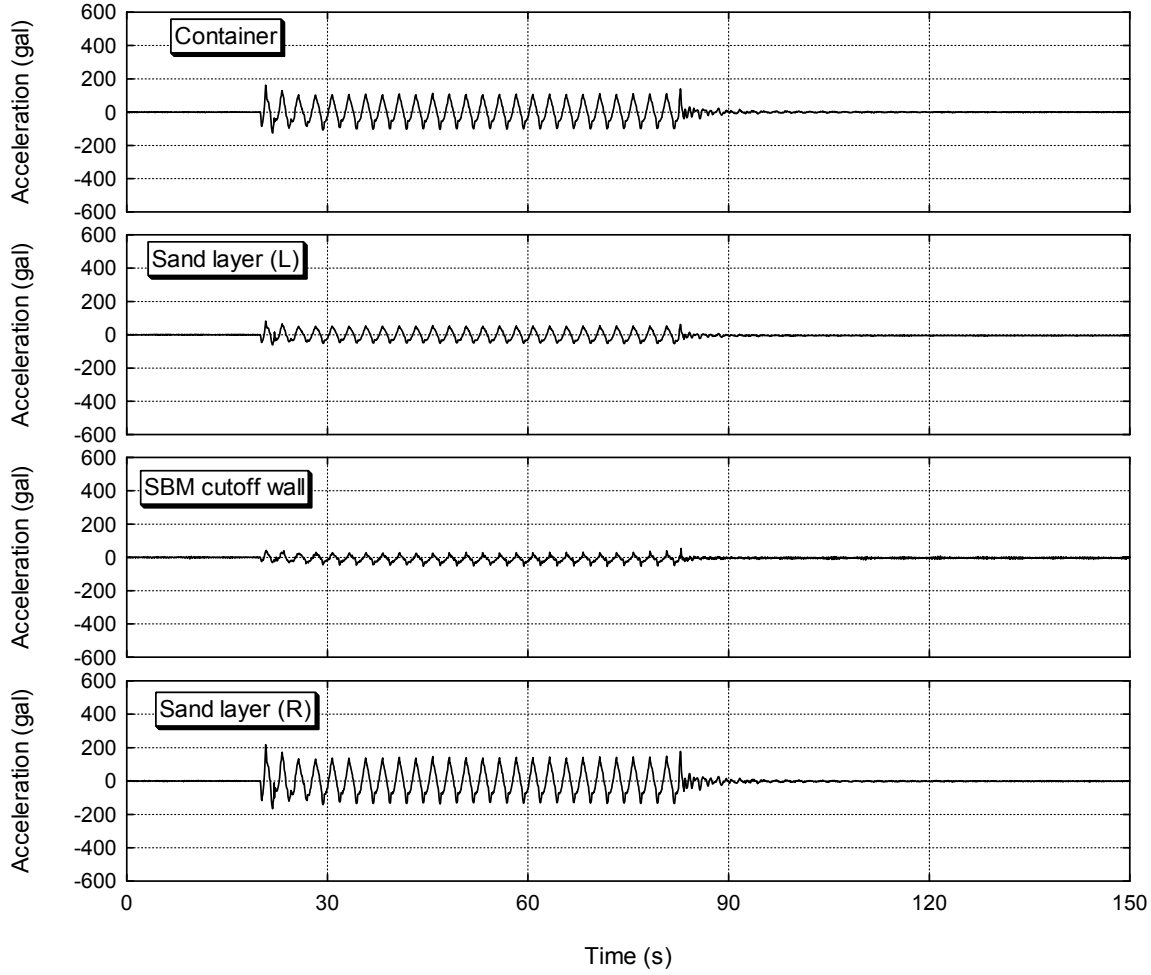

Figure 4.36 Time history of acceleration (Case-9, at 5.5 m-depth).

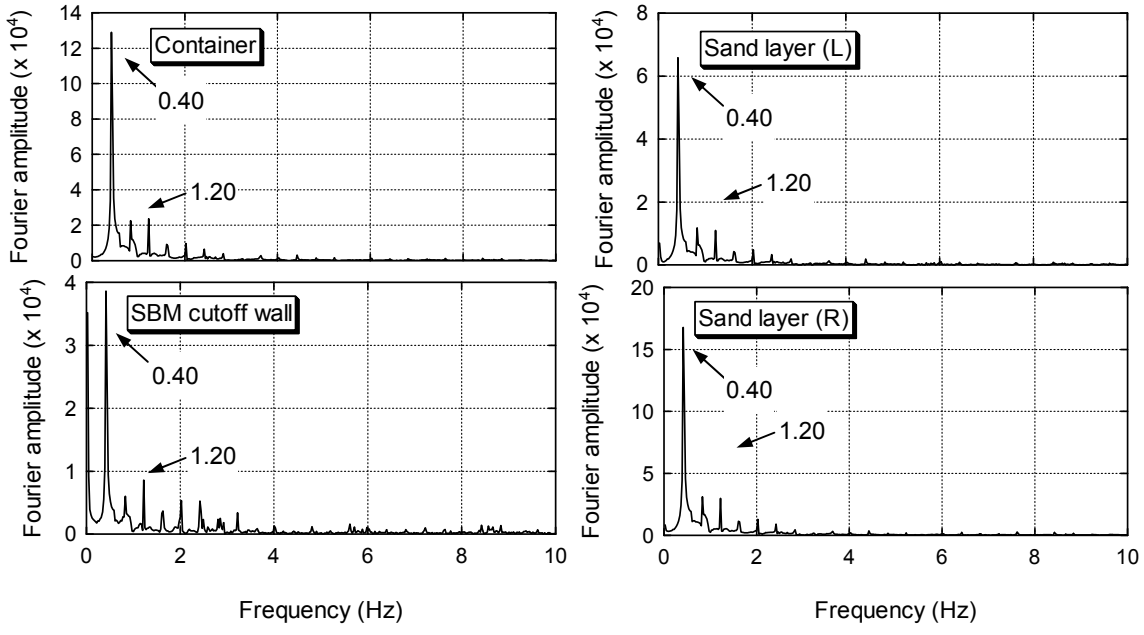

Figure 4.37 Comparison of Fourier spectrum (Case-9, at 5.5 m-depth).

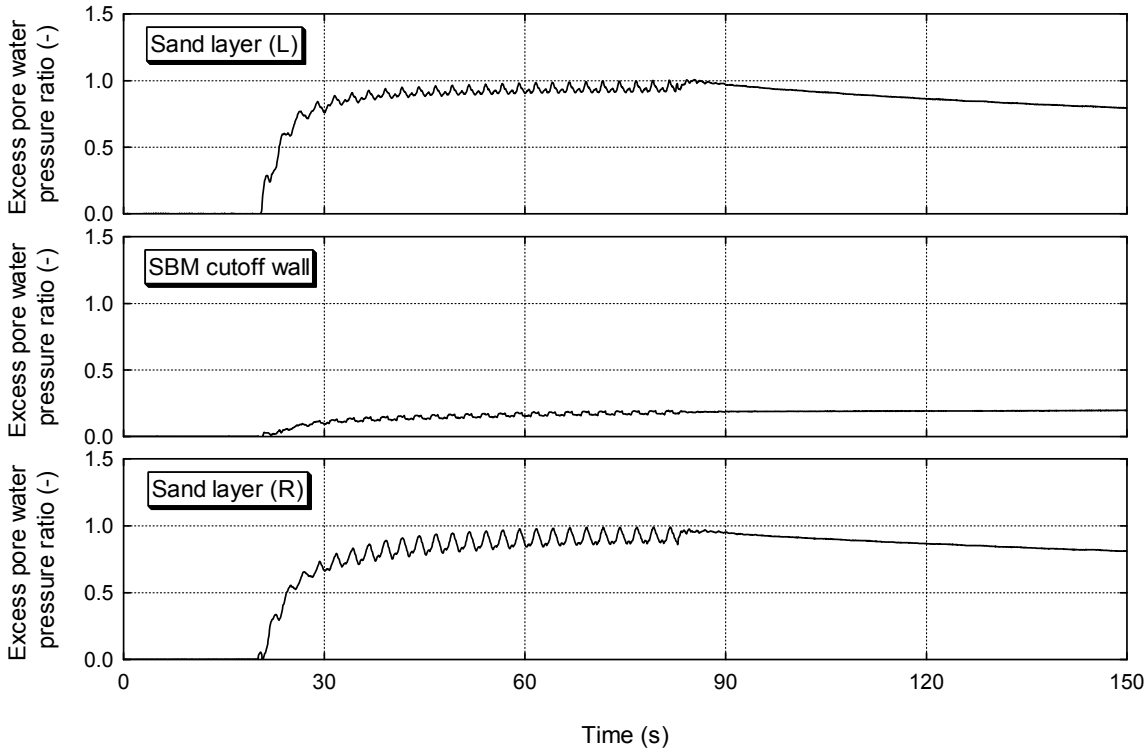

Figure 4.38 Time history of excess pore water pressure ratio (Case-9, at 5.5 m-depth).

4.5.2 Surface settlement by seismic excitation

Surface settlement due to the seismic excitation was obtained by measuring the distance between the ground and the top edge of container before and after the shaking. Figure 4.39 demonstrates a three-dimensional representation of the ground settlement in each testing case. In this figure, x value represents the longitudinal length in prototype scale, and the amount of settlement is represented by the color density.

In Case-1~3, in which both sand layers were loosely prepared and SBM was made with composite soil, the ground surfaces of sand layers settled down symmetrically due to liquefaction by the seismic excitation. The surface settlement of sand layers close to the side wall of container becomes smaller than the layer near the center because of mutual friction between the container and sand layer. On the other hand, since liquefaction did not occur in SBM cutoff wall, its surface settlement was limited. In Case-4, in which one sand layer was densely prepared and another was loosely prepared to simulate the unsymmetrical earth pressure, the surface settlement in left dense sand layer is obviously smaller than that in right loose layer because the increase in excess pore water pressure is limited especially in the deeper zone in dense sand layer. In Case-5~10, a similar trend with Case-1~3 can be observed. The surface settlement of SBM cutoff wall is smaller than that of adjacent sand layers.

Table 4.6 summarizes the average surface settlement of SBM cutoff wall and of adjacent sand layers in each case. As shown in this table, the average surface settlement of SBM cutoff wall is relatively smaller than that of adjacent sand layers in all cases except Case-4. Although

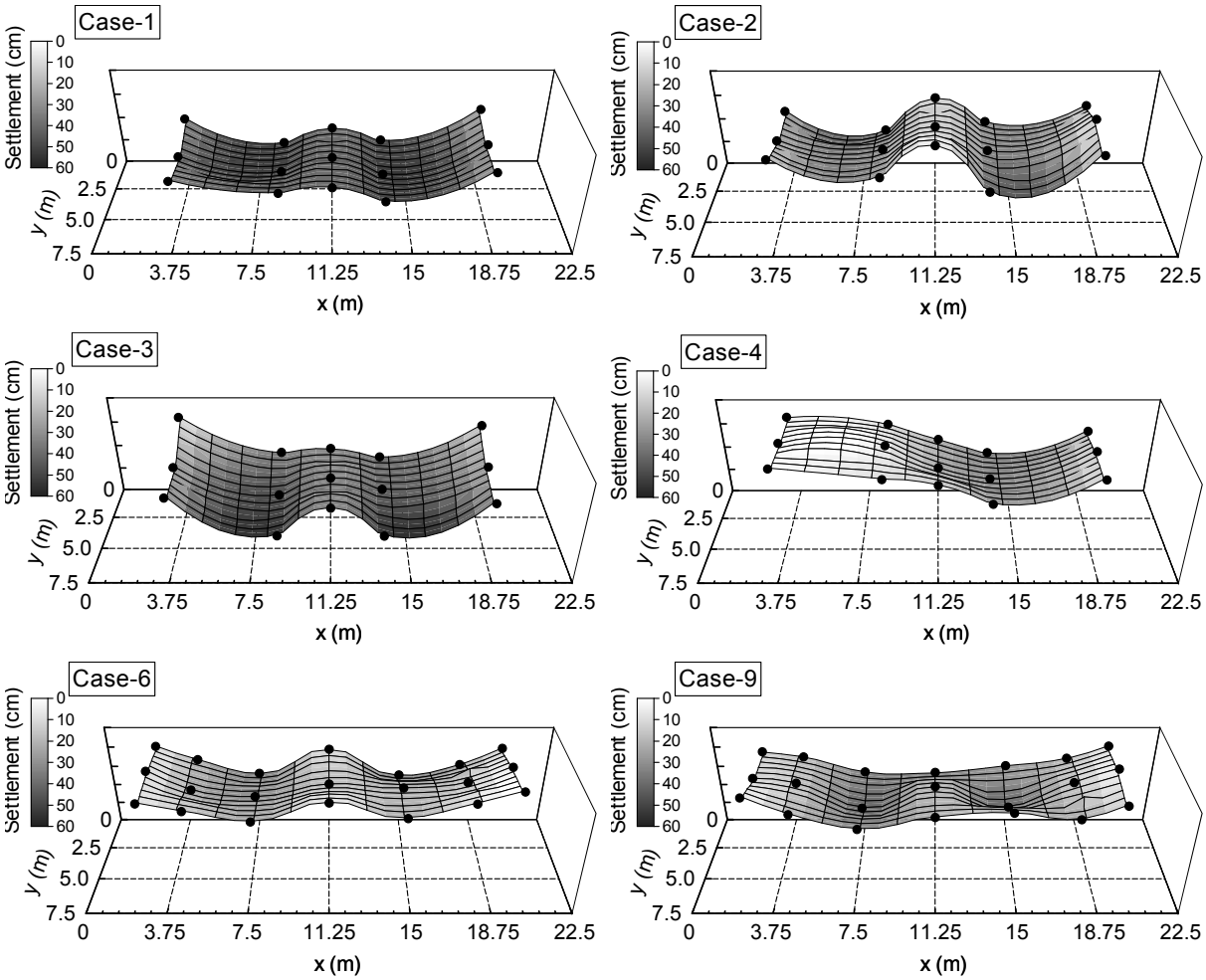

Figure 4.39 Three-dimensional view of surface settlement by seismic excitation.

Table 4.6 Average surface settlement in each case.

Case No.	Density of sand layer		Average settlement of SBM cutoff wall (cm)	Average settlement of sand layer* (cm)	
	Left	Right		Left	Right
Case-1	Loose	Loose	38.5	48.3	50.5
Case-2	Loose	Loose	9.3	32.6	34.3
Case-3	Loose	Loose	31.9	45.4	45.1
Case-4	Dense	Loose	19.5	7.9	31.1
Case-5~7	Loose	Loose	26.2	36.2	29.4
Case-8~10	Dense	Dense	20.4	31.8	30.9

* At adjacent measurement point of SBM cutoff wall

the surface settlement of silica sand-based SBM (Case-5~10) could have been considered to become larger than that of composite soil-based SBM (Case-1~4) because of the lower cyclic strength ratio, the measured ground settlement in silica sand-based SBM was relatively smaller. The same trend can also be observed in the average surface settlement of sand layers.

These are probably because the smaller maximum acceleration was applied in these cases. By comparing the results in Case-1~3, the average surface settlement of SBM cutoff wall in Case-2 is extremely small probably due to short period of the seismic excitation. Thus, it can be considered that both acceleration and period of the vibration may affect on the surface settlement of SBM cutoff wall. When the result in Case-8~10 is compared with that in Case-5~7, the smaller average surface settlement is observed in Case-8~10 because of the difference in the density of sand layer. Considering the fact that the stiffness of SBM cutoff wall should be equivalently degraded in Case-5~10, the difference in the magnitude of settlement can attribute to a down-drag by adjacent sand layers. These observations indicate that the SBM cutoff wall settled down due to both the degradation of stiffness by seismic excitation and down-drag by negative friction derived from the settlement of sand layers.

4.5.3 Horizontal deformation characteristic of SBM cutoff wall

In Case-1~4, the SBM cutoff wall showed little change about the horizontal deformation. This is because high friction acted between the silicone grease and the rigid container. In this section, the horizontal deformation characteristic of SBM cutoff wall is discussed based on the results in Case-5~10. In these cases, horizontal displacements of the round head pins were measured by image analysis on a picture taken after the test as shown in Photo 4.9. Afterwards, horizontal shear strain and curvature of each section was calculated from the measured horizontal displacement.

The experimental results related to the horizontal deformation characteristics are shown in Figure 4.40~4.45 with respect to each case. In Case-5 and Case-7, SBM cutoff wall is deformed with a similar shape that the cutoff wall is inflected to left and right side from top to bottom. In these cases, a relatively large shear strain is produced in shallow zone. On the other hand, although all testing conditions are completely the same, a different trend is observed in Case-6. In this case, while a maximum displacement is produced at 0.5 m-depth, a maximum shear strain and a maximum curvature are observed at relatively-shallow area of 11.0 m and5.5 m-depth, respectively. Besides, in this case, the SBM cutoff wall is deformed with a mode of inclination to one side. Similarly, the deformation characteristics of SBM cutoff wall in dense sand layer are also varied by the test case. In Case-8 and 9, the SBM cutoff wall has a similar deformation mode that the wall inflects to left and right. However, although the maximum shear strain is obtained at the shallowest part in Case-8, the maximum value is obtained in deep zone of 9.0 m-depth in Case-9. In Case-9, large curvature of more than 0.2 1/m is obtained in both shallow and deep part, even though the magnitude of displacement is relatively small in whole domain. This is because the SBM cutoff wall is inflecting from one side to another in these points. In Case-10, the SBM cutoff wall is inclined to one direction from bottom to top.

The maximum value of displacement, shear strain and curvature are summarized in Table 4.7 in conjunction with the depth of measure point. The maximum curvature of 0.22 1/m is

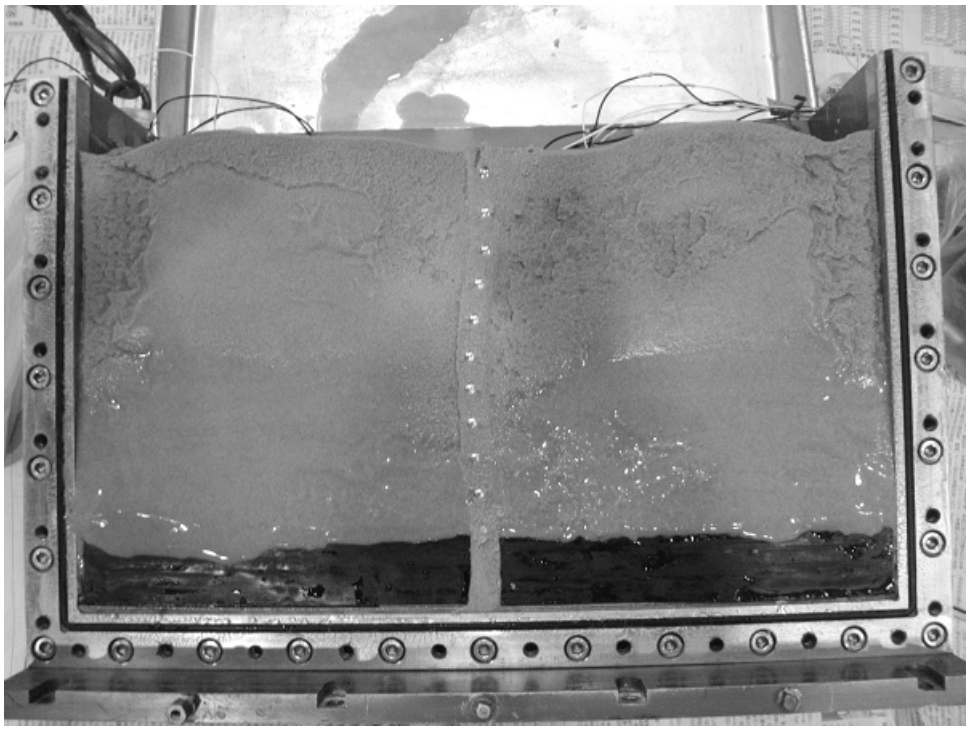

Photo 4.9 Typical front view of model ground after the test (Case-5).

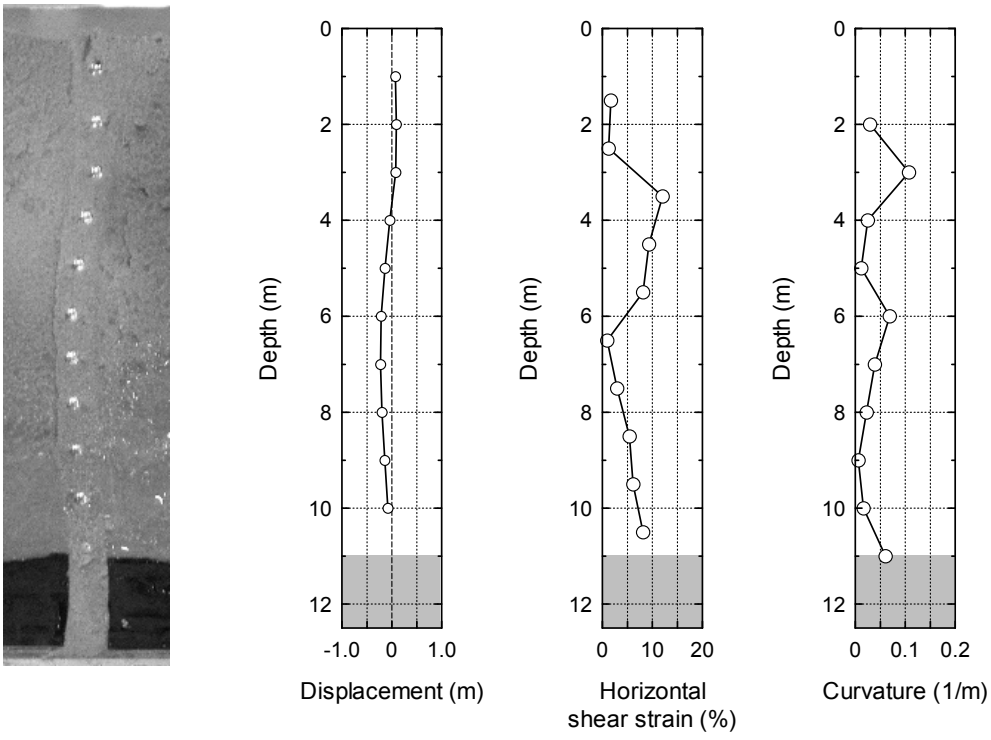

Figure 4.40 Horizontal deformation of SBM cutoff wall in Case-5.

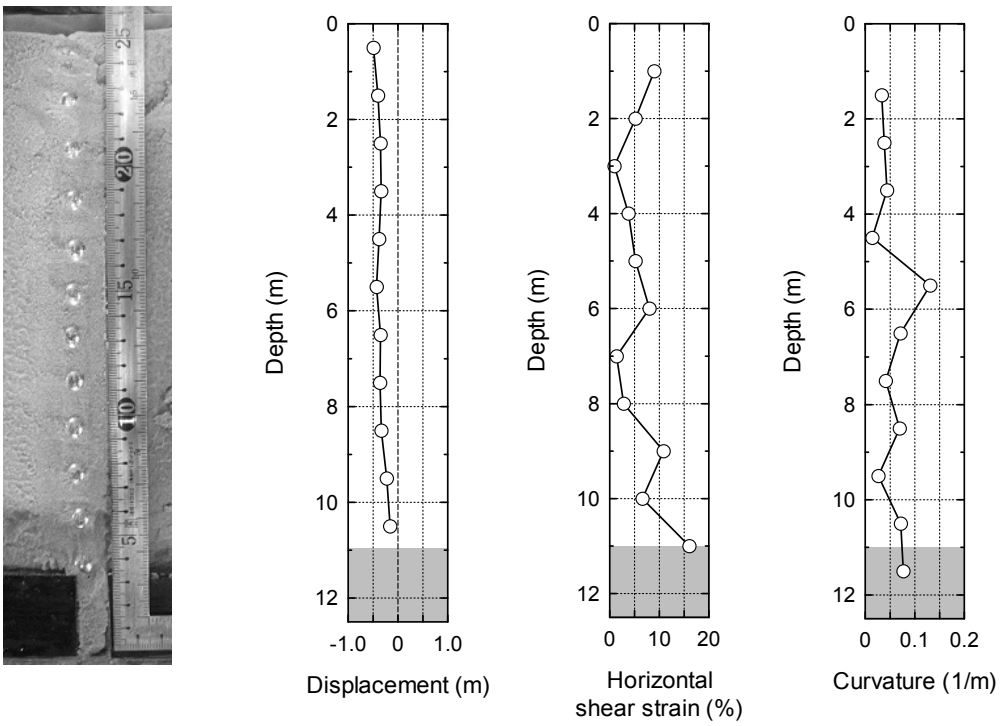

Figure 4.41 Horizontal deformation of SBM cutoff wall in Case-6.

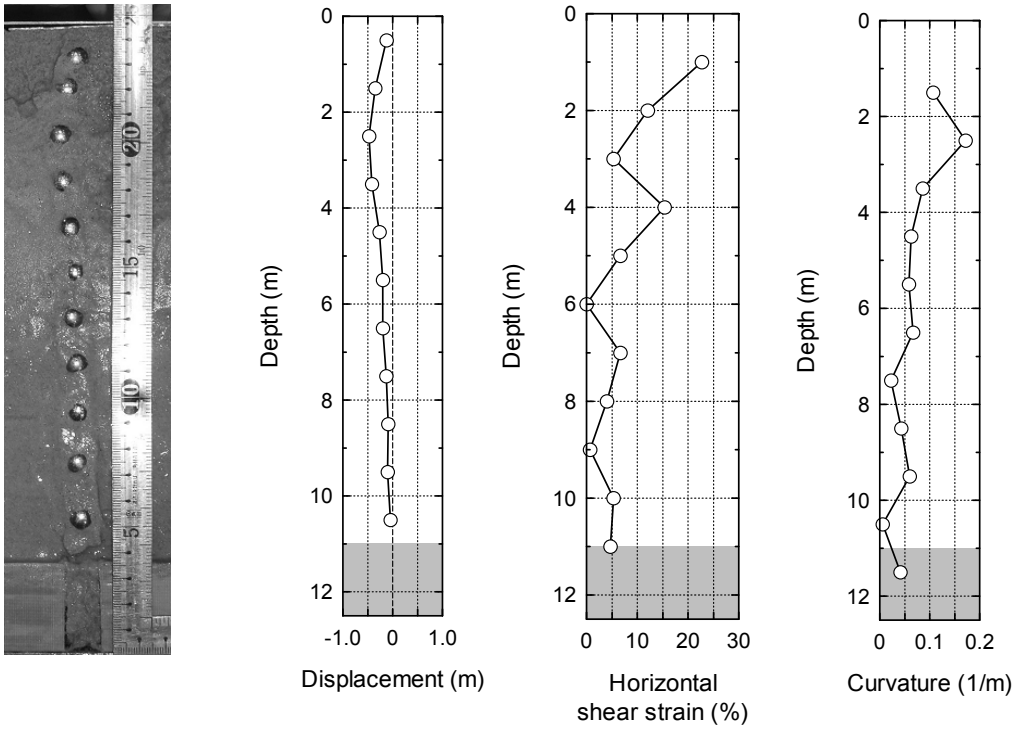

Figure 4.42 Horizontal deformation of SBM cutoff wall in Case-7.

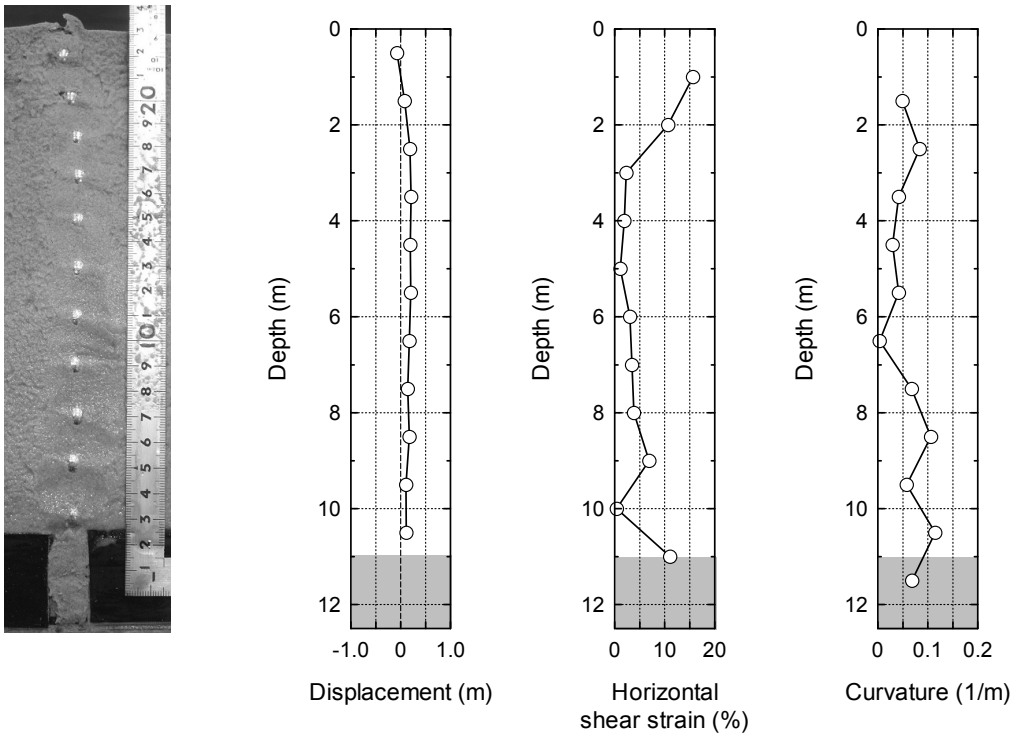

Figure 4.43 Horizontal deformation of SBM cutoff wall in Case-8.

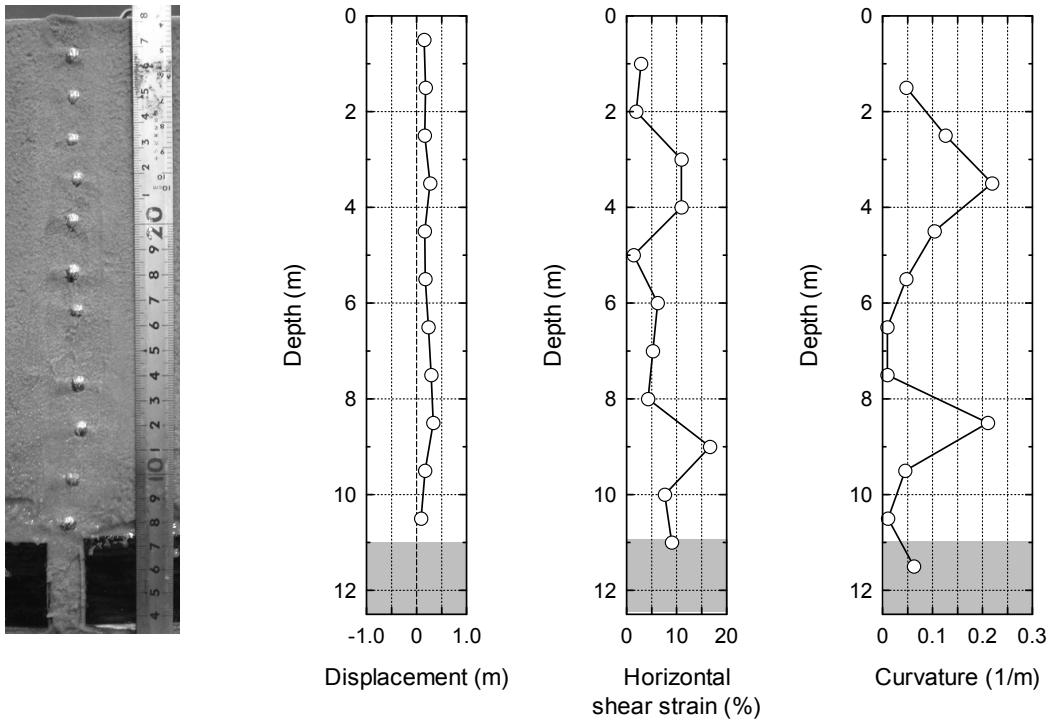

Figure 4.44 Horizontal deformation of SBM cutoff wall in Case-9.

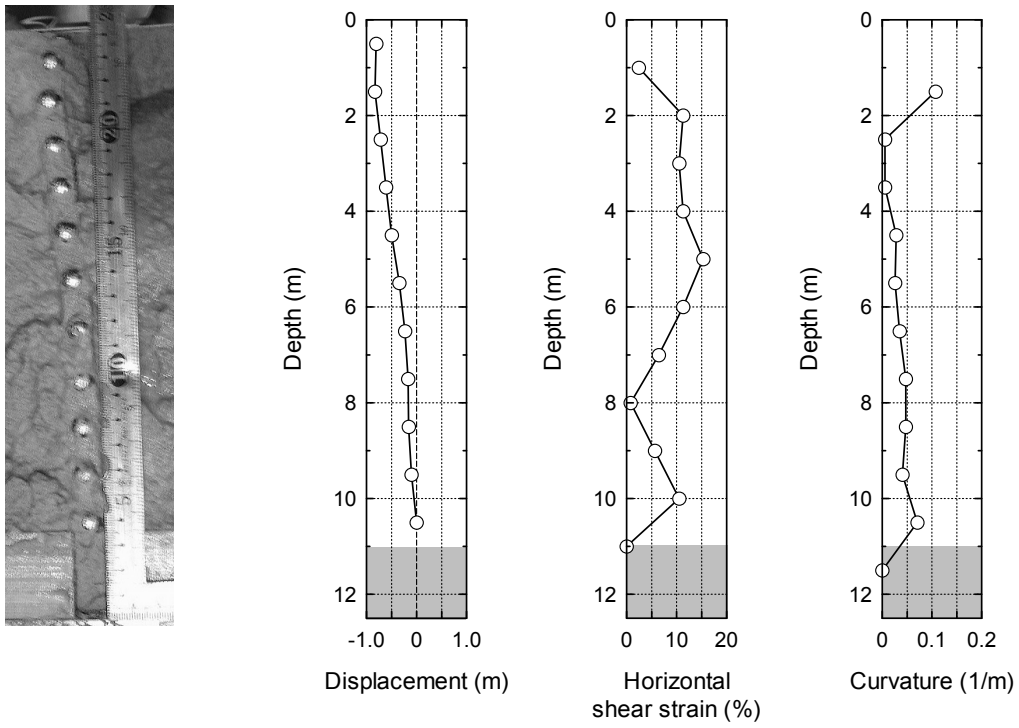

Figure 4.45 Horizontal deformation of SBM cutoff wall in Case-10.

observed in Case-9 at 3.5 m-depth. As seen from this table, the maximum values of displacement and shear strain have variability even in the test cases with completely identical conditions. Furthermore, an apparent difference between the densities of sand layer cannot be confirmed. This variability might be caused by a slight difference in ground conditions during the model preparation. However, it can be seen that the maximum curvature is obtained in the area shallower than 5.5 m-depth in 5 of 6 cases. Besides, the maximum shear strain is produced in the shallower area in 4 of 6 cases. These confirmations indicate that the large deformation of SBM cutoff wall is likely to happen in the shallow zone, although the deformation mode is sensitively affected by difference in ground conditions.

Table 4.7 Maximum displacement, shear strain and curvature in each case.

Case No.	Density of sand layer	Max. displacement (m) and depth (m)	Max. shear strain (%) and depth (m)	Max. curvature (1/m) and depth (m)
Case-5	Loose	0.23 (7.0)	12 (3.5)	0.11 (3.0)
Case-6	Loose	0.49 (0.5)	16 (11.0)	0.13 (5.5)
Case-7	Loose	0.47 (2.5)	23 (1.0)	0.17 (2.5)
Case-8	Dense	0.16 (3.5)	12 (1.0)	0.11 (10.5)
Case-9	Dense	0.33 (8.5)	17 (9.0)	0.22 (3.5)
Case-10	Dense	0.83 (1.5)	15 (5.0)	0.11 (1.5)

After the test, physical damage on SBM cutoff wall by the seismic excitation was visually inspected. As a result, SBM cutoff wall could maintain its soundness without any damage, such as cracks and fractures. Although further researches should be conducted to ensure the effects of changes in microstructure on the hydraulic barrier performance, SBM cutoff wall can maintain its integrity for a range of seismic excitation with maximum acceleration of around 500 gal.

4.6 Summary and conclusions

The containment barriers including SBM cutoff wall have to maintain its hydraulic barrier performance even when an earthquake occurs to completely contain contaminants. Especially for SBM cutoff wall, large deformation can be produced by seismic excitation due to its softness even after the construction. Therefore, the seismic behavior of SBM cutoff wall is needed to be properly assessed. In this chapter, cyclic strength and dynamic behavior of SBM cutoff walls against seismic loading were verified by cyclic undrained triaxial test and centrifuge modeling test. In centrifuge modeling test, the horizontal deformation of SBM cutoff wall was discussed as well as the response characteristics of each layer to the seismic excitation. The main achievement obtained in this chapter can be summarized as follows:

(1) Experimental results of cyclic undrained triaxial test indicate that the axial strain of composite soil-based SBM dramatically increased from 1% to 5% after a gradual increase up to approximately 1%. The axial strain of silica sand-based SBM linearly increased at the same rate of 0.40% per cycle.
(2) The excess pore water pressure during cyclic loading was large in silica sand-based SBM compared with the composite soil-based SBM because the silica sand-based SBM showed sand-like behavior due to few fine particles of base soil.
(3) The ratio of excess pore water pressure to the effective stress is approximately 0.03 for composite soil-based SBM and approximately 0.5 in silica sand-based SBM at the maximum. Thus, liquefaction may not have occurred in SBM cutoff wall due to little change in the excess pore water pressure, but large strain can be produced according to degradation of stiffness.
(4) Silica sand-based SBM has cyclic strength lower than composite soil-based SBM because the larger excess pore water pressure is generated.
(5) Cyclic strength ratio of composite soil-based SBM with the maximum grain size of 4.75 mm, that of 0.85 mm, and silica sand-based SBM was calculated to be approximately 0.225, 0.230, and 0.155, respectively. These values are consistent with that in a previous research, which dealt with specimens made with various clay/sand ratio.
(6) Acceptable accelerations back calculated by the factor of liquefaction, F_L, were

approximately 100 gal and 60 gal for composite soil-based SBM and silica sand-based SBM, respectively. Thus, while the excess pore water pressure will be progressively increased during an earthquake, the SBM cutoff walls can be highly deformed with seismic excitation with its acceleration larger than these values.

(7) From a series of centrifugal modeling test, although excess pore water pressure ratio in sand layers gradually increase with shaking regardless of the depth and eventually attain approximately 1.0, that in SBM cutoff wall did not increase as much. Therefore, liquefaction may not be occurred in SBM cutoff wall because the excess pore water pressure did not significantly develop throughout the entire shaking, although the sand layers are liquefied.

(8) The excess pore water pressure ratio in the upper SBM cutoff wall increase to 0.8 during shaking with maximum acceleration of around 500 gal. The pore water pressure can be increased by seismic excitation with high acceleration, although a certain amount of effective stress can be maintained in SBM cutoff wall.

(9) In some cases, drastic reduction of pore water pressure and/or amplified response acceleration, which are assumed to be due to cyclic mobility during the shaking, are observed.

(10) Predominant frequency of response acceleration corresponds to frequency of input sinusoidal wave. Thus, SBM cutoff wall is assumed to be shaken together with adjacent sand layers during the seismic excitation. The vibration characteristics of SBM cutoff wall depends on that of surrounding ground even when the liquefaction is occurred in the adjacent ground. However, the Fourier spectra in the case of high acceleration poorly-matched each other.

(11) Ground surface of sand layers is settled down due to the liquefaction by seismic excitation; however, since liquefaction did not occur in SBM cutoff wall, its surface settlement is limited. Accordingly, the surface settlement of SBM cutoff wall is smaller than that of adjacent sand layers in all cases.

(12) The surface settlement of SBM cutoff wall increases with the increasing of the surface settlement of adjacent sand layers even against the same input wave. This result indicates that the SBM cutoff wall settled down due to both the degradation of stiffness by seismic excitation and down-drag by negative friction generated by the settlement of sand layers.

(13) A maximum curvature of 0.22 1/m is observed at 3.5 m-depth of SBM cutoff wall in dense sand layer. However, the horizontal deformation characteristic has variability even in the test cases with completely same conditions. Besides, an apparent difference between the densities of sand layer cannot be confirmed. This variability might be caused by a slight difference in ground conditions during the model preparation.

(14) However, it can be seen that the maximum curvature is obtained in the area shallower than 5.5 m-depth in 5 of 6 cases. Besides, the maximum shear strain is produced in the shallower area in 4 of 6 cases. Therefore, the large deformation of SBM cutoff wall is likely to be produced in the shallow zone.

(15) By visual inspection of SBM cutoff wall after the experiment, it was confirmed that SBM cutoff wall can maintain its soundness without any damage, such as cracks and fractures. Thus, SBM cutoff wall can maintain its integrity for a range of seismic excitation with maximum acceleration of around 500 gal.

References for Chapter 4

American Society of Civil Engineers, Los Angeles Section (1974): Earthquake damage evaluation and design considerations for underground structures.

Brandenberg, S.J., Boulanger, R.W., Kutter, B.L., and Chang, D. (2005): Behavior of pile foundations in laterally spreading ground during centrifuge tests, *Journal of Geotechnical and Geoenvironmental Engineering*, Vol.131, No.11, pp.1378-1391.

Dowding, C.H., and Rozen, A. (1978): Damage to rock tunnels from earthquake shaking, *Journal of the Geotechnical Engineering Division*, ASCE, Vol.104, No.GT2, pp.175-191.

Graham, M.D., Xiao, M., and Owaidat, L.M. (2012): Seismic performances of slurry walls, *GeoCongress 2012 - State of the Art and Practice in Geotechnical Engineering -, Geotechnical Special Publication, No.225*, R.D. Hryciw, A.A. Zekkos, and N. Yesiller (eds.), ASCE, pp.1879-1887.

Gratchev, I.B., and Sassa, K. (2013): Cyclic shear strength of soil with different pore fluids, *Journal of Geotechnical and Geoenvironmental Engineering*, Vol.139, No.10, pp.1817-1821.

Hioki, K., Hirata, T., Nishigaki, M., Egusa, N., and Kushihara, S. (2007): Physical and dynamic properties of soil cement diaphragm walls and seismic performance evaluation using seismic response analysis, *Journal of the Japan Society Waste Management Experts*, Vol.18, No.4, pp.230-239. (in Japanese)

Iai, S., Tobita, T., and Nakahara, T. (2005a): Generalised scaling relations for dynamic centrifuge tests, *Géotechnique*, Vol.55, Issue 5, pp.355-362.

Iai, S., Tobita, T., Nakamichi, M, and Kaneko, H. (2005b): Soil-pile interaction in horizontal plane: *Proceedings of a Workshop on Simulation and Seismic Performance of Pile Foundations in Liquefied and Laterally Spreading Ground*, Geotechnical Special Publication, ASCE, Vol.145, pp.294-305.

Iai, S., and Ichii, K. (2011): Soils and foundations during earthquake, *Soils and Foundations*, Vol.50, No.6, pp.937-953.

Iida, H., Hiroto, T., Yoshida, N., Iwafuji, M., (1996): Damage to Daikai subway station, *Soils and Foundations*, Special Issue on Geotechnical Aspects of the January 17 1995 Hyogoken-Nambu Earthquake, Japanese Geotechnical Society, pp.283-300.

Ito, S., Hyodo, M., Fujii, T., Yamamoto, Y., and Taniguchi, T. (2001): Undrained monotonic

and cyclic shear characteristics of sand, clay and intermediate soils, *Journal of JSCE*, Vol.680, pp.233-243. (in Japanese)

Japan Society of Civil Engineers (1988): Earthquake resistant design for civil engineering structures in Japan, Japanese Society of Civil Engineers.

JGS (2000): 0541-2000 Method for cyclic undrained triaxial test on soils.

Kang, G.C, Tobita, T., Iai, S., and Ge, L. (2013): Centrifuge modeling and mitigation of manhole uplift due to liquefaction, *Journal of Geotechnical and Geoenvironmental Engineering*, Vol.139, No.3, pp.458-469.

Ling, H., and Ling, H.I. (2012): Centrifuge model simulations of rainfall-induced slope instability, *Journal of Geotechnical and Geoenvironmental Engineering*, Vol.138, No.9, pp.1151-1157.

Nakamura, S., Yoshida, N., Iwatate, T. (1996): Damage to Daikai subway station during the 1995 Hyogoken-Nambu Earthquake and its investigation, Japan Society of Civil Engineers, Committee of Earthquake Engineering, pp.287-295.

Owen, G.N., and Scholl, R.E. (1981): Earthquake engineering of large underground structures, Report no. FHWA_RD-80_195, Federal Highway Administration and National Science Foundation.

Power M.S., Rosidi D., and Kaneshiro J.Y. (1998), Seismic vulnerability of tunnels and underground structures revisited, *Proceedings of North American Tunneling '98*, pp.243-250.

Procter, D.C. and Khaffaf, J.H. (1984): Cyclic Triaxial Tests on Remoulded Clays, *Journal of Geotechnical Engineering*, Vol.110, No.10, pp.1431-1445.

Sharma, S., and Judd, W.R. (1991): Underground opening damage from earthquakes, *Engineering Geology*, Vol.30, pp.263-276.

St. John, C.M., and Zahrah, T.F. (1987): A seismic design of underground structures, *Tunneling Underground Space Technology*, Vol.2, No.2, pp.165-197.

Tatsuoka, F., Iwasaki, T., Tokida, K., Yasuda, S., Hirose, M., Imai, T., and Kon-no, M. (1980): Standard penetration tests and soil liquefaction potential evaluation, *Soils and Foundations*, Vol.20, No.4, pp.95-111.

Tatsuoka, F., Toki, S., Miura, S., Kato, H., Okamoto, M., Yamada, S., Yasuda, S., and Tanizawa, F. (1986): Some factors affecting cyclic undrained triaxial strength of sand, *Soils and Foundations*, Vol.26, No.3, pp.99-116.

Tobita, T., Kang, G.C., and Iai, S. (2011): Centrifuge modeling on manhole uplift in a liquefied trench, *Soils and Foundations*, Vol.51, No.6, pp.1091-1102.

Toki, S., Tatsuoka, F., Miura, S., Yoshimi, Y., Yasuda, S., and Makihara, Y. (1986): Cyclic undrained triaxial strength of sand by a cooperative test program, *Soils and Foundations*, Vol.26, No.3, pp.117-128.

Viswanadham, B.V.S., and Rajesh, S. (2009): Centrifuge model tests on clay based engineered barriers subjected to differential settlements, *Applied Clay Science*, Elsevier, Vol.42, pp.460-472.

Wang W.L., Wang T.T., Su J.J., Lin C.H., Seng C.R., and Huang T.H. (2001), Assesment of damage in mountain tunnels due to the Taiwan Chi-Chi earthquake, *Tunneling and Underground Space Technology*, Vol.16, pp.133-150.

Yasuhara, K., Murakami, S., Komine, H., and Unno, T. (2005): Effects of Initial Static Shear Stress and Principal Stress Reversal on Cyclic and Post-cyclic Undrained Shear of Sand, *Proceedings of the 16th International Conference on Soils Mechanics and Geotechnical Engineering*, Vol.2, pp.459-463.

CHAPTER 5

Practical Implications

5.1 Design considerations

The primary design consideration for SBM used for groundwater control applications is low hydraulic conductivity. A k value of 1×10^{-9} m/ s is typically required for containment barriers. This value is readily achieved with SBM employing appropriate materials and construction technique. However, factors affecting the hydraulic barrier performance should be preliminarily assessed according to ground conditions. For example, the k of SBM is stress dependent (Evans 1994) and designers need to specify the effective confining pressures used in laboratory testing for hydraulic conductivity. When used in environmental applications, chemical compatibility with the permeating fluid is an important consideration (Opdyke and Evans 2005). Additionally, Japan is an island nation surrounded by the sea, and the most urban areas are developed along seashore. Thus, the chemical compatibility of SBM with pore water containing electrolytes is another important consideration.

Implementation of the hydraulic conductivity tests is a crucial step doing the designing process at the pre-construction stage to determine adequate mixing ratio of SBM for high hydraulic barrier performance. It is necessary to assess the k value with a low confining pressure as much as possible to ensure the hydraulic barrier performance in shallow area. The bentonite powder content should be determined according to physical and chemical properties of in-situ soil, such as particle size distribution and chemical concentration in the soil pore water. As validated in this research, the chemical concentration in the soil pore water is an especially essential consideration for the subsequent hydraulic barrier performance of SBM because the k value of SBM containing 0.1 M $CaCl_2$ in the soil pore water can become 20 times or more higher than that of SBM without chemicals in the soil pore water. By measuring the groundwater quality, the possible effect on the hydraulic barrier performance should be preliminarily evaluated. If the designers consider the severest condition with calcium cation for SBM, 0.1 M is necessary and sufficient because the effect of $CaCl_2$ on the swelling characteristic of bentonite is negligible in a range higher than 0.1 M. Regarding the

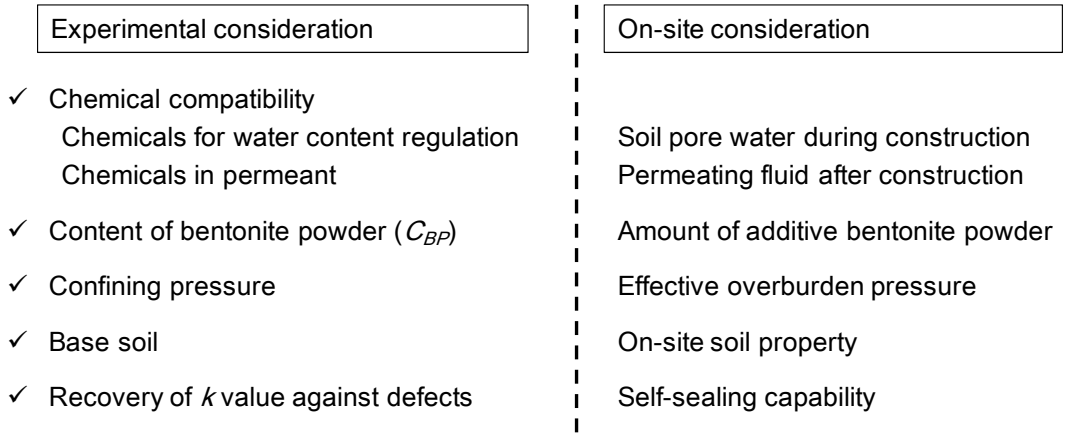

Figure 5.1 Design considerations for SBM cutoff wall.

permeating fluid, it was confirmed that the effect of chemicals in permeant on the k value of SBM is smaller than that of soil pore water. However, since the increase of k value is not negligible as 4 times at the maximum, it is preferable to evaluate the influence of permeant when exposure of SBM cutoff wall to the groundwater containing electrolytes is considerable. Figure 5.1 summarizes experimental considerations for the designing process of SBM cutoff wall and corresponding considerations in the field. For the designing of SBM cutoff walls, these considerations should be taken into account to determine an appropriate mixing condition according to each site characteristics.

5.2 Post-construction verifications

After SBM cutoff wall is constructed with adequate mixing ratio according to results of hydraulic conductivity tests, quality of the cutoff wall has to be verified from view points of homogeneity and in-situ hydraulic barrier performance. Homogeneity plays a fundamental role on the quality of containment barriers since a larger variability in the hydraulic conductivity leads to a higher flux of contaminant out of the barrier system even if the average hydraulic conductivity values are equivalent (Britton and Filz 2007, Yesiller and Shackelford 2010). The variability in SBM may be raised by some factors such as natural variability in the base soils, accumulation of soil particles at the bottom and time-dependent chemical interactions (Evans 1993).

Currently, in-situ k value is mainly evaluated by conducting hydraulic conductivity tests in laboratories on grab samples collected at and delivered from sites. However, the k value assessment by hydraulic conductivity test takes a long period of at least several weeks. In this study, it was validated that the k values of SBM have good correlation with some physical

properties such as swelling pressure, plasticity index, water content after permeation, total fine particle content, etc. Therefore, since the measurement of these properties is easier and faster than the k assessment, these values can be employed as good indicators for the approximate estimation of k value in QC/QA. However, the k value assessment by these methods contains some problems such as: 1) the samples are disturbed by people, 2) the number of samples which can be tested is limited and 3) the measured k values have to represent whole domain of the cutoff wall because a linearly continuous evaluation is not feasible. Hence, while requirements about quality depend on the specifications of each site, in-situ and on-site QC/QA method is essential to ensure the designed hydraulic barrier performance; moreover, the linearly continuous evaluation can enhance the reliability of in-situ containment techniques.

Given such background, a feasibility of CPTU was studied with a laboratory test in this research. As indicated in this research, although the applicability depends on the strength characteristics of SBM, the tendency of q_c, f_s and u values can change according to bentonite content. Thus, it might be possible to check homogeneity of constructed SBM cutoff wall by the profiles of three parameters, which can be obtained during cone penetration. Therefore, the homogeneity assurance using CPTU should be operated at a certain intervals along the wall because it is not economically feasible to evaluate the whole domain of the walls. If the profile of parameters during CPTU has any unstable trends, there is a possibility that heterogeneous part exists inside the wall. In such cases, re-mix in the cutoff wall should be considered to improve the homogeneity until uniform profiles can be obtained. After the homogeneity is ensured, excess pore pressure dissipation test should be conducted to estimate on-site k values at a certain depth intervals. Since the k value will become lower with higher overburden pressure in the deeper area of the cutoff wall as demonstrated in this study, it is more important to obtain reasonable k values in the shallow area. When the k values from CPTU are more than one order of magnitude higher than k values obtained by hydraulic conductivity test, re-addition of bentonite powder should be considered to enhance the hydraulic barrier performance.

5.3 Seismic stability assessment

During, as well as after, the construction of SBM cutoff walls, seismic excitation may affect the structure of containment barrier system, such as shear failure, ground movement, residual deformation, liquefaction, etc. Besides, the cutoff walls for seepage control are often installed in sand strata that are subject to liquefaction. Therefore, seismic stability of SBM cutoff walls should be assessed especially in earthquake-prone countries, such as Japan.

In this research, cyclic strength and liquefaction potential was revealed by cyclic undrained triaxial test using SBMs prepared with two different base soils. Since the ratio of

excess pore water pressure to initial effective stress is approximately 0.03 for composite soil-based SBM and approximately 0.5 in silica sand-based SBM at the maximum, SBM cutoff wall is not subject to liquefaction. However, large axial strain was generated by the cyclic loading. These facts prove that large deformation can be produced on SBM cutoff wall according to the degradation of stiffness, although SBM cutoff walls have low liquefaction potential compared with surrounding sand strata. As discussed in chapter 2, swelling of bentonite will be affected by chemicals existing in the solution. Under conditions disturbing the swelling of bentonite, viscosity of hydrated bentonite inside SBM become low because water retention capacity would be decayed. In such cases, since strength characteristic of SBM can be assumed to be disparate, the cyclic strength of SBM should be verified according to the site. Especially, the liquefaction potential of SBM is an important consideration and should be appropriately assessed. The contaminants would be transported during the liquefaction of SBM cutoff walls when unsymmetrical water pressure is produced in the ground. Thus, it is preferable that the mixing condition of SBM is determined with considering this viewpoint. Since the SBM cutoff walls have high softness and self-sealing capability as validated in chapter 2 and 4, SBM cutoff walls will basically sustain its soundness against earthquake. However, deformation of the SBM cutoff walls may occur by the seismic excitation due to their softness or residual deformation of surrounding ground as demonstrated in the results of centrifuge modeling test in chapter 4. The results indicated that curvature of 0.22 1/m is potentially generated in SBM cutoff wall by the seismic excitation. Because the underground deformation is invisible from the ground surface, horizontal deformation of SBM cutoff wall should be evaluated by the centrifuge modeling test with simulating an actual condition if necessary. Moreover, since CPTU can obtain vertically continuous logs in the ground, CPTU might have a potential to briefly verify the vertical soundness.

5.4 Mutual relations among considerations

Figure 5.2 illustrates mutual relations between contents obtained in each chapter. As explained above, it is preferable to consider both factors affecting k value and liquefaction potential at the pre-construction stage for determining adequate mixing conditions of SBM. If a rough estimate of k value is required before the laboratory hydraulic conductivity test, some compatible factors, such as swelling pressure, plasticity index, etc., should be measured as an indicator of laboratory k value. These factors are also employed as an indicator of on-site k value in QC/QA at a site. Thus, the measurement of these factors is concerned with both pre- and post-construction stages. Needless to say, since direct measurement of on-site k value is rather reliable to ensure the hydraulic barrier performance, the k value assessment by pore water dissipation test during CPTU was proposed in this study. Other advantages to use

CPTU are vertically continuous profiles and simultaneous verification of homogeneity in depth direction of SBM cutoff walls. Another important aspect for the on-site characteristics related to the geoenvironmental reliability is seismic behavior of SBM cutoff walls. If an earthquake will occur, evaluation of seismic behavior will contribute to maintenance and repairment of SBM cutoff walls.

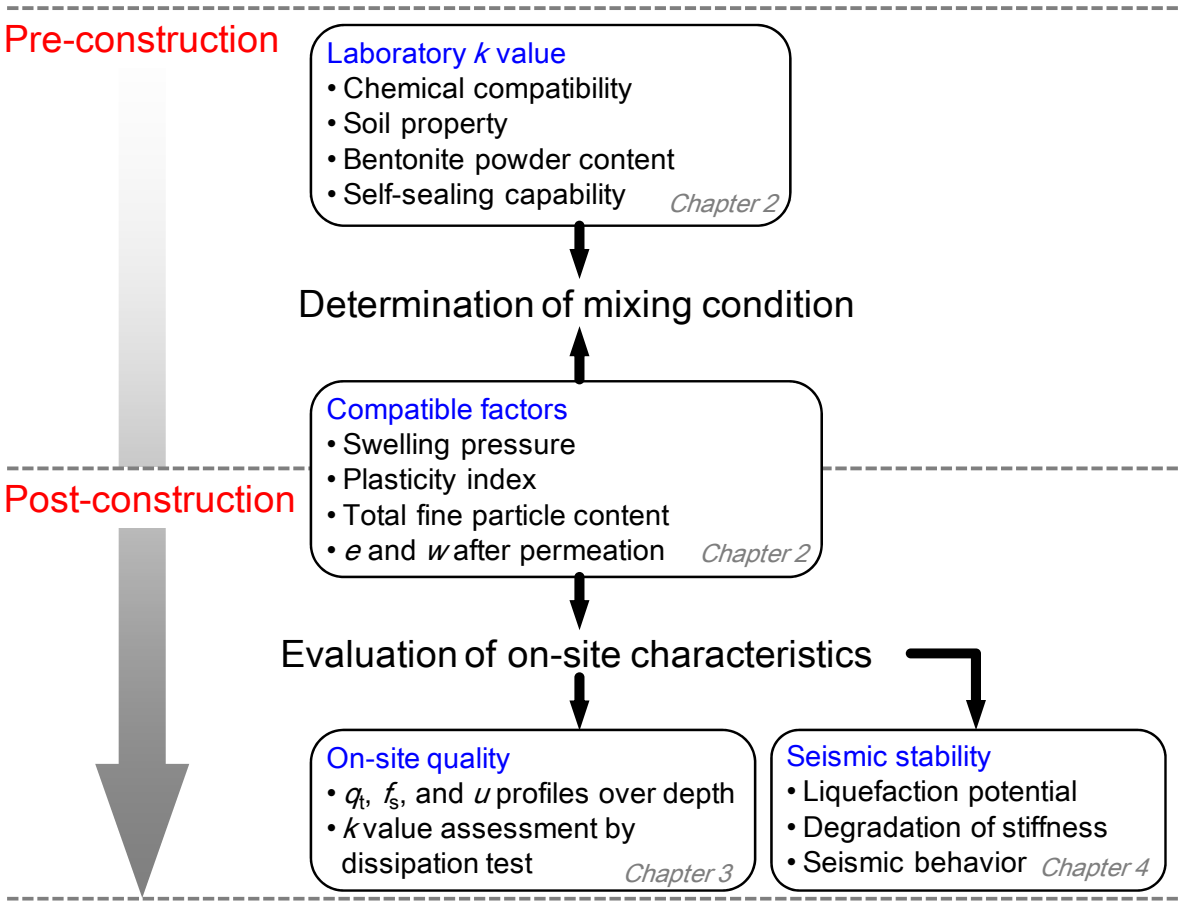

Figure 5.2 Sequential relations between contents obtained in each chapter.

References for Chapter 5

Britton, J.P. and Filz, G.M. (2007): High uniformity versus low hydraulic conductivity for vertical barriers in contaminant containment applications, *Geoenvironmental Engineering*, S.E. Burns, P.J. Culligan, J.C. Evans, P.J. Fox, K.R. Reddy, and N. Yesiller (eds.), pp.1-10.

Evans, J.C. (1993): Vertical cutoff walls, *Geotechnical practice for waste disposal*, D.E.

Daniel (ed), Chapman and Hall, London, U.K. pp.430-454.
Evans, J. C. (1994): Hydraulic conductivity of vertical cut-off walls, *Hydraulic Conductivity and Waste Contaminant Transport in Soils*, ASTM STP 1142, D. E. Daniel and S. J. Trautwein, eds. American Society for Testing and Materials, Philadelphia, pp.79-94.
Opdyke, S.M., and Evans, J.C. (2005): Slag-cement-bentonite slurry walls, *Journal of Geotechnical and Geoenvironmental Engineering*, Vol.131, No.6, pp.673-681.
Yesiller, N., and Shackelford, C.D. (2010): Chapter 13: Geoenvironmental Engineering, B.M. Das (ed.), *Geotechnical Engineering Handbook*, pp.13-52.

CHAPTER 6

Conclusions and Future Directions

6.1 Conclusions

This dissertation presents various aspects of SBM cutoff walls used for in-situ containment technique toward the enhancement of its geoenvironmental reliability. Particularly, factors affecting hydraulic barrier performance of SBM cutoff walls were experimentally and comprehensively verified from viewpoints of laboratory *k* value, on-site QC/QA, liquefaction potential and seismic stability. Since SBM cutoff walls have some unique characteristics, such as high flexibility and self-sealing capability, comprehensive assessment is essential to ensure the effectiveness for geoenvironmental problems. The main achievement in each chapter can be summarized as follows:

In Chapter 1, the objectives and the contents of this dissertation were presented in conjunction with general information related to this research. The general information includes fundamentals of soil and groundwater contamination and a simple overview of what SBM cutoff walls are.

In Chapter 2, hydraulic barrier performance of SBM was discussed in terms of laboratory *k* value especially based on results of hydraulic conductivity test, swelling-pressure test and consistency characterization.

As a result of free swell test of bentonite, which was conducted as a fundamental study of bentonite swelling, the bentonite resulted in significant decrease in its swell volume when the $CaCl_2$ concentration was higher than 0.01 M, but showed similar volume against the solutions of $CaCl_2$ concentration higher than 0.1 M. In hydraulic conductivity test, although original *k* values of base soils have variation, the values of SBMs made with each soil could be lower than 1.0×10^{-10} m/s with 100 kg/m^3 powder bentonite addition. Since the SBM represented sufficiently low *k* value even at the lowest confining pressure, SBM can be

assumed to have an appropiate hydraulic barrier performance even when the effective overburden pressure is lowered due to the arching effect. The fact that the prehydrated SBMs could maintain its hydraulic barrier performance also against the permeation of inorganic solutions, seawater and 50%-ethanol confirms that the k value of SBM does not significantly increase by permeating fluids containing inorganic/organic chemicals when the bentonite in the SBM can be preliminarily and adequately hydrated with the soil pore water. On the other hand, in the case that $CaCl_2$ concentration in the soil pore water is 0.1 M, the k became higher than 1.0×10^{-9} m/s, which is the performance target in this study. Although the pore water containing cations was diluted by the water fraction of the bentonite slurry, a significant increase was observed. By comparing the effects of divalent cations on the k when they exist in the permeant or in the pore water, the cation in the pore water caused more significant increase in the k value. Thus, the prehydration of bentonite is absolutely essential for the chemical compatibility of the SBM. However, because the k could be lowered by 50% by increasing the bentonite powder content by 1.5 times in the case of 0.1 M $CaCl_2$ in the soil pore water, the hydraulic barrier performance of SBM cutoff walls can be enhanced by increasing the additive amount of bentonite powder.

It was confirmed that the k value of SBM has strong correlation with some compatible factors such as maximum swelling pressure, normalized void ratio after permeation, swell volume of bentonite, plastic index and water content of specimen after the permeation. Thus, the change in these values, influenced by the cations of the pore water and the bentonite content, can be useful indices of these effects on the k value. While it takes a long period to measure the k of low-permeable materials such as SBM, these compatible factors can be measured within a couple of weeks or so. Considering this fact, the compatible factors are expected to be employed as indicators for the rough estimation of the hydraulic barrier performance of the SBM in laboratories and/or in the field.

Regarding its self-sealing capability, which is one of the striking characteristics of SBM, recovery of the k value could be demonstrated when the specimen has an intentional defect (a vertical interface or a circular hole penetrating the specimen) due to the combined effects of its deformability and the reswelling of bentonite. However, when permeated with $CaCl_2$ solution, leakage through the circular hole continued to exist because the reswelling of the bentonite was impeded.

In Chapter 3, applicability of piezocone test (CPTU) as QC/QA method was verified using a large-scale soil tank to study feasibility to expand this technique to the field. The strength characteristic of SBM was studied by an unconsolidated-undrained triaxial compression test. In the results of unconsolidated-undrained triaxial compression test, since clear peaks were not observed in deviator stress changes with time regardless of base soil and bentonite powder amount, SBM presented ductile fracture against the compression due to its high softness. Pore water pressure of SBM with C_{BP} = 50 kg/m^3 decreased after 5% strain, and dropped into negative values under some confining pressure. These observations are

consistent with the fact that pore water pressure lower than hydrostatic pressure was observed during CPTU. This is due to negative dilatancy during the shearing steps caused by less clay fraction of approximately 6%. In contrast, a significant difference was not observed in fine sand-based SBMs with two different C_{BP} probably because fine particles were originally contained in the fine sand itself to some degree.

As a result of laboratory CPTU, q_t values in SBM layer with 50 kg/m^3 bentonite powder were larger than the values in the SBM layers with 100 kg/m^3 bentonite powder. Since SBM with 50 kg/m^3 bentonite powder contains less clay fraction (approximately 6% by dry mass basis), the strength characteristic of sand was dominant in such SBM. Pore water pressure also had obviously different trend with the composition of SBMs as same as the results of triaxial test. Although excess pore water pressure was generated in the well bentonite added layers, u values in a layer with 50 kg/m^3 bentonite powder were negative throughout the layer. However, clearly different tendencies in the results of fine sand-based SBMs were not observed because both SBMs with 25 kg/m^3 and 100 kg/m^3 bentonite powder had similar strength characteristics. Overall, relatively higher q_t values could be obtained by CPTU from the SBMs with higher undrained shear strength. About the borehole left after CPTU, although residual deformation due to the cone penetration was observed within approximately 2.0 cm depth at the soil surface, the deeper area of the borehole was sealed due to the self-sealing capability of SBM with time. This observation indicated that SBM cutoff walls can maintain the designed hydraulic barrier performance even after CPTU operation. Thus, CPTU is applicable to detect the lean-mix part in the SBM cutoff walls when the strength characteristics of SBM were significantly influenced by the amount of bentonite powder.

Horizontal k values were measured by pore pressure dissipation test with a temporal stop of cone penetration applying each dissipation degree of 20%, 30% and 50%. The calculated horizontal k values were almost equivalent regardless of the dissipation degree so that the k values calculated at any dissipation degree were in a range of 1.4 - 1.6 times of the k values measured by the hydraulic conductivity test. Thus, the hydraulic barrier performance of SBM can be measured in a shorter time with same accuracy when 20% or 30% dissipation degree is applied. Since the k value measured by the pore pressure dissipation test showed a good correlation with the value measured by hydraulic conductivity test, the k value can be assessed by CPTU within one order of magnitude difference. Therefore, the operation of dissipation test is valid as QC/QA at the post-construction stage of SBM cutoff walls.

In this chapter, a process of QC/QA using CPTU was also suggested. The QC/QA using CPTU should be implemented after the laboratory-scale calibration to obtain the dependency of strength properties on bentonite powder amount. First, CPTU should be operated on the constructed SBM cutoff wall to obtain the profiles of three physical properties at a certain intervals along the wall. During the CPTU, if q_t values have variation or u values change with different rate with penetration depth, SBM cutoff walls may have heterogeneous part inside. In such cases, re-mixing of the cutoff wall should be considered to enhance its homogeneity. Afterward, pore pressure dissipation test should be implemented at certain depth intervals to

ensure the on-site k values. If the k values from CPTU are more than one order of magnitude higher than those values obtained from hydraulic conductivity test, re-addition of bentonite powder should be considered to enhance the hydraulic barrier performance.

In Chapter 4, dynamic behavior of SBM cutoff walls against seismic loading was verified by centrifuge modeling test and cyclic undrained triaxial test. Experimental results of cyclic undrained triaxial test indicated that the axial strain of composite soil-based SBM dramatically increased from 1% to 5% after the gradual increase up to approximately 1%, although that of silica sand-based SBM linearly increased at the same rate of 0.40% per cycle. The excess pore water pressure during cyclic loading was large in silica sand-based SBM compared with the composite soil-based SBM because the silica sand-based SBM showed sand-like behavior due to few fine particles of base soil. However, it was confirmed that the liquefaction may have occurred in SBM cutoff walls due to relatively little change in the excess pore water pressure with cyclic loadings, although large strain can be accumulated according to degradation of stiffness. Silica sand-based SBM had cyclic strength lower than composite soil-based SBM because of the larger excess pore water pressure. Cyclic strength ratios of SBMs calculated in this research were consistent with the results from a previous study, which dealt with various clay/sand mixtures. Acceptable accelerations back calculated by the factor of liquefaction, F_L, were approximately 100 gal and 60 gal for composite soil-based SBM and silica sand-based SBM, respectively. Thus, while the excess pore water pressure will not be progressively increased during the earthquake, the SBM cutoff walls can be highly deformed with seismic excitation with its acceleration larger than these values.

From a series of centrifugal modeling tests, although excess pore water pressure ratio in sand layers gradually increased with shaking regardless of the depth, and eventually attained approximately 1.0, that in SBM cutoff wall increased up to 0.8 with a shaking of a maximum acceleration of 500 gal. Thus, liquefaction may not have occurred in SBM cutoff walls because excess pore water pressure may not have been significantly produced. Since predominant frequency of response acceleration corresponds to the frequency of input wave, SBM cutoff wall shook together with adjacent sand layers during the shaking. This fact implies that the vibration characteristics of SBM cutoff wall depends on that of surrounding ground even when the liquefaction occurred in the adjacent ground. However, the Fourier spectra poorly-matched each other in the case of high acceleration.

Ground surface settlement by the seismic excitation was also measured in the centrifugal modeling test. Ground surface of sand layers was settled down due to the liquefaction; however, ground surface settlement in SBM cutoff wall was limited because it was not liquefied. Another finding is that the surface settlement of SBM cutoff wall increased with the increasing of the surface settlement of the adjacent sand layers, even against the same input wave. This result indicates that the SBM cutoff wall settled down due to both the degradation of its stiffness and down-drag by negative friction caused by the settlement of adjacent sand layers. Regarding horizontal deformation characteristics of SBM cutoff wall, a maximum

curvature of 0.22 1/m was observed at 3.5 m-depth of SBM cutoff wall. However, various deformation modes have been observed even in the cases with completely identical conditions. Besides, apparent differences between the densities of sand layer cannot be confirmed. This variation might be caused by a slight difference in ground conditions during the model preparation. One finding about the horizontal deformation characteristics is that the large deformation is likely to be produced in the shallow zone of SBM cutoff wall. In 5 of 6 cases, the maximum curvature was obtained in the area shallower than 5.5 m-depth. Besides, the maximum shear strain was produced in the shallower area in 4 of 6 cases. Although such large deformation might be arisen by the seismic excitation, significant damage such as cracks or fractures were not observed in SBM cutoff wall by visual inspection after the experiment. Therefore, it was confirmed that SBM cutoff walls can maintain their soundness for a range of seismic excitation with maximum acceleration of around 500 gal.

In Chapter 5, interpretation of experimental results were described in consideration with practical implications. At a pre-construction stage, achievements of hydraulic conductivity test will make a great contribution to a designing process for optimizing a mixing condition in a field. Various considerations, which should be taken into account, were also summarized in this chapter. Moreover, QC/QA methods using some factors compatible with the k value and CPTU were mentioned. The application of CPTU is more preferable for QC/QA of constructed SBM cutoff walls because vertically continuous evaluation is possible with CPTU. Since contaminants would be transported during the liquefaction of SBM cutoff walls if unsymmetrical water pressure is produced in the ground, it is preferable that the mixing condition of SBM is determined with considering the liquefaction potential of SBM. Moreover, since the results of centrifuge modeling test indicated that curvature of 0.22 1/m is potentially generated in SBM cutoff wall at an earthquake, horizontal deformation of SBM cutoff walls should be evaluated by the centrifuge modeling test with simulating an actual condition if necessary. In this chapter, mutual relations between the results in each chapter were also discussed.

6.2 Future directions

In Chapter 2, effects of various factors on the k value were experimentally quantified. However, self-sealing capability was studied on SBM made with only one mixing condition, and an interrelation between chemical compatibility and self-sealing capability was not yet established. Since the self-sealing capability of SBM depends on its stiffness and swelling property of bentonite as discussed in this research, the magnitude of recovery in k value may be also impeded under the conditions when the swelling of bentonite is be degraded. Thus,

further research should focus on the quantification of the self-sealing capability, employing SBMs made with various chemical concentrations in the original soil pore water and with various C_{BP}. Also, the factors compatible with the k value was fundamentally studied using composite soil-based SBM. In order to enhance the versatility of these factors as the indicators of the k value, a correlation is needed to be generalized using SBMs made with base soils.

Regarding applicability of CPTU as QC/QA method, although feasibility of this method was demonstrated in the case of silica sand-based SBM, CPTU could not detect the difference in composition of fine sand-based SBM. Another challenge is to reveal the detectable shape and size of lean-mix part. In this way, the application limit of CPTU should be studied with the change of experimental conditions. Furthermore, a larger scale test such as a pilot-scale test must be conducted to expand this technique to the field. In order to improve the reliability of this method, the validity of the laboratory-scale results obtained in this research should be confirmed by comparing with the results of pilot-scale test.

As far as the seismic stability is concerned, since relatively high excess pore water pressure was generated in the SBM cutoff wall when the wave with the maximum acceleration of 500 gal, the greatest potential assessment is required in terms of pore water pressure generation in the SBM cutoff wall. Moreover, the soundness also should be verified under such high acceleration conditions. Since the Fourier spectra poorly-matched each other in the case of high acceleration, vibration characteristics of SBM cutoff walls with high acceleration should be studied in conjunction with the improvement of experimental accuracy. In this research, uniform deformation modes were not obtained even in completely identical conditions; therefore, the experimental accuracy should be considered in terms of how accurate the model ground can be prepared to simulate the actual ground condition. Although the self-sealing capability and deformation characteristics were separately confirmed in this study, the effect of the deformation on the hydraulic barrier performance should be studied to validate seismic stability in a real sense.

APPENDIX

Appendix 1　Base machine of TRD method.

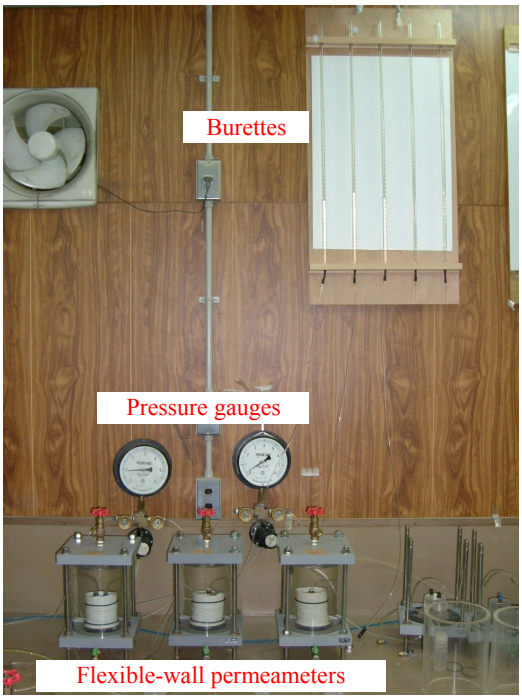

Appendix 2　Full view of system for hydraulic conductivity test.

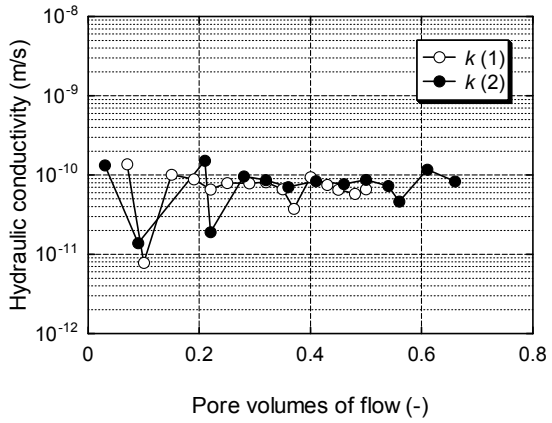

Appendix 3 Changes in *k* value (C-1).

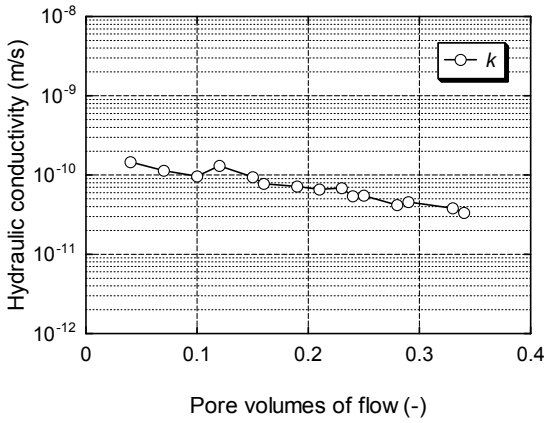

Appendix 4 Change in *k* value (C-2).

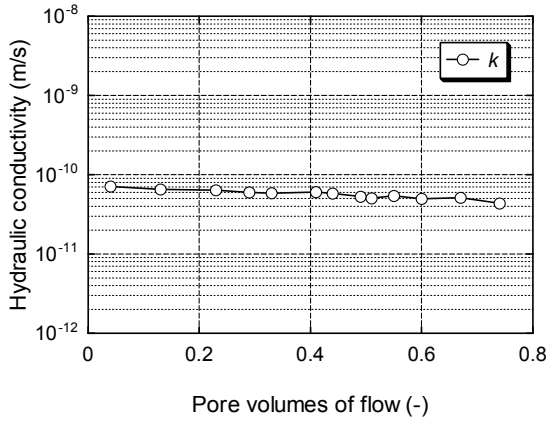

Appendix 5 Change in *k* value (C-3).

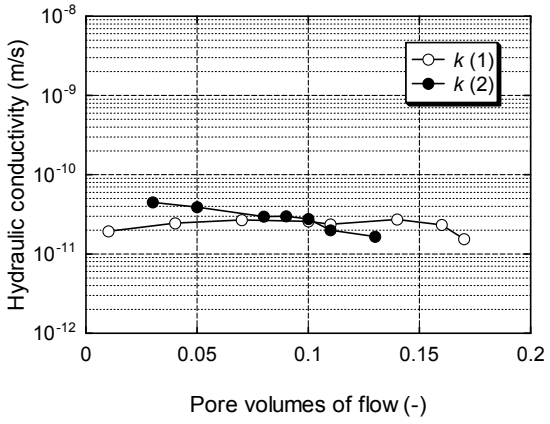

Appendix 6 Changes in *k* value (C-4).

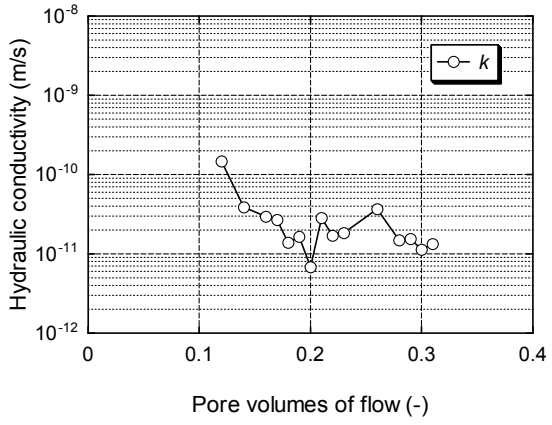

Appendix 7 Change in *k* value (C-5).

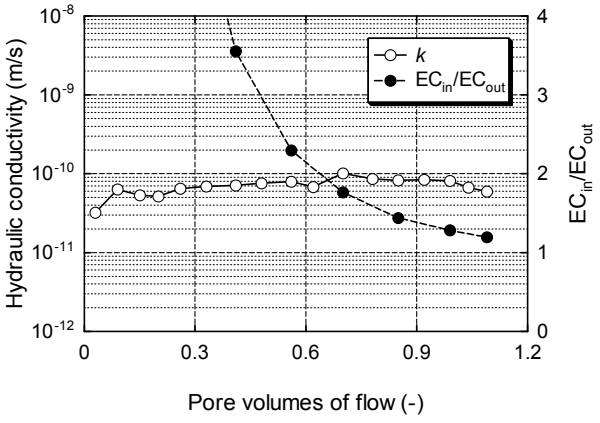

Appendix 8 Changes in *k* value and EC_{in}/EC_{out} (C-6).

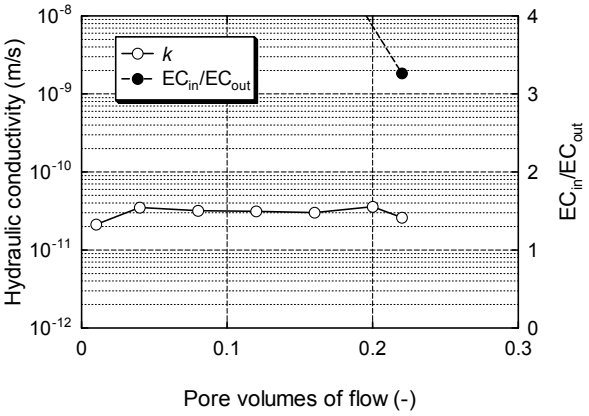

Appendix 9 Changes in k value and EC_{in}/EC_{out} (C-7).

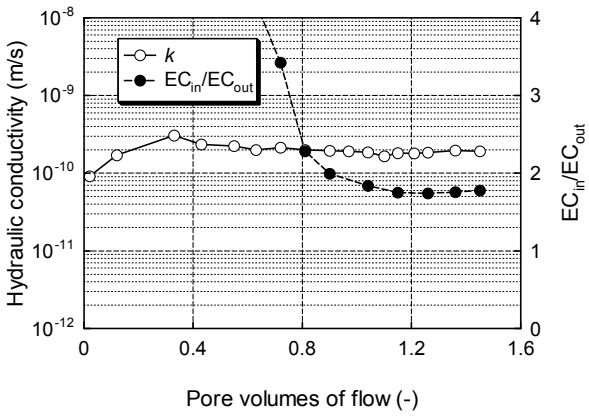

Appendix 10 Changes in k value and EC_{in}/EC_{out} (C-8).

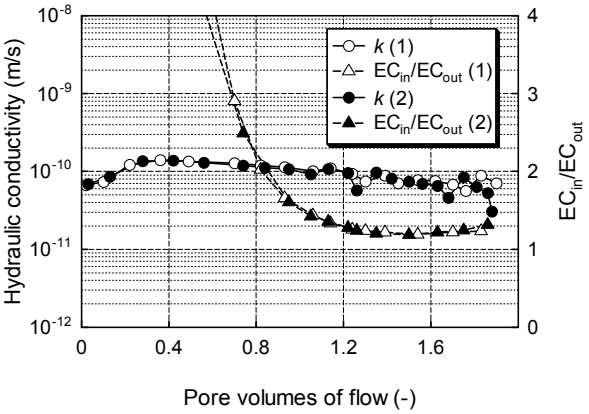

Appendix 11 Changes in k value and EC_{in}/EC_{out} (C-9).

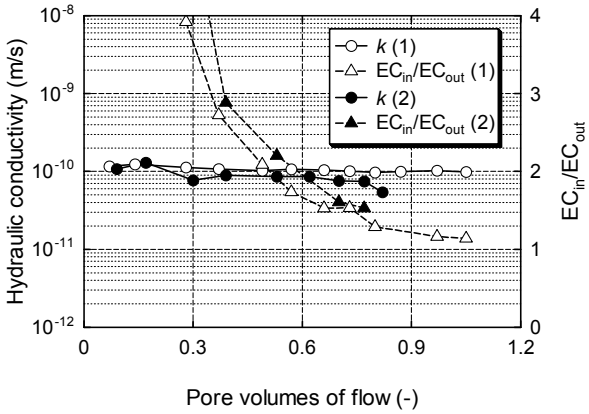

Appendix 12 Changes in k value and EC_{in}/EC_{out} (C-10).

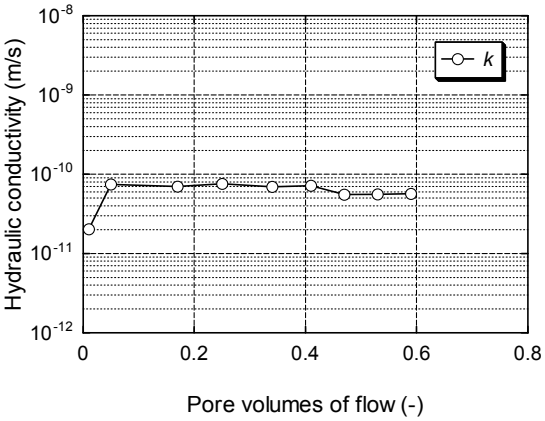

Appendix 13 Change in k value (C-11).

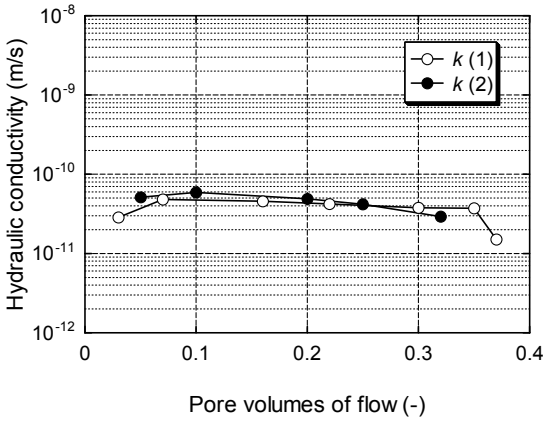

Appendix 14 Changes in k value (C-12).

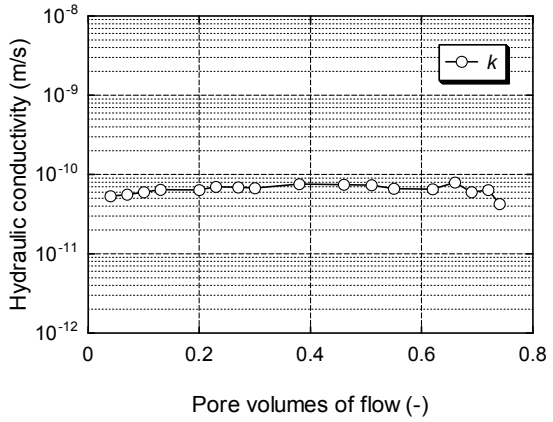

Appendix 15 Change in k value (C-13).

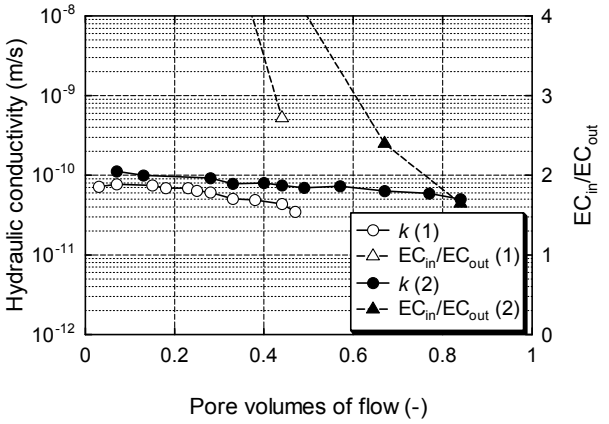

Appendix 16 Changes in k value and EC_{in}/EC_{out} (C-14).

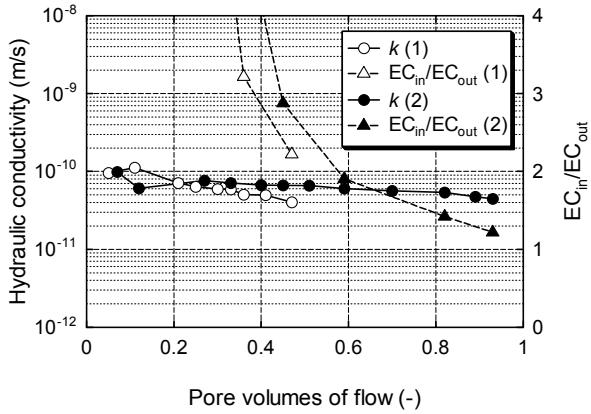

Appendix 17 Changes in k value and EC_{in}/EC_{out} (C-15).

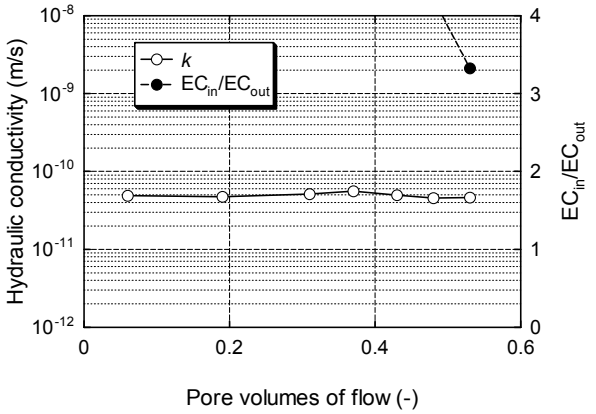

Appendix 18 Changes in k value and EC_{in}/EC_{out} (C-16).

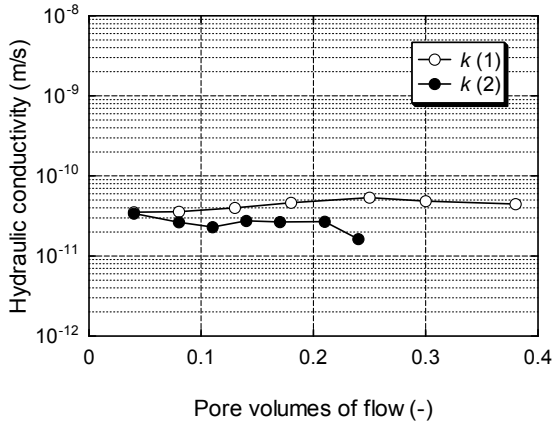

Appendix 19 Changes in k value (C-17).

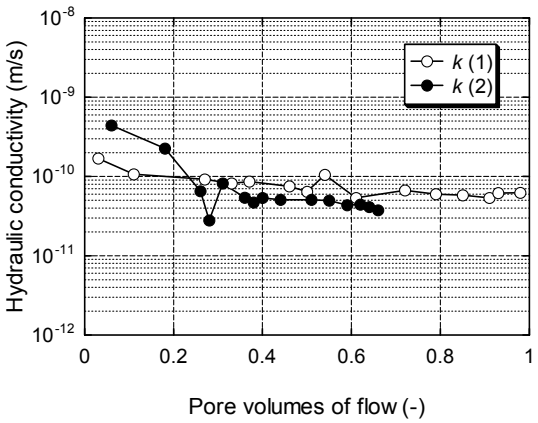

Appendix 20 Changes in k value (P-1).

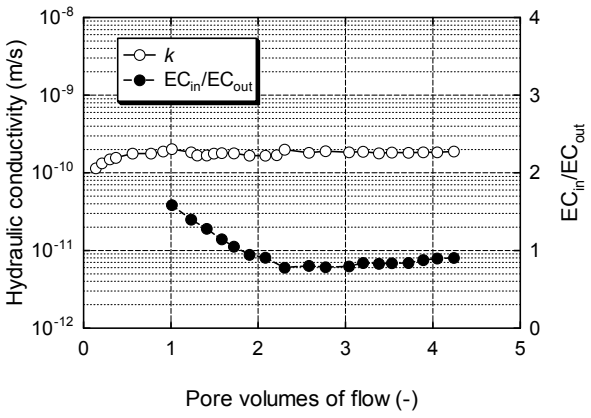

Appendix 21 Changes in k value and EC_{in}/EC_{out} (P-2).

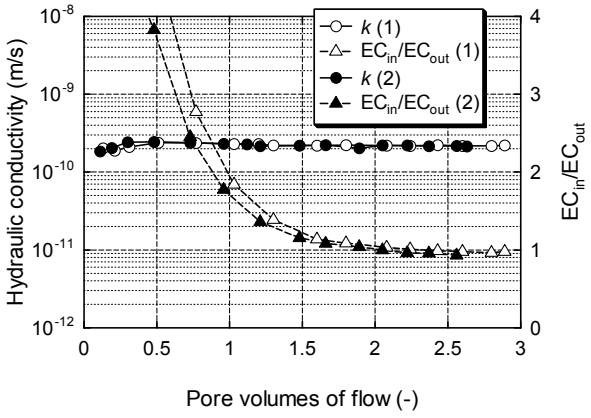

Appendix 22 Changes in k value and EC_{in}/EC_{out} (P-3).

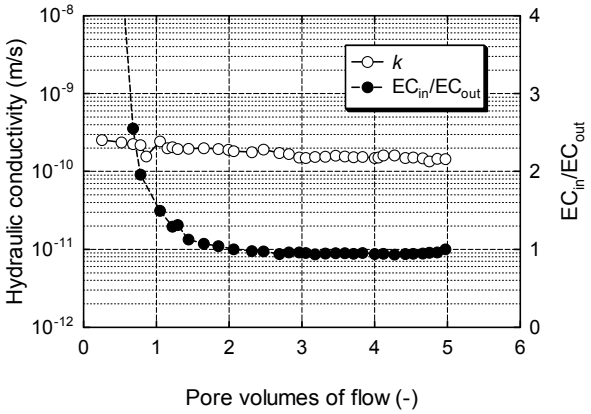

Appendix 23 Changes in k value and EC_{in}/EC_{out} (P-4).

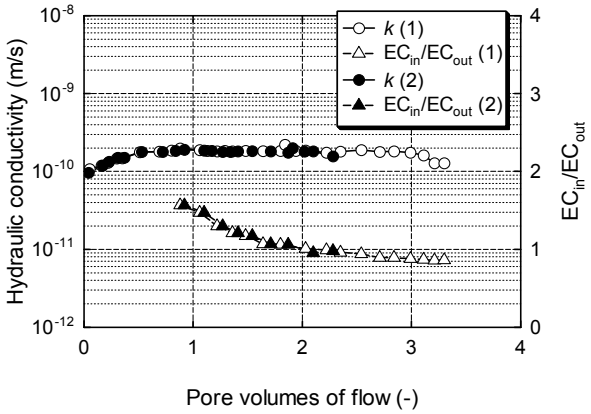

Appendix 24 Changes in k value and EC_{in}/EC_{out} (P-5).

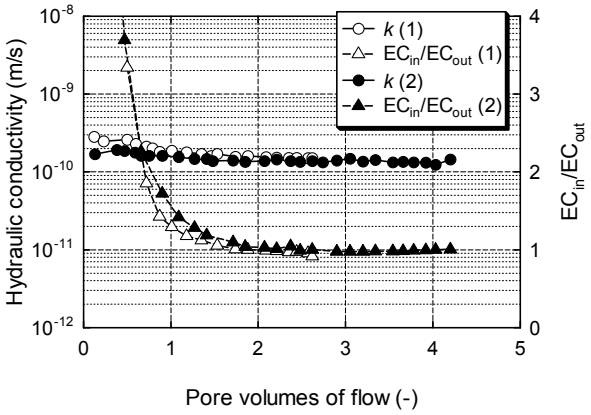

Appendix 25 Changes in k value and EC_{in}/EC_{out} (P-6).

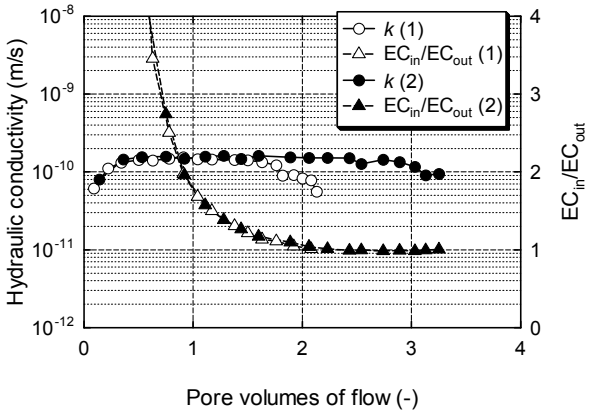

Appendix 26 Changes in k value and EC_{in}/EC_{out} (P-7).

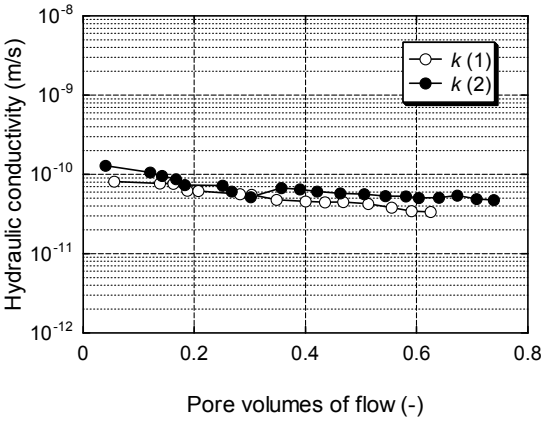

Appendix 27 Changes in k value (P-8).

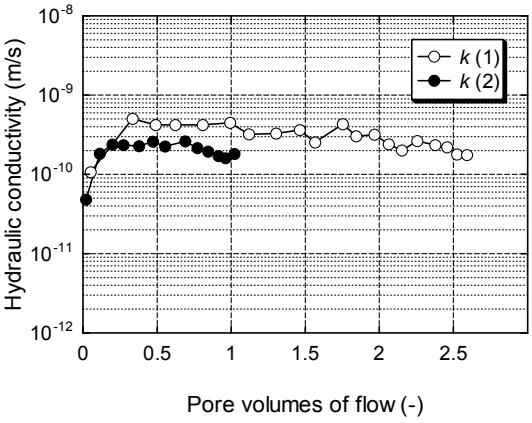

Appendix 28 Changes in k value (N-1).

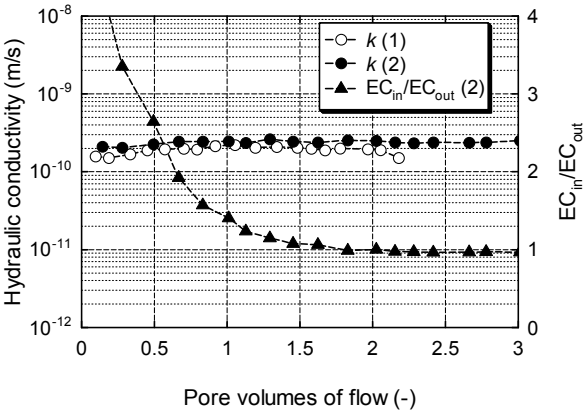

Appendix 29 Changes in k value and EC_{in}/EC_{out} (N-2).

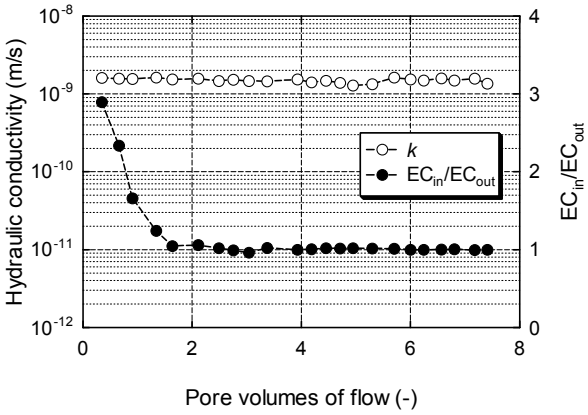

Appendix 30 Changes in k value and EC_{in}/EC_{out} (N-3).

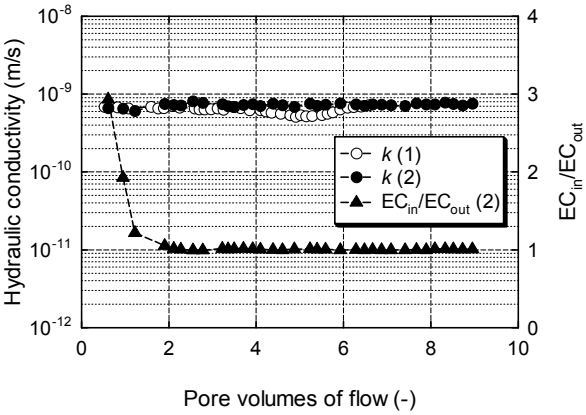

Appendix 31 Changes in k value and EC_{in}/EC_{out} (N-4).

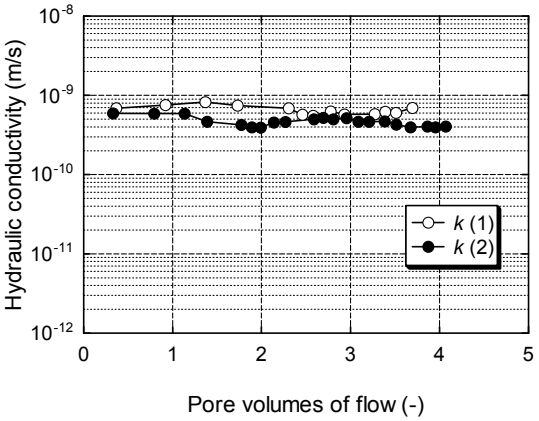

Appendix 32 Changes in k value (N-5).

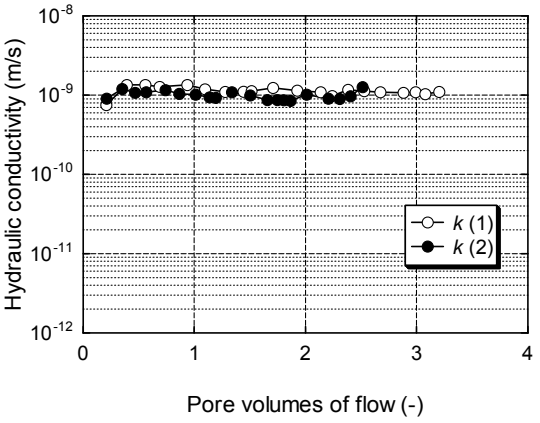

Appendix 33 Changes in k value (N-6).

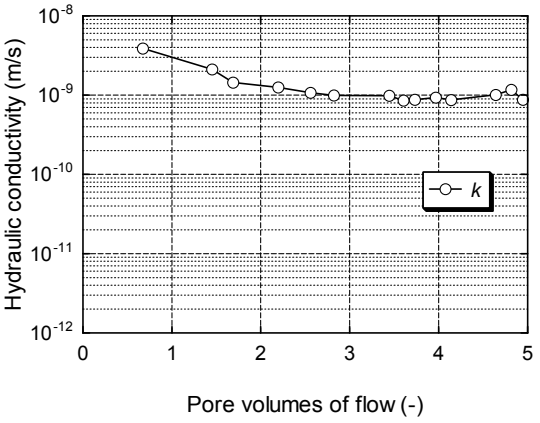

Appendix 34 Change in k value (N-7).

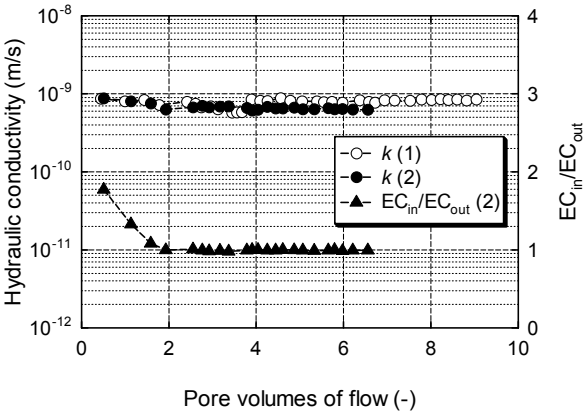

Appendix 35 Changes in k value and EC_{in}/EC_{out} (N-8).

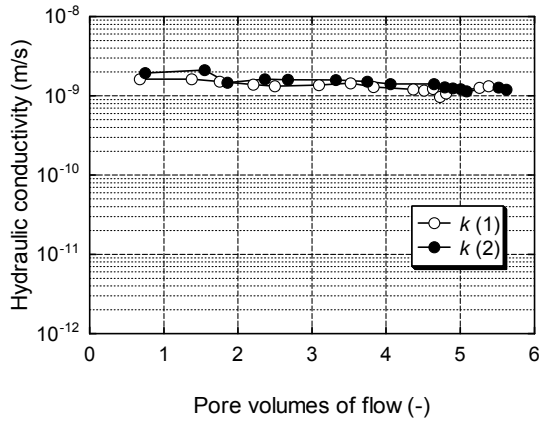

Appendix 36 Changes in k value (N-9).

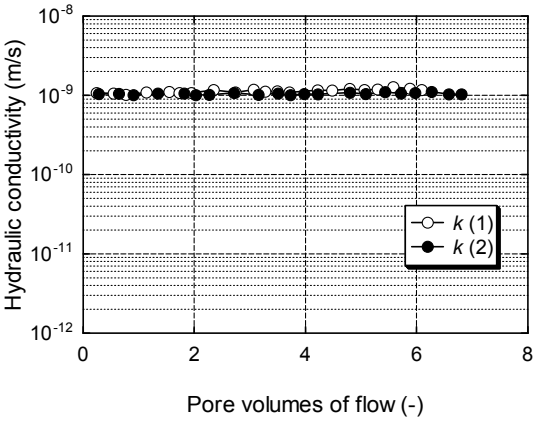

Appendix 37 Changes in k value (N-10).

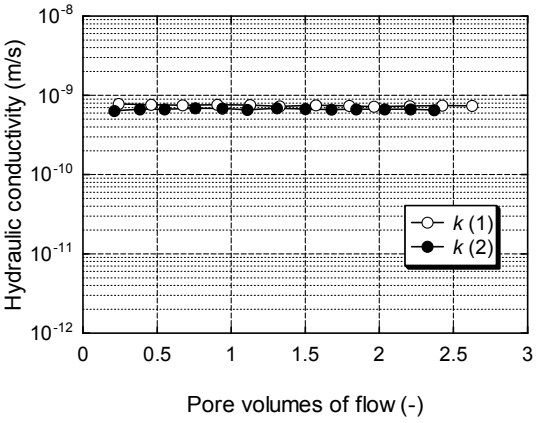

Appendix 38 Changes in k value (N-11).

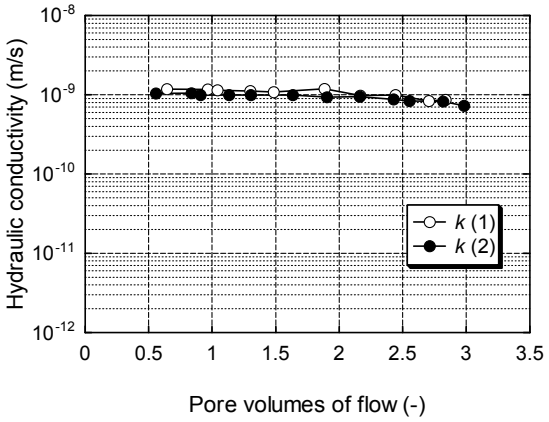

Appendix 39 Changes in *k* value (N-12).

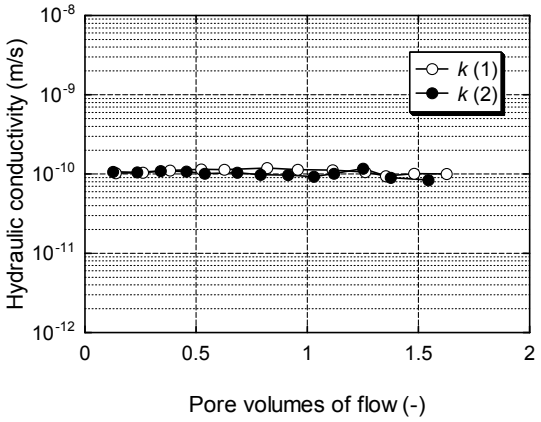

Appendix 40 Changes in *k* value (N-13).

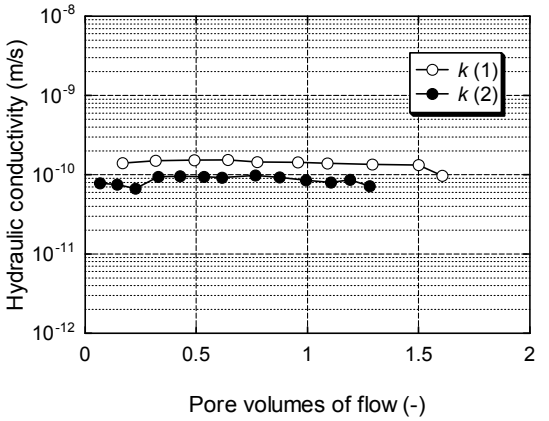

Appendix 41 Changes in *k* value (N-14).

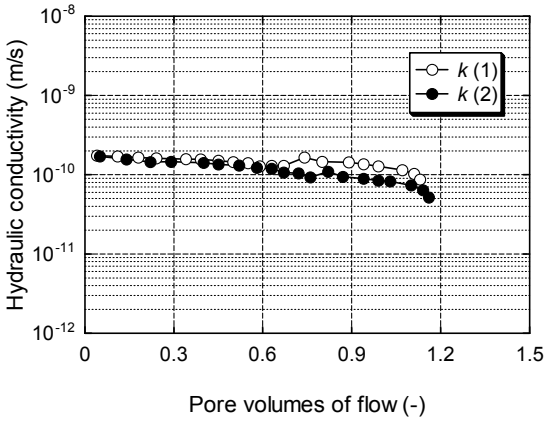

Appendix 42 Changes in *k* value (S-1).

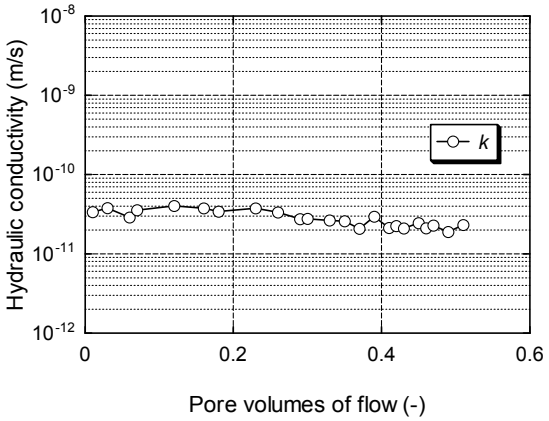

Appendix 43 Change in *k* value (S-2).

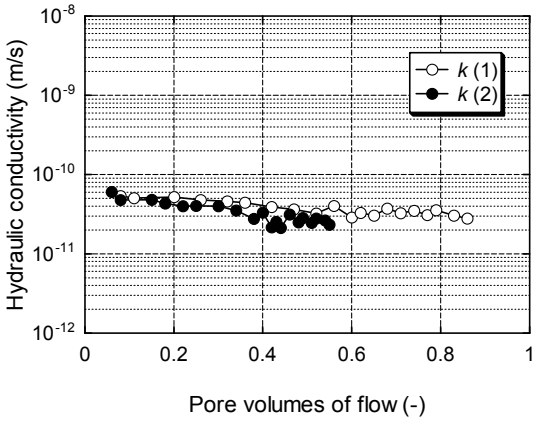

Appendix 44 Changes in *k* value (S-3).

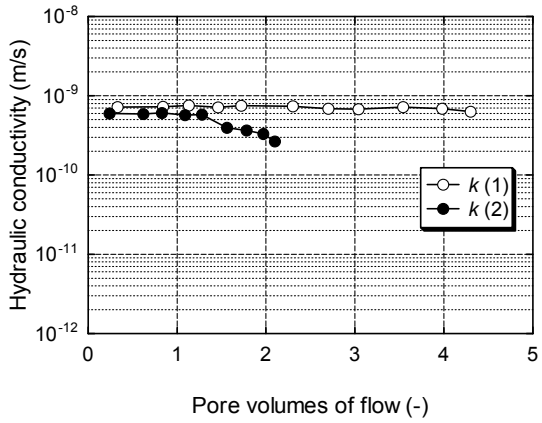

Appendix 45 Changes in *k* value (S-4).

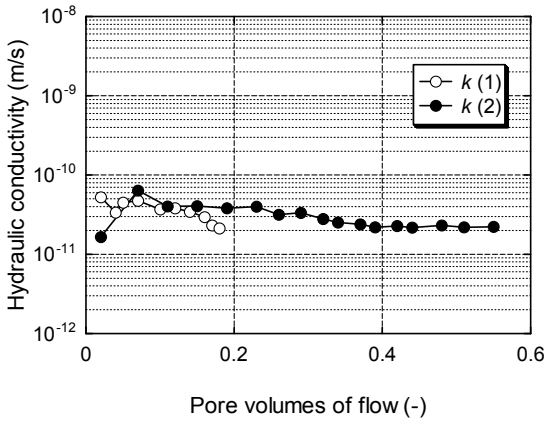

Appendix 46 Changes in *k* value (S-5).

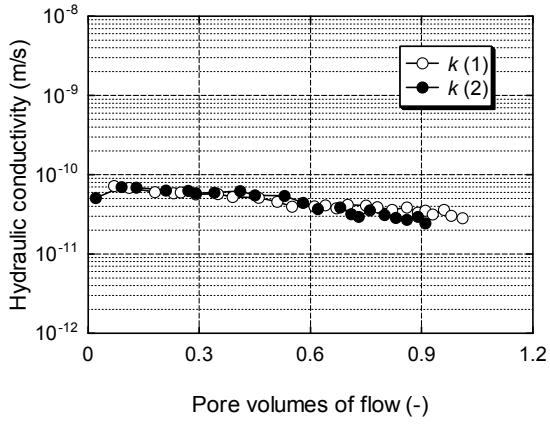

Appendix 47 Changes in *k* value (S-6).

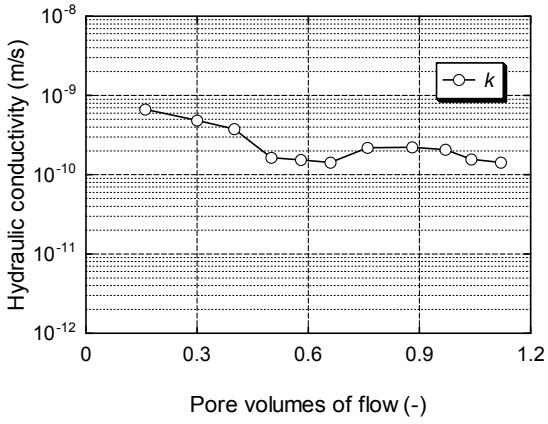

Appendix 48 Change in *k* value (S-7).

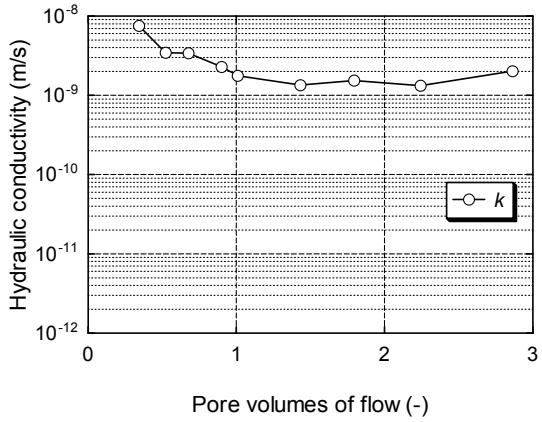

Appendix 49 Change in *k* value (S-8).

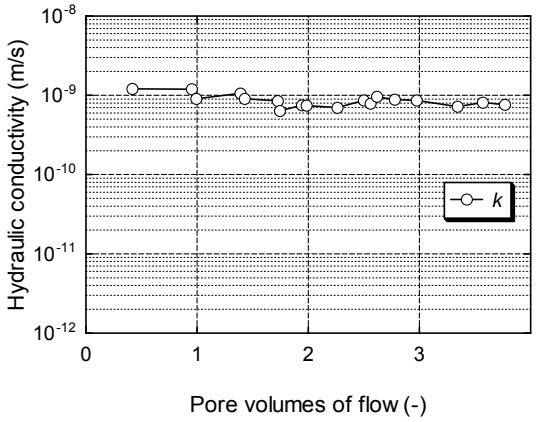

Appendix 50 Change in *k* value (S-9).

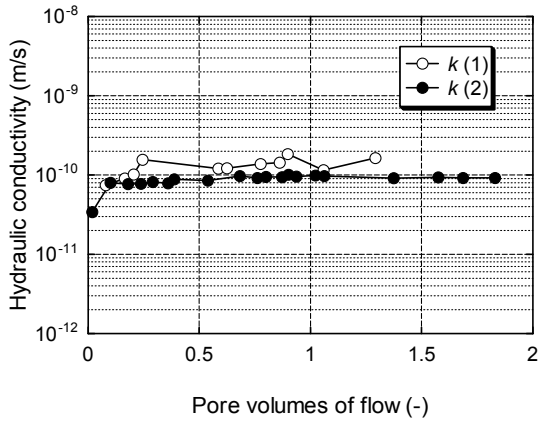

Appendix 51 Changes in *k* value (S-10).

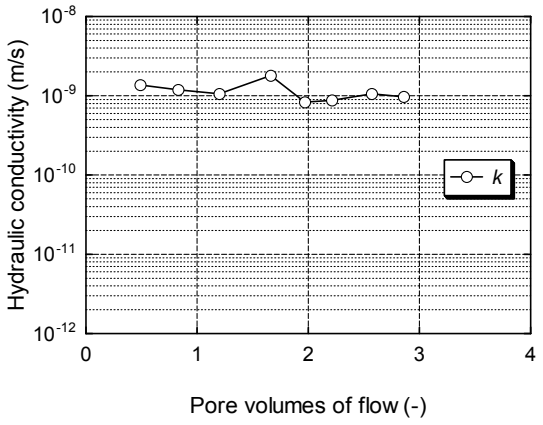

Appendix 52 Change in *k* value (S-11).

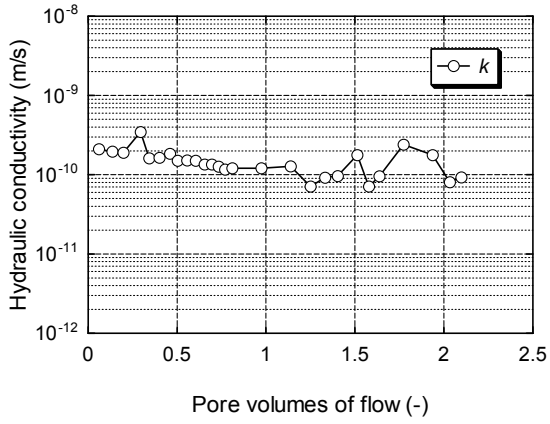

Appendix 53 Change in *k* value (S-12).

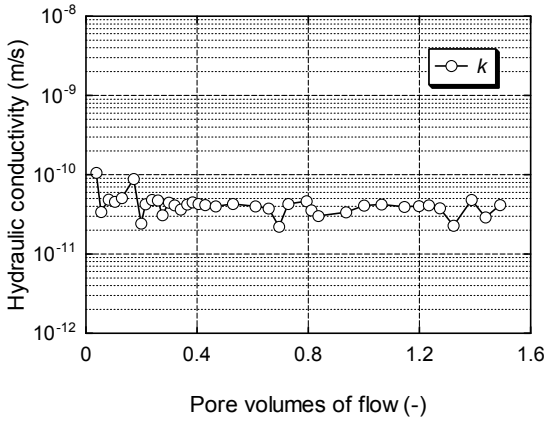

Appendix 54 Change in *k* value (S-13).

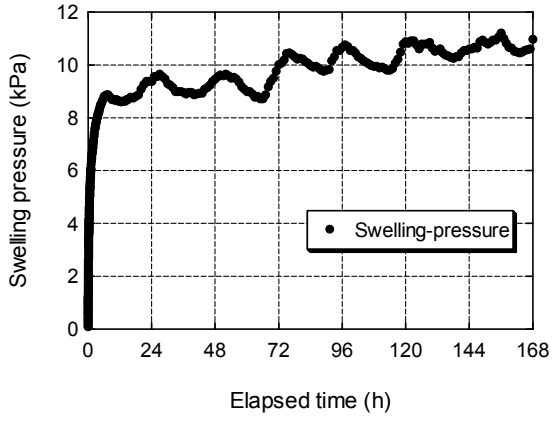

Appendix 55 Change in swelling-pressure value (P-2).

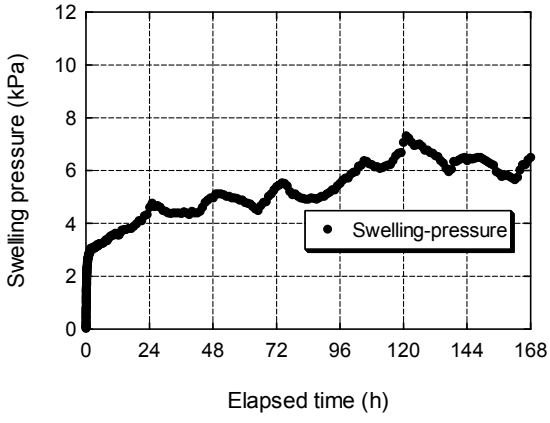

Appendix 56 Change in swelling-pressure value (N-1).

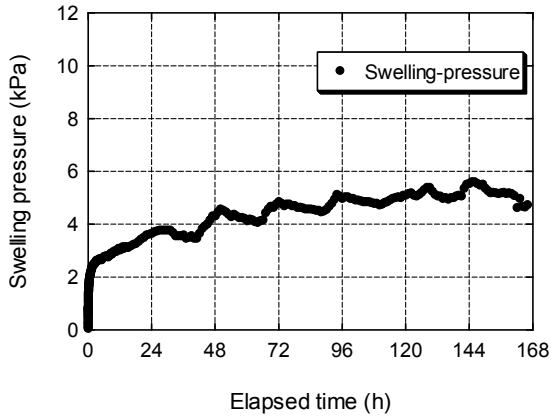

Appendix 57 Change in swelling-pressure value (N-9).

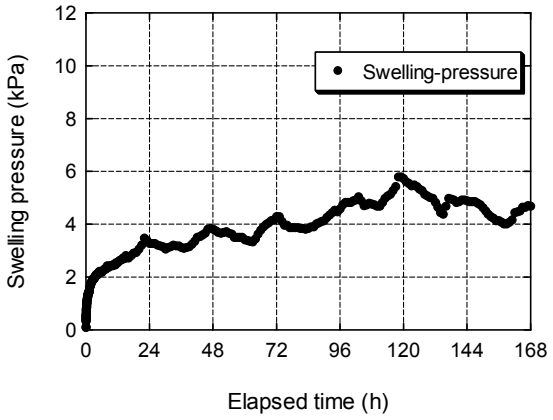

Appendix 58 Change in swelling-pressure value (N-11).

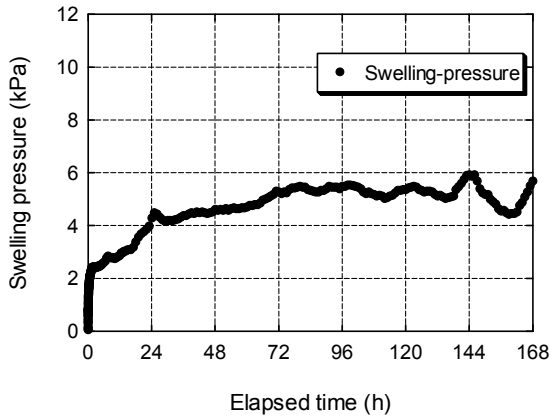

Appendix 59 Change in swelling-pressure value (N-12).

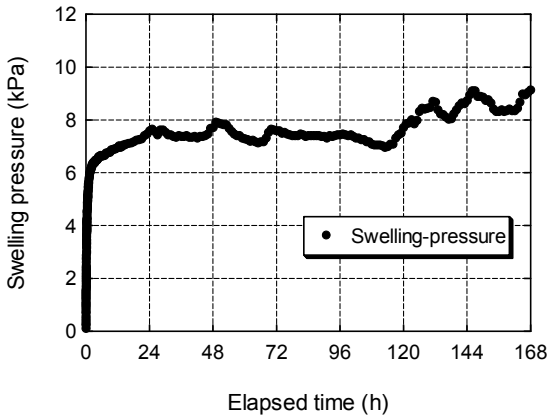

Appendix 60 Change in swelling-pressure value (N-13).

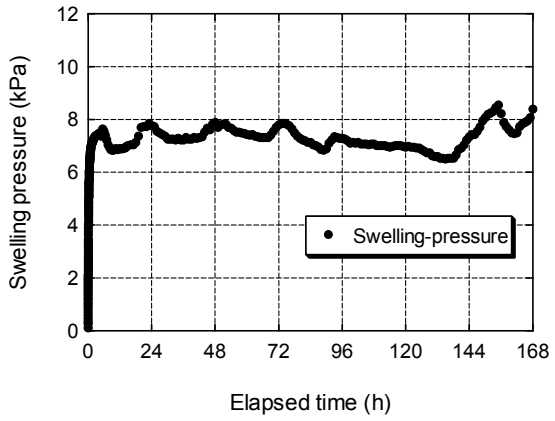

Appendix 61 Change in swelling-pressure value (N-14).

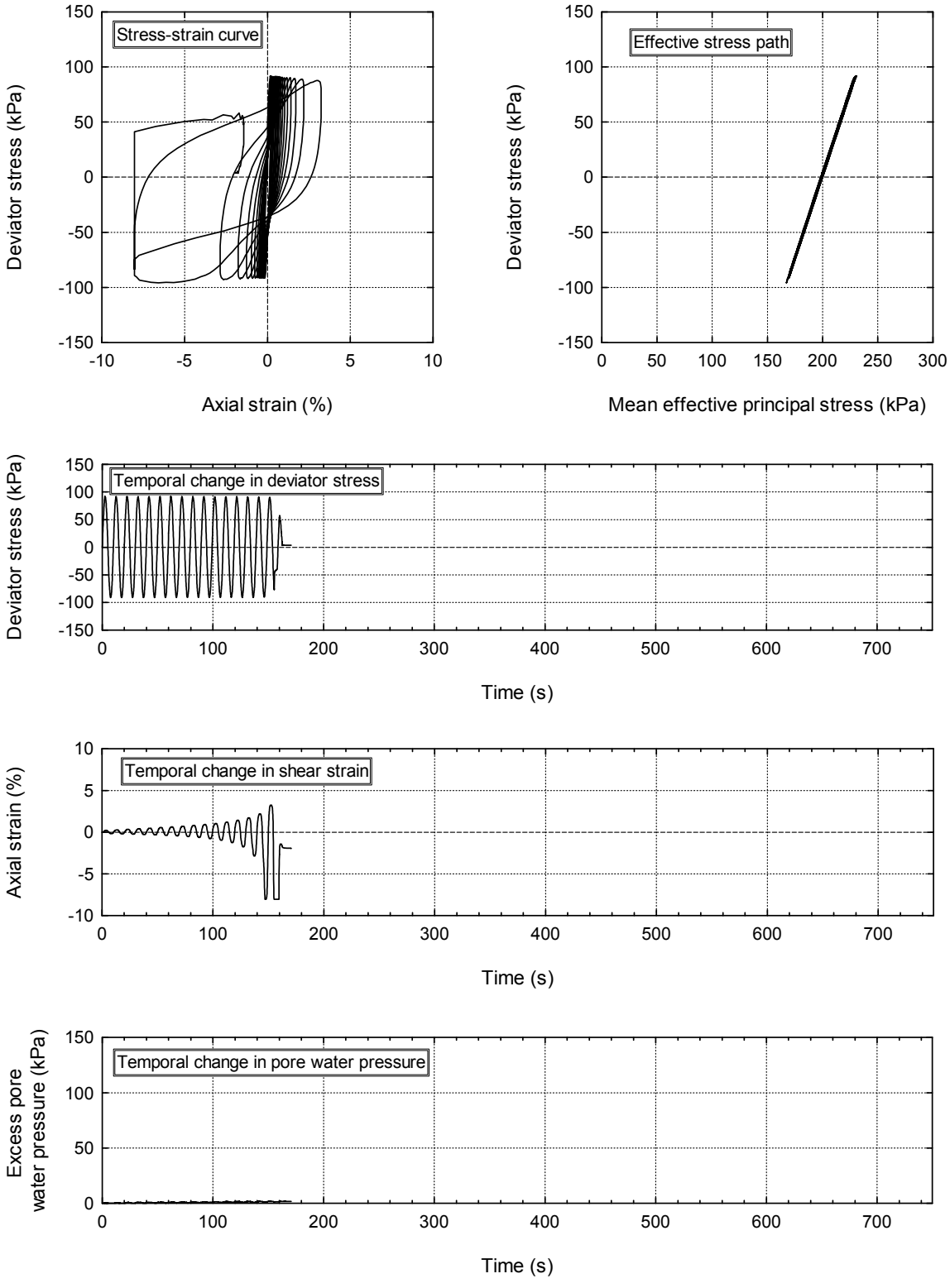

Appendix 62　Result of cyclic undrained triaxial test (Case-1).

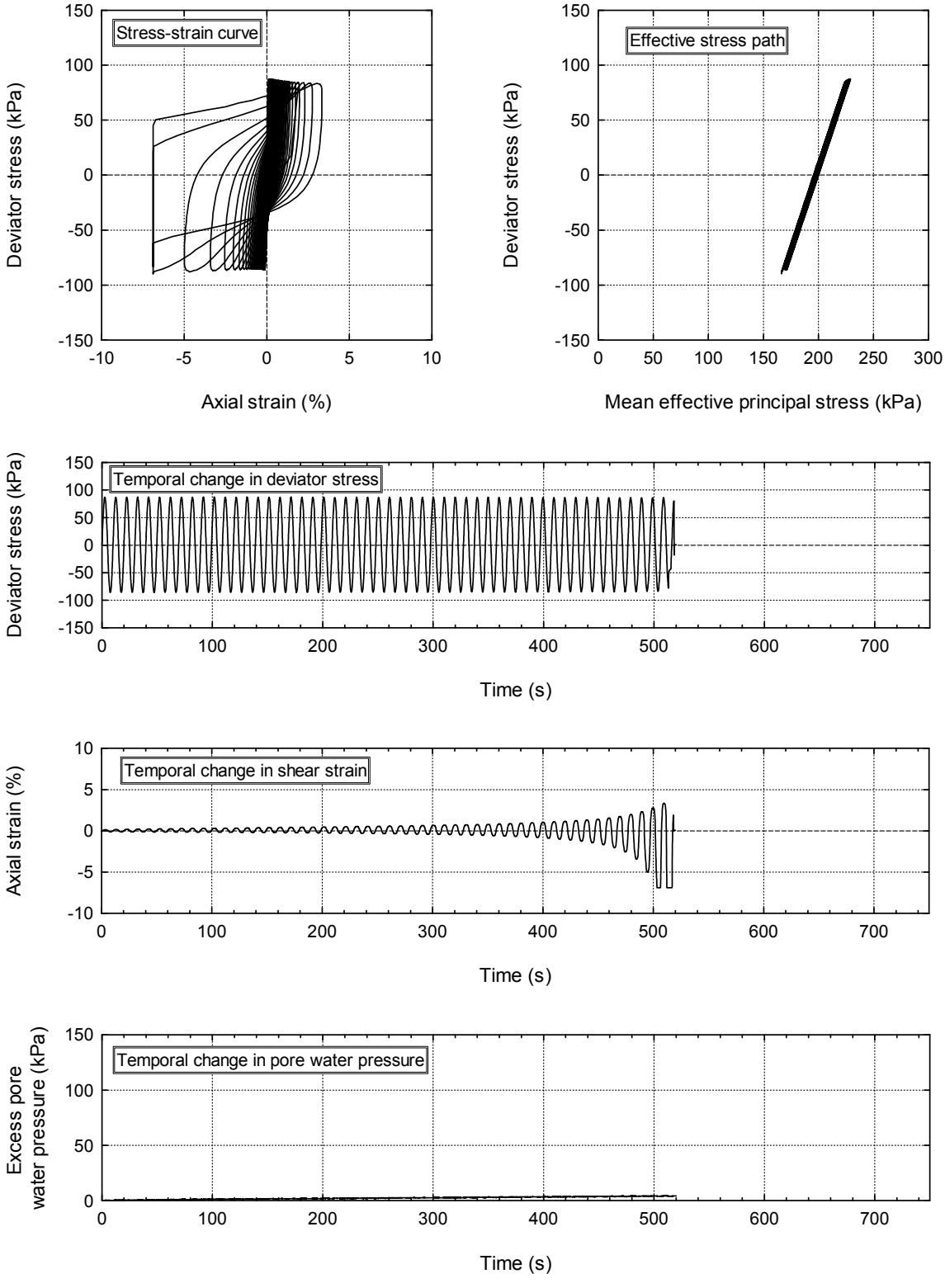

Appendix 63　Result of cyclic undrained triaxial test (Case-2).

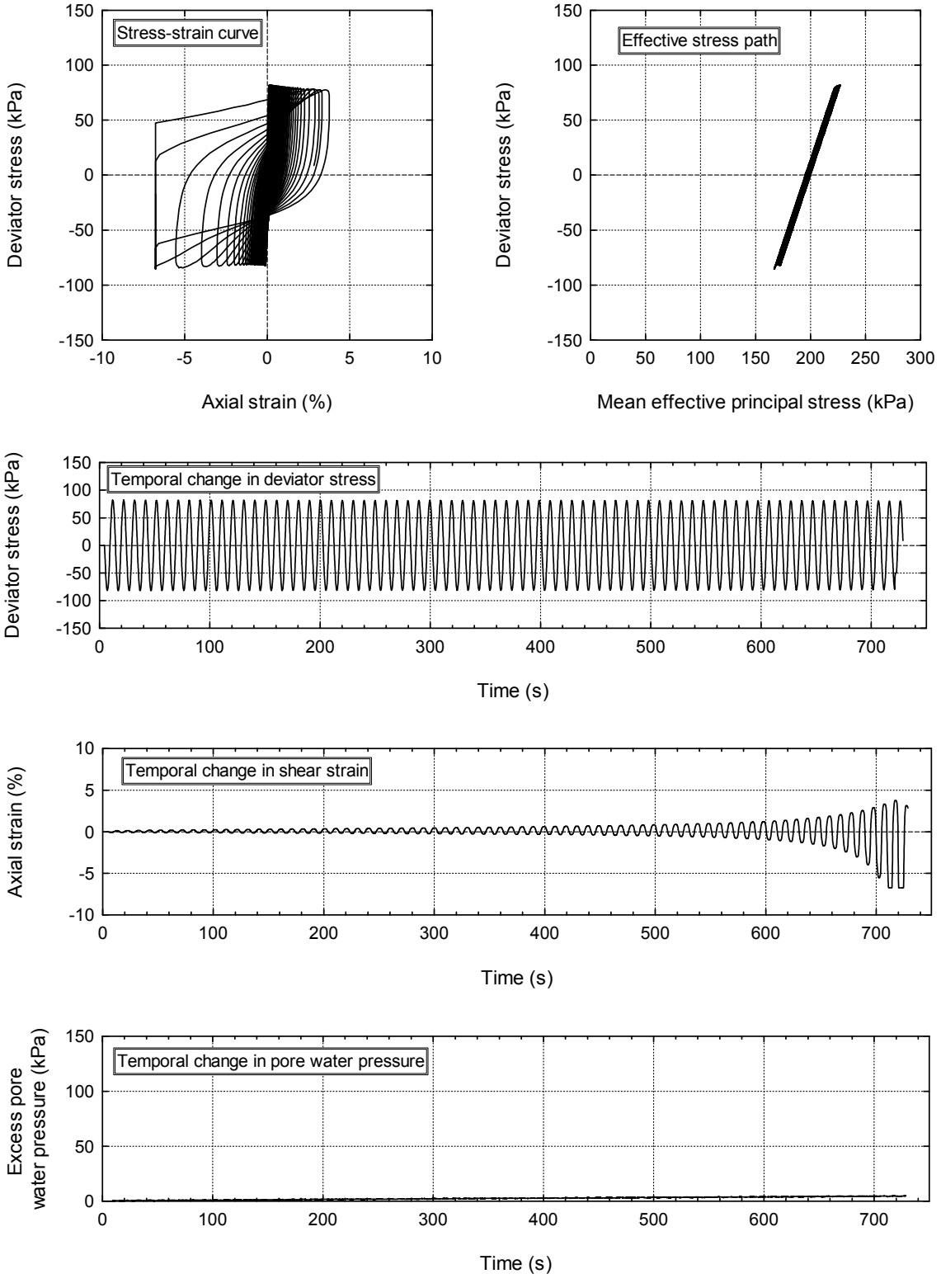

Appendix 64 Result of cyclic undrained triaxial test (Case-3).

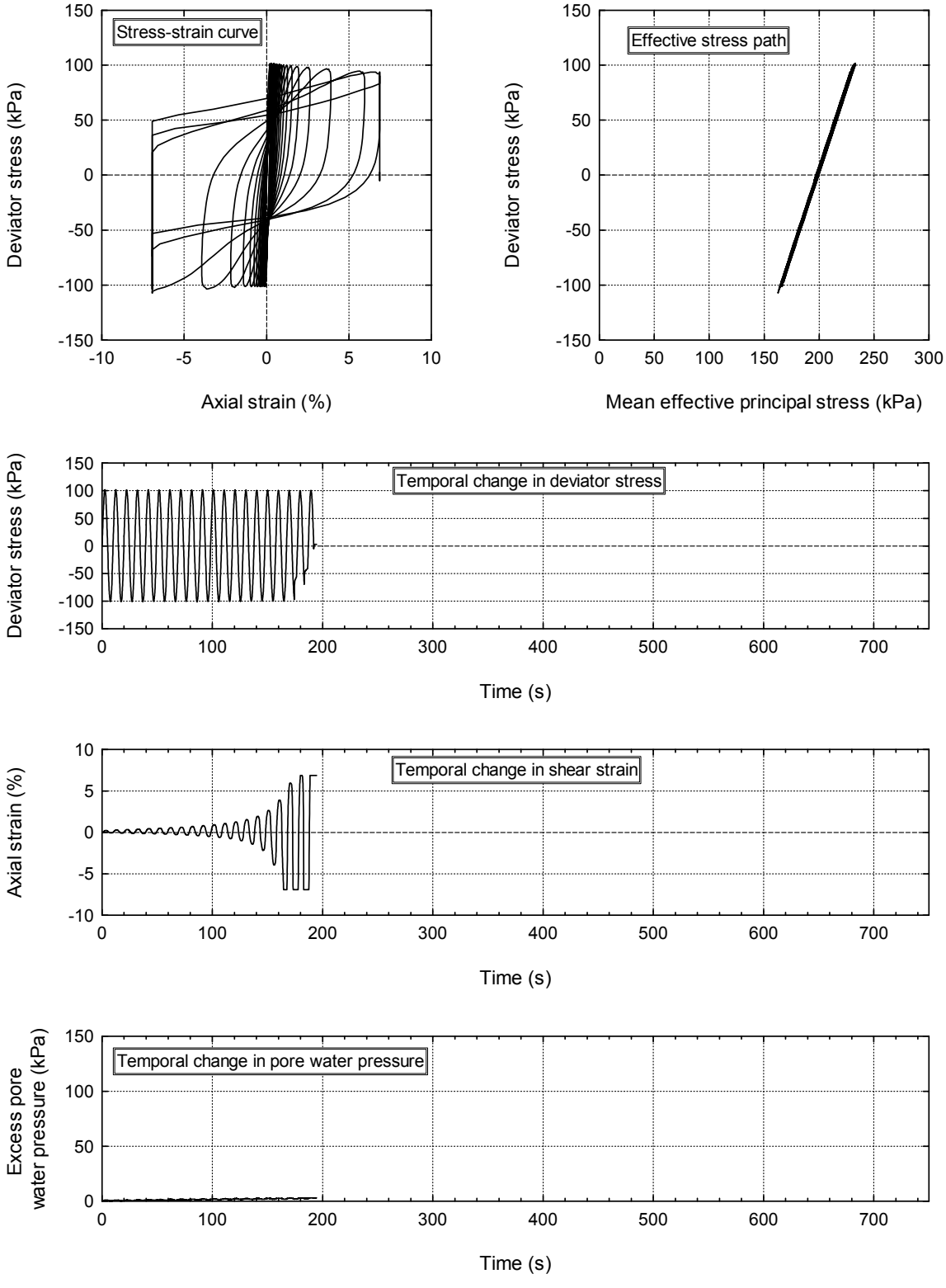

Appendix 65 Result of cyclic undrained triaxial test (Case-4).

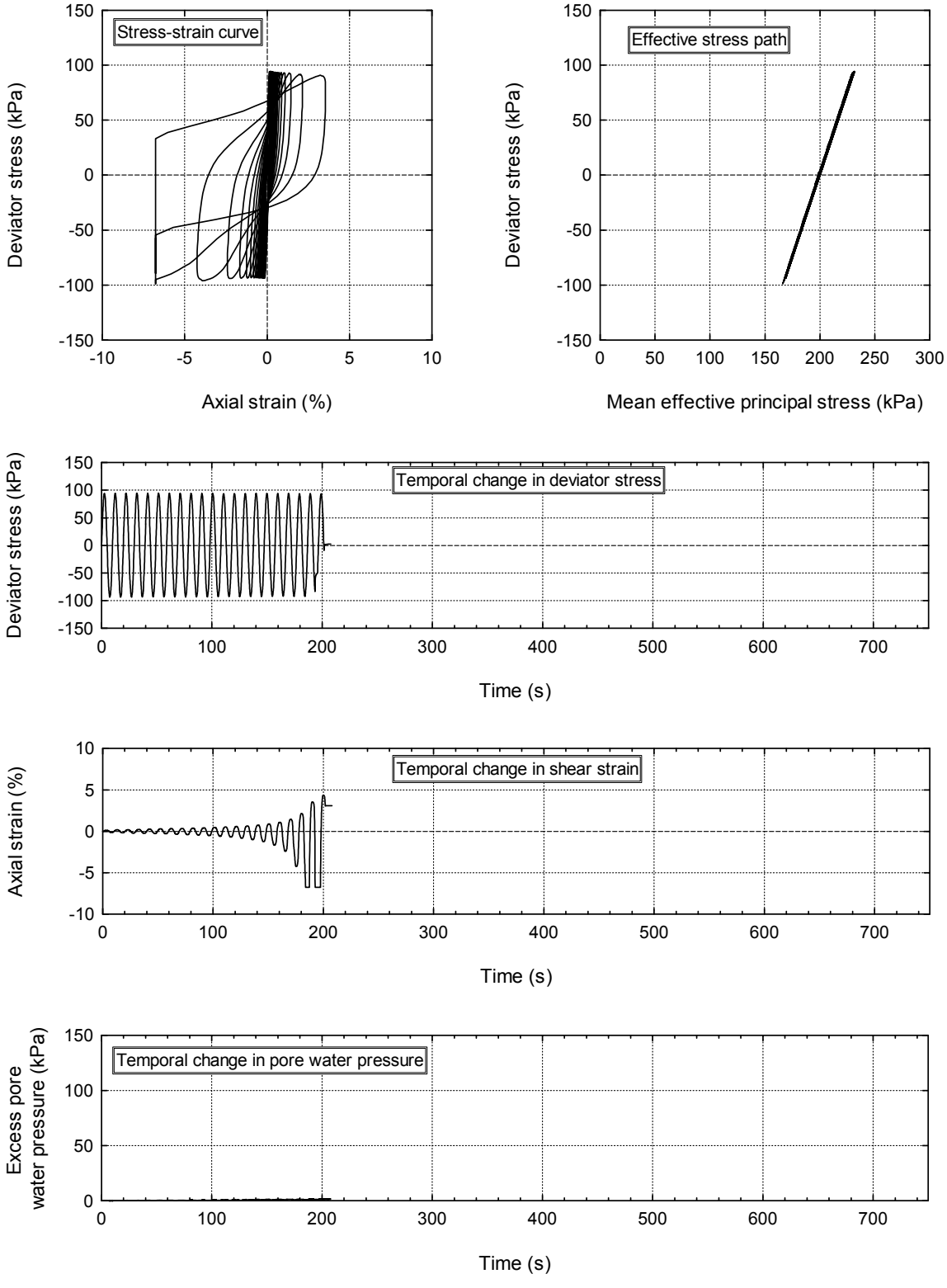

Appendix 66　Result of cyclic undrained triaxial test (Case-5).

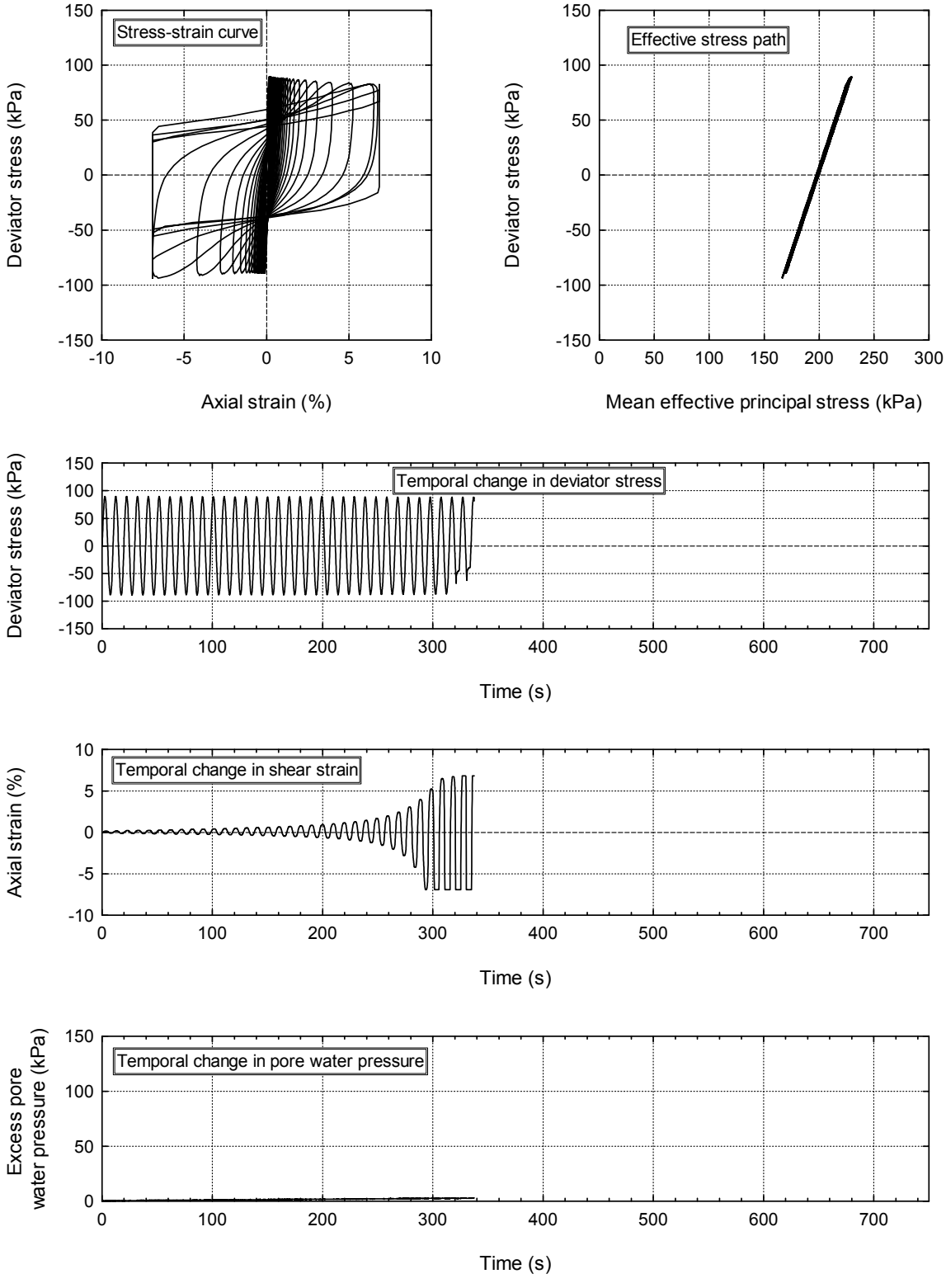

Appendix 67　Result of cyclic undrained triaxial test (Case-6).

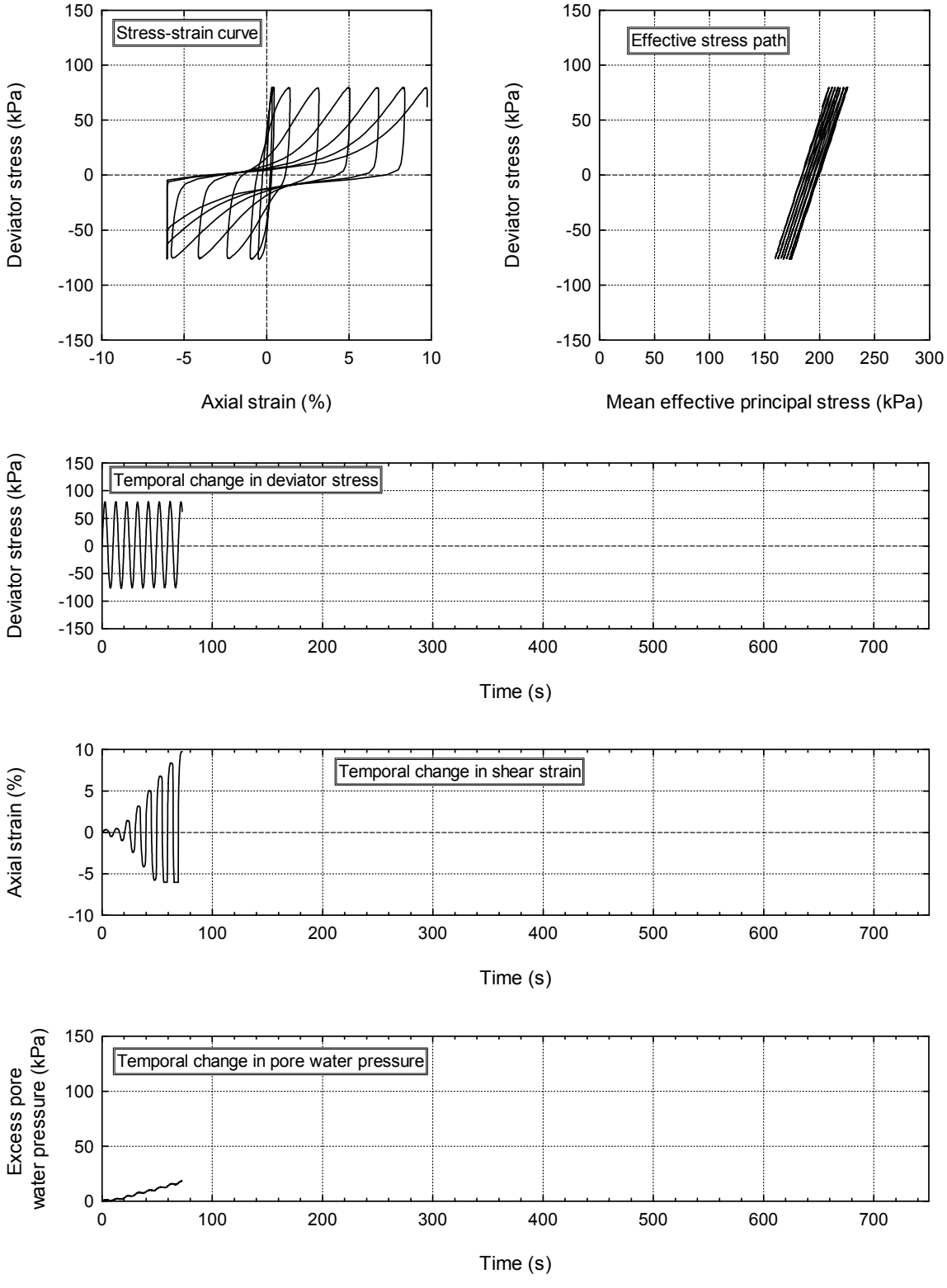

Appendix 68　Result of cyclic undrained triaxial test (Case-7).

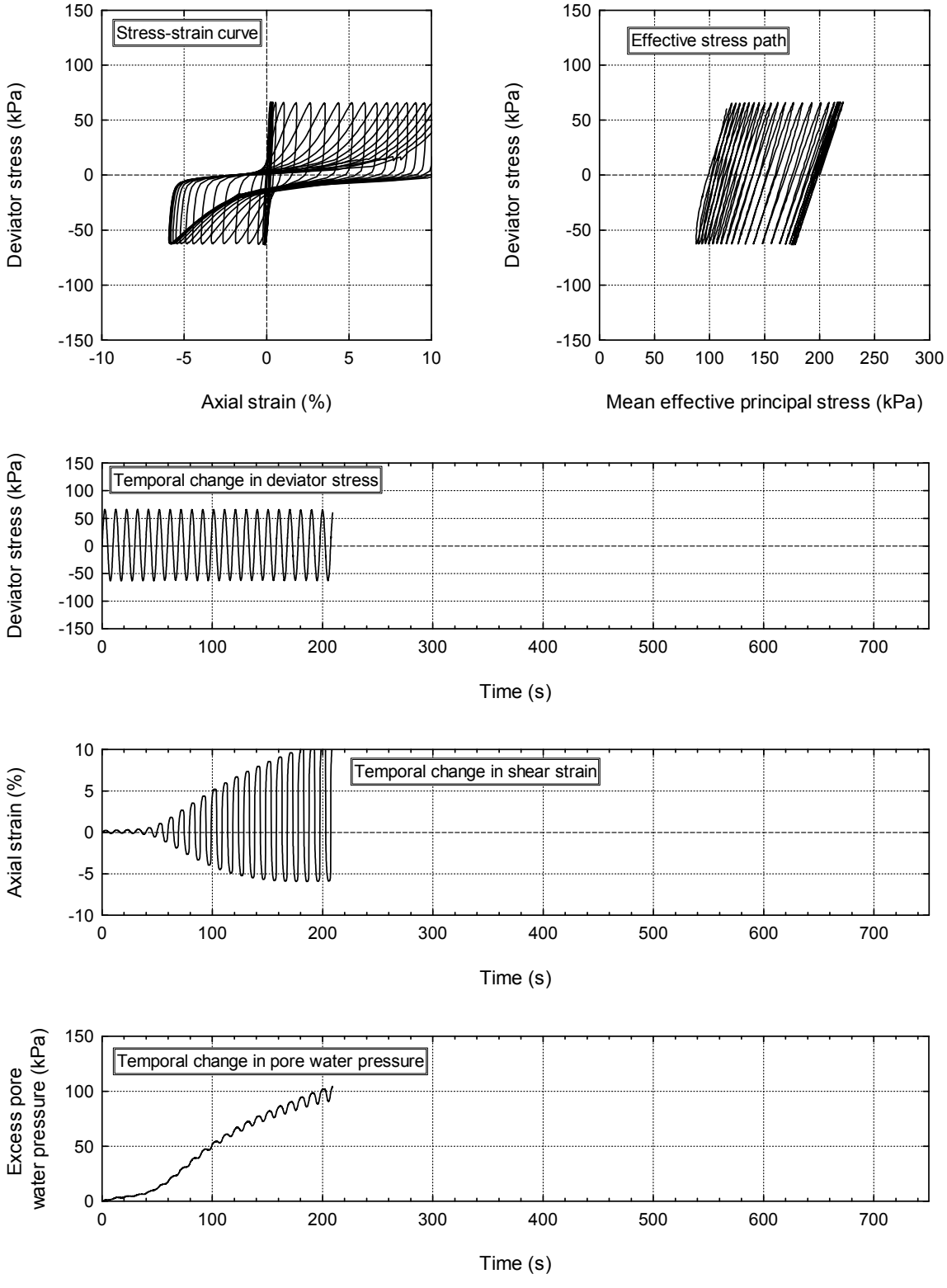

Appendix 69　Result of cyclic undrained triaxial test (Case-8).

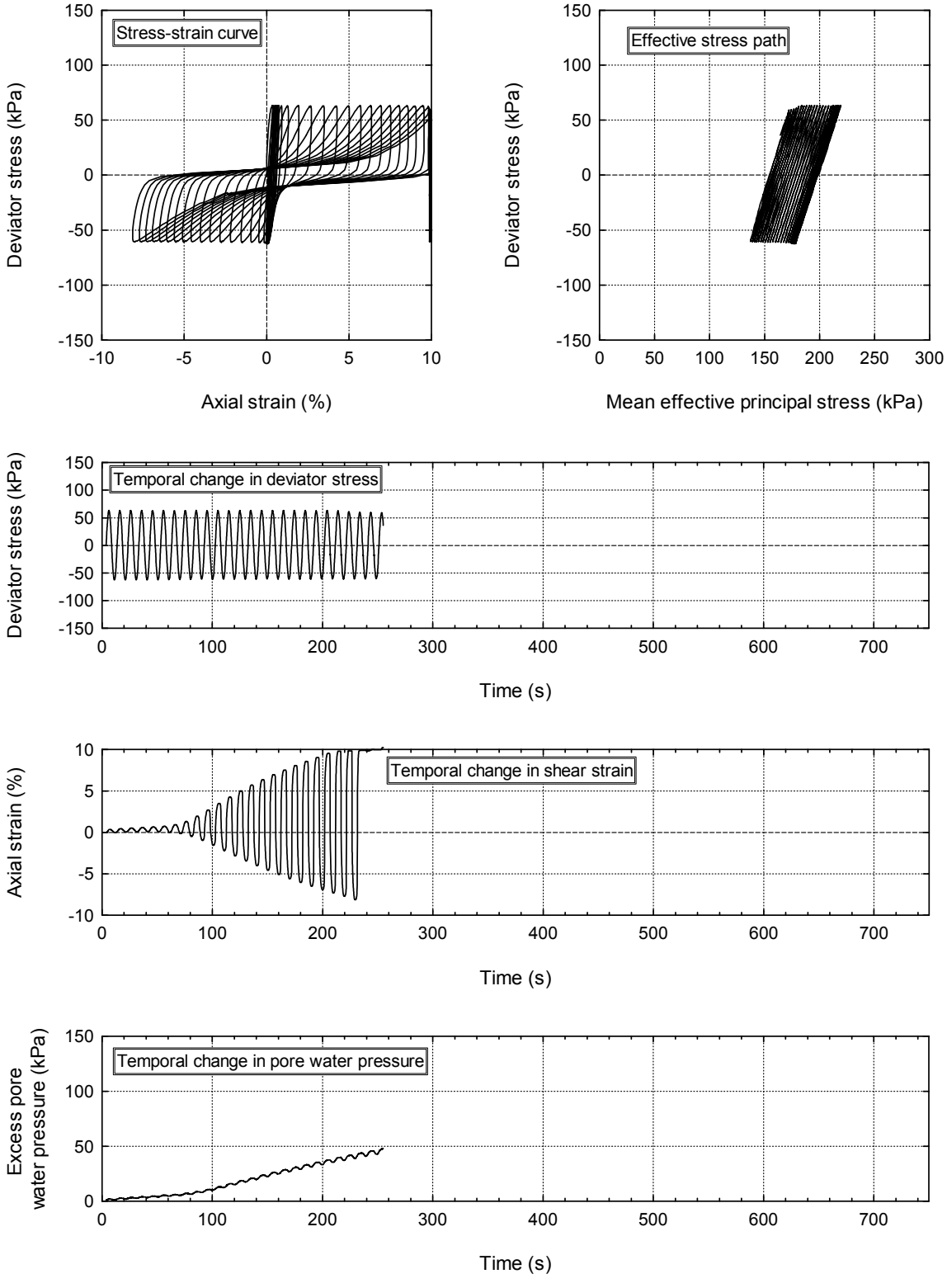

Appendix 70　Result of cyclic undrained triaxial test (Case-9).

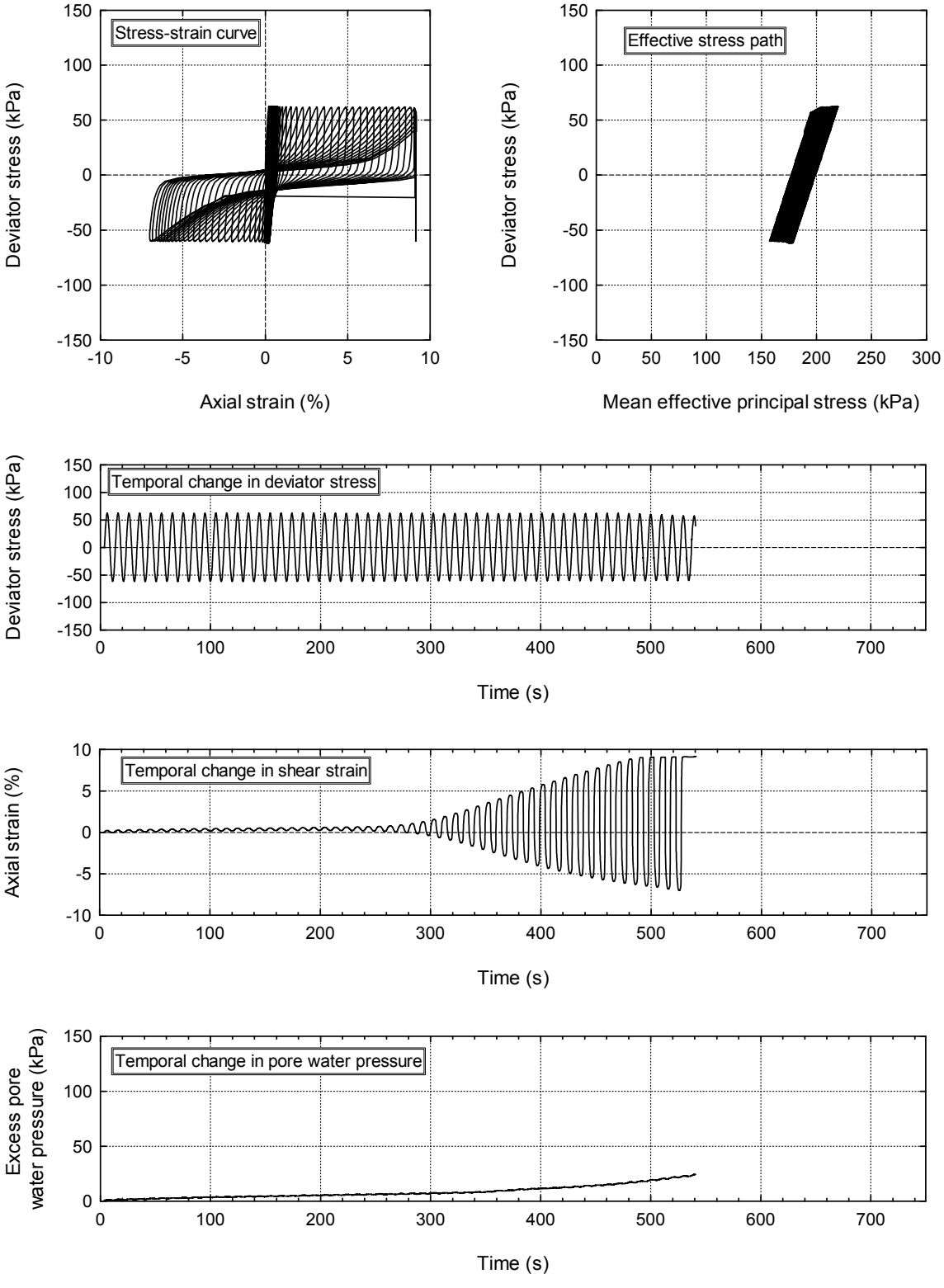

Appendix 71 Result of cyclic undrained triaxial test (Case-10).

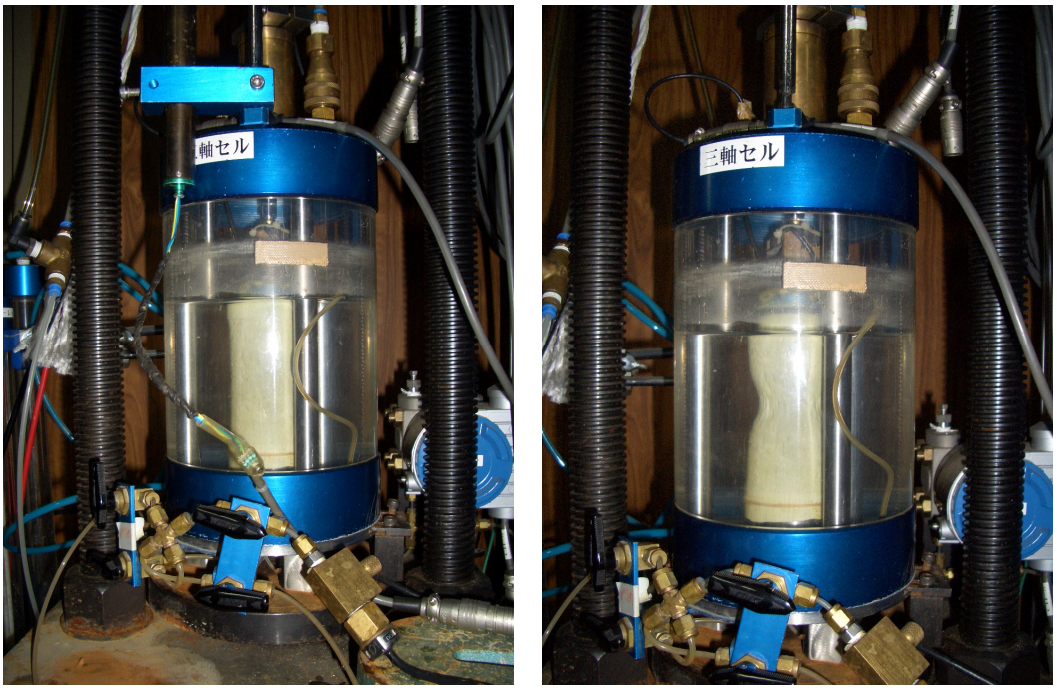

Appendix 72　Appearance of specimen before and after cyclic undrained triaxial test.